

AD-A107 255

AIR FORCE INST OF TECH WRIGHT-PATTERSON AFB OH
MECHANISMS OF RECOVERING LOW CYCLE FATIGUE DAMAGE IN INCOLOY 90--ETC(U)
1979 R E SCHAFRIK
AFIT-CI-79-212D

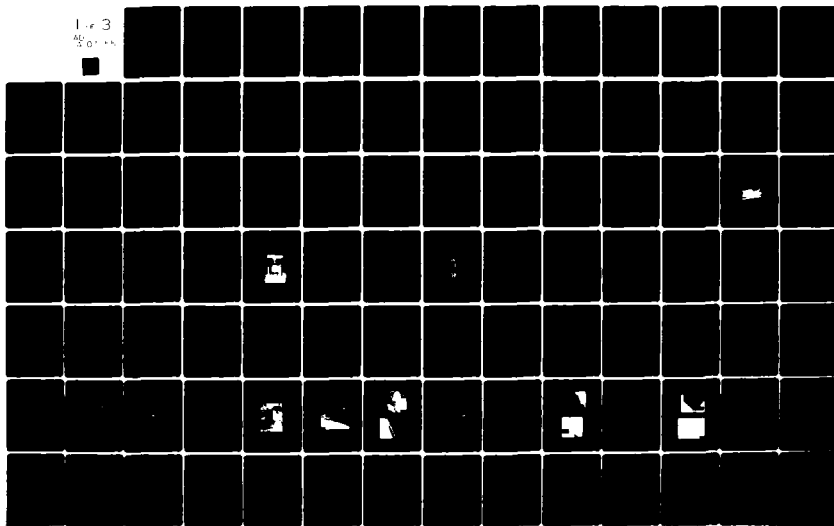
F/G 11/6

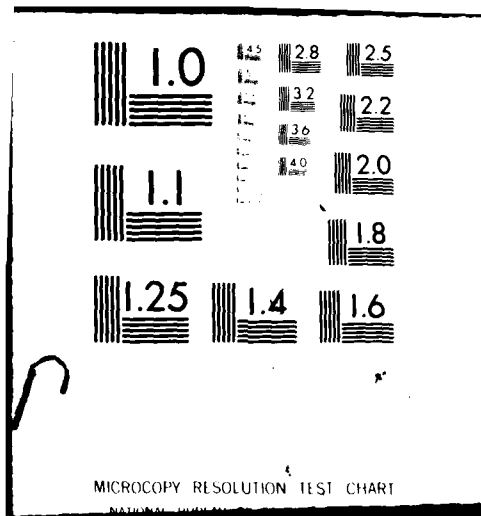
UNCLASSIFIED

NL

1 of 3

AD-A107 255





UNCLASS

SECURITY CLASSIFICATION OF THIS PAGE (When Data Entered)

REPORT DOCUMENTATION PAGE		READ INSTRUCTIONS BEFORE COMPLETING FORM
1. REPORT NUMBER 79-212D	2. GOVT ACCESSION NO. AD-A107255	3. RECIPIENT'S CATALOG NUMBER 255
4. TITLE (and Subtitle) Mechanisms of Recovering Low Cycle Fatigue Damage in Incoloy 901		5. TYPE OF REPORT & PERIOD COVERED THESIS/DISSERTATION
7. AUTHOR(s) Capt Robert E. Schafrik		6. PERFORMING ORG. REPORT NUMBER
9. PERFORMING ORGANIZATION NAME AND ADDRESS AFIT STUDENT AT: The Ohio State University		8. CONTRACT OR GRANT NUMBER(s)
11. CONTROLLING OFFICE NAME AND ADDRESS AFIT/NR WPAFB OH 45433		10. PROGRAM ELEMENT, PROJECT, TASK AREA & WORK UNIT NUMBERS
14. MONITORING AGENCY NAME & ADDRESS (if different from Controlling Office) LEVEL II		12. REPORT DATE 1979
		13. NUMBER OF PAGES 239
		15. SECURITY CLASS. (of this report) UNCLASS
16. DISTRIBUTION STATEMENT (of this Report) APPROVED FOR PUBLIC RELEASE; DISTRIBUTION UNLIMITED		15a. DECLASSIFICATION/DOWNGRADING SCHEDULE
17. DISTRIBUTION STATEMENT (of the abstract entered in Block 20, if different from Report) 22 OCT 1981 Fredric C. Lynch FREDRIC C. LYNCH, Major, USAF Director of Public Affairs Air Force Institute of Technology (ATC) Wright-Patterson AFB, OH 45433		
18. SUPPLEMENTARY NOTES APPROVED FOR PUBLIC RELEASE: IAW AFR 190-17		
19. KEY WORDS (Continue on reverse side if necessary and identify by block number)		
20. ABSTRACT (Continue on reverse side if necessary and identify by block number) ATTACHED		

AD A107255

FILE COPY

DD FORM 1 JAN 73 1473

EDITION OF 1 NOV 65 IS OBSOLETE

UNCLASS

SECURITY CLASSIFICATION OF THIS PAGE (When Data Entered)

811030051

MECHANISMS OF RECOVERING LOW CYCLE FATIGUE DAMAGE
IN INCOLOY 901

BY

Robert E. Schafrik, Capt. USAF (Ph.D.)
The Ohio State University, 1979
Professor James A. Begley, Adviser

ABSTRACT

The effect of thermal treatment and hot isostatic pressing (HIP) on eliminating low cycle fatigue (LCF) damage in the iron-nickel superalloy, Incoloy 901, was investigated. Testing was done in air at 500°F at a total strain range of 0.75%. The mechanisms of crack initiation and crack propagation in baseline specimens were determined and used as the basis of comparison for the rejuvenated specimens.

Crack initiation in the baseline specimens was due to decohering of blocky grain boundary carbides. Pre-crack initiation damage consisted of extrusions and intrusions formed at persistent slip bands and partially decohered grain boundary carbides.

A pre-rejuvenation damage level of 800 cycles (60% of crack initiation) was selected. Some specimens to be HIP processed were ceramic coated; the rest were left uncoated. Post-HIP testing revealed that LCF properties were adversely affected by surface microstructural damage caused by the HIP processing.

Thermal rejuvenation, consisting of a standard solution treatment and double aging, was partially successful in recovering fatigue properties with a pre-rejuvenation damage level of 800 cycles. Initiation life was extended by 400 cycles and cycles to failure was extended by 600 cycles. This behavior is explained in terms of microstructural damage which is resistant to thermal treatment.

Total Pages - 259

Selected Bibliography

1. M.N. Menon and W.H. Reiman, "Low Cycle Fatigue Crack Initiation Study in René 95", J. Mater. Sci. 10, 1571-1581 (1975).
2. B. Leis and A. Clauer, Investigation of Rejuvenation of Fatigue Damage in IN-718, AFML TR-78-90, Wright-Patterson AFB, OH.
3. H.F. Merrick, "The Low Cycle Fatigue of Three Wrought Nickel-Base Alloys", Met Trans 5, 891-897 (1976).
4. C. Laird, Mechanisms and Theories of Fatigue, presented at the Materials Science Seminar, ASM, St. Louis Mo. (1978).

MECHANISMS OF RECOVERING LOW CYCLE FATIGUE DAMAGE
IN INCOLOY 901

DISSERTATION

Presented in Partial Fulfillment of the Requirements for
the Degree Doctor of Philosophy in the Graduate
School of The Ohio State University

By

Robert E. Schafrik, B.S.Met., M.S.

The Ohio State University
1979

Reading Committee:

Dr. G. W. Powell

Dr. J. P. Hirth

Dr. J. A. Begley

Approved By


Adviser

Department of Metallurgical Engineering

Accession For
NHS GRAI
DTIC TAB
Unannounced
Justification
By
Distribution
Availability
Dist

A

DEDICATION

To my wife, Mary; and to my children: Catherine,
Frances, Robert Jr., and Steven.

ACKNOWLEDGEMENTS

The author wishes to express his sincere appreciation to Dr. J. A. Begley of The Ohio State University for his guidance and encouragement throughout this project. The author is thankful for the constructive comments of the following individuals in the early stages of this effort: Dr. B. Wilshire of University College, University of Wales; A. Adair, Dr. W. Reimann, and Dr. H. A. Lipsitt of the Air Force Materials Laboratory, Wright-Patterson Air Force Base; Drs. A. Clauer and B. Leis, Battelle-Columbus Laboratories; and Dr. J. C. Williams, Carnegie-Mellon University. Also, the author is grateful for the excellent training in practical aspects of transmission electron microscopy provided by Dr. J. C. Williams.

Appreciation is due to Captain P. Martin and R. Kerans of the Air Force Materials Laboratory for helpful advice, instruction, and troubleshooting assistance in using the many different pieces of laboratory equipment required to complete this dissertation; and for helpful discussions on the research work throughout the project. Also, appreciation is due to Mr. Dwelle Butts of the Air Force Materials Laboratory for his efforts in obtaining necessary supplies.

I wish to thank my wife, Mary, and our four children for their support and extreme patience throughout my graduate education.

The author is obliged to the following for supplying materials: M. M. Allen, Government Products Division, Pratt-Whitney Aircraft Co.,

for providing a section of a compressor shaft forging; P. Bailey, Aircraft Engine Group, General Electric Co., for providing ceramic coating for some specimens; and D. Weaver, Kelsey-Hayes, Detroit, for a piggybacked hot-isostatic-pressing run.

I would like to recognize the cooperation and help of the following: S. Leffler, J. Henry, M. Henry, G. Cornish, and J. Barlowe. Many thanks are due to Ms. S. Ehlers for typing this manuscript.

Able assistance in transferring my fatigue data from paper punch tape format to computer disk file was provided by Captain D. Summer and Ms. C. Johnson of the Air Force Materials Laboratory.

This research was performed under the auspices of the Air Force Materials Laboratory. I am appreciative of the moral and financial support provided by Dr. H. A. Lipsitt, and for his helpful advice during various stages in this project. I am likewise appreciative of the encouragement given me by Dr. H. Burte and L. Hjelm of the Air Force Materials Laboratory.

Finally, I wish to thank the Air Force Institute of Technology and the U. S. Air Force for the opportunity to complete my graduate education. I would like to acknowledge the administrative assistance provided by my Program Managers, Captains S. Brown and D. Cain.

VITA

February 6, 1946 Born - Cleveland, Ohio

1963-1967 B.S.Met., Case-Western Reserve University, Cleveland, Ohio

1967-1968 Applications Engineer, American Air Filter Co., Louisville, KY

1968 Commissioned and entered U. S. Air Force

1968-1972 Base Civil Engineer, Hanscom Air Force Base, Bedford, MA

1972-1974 M.S., Aerospace Engineering, Air Force Institute of Technology, Wright-Patterson Air Force Base, Ohio

1974-1975 Materials Development Engineer, Metallurgy and Ceramics Laboratory, Aerospace Research Laboratories, Wright-Patterson Air Force Base, Ohio

1975-1977 Assistant Branch Chief, Metals Branch, Manufacturing Technology, Air Force Materials Laboratory, Wright-Patterson Air Force Base, Ohio

PUBLICATIONS

"Determination of Texture Pole Figures Using Picker FACS-1 Apparatus," with L. A. Jacobson, ARL TR 75-0190, Aerospace Research Laboratories, Wright-Patterson Air Force Base, Ohio (1975).

"The Deformation and Fracture of TiAl at Elevated Temperatures," with H. A. Lipsitt and D. S. Schechtman, Met. Trans. A 6A, 1991-1996 (1975).

"Dynamic Elastic Moduli of the Titanium Aluminides," Met. Trans. A 8A, 1003-1006 (1977).

"Manufacture of TiAl by Extrusion of Blended Elemental Powders,"
Met. Trans. B 7B, 713-716 (1976).

"Manufacture of TiAl by Extrusion of Blended Elemental Powders,"
DDC Report AD-780630, Defence Documentation Center, Arlington, VA
(1974).

TABLE OF CONTENTS

DEDICATION	Page 11
ACKNOWLEDGEMENTS	111
VITA	v
LIST OF TABLES	x
LIST OF FIGURES	xi
Chapter	
1. INTRODUCTION	1
I. Crack Initiation	2
II. Stage I Crack Propagation	4
III. Stage II Crack Propagation	5
IV. Physical Metallurgy of Incoloy 901	5
V. Rejuvenation	9
2. EXPERIMENTAL PROCEDURE	11
I. Metallography Techniques	11
A. Optical Microscopy	11
B. Transmission Electron Microscopy	12
C. Scanning Electron Microscopy	13
D. Surface Replication	13
II. Aging Response of Incoloy 901	14
A. Material Specification	14
B. Thermal Treatments	14
III. Low Cycle Fatigue	18
A. LCF Specimen Design and Manufacture	18
B. Ceramic Coating Procedure	24
C. Specimen Preparation after Rejuvenation	27
D. Load Train Configuration	27
E. Strain Measuring System	27
F. Low Cycle Fatigue Testing	34
G. Computation of Strain Range and Stress Range	37
H. In Situ Surface Replication	40

TABLE OF CONTENTS (CONT'D)

Chapter	Page
IV. Tensile Testing	41
A. Specimen Configuration	41
B. Machine Description	41
C. Computation of Stress and Strain	41
V. Rejuvenation Treatments	42
A. Thermal Treatments	42
B. Hot Isostatic Pressing (HIP) Treatments	45
VI. Sonic Modulus Testing	49
3. RESULTS AND DISCUSSION	51
I. Aging Response of Incoloy 901	51
A. Characterization of As-Received Microstructure	51
B. Development of Standard Solution and Double-Aged Treatment	55
C. Microstructure Response at Elevated Temperatures	62
D. Microstructure Resulting from Hot Isostatic Pressing	62
II. Mechanical Properties	65
A. Tensile Testing	65
B. Elastic Constants	65
III. Low Cycle Fatigue Baseline Testing	68
A. Determination of Effective Gauge Length	68
B. Cyclic Stress-Strain Curve	71
C. Characterization of Fatigue Damage	73
i. Baseline Data	73
ii. Dislocation Substructure	90
iii. Fractography	90
D. Crack Initiation Mechanisms	96
i. Surface Replication	96
ii. Surface Scanning Electron Microscopy	107
iii. Proposed Mechanism	126

TABLE OF CONTENTS (CONT'D)

Chapter	Page
IV. Rejuvenation Effects	127
A. Results of HIP Treatments	127
i. Presentation of Data	127
ii. Mechanisms	158
B. Results of Thermal Treatments	159
i. Presentation of Data	159
ii. Mechanisms	179
C. Conclusions	181
4. SUMMARY	185
5. APPENDIX	189
Listing of Computer Programs	
I. Source Listing of Modified Instron Low Cycle Fatigue Application Program APP-900-A3A8	190
II. Source Listing of FORTRAN Program for Stress and Strain Computations and Plotting	224
BIBLIOGRAPHY	239

LIST OF TABLES

Table		Page
1	Chemical Analysis of Billet	15
2	Commercial Heat Treatment Specifications for Incoloy 901	16
3	Furnace Cool Rates - Vacuum Cool and Helium Gas Quench	19
4	Standard Heat Treatment, STA 3A, for Incoloy 901	25
5	Low Stress Grinding Parameters	26
6	Typical LVDT Calibration Curve Data	33
7	Incoloy 901 Tensile Data	66
8	Effective Elastic Gauge Length	68
9	Summary of Baseline LCF Properties	74
10	Line Constants for Log $\Delta\epsilon$ vs Log N Curves	75
11	Calculation of Crack Growth Rate from Fracture Mechanics	106
12	Summary of HIP Rejuvenation on LCF Properties	128
13	Effect of Vapor Honing on LCF Properties	141
14	Summary of Thermal Rejuvenation on LCF Properties	160
15	Summary of Repolishing on LCF Properties	161
16	Summary of LCF Data for Multiple Thermal Rejuvenation - LCF Specimen 41	172
17	Summary of Cycles to Crack Initiation, 0.70-0.80 Total Strain Range, 500 F Test Temperature	182
18	Summary of Cycles to Failure, 0.70-0.80 Total Strain Range, 500 F Test Temperature	183

LIST OF FIGURES

Figure		Page
1	Low Cycle Fatigue Specimen Design	21
2	View of Incoloy 901 Shaft Forging	22
3	Load Train Sketch	28
4	LCF Specimen Grip Design	30
5	Strain Measuring System	31
6	LVDT Calibration Curve	35
7	Plot of Displacement vs Cycles	38
8	Heat Treatment Fixture Design	43
9	HIP Fixture Design	46
10	Plot of Temperature vs Time for HIP Run	47
11	Plot of Pressure vs Time for HIP Run	48
12	Micrograph of As-Received Material	52
13	Electron Micrograph of Inclusions	54
14	Electron Microprobe Image of Carbide Inclusion	56
15	TEM Micrograph of γ'	57
16	TEM Micrograph of Grain Boundary MC Carbides	58
17	TEM Micrograph of Precipitate-Free Grain Boundary	59
18	TEM Micrograph of Undesirable Grain Boundary Precipitate Morphology	61
19	TEM Micrograph of η Platelets	63
20	Micrograph of η Platelets	64
21	Micrograph of As-HIP'd Material	67

LIST OF FIGURES (CONT'D)

Figure		Page
22	Plot of Stress vs Displacement at 70°F	69
23	Plot of Stress vs Displacement at 500°F	70
24	Plot of Cyclic Stress-Strain Curve	72
25	Plot of Stress Range vs Cycles - Expanded Scale	76
26	Plot of Baseline Strain Range vs Cycles to Failure	77
27	Plot of Baseline Strain Range vs Cycles to Initiation	78
28	Plot of Stress Range vs Cycles - LCF Specimen 2	79
29	Plot of Stress Range vs Cycles - LCF Specimen 4	80
30	Plot of Stress Range vs Cycles - LCF Specimen 5	81
31	Plot of Stress Range vs Cycles - LCF Specimen 6	82
32	Plot of Stress Range vs Cycles - LCF Specimen 7	83
33	Plot of Stress Range vs Cycles - LCF Specimen 8	84
34	Plot of Stress Range vs Cycles - LCF Specimen 11	85
35	Plot of Stress Range vs Cycles - LCF Specimen 12	86
36	Plot of Stress Range vs Cycles - LCF Specimen 32	87
37	Plot of Stress Range vs Cycles - LCF Specimen 33	88
38	Plot of Stress Range vs Cycles - LCF Specimen 53	89
39	TEM Micrograph of Fatigued Specimen with Planar Dislocations	91
40	SEM Fractograph - LCF Specimen 33	92
41	SEM Fractograph, Initiation Site - LCF Specimen 33	93
42	SEM Fractograph, Fatigue Striations - LCF Specimen 33	94
43	SEM Fractograph, Cracked Carbides - LCF Specimen 33	95
44	Micrographs of Replicas, Cracks - LCF Specimen 7	97

LIST OF FIGURES (CONT'D)

Figure		Page
45	Plot of Crack Length vs Cycles - LCF Specimen 7	99
46	Micrographs of Replicas, Cracks - Specimen 8	101
47	Plot of Crack Length vs Cycles - LCF Specimen 8	104
48	Electron Micrographs Depicting Grain Boundary Offsets	109
49	SEM Micrograph, Crack at Carbide - LCF Specimen F2	111
50	SEM Micrograph, Crack at Carbide - LCF Specimen F2	113
51	Micrograph of Replica - LCF Specimen 36	114
52	Micrograph of Replica, Crack at Carbide - LCF Specimen 36	115
53	SEM Micrograph, Main Crack - LCF Specimen 53	116
54	SEM Micrograph, Fatigue Striations - LCF Specimen 53	117
55	SEM Micrograph, Secondary Cracking - LCF Specimen 53	118
56	SEM Micrograph, Extrusion after 800 Cycles - LCF Specimen 38	120
57	SEM Micrograph, Decohering Carbide after 800 Cycles - LCF Specimen 38	121
58	SEM Micrograph, Longitudinal Section after 2103 Cycles - LCF Specimen 39	122
59	SEM Micrograph, Cracks in Longitudinal Section after 2103 Cycles - LCF Specimen 39	123
60	Plot of Stress Range vs Cycles - LCF Specimen 14	129
61	Plot of Stress Range vs Cycles - LCF Specimen 16	130
62	Plot of Stress Range vs Cycles - LCF Specimen 18	131
63	Plot of Stress Range vs Cycles - LCF Specimen 19	132
64	Plot of Stress Range vs Cycles - LCF Specimen 20	133
65	Plot of Stress Range vs Cycles - LCF Specimen 21	134
66	Plot of Stress Range vs Cycles - LCF Specimen 22	135

LIST OF FIGURES (CONT'D)

Figure		Page
67	Plot of Stress Range vs Cycles - LCF Specimen 23	136
68	Plot of Stress Range vs Cycles - LCF Specimen 24	137
69	Plot of Stress Range vs Cycles - LCF Specimen 25	138
70	Plot of Stress Range vs Cycles - LCF Specimen 29	139
71	SEM Micrograph, As-Vapor-Honed Surface - LCF Specimen 55	142
72	Plot of Stress Range vs Cycles - LCF Specimen 27	143
73	Plot of Stress Range vs Cycles - LCF Specimen 28	144
74	SEM Micrograph, Secondary Cracking - LCF Specimen 28	146
75	SEM Micrograph, Secondary Cracking - LCF Specimen 28	147
76	SEM Micrograph, Secondary Cracking - LCF Specimen 28	148
77	Micrograph, Coating Reaction - LCF Specimen 20	149
78	SEM Fractograph - LCF Specimen 25	150
79	Micrographs of Replicas, Cracks - LCF Specimen 21	151
80	Plot of Crack Length vs Cycles - LCF Specimen 21	152
81	Micrograph, Surface Oxidation - LCF Specimen 26	154
82	SEM Micrographs, Main Crack - LCF Specimen 16	155
83	SEM Micrographs, Secondary Cracking - LCF Specimen 16	157
84	Plot of Stress Range vs Cycles - LCF Specimen 13	162
85	Plot of Stress Range vs Cycles - LCF Specimen 34	163
86	Plot of Stress Range vs Cycles - LCF Specimen 35	164
87	Plot of Stress Range vs Cycles - LCF Specimen 42	165
88	Plot of Stress Range vs Cycles - LCF Specimen 43	166
89	Plot of Stress Range vs Cycles - LCF Specimen 51	167
90	Plot of Stress Range vs Cycles - LCF Specimen 54	168

LIST OF FIGURES (CONT'D)

Figure		Page
91	Plot of Stress Range vs Cycles - LCF Specimen 38	169
92	Plot of Stress Range vs Cycles - LCF Specimen 40	170
93	SEM Micrograph, Cracking at Inclusions - LCF Specimen 42	173
94	TEM Micrograph, Dislocation Network after 800 Cycles - LCF Specimen 31	174
95	TEM Micrograph, Annealed Dislocation Network - LCF Specimen 31	175
96	Plot of Stress Range vs Cycles - LCF Specimen 41	176
97	SEM Micrograph, Surface Cracking after 1606 Cycles - LCF Specimen 41	177
98	SEM Micrograph, Cracking after Failure - LCF Specimen 41	180
99	Plot of Strain Range vs Cycles to Failure with Baseline Trend Line and Rejuvenation Data	188

Chapter 1

INTRODUCTION

The modern gas turbine engine demands the ultimate in performance from materials. Typical material requirements include high strength and stiffness at operating temperatures, good oxidation resistance, low creep rates and high stress rupture values, and good low-cycle and high-cycle fatigue resistance. Since the results of component failure, especially of rotating components, usually are catastrophic, design approaches and material specifications tend to be conservative (1,3,4,61).

A turbine disk is that component which transmits the work done by hot, expanding gases on the turbine blades to the power shaft of the engine. Experience has indicated that turbine disks can fail either by stress rupture at the rim where the blades are attached with dovetail slots; or, as is usually the case, by low-cycle fatigue at cross-sectional changes or at bolt holes (10). The low-cycle fatigue results from vibration, changing engine operating speeds and thermal gradients (3,12). When a turbine disk is limited by low-cycle fatigue (LCF) life, the design approach is to establish a probability of failure of 0.5%, with failure defined as extension of a detectable crack and not component disintegration. Therefore, most turbine disks reach their LCF life with a high probability of additional life remaining (1). Since these disks are quite expensive, there is a great deal of interest in processing the disks in some manner (i.e., rejuvenating the disks)

to remove the microstructural damage which leads to LCF failure, so that the disks can be returned to service safely and reliably at low cost (2).

This investigation was undertaken to determine how the LCF process causes crack initiation in Incoloy 901, and to find which rejuvenation treatments can lead to recovery of the initiation life. Incoloy 901 was selected for study because it is a commonly used superalloy and, thus, there are many disks which potentially can be returned to service after rejuvenation.

Subsequent portions of this introduction will briefly review LCF crack initiation and propagation in superalloys, the physical metallurgy of Incoloy 901, and rejuvenation.

I. CRACK INITIATION

Dieter divides the fatigue process into four steps: crack initiation, Stage I crack growth, Stage II crack growth, and ultimate ductile failure (14). This classification will be used in the following discussion.

The mechanisms for LCF crack initiation generally involve the interaction between the deformation processes and the alloy microstructures (1,4,5,6,7,8,9,11,46,64,67,68). The mode of crack nucleation depends on such factors as the amount of deformation, the degree of slip dispersal, test temperature and environment, and the amount and type of microstructural defects (carbo-nitrides, borides, porosity, brittle second phases, etc.). Kim and Laird point out that in pure metals, crack initiation occurs at persistent slip bands at low stress ranges and at grain boundaries at high stress ranges exclusive of severe

environmental effects (47). In lower temperature regimes (less than about 700°F or 370°C), superalloys deform by planar slip which is heterogeneous in nature (4). Kuhlmann-Wilsdorf and Laird have developed a dislocation model to explain how persistent slip bands can lead to the formation of intrusions and extrusions on the specimen surface which in turn lead to crack initiation (49,46). This model presents the rationale for the simple stress-raiser mechanism proposed by Wood 20 years ago (50).

At high cyclic ranges, cracks generally initiate at the grain boundaries. Recent work by Kim and Laird (47,48) have developed three criteria for crack initiation in pure metals at grain boundaries:

- (a) The grain boundaries must have a high degree of lattice mismatch;
- (b) The slip on the active slip system in either one or both of the adjacent grains should be directed at the intersection of the boundary with the specimen surface; and (c) The trace of the boundary at the free surface should lie at an angle of 30-90° with respect to the stress axis. Kim and Laird also observed grain boundary sliding in their LCF experiments on pure copper (47). The cracks were observed to have initiated at grain boundary steps.

Superalloys contain a substantial amount of carbides, carbo-nitrides, and borides intentionally added to control the grain size, improve creep resistance, increase grain boundary strength, and to vitiate the adverse effects of trace elements (17). Unfortunately, it has been found that these nonmetallic inclusions serve as favorable sites for crack initiation. In a study by Gell and Leverant on the LCF behavior of Mar-M200, it was found that metal carbides played a key role in

determining the crack initiation life (8). The carbides can be pre-cracked due to differential contraction during the solidification process or during the various metalworking processes. Also, the carbides can de-cohere from the matrix, especially at the surface, leading to a localized strain concentration region. As recently shown by Reimann and Menon, carbides provide a preferential path for developing LCF cracks in René 95 and seem to be associated with initiation of the cracks themselves (1).

Many investigators have found coherent twin boundaries to be significant sites for crack initiation at lower stress ranges (4).

II. STAGE I CRACK PROPAGATION

There is some disagreement in the literature about a definition of Stage I cracking. Coffin suggests that Stage I is early growth of a crack to some detectable limit and then propagation through a plastic regime (12). A more accepted definition is that Stage I cracking is that stage where cracks propagate along specific crystallographic planes which are oriented near 45° to the applied stress axis (46). But Laird points out that this definition is not strictly applicable to LCF where crack nucleation and growth may occur along sections which are not crystallographic (47).

Since persistent slip bands develop on the most active slip plane, cracks initiated at them generally continue to propagate along them (46). Thus, a persistent slip band can lead to the development of intrusions/extrusions, to a crack nucleus, and finally to crack propagation.

Similarly, cracks nucleated at grain boundaries tend to grow along the boundary both on the surface and into the bulk (47). Thus, the

crack front develops a thumbnail shape. Also, Kim and Laird predicted and observed a crack path which is asymmetric with respect to the boundary, with the crack occurring in that grain with the most favorably oriented active slip system (48).

III. STAGE II CRACK PROPAGATION

Coffin proposes that Stage I cracking leads to Stage II cracking when the crack overcomes the plastic zone which envelops it during its early stages, and thus it begins to grow elastically (12).

Usually, however, Stage II is denoted as the transition of the crack from growing along the maximum shear direction to growing normal to the applied stress direction. At high stress ranges, the crack will almost immediately propagate by Stage II processes (46).

It is during Stage II crack growth that fatigue striations are generated, although not all materials develop a striation pattern. Striations are usually observed in superalloys (53). It is generally accepted that each striation represents the propagation distance of a fatigue crack during each cycle. A crack plastic blunting process proposed by Laird requiring two slip systems (51) is a very reasonable explanation for the formation of striations (52).

Stage II continues until the crack becomes long enough to cause the final instability. In brittle materials, the crack begins to propagate unstably after a critical length is reached. In ductile materials, the crack grows until a tensile overload occurs, at which time fracture occurs by shear rupture on planes inclined 45° to the tensile axis (52).

IV. PHYSICAL METALLURGY OF INCOLOY 901

Incoloy 901 is an iron-nickel superalloy widely used as a turbine disk material since the early 1960's (17). Its nominal composition is (in weight percent): Ni-42.5, Fe-36.0, Cr-12.5, Mo-5.7, Ti-2.8, Al-0.2, C-0.05, and B-0.015. Since it is fairly strong and ductile at intermediate temperatures (up to 1000°F/540°C) and contains substantial iron and relatively low chromium, it is widely used due to its comparatively low cost. It also possesses the advantage of being in that group of superalloys which can be forged and machined fairly conventionally (19).

Incoloy 901 has an austenitic (γ -f.c.c.) iron-nickel-chromium matrix. Molybdenum, titanium, carbon, and boron are the other principal substitutional solid-solution strengtheners of the matrix (17). The stacking fault energy is not known, but from data presented by Decker and Floreen, it can be estimated to be greater than 60 ergs/cm² (18).

The primary precipitate is γ' , an intermetallic compound of the type Cu₃Au, possessing a Strukturbericht structure type Ll₂. Its stoichiometric composition is Ni₃Al with a lattice parameter of 3.60 Å. In actual fact, γ' contains some iron on the nickel lattice sites, and some titanium on the aluminum lattice sites, so that γ' is usually denoted as (Ni,Fe)₃(Al,Ti). The lattice mismatch between γ' and the γ matrix is low, so that the γ' nucleates homogeneously. The γ' grows in a spherical morphology which indicates that the lattice misfit is less than 0.5% (17,20). The solvus temperature is 1725°F (940°C) (17).

Actually, in Incoloy 901, γ' is a metastable precipitate (18). The equilibrium precipitate is η , an h.c.p.-ordered intermetallic compound with a Strukturbericht structure type DO₂₄. It has the stoichiometric

composition Ni_3Ti . Unlike γ' , it does not dissolve substantial amounts of other elements (20). The precipitation of η may occur in two forms: at the grain boundaries in a cellular morphology or intergranularly as plates (22,20). The cellular precipitation nucleates at a lower temperature than the plate-shaped precipitates. The solvus temperature for η is 1825°F (996°C) (17). Significant precipitation occurs in the temperature range $1500\text{--}1750^\circ\text{F}$ ($816\text{--}954^\circ\text{C}$), with the most rapid precipitation rate in the temperature region $1600\text{--}1650^\circ\text{F}$ ($871\text{--}899^\circ\text{C}$) (25).

The cellular precipitation reaction consists of alternating lamellae of γ and η . These cells have a random orientation with respect to the grain into which they are growing. But the close-packed planes and directions of the h.c.p. η and the f.c.c. γ are parallel to one another (20). These orientation relationships are also true for the plate morphology which are thought to nucleate on stacking faults in γ' (18). The interface between γ and η is semi-coherent, with a lattice mismatch of 0.65% (19). The η phase is associated with severe degradation in mechanical properties. Not only is the phase itself brittle, but also it grows at the expense of the γ' . However, η has successfully been used to control the grain size of Incoloy 901 during forging by the utilization of special thermomechanical processing (25).

Carbides play a key role in superalloys. They help to control grain size since some carbide types are stable nearly to the melting point of the alloys. Also, the carbides which precipitate in the grain boundary greatly increase stress rupture strength at elevated temperatures. And, carbides can increase the chemical stability of the matrix by removing reacting elements (26). MC carbides form shortly after freezing and,

hence, they occur as discrete particles distributed homogeneously throughout the alloy. In Incoloy 901, these MC carbides have the composition TiC with an f.c.c. structure. Some molybdenum can substitute on the titanium lattice sites, so that a carbide of the type (Ti,Mo)C is possible (26,70).

Although carbides of the type $M_{23}C_6$ usually form in superalloys during low-temperature heat treatment and service in the temperature range 1400-1800°F (760-980°C), they are not found in Incoloy 901. Instead, MC carbides of the type (Ti,Mo)C precipitate at the grain boundaries during the stabilization portion of the heat treatment (70). The morphology of these grain boundary carbides is similar to that for a Laves phase and they have been incorrectly identified as Laves phases (24).

The formation of carbo-nitrides and titanium nitrides has been reported (24). Cubic TiN is as thermally inert in the superalloy as is TiC.

The boron which is added to improve creep properties results in the precipitation of hard, refractory M_3B_2 borides (26). Typical composition of these borides is: (Mo,Ti,Al,Cr,Fe,Ni,Si) $_3B_2$ (24,69).

In addition to the intentional precipitates, various topologically close-packed (t.c.p.) intermetallic compounds form in superalloys due to solid-state bonding phenomena (t.c.p. phases are also referred to as "Hume-Rothery compounds" and "electron compounds"). A hexagonal Laves phase of the type $(Fe,Cr,Mn,Si)_2(No,Ti,Cb)$ has been found in Incoloy 901 after aging for long times in the temperature range 1200-2000°F (649-1093°C). The morphology varies from general intergranular to grain

boundary precipitation (24,23,18). The trigonal μ phase has been observed in Incoloy 901 with high boron additions (0.1 weight percent) (24). This phase has a close structural relationship to the M_6C carbides and, thus, it may be that M_6C can precipitate in this alloy, although it has not been reported. The chemical composition of the μ phase can be quite complex. It is, in general, $(Ti,Mo)_6(Fe,Ni)_7$ (24). The precipitation is intragranular as thin platelets parallel to γ close-packed planes.

V. REJUVENATION

Metallurgical engineers who are responsible for the maintenance of turbine engines have long expressed a desire to be able to restore at least a portion of the design life of expensive engine components through some sort of processing operation. This process has been given the name "rejuvenation." Recent advances made by Wilshire and others have shown that thermal treatments are successful in recovering the creep life of superalloys (28,29). Wilshire found that the onset of tertiary creep is caused either by development and growth of grain boundary cavities or by microstructural changes which cause changes in volume fraction and morphology of the γ' (28). Thus, suitable heat treatments could be devised to sinter out the cavities in the first case, or to restore the original microstructure in the second case in order to recover the creep life.

The success with creep damage has given impetus to finding suitable processing conditions for recovering the low-cycle fatigue (LCF) life of superalloys. The use of hot-isostatic-pressing (HIP) technology to consolidate metal powders has been quite successful (31) and it was

inferred that this technology would be useful in heatling LCF damage. The HIP process involves the introduction of high pressure gas into an autoclave at elevated temperature. Thus, some mechanical energy is available as well as thermal energy.

Researchers at the Stellite Division of the Cabot Corporation obtained some preliminary data on turbine blades which indicated that some recovery of creep and fatigue properties was possible with HIP processing (30). An Air Force funded study on HIP rejuvenation in IN-718 concluded that there was no rejuvenation of pre-crack initiated damage, but that there was some rejuvenation of post-crack initiation life due to the closure and bonding of fatigue cracks (2). However, this work was not conclusive because the HIP cycle chosen for the rejuvenation effort substantially changed the baseline properties of the material, and there was relatively little effort devoted to microstructural characterization.

It is the purpose of this dissertation to report the results of the experimental investigation to recover some portion of pre-crack initiated LCF life using thermal and HIP processing. Pertinent aspects of the physical metallurgy of Incoloy 901 are presented. The LCF behavior of Incoloy 901 at various strain ranges is reported. The microstructural mechanisms of LCF damage and the resultant effects of the rejuvenation processes are detailed.

Chapter 2

EXPERIMENTAL PROCEDURE

I. METALLOGRAPHY TECHNIQUES

A. Optical Microscopy

The samples to be examined were mounted in Bakelite, hand polished through 600-grit silicon carbide paper using water as a lubricant, and polished successively with 6- μ , 1- μ , and 1/4- μ diamond paste. Several different etchants were utilized. ASTM Etchant 105 (32) was most generally used to reveal microstructural details. It was freshly mixed each time in these proportions: 92% HCl, 5% H₂SO₄, and 3% HNO₃. Immersion for 5-30 seconds was usually sufficient. Marble's Reagent (ASTM Etchant 25) was effective in highlighting the grain boundaries. It was mixed in these proportions: 10 g CuSO₄, 50 ml HCl, and 50 ml water (32). Etchant times were generally 10-30 seconds. Glyceregia (ASTM Etchant 87) was useful in highlighting microstructural details when the other etchants were not adequate. It was freshly mixed each time according to the formula: 10 ml HNO₃, 50 ml HCl, 30 ml glycerin (32). The samples were bathed in hot water prior to immersion in the glyceregia. Etchant times depended on the surface temperature of the specimen. Average times were between 20 seconds and 1 minute. Sometimes the samples were immersed in HF for a few seconds to remove a passive layer prior to etching.

After the samples were satisfactorily etched, they were thoroughly rinsed in water and bathed in a saturated sodium bicarbonate solution placed in an ultrasonic cleaner for several minutes. This step was necessary to prevent etching of the microscope objective piece. The etched surface was then dried using a methanol wash and a blower. The samples were examined and photographed in a Bausch and Lomb Research II Metallograph using a xenon light source.

B. Transmission Electron Microscopy

Thin slices of Incoloy 901, approximately 0.010 inch thick, were cut using a thin abrasive cut-off wheel. These slices were then ground flat on 240- and 320-grit silicon carbide paper using water as a lubricant. The slices were attached to the bottom of a stainless steel mount using balsam wax. The slice was further ground down to a thickness of 5-6 mils on 320- and 400-grit silicon carbide paper using a water lubricant. The thin slices were then dismounted and the residual balsam was removed by slight grinding on the 400-grit paper. A punch-out die, with a 3-mm opening, was used to cut out the disks. In the case of the fatigue specimens where the disks were taken normal to the longitudinal axis, the above procedure was simplified somewhat since the fatigue specimens had a nominal 3-mm diameter.

Electropolishing was done with a dual-jet Tenupol. The electrolyte had the following composition: 600 ml methanol, 250 ml butanol, and 60 ml perchloric acid (70%). The electrolyte was maintained at a temperature of about -60°C by constantly adding liquid nitrogen to a methanol bath surrounding the electrolyte.

The controls on the polisher were set for minimum flow rate and maximum sensitivity of the photocell detector which turned off the

electrolyte pump after perforation of the disk. A two-step polishing sequence worked best. Electropolishing for 15-30 minutes at 30 volts followed by final polishing at 16-20 volts produced dished disks with holes close to the center. After electropolishing, the disks were washed in methanol. Great care was taken in handling to prevent inducing artifact dislocations into the structure.

C. Scanning Electron Microscopy (SEM)

An AMR Model 1000 Scanning Electron Microscope was used in this investigation. An Energy Dispersive Analysis of X-Rays (EDAX) attachment to the SEM was used to identify chemical elements. Sample preparation involved cutting the LCF specimen just below the extensometer flange, and mounting it on an aluminum stud using a silver paste.

D. Surface Replication

Acetyl cellulose replicating film was used to replicate the surface in the gauge section of the low-cycle fatigue specimen. The replication was done on loose specimens and while the specimens were mounted in the Instron Hydraulic Testing Machine (37). The replicating film, 0.034 mm thick (1.34 mils), was cut into strips 0.30 in. wide (the approximate length of the gauge section). The strips were cut into lengths 0.25-0.30 in. long. Strips of this length covered about 75% of the gauge length area. A reference line was made on the LCF specimen above the extensometer flange so that the location of each replica could be noted. At least six replicas were made for each gauge length, with adequate overlap of areas between adjacent replicas. Thus, the gauge section was completely replicated about three times. This provided insurance against an artifact in the replica obscuring a vital surface detail.

The replicating film was prepared for use by submerging it in acetone for 8-10 seconds, holding a corner with tweezers. The film was removed from the acetone and quickly applied to the surface. The film "grabbed" onto the surface almost immediately. The film dried on the surface for 5-10 minutes, and then was stripped off with tweezers. It was placed on a piece of double-sided sticky tape mounted on a glass slide. The position of the reference mark on the LCF specimen with respect to the replica was scribed into the sticky tape at the appropriate position. A piece of masking tape on the reverse of the glass contained the identification data. Two glass slides at a time were then placed in a vacuum evaporator, and the belljar evacuated to 2×10^{-5} torr. The slides were rotated and a uniform thin coating of 99.99% purity aluminum was applied. The replicas were then examined using a light microscope or a scanning electron microscope.

II. AGING RESPONSE OF INCOLOY 901

A. Material Specification

The Incoloy 901 was received in the form of a segment of a partially finished compressor shaft. The shaft had been cast, forged, and pierced. A chemical analysis is presented in Table 1. A band saw with a bi-metal blade was used to cut pieces of material for study. The material was received in solution-treated and double-aged condition. The commercial heat treatment specification is shown in Table 2 (34).

B. Thermal Treatments

Heat treating studies were conducted in two different furnaces. A vertical tube drop Marshall furnace was used when rapid quenching

TABLE 1
CHEMICAL ANALYSIS OF BILLET

Element	Weight Percent	Atomic Percent
C	0.034	0.162
Mn	0.10	0.104
P	0.019	0.035
S	0.005	0.009
Si	0.10	0.203
Cr	12.41	13.63
Ni	41.33	40.21
Mo	5.31	3.16
Ti	2.99	3.57
Al	0.29	0.61
Cu	0.09	0.08
Co	0.29	0.28
Bi	0.00005	0.00001
Pb	0.0003	0.00008
B	0.015	0.079
Fe	Balance (37.02)	37.86

TABLE 2
COMMERCIAL HEAT TREATMENT SPECIFICATION
FOR INCOLOY 901

SOLUTION	Heat to 1975-2025 F Hold within ± 25 F for 2 hours Cool at rate equivalent to air cool or faster
STABILIZATION	Heat to 1400-1475 F Hold within ± 15 F for 2-4 hours Cool in air or quench in water
PRECIPITATION	Heat to 1300-1375 F Hold within ± 15 F for 24 hours Cool in air

Reference: Pratt & Whitney Aircraft Specification 1003H, 20 Nov. 1973.

of the specimen was desired. A thin piece of alumel wire was used to suspend a tantalum specimen basket in the furnace hot zone. The alumel wire was formed into a loop and each end was connected to a metal post in a cap at the top of the furnace. Heavy gauge nichrome wire, bent at each end in the form of a "U", was used to connect the basket to the alumel wire. Helium gas was passed through a gas train to remove impurities and then introduced into the top cap of the tube. The bottom tube opening was covered with a thin sheet of plastic held in place by a rubber band wrapped around the tube. Tygon tubing, connected to a side tap in the tube, near the bottom, directed the helium gas into a beaker of vacuum pump oil. Minimal pressure and flow rate of the gas was maintained, i.e., only sufficient pressure to generate a bubble every few seconds in the oil was used. A chromel-alumel thermocouple placed at the same height in the tube as the basket was used to monitor temperature. When the heat treatment was completed, the thin alumel wire loop was broken by passing a 110-volt line current through it. The basket, with the specimen in it, fell out the bottom of the tube, easily penetrating the plastic membrane on the bottom. A pail of water was placed under the tube to serve as the quenching medium.

A Brew High Vacuum Furnace was also used for heat treatment studies. Vacuums on the order of 10^{-6} torr were easily obtainable at the temperatures used in this study. A platinum/platinum-10% rhodium thermocouple was used to monitor temperature. The hot zone of the furnace was 6 inches in diameter by 14 inches high. Tantalum heating elements and shields were used. The furnace design was of the cold wall type. Temperature was controlled within $\pm 5^{\circ}\text{F}$. The specimens were either

cooled in vacuo or by backfilling the furnace chamber with helium gas, which passed through the gas train, to a partial pressure of 640 torr (about 0.83 atmosphere). The cooling rates, as measured by a thermocouple, for the vacuum cool and the helium quench, are presented in Table 3.

III. LOW-CYCLE FATIGUE

A. LCF Specimen Design and Manufacture

The specimen design is shown in Figure 1. The outstanding feature of the specimen is the extensometer ridges located on either side of the gauge section. This allows accurate measurement of displacement and the ability to maintain constant, uniform temperature in the gauge section using a clamshell furnace. The disadvantages of the system are the long times required for the entire system to reach equilibrium (typically 2-3 hours) and the fact that the calculation of strain necessarily involves the application of effective gauge lengths. The details of the load train, the strain measuring system, and the equations required to convert displacement to strain are discussed in following sections.

The specimens were manufactured by Metcut Research Associates from blanks sawed from a portion of a forged shaft. Figure 2(a) shows a photograph of the shaft segment. Specimen blanks were sawed from this segment parallel to the shaft axis. A typical cutout configuration is depicted in Figure 2(b). The blanks were then rounded by straight wheel grinding, and rough machined to ~ 0.020 in. oversize in the gauge section. The specimens were given a standard heat treatment, designated as STA 3A

TABLE 3
FURNACE COOLING RATES

Vacuum Cool

A. Heat Treatment Temperature: 1975 F

Temperature (°F)	Average Cooling Rate (°F/min.)
1400	192.0
1299	97.6
1072	72.2
893	55.8
709	47.8
509	27.1

B. Heat Treatment Temperature: 1400 F

1299	100.0
1072	50.5
893	40.2
709	28.2
509	15.1

C. Heat Treatment Temperature: 1300 F

1072	46.5
893	35.4
709	25.1
509	33.7

TABLE 3 (CONT'D)

Helium Gas Quench (640 torr)

A. Heat Treatment Temperature: 1975 F

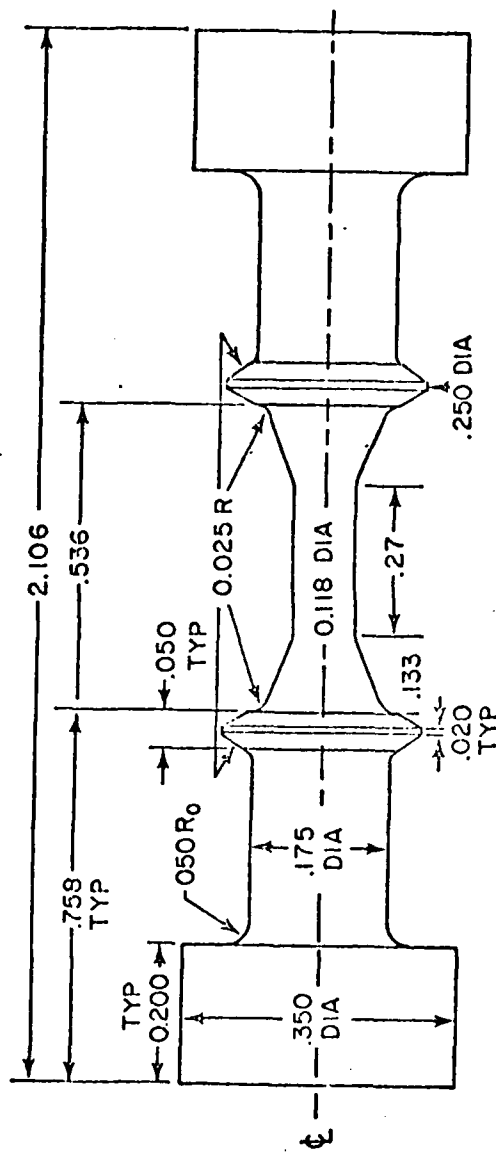
<u>Temperature (°F)</u>	<u>Average Cooling Rate (°F/min.)</u>
1400	243.4
1299	214.6
1072	166.2
893	137.4
709	120.0
509	116.4

B. Heat Treatment Temperature: 1400 F

1299	85.5
1072	104.1
893	92.0
709	83.6
509	75.4

C. Heat Treatment Temperature: 1300 F

1072	82.7
893	86.1
709	75.1
509	67.0



SCALE:
ALL DIMENSIONS IN INCHES

Figure 1. Low-Cycle Fatigue Specimen Design



Figure 2a. IncoLOY 901 Shaft Forging Photograph

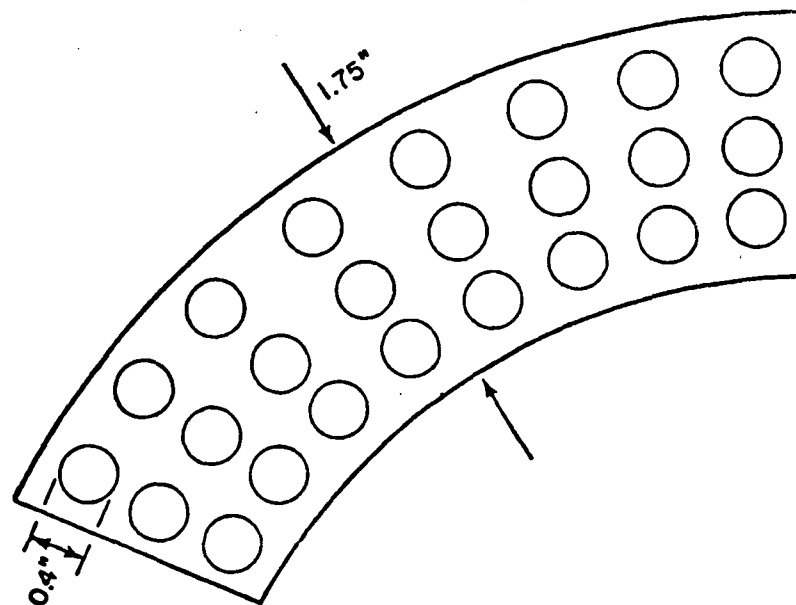


Figure 2b. Incoloy 901 Shaft Forging Segment Indicating Cut-Out Pattern for LCF Test Specimens

prior to final machining. The heat treatment parameters for STA 3A are contained in Table 4. The specimens, in groups of nine, were heat treated in a Brew High Vacuum Furnace. The fixture used to support the specimens in the furnace chamber is described in Section V of this chapter.

Final machining of the gauge section was done using a low-stress grinding approach (35). The machining parameters are summarized in Table 5. Final polishing of the gauge section was done with 400-grit silicon carbide paper using water as a lubricant, followed by 3/0 and 4/0 Emery polishing paper using Buehler Isocut Fluid as a lubricant. The paper was cut into strips approximately 0.20 inches wide, and polishing was done axially with the specimen chucked in a jeweler's lathe.

B. Ceramic Coating Procedure

A gas-tight ceramic coating, Solaramic 5210, was applied to the gauge sections of some specimens at General Electric's Materials and Processing Laboratory in Evendale, Ohio. Before the coating was applied, the gauge section was vapor blasted; this procedure entailed impinging fine alumina powder (Novacite 1250/150, supplied by Malvern Minerals) in a water stream at 0.31 MPa at the specimen surface. The specimen-to-surface distance was kept at about 5 cm, and total honing time was approximately 1 minute. The surface had a bright matte finish after the vapor blasting.

The ceramic coating was then applied, and baked in air at 1750°F for 20 minutes, and air cooled. The gauge section was inspected for spallation of the coating.

TABLE 4
STANDARD HEAT TREATMENT STA 3A
FOR INCOLOY 901

SOLUTION	Heat to 1975°F in vacuum
	Hold within ± 4 F for 2 hours
	Backfill furnace with helium gas to a partial pressure of 640 torr
STABILIZATION	Heat to 1400°F in vacuum
	Hold within ± 4 F for 2 hours
	Backfill furnace with helium gas to a partial pressure of 640 torr
PRECIPITATION	Heat to 1300°F in vacuum
	Hold within ± 4 F for 24 hours
	Backfill furnace with helium gas to a partial pressure of 640 torr

TABLE 5
LOW STRESS GRINDING PARAMETERS

SPEEDS	Work surface: 8-26 ft/min.
	Table speed: 7 in./min.
	Wheel speed for traverse grinding: 2800-3250 ft/min.
FEEDS	Traverse grinding
	Roughing: 0.001 in./pass
	Finishing: Last 0.010 in. (250 μ m)
	First 0.0080 in.: 0.0005 in./pass
	Next 0.0008 in. : 0.0004 in./pass
	Final 0.0012 in.: 0.0002 in./pass
	Plung grinding: 0.00002 to 0.00008 in./rev.

C. Specimen Preparation after Rejuvenation

After the specimens were thermally rejuvenated (see Section V-A), the gauge section was axially repolished with 3/0 and 4/0 emery polishing paper as described above in Section III-A. This provided a good quality surface for replication; an oxidized surface could not be replicated without loss of detail.

After the specimens were HIP rejuvenated (see Section V-B), those specimens which were ceramic coated were mechanically polished with 240-grit polishing paper to remove the coating. The specimens were given the standard STA 3A (Table 5) to restore the morphology of the precipitates in the matrix. The gauge length was then lightly polished through 4/0 emery polishing paper as previously described.

D. Load Train Configuration

A photograph of the load train is shown in Figure 3(a). Note that a resistance-wound clamshell furnace was used for heating. A sketch of the load train with the various components labelled is illustrated in Figure 3(b). The grip design is contained in Figure 4. A molybdenum di-sulfide lubricant was effective in preventing binding in the grips.

E. Strain Measuring System

Although commonly referred to as a strain measuring system, the system employed actually measured displacement which must then be converted to strain. The necessary equations to accomplish this are described in Sections III-F and IV-C. Figure 5 is a photograph of the extensometer system used in this investigation. The system features a Satek PSH-6MS High Temperature Extensometer with a Microformer (Linear

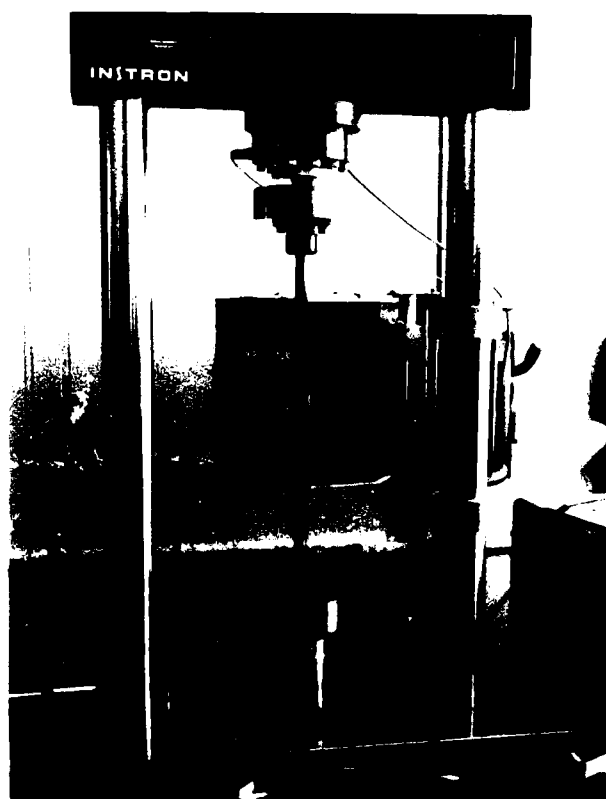


Figure 3a. Photograph of Load Train

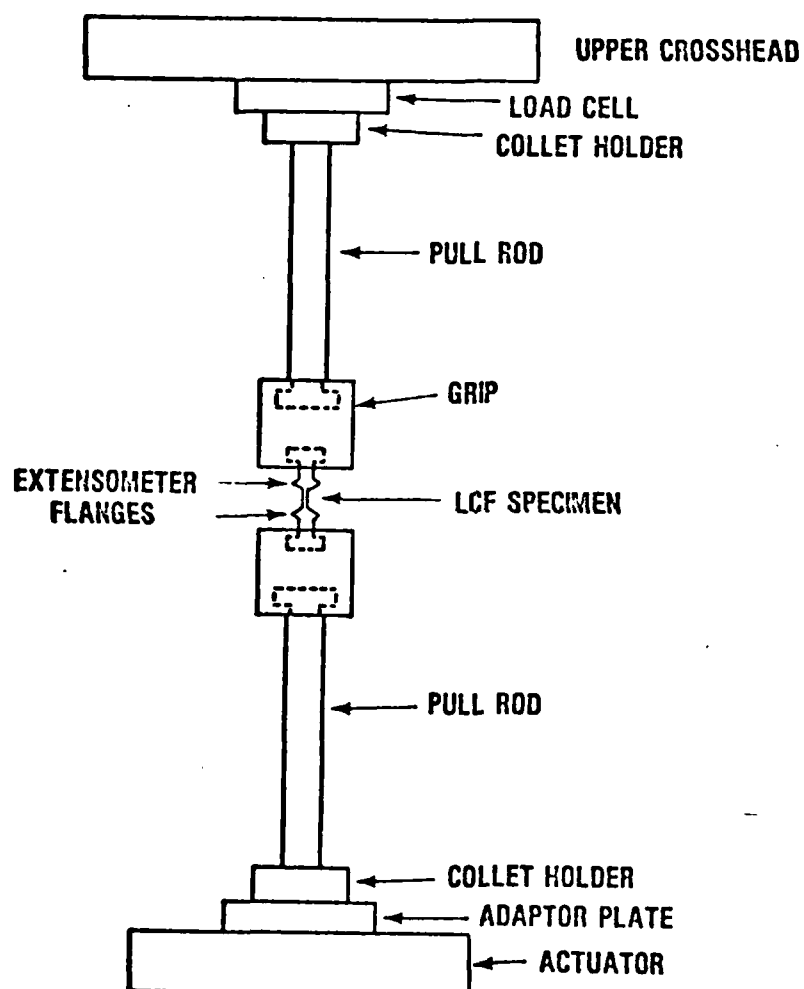


Figure 3b. Sketch of Load Train

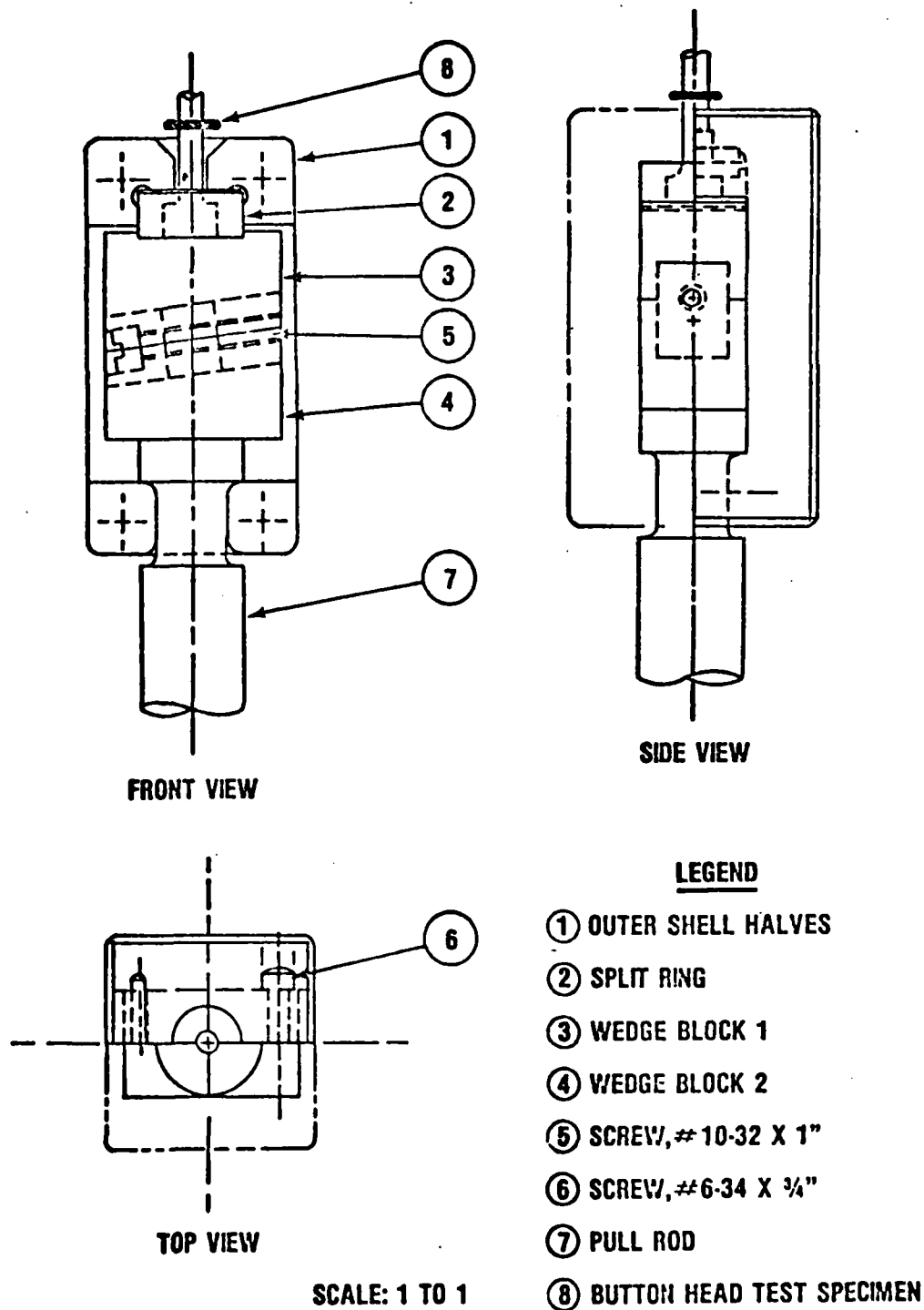


Figure 4. LCF Specimen Grip Design

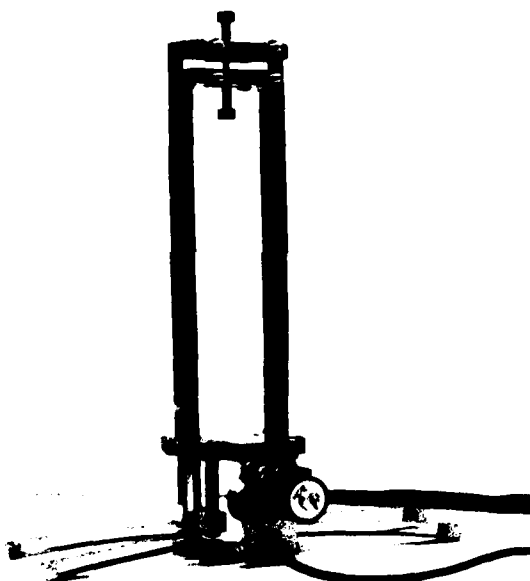


Figure 5. Photograph of Strain Measuring System

Variable Differential Transducer or "LVDT") to measure displacement. The suspension arms, which lock into the extensometer fixture, bolt around the flanges on the LCF specimen and effectively transmit the displacement of the specimen to the LVDT located beneath the furnace. The length of the suspension arms was governed by two criteria: (a) adequate length to allow the center of the specimen gauge length to be located in the center of the furnace hot zone with a one-inch clearance between the top of the extensometer fixture and the bottom of the furnace; and (b) proper difference in length between the top and bottom arms so that they would lock into the fixture for the particular flange separation distance used for the LCF specimen.

Calibration of the strain measuring system was accomplished as follows: The extensometer system was mounted in a Boeckeler Instrument Calibration Fixture. The top extension arm remained fixed and the bottom arm was movable using a dial calibrated in increments of 0.0001 inch. The LVDT was connected to an Instron Model 602A Stroke Controller. A Resistance-Capacitance (R-C) balancing network was adjusted to compensate for the resistive and capacitive characteristics of the system.

The zero suppression control was used to give a zero voltage when the LVDT core was in the center position of the LVDT. Output was read as a voltage on a digital voltmeter. Voltage readings were then taken as the dial was advanced in increments of a thousandths of an inch from 0 mils to 10 mils to -10 mils, and back to 0 mils. These 41 data points were then used to compute a linear least-square error line of the form $y = mx + b$ (36) where y is the displacement in volts, x is the displacement in mils, m is the slope of the line in volts/mil, and b is the y-intercept value. Table 6 contains typical data obtained from a

TABLE 6
TYPICAL LVDT CALIBRATION CURVE DATA

<u>Inches $\times 10^3$</u>	<u>Output Voltage</u>	<u>Inches $\times 10^3$</u>	<u>Output Voltage</u>
0.0	0.003	-1.0	-0.687
1.0	0.723	-2.0	-1.397
2.0	1.429	-3.0	-2.120
3.0	2.129	-4.0	-2.835
4.0	2.828	-5.0	-3.552
5.0	3.534	-6.0	-4.269
6.0	4.230	-7.0	-4.991
7.0	4.927	-8.0	-5.707
8.0	5.622	-9.0	-6.428
9.0	6.320	-10.0	-7.153
10.0	6.994	-9.0	-6.421
9.0	6.324	-8.0	-5.700
8.0	5.630	-7.0	-4.980
7.0	4.926	-6.0	-4.258
6.0	4.243	-5.0	-3.538
5.0	3.553	-4.0	-2.821
4.0	2.848	-3.0	-2.110
3.0	2.130	-2.0	-1.396
2.0	1.421	-1.0	-0.678
1.0	0.721	0.0	0.023
0.0	0.007		

calibration run. The data is plotted in Figure 6. Note that it is very linear. The inverse slope of this graph, or $1/m$, is the desired calibration factor, λ , in volts per mil. These calibration runs were typically done before and after each LCF test.

F. Low Cycle Fatigue Testing

All LCF testing was performed on an Instron Dynamic Materials Testing System. The testing was done using a saw-tooth wave form at a frequency of 0.4 Hz under strain control (actually displacement control, as explained above) with zero mean level (i.e., fully reversed). The signal cable connecting the actuator LVDT with the Stroke Controller was disconnected and attached to the extensometer LVDT by means of an adapter cable. Specimen displacement thus served as the feedback to the controller. Command signals to the servovalve were generated by two different techniques: (a) Instron Model 860 Function Generator (i.e., an analog computer), and (b) Instron Series 900 Computer System, utilizing a Computer Automation Alpha 16 Minicomputer. Load-displacement hysteresis loops were plotted on a Hewlett Packard Model 7004B X-Y Plotter.

The load train alignment was checked and the load cell calibrated prior to each test. To begin the actual testing, the specimen was loaded into the grips, the extension arms were attached, and a chromel-alumel thermocouple was placed in close proximity to the LCF specimen surface in the center of the gauge length. Then the clamshell furnace was placed around the assembly. All testing was done at 500°F. Temperature was controlled using a West Guardsman Controller. The specimen was heated under load control at a tensile stress of ~ 3 ksi.

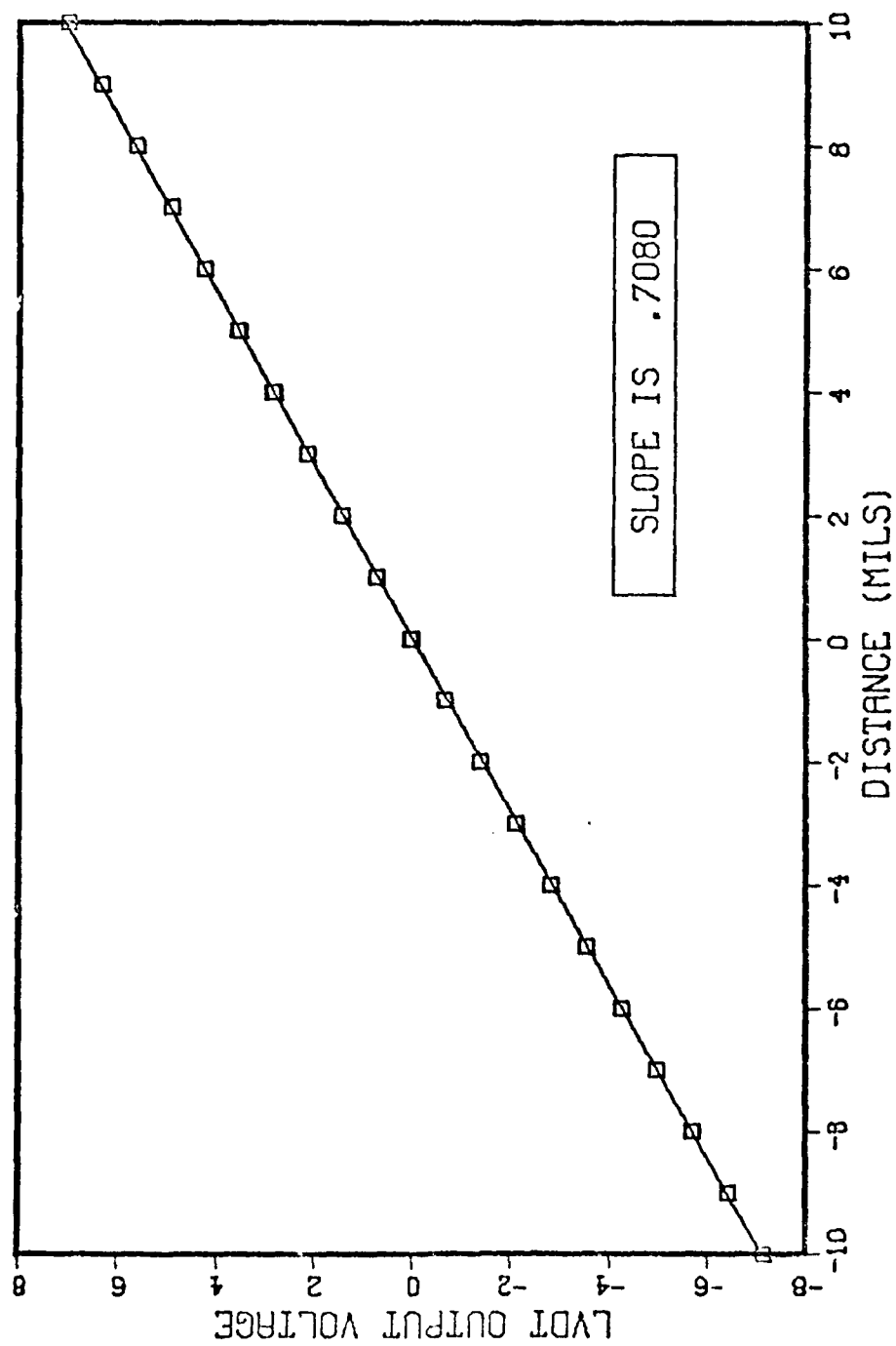


Figure 6. LVDT Calibration Curve

Once the temperature and the indicated specimen displacement readings had equilibrated, the Stroke Zero Suppression control was used to obtain zero voltage output of the LVDT at zero load.

The operation of the Function Generator was fairly straightforward. The proper amplitude setting to provide the desired strain range was empirically determined, using several specimens.

Testing under computer control required the use of a computer program. Instron's Low Cycle Fatigue Application Program APP-900-A3A8 (1974) was modified to provide more frequent and better formatted data output. The Appendix contains the source listing of the modified program. The address locations are in hexadecimal notation. The program was assembled using an Alpha 16 Assembler. Program parameters were entered via a teletype keyboard. Output was accomplished by teletype printer and punched paper tape. The frequency of data output was governed only by the speed of the paper tape punch. The fastest rate that data could be recorded was every three cycles at the test strain rate. The data on paper tape was processed by another program, written in Fortran, on a CDC 6600 computer. This program provided data, typically every five cycles, in tabular format for the following parameters: total displacement, plastic displacement, maximum elongation, minimum elongation, stress range, maximum stress, minimum stress, the ratio of maximum stress to minimum stress, elastic strain range, plastic strain range, and total strain range. Also, the program generated plots of stress range versus cycles, ratio of maximum stress to minimum stress versus cycles, and strain range versus cycles. A source listing of the computer program is contained in the Appendix.

The Instron computer program required a specification of strain rate, rather than frequency. Equation 1 is the appropriate expression relating frequency to strain rate:

$$\dot{u} = 2v \Delta u \quad (1)$$

where \dot{u} is "strain" rate (actually displacement rate) in mils per second, v is frequency in hertz (cycles per second), and Δu is displacement in mils.

The Instron was capable of controlling displacements to ± 0.00004 in. A typical plot of displacement versus cycles is shown in Figure 7.

G. Computation of Strain Range and Stress Range

As previously explained, the strain measuring system actually measured displacement. Since the cross-section of the LCF specimen between the extensometer flanges was not uniform, as is apparent from Figure 1, the computation of strain involved consideration of an effective gauge length. An effective gauge length is defined as that gauge length of uniform cross-sectional area which produces the same displacement under the application of a given load as does the gauge section of variable geometry. Use of the effective gauge length concept is made in the following equation which allows the computation of strain from displacement data:

$$\Delta \epsilon_t = \Delta \epsilon_e + \Delta \epsilon_p = \frac{u_t - u_p}{L_{eff}^e} + \frac{u_p}{L_{eff}^p} \quad (2)$$

where $\Delta \epsilon_t$ is the total strain range, $\Delta \epsilon_e$ is the elastic strain range, $\Delta \epsilon_p$ is the plastic strain range, u_t is the total specimen displacement (in inches), u_p is the plastic displacement (in inches), L_{eff}^e is the effective gauge length in the elastic regime (in inches), and L_{eff}^p is

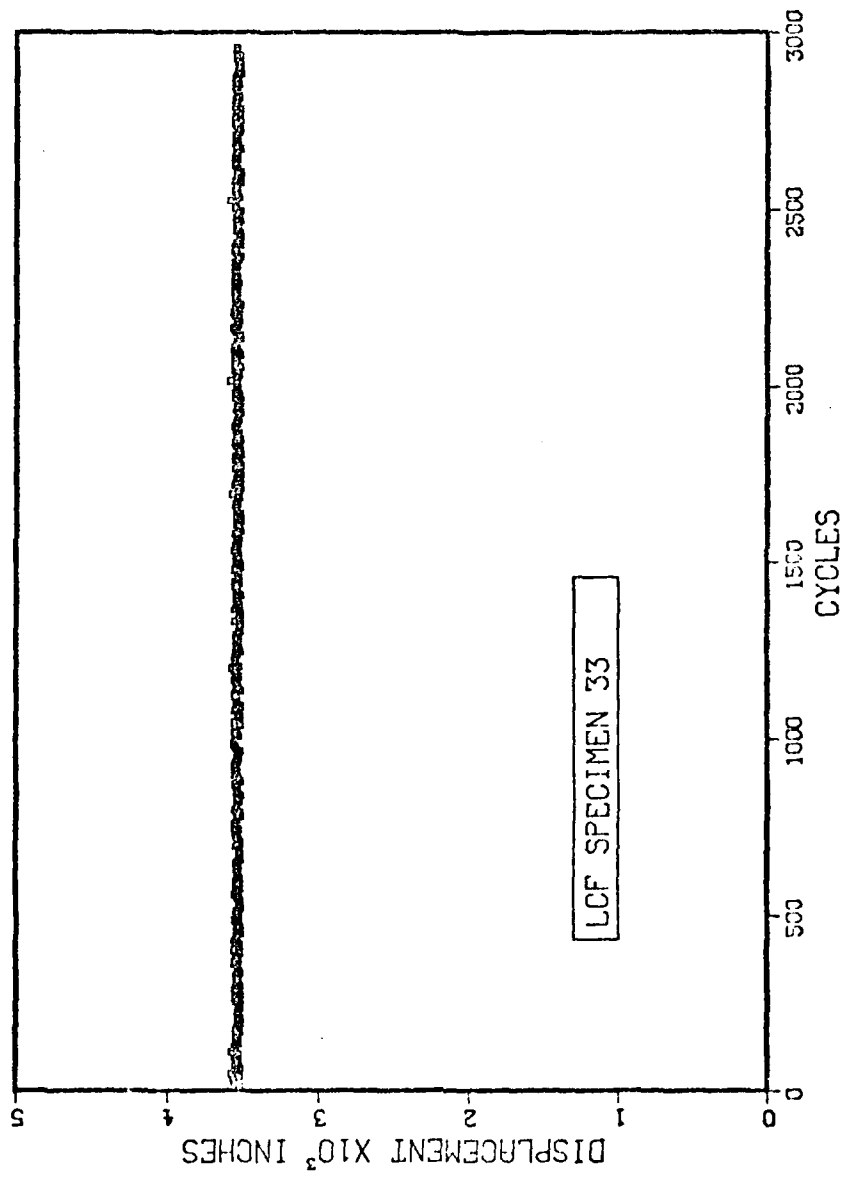


Figure 7. Plot of Displacement vs Cycles

the effective gauge length in the plastic regime (in inches). Now, u_t and u_p can be measured directly from the hysteresis loop plots or can be obtained from the computer data.

Equation 3 was used to compute displacement in thousandths of an inch when displacement distances were measured from hysteresis loop plots:

$$u = \lambda \cdot s \cdot \ell_D \quad (3)$$

where u is displacement (in mils), λ is the LVDT calibration factor, m^{-1} (in mils/volt), s is the plotter chart scale factor (in volts/inch of chart), and ℓ_D is the measured chart distance along the displacement axis of the hysteresis loop plot (in inches).

The plastic effective gauge length, L_{eff}^p , was assumed to be the straight portion of gauge length. This straight segment was measured for each specimen using a traveling microscope. Measurements were made along the top and bottom surfaces of a specimen supported horizontally; these were then averaged and rounded off to two significant figures.

The experimental determination of the elastic effective gauge length, L_{eff}^e , involved comparing the slope of a stress-displacement curve to a known elastic modulus value. The equation of interest was:

$$L_{eff}^e = \frac{E_{ACT}}{\Delta\sigma/\Delta u} \quad (4)$$

where L_{eff}^e is the effective elastic gauge length (in inches), E_{ACT} is the known Young's Modulus (in psi), $\Delta\sigma$ is the stress range (in psi), and Δu is the displacement range (in inches).

The calculation of stress, using distances measured along the load axis on the fatigue hysteresis loop, was done by applying Equation 5:

$$\sigma = k \cdot (1/d_o^2) \cdot t \cdot \ell_L \quad (5)$$

where σ is stress (in psi), k is a constant $= 6.367 \times 10^2$ when the full scale load is 5000 lbs, d_o is the specimen diameter (in inches), t is the plotter chart scale factor (in volts/inch of chart), and ℓ_L is the measured chart distance (in inches) along the load axis of the hysteresis loop plot.

H. In Situ Surface Replication

When it was necessary to interrupt a fatigue test in order to replicate the gauge length of the specimen, the specimen was not removed from the load train but rather replicated in place in order to maintain the same alignment (37). The procedure is detailed below.

After the LCF test was halted, while the specimen was going into compression, the system was placed in Load Control with a mean level of zero. Then the stroke value was recorded. A mean tensile stress of about 3 ksi was then imposed on the specimen. The furnace was removed and a small fan was used to speed the cooling of the load train. After the system was at room temperature, the actuator was turned off, the thermocouple pulled back, and the extensometer removed. These procedures exposed the gauge section. The gauge section was cleaned with acetone and the replication was accomplished as explained in Section I-D.

In order to restart the test, the extensometer was reattached and the thermocouple placed back in position. The actuator was turned on, and a mean tensile stress of about 3 ksi was imposed. The furnace was placed back around the load train. When the system was equilibrated, both with respect to temperature and dimensions, a zero mean level was

imposed and the Stroke Zero Suppression Control was used to set the same stroke value which was recorded when test was initially stopped. Then the test was restarted.

IV. TENSILE TESTING

A. Specimen Configuration

The same specimen design, shown in Figure 1 for LCF testing, was used for tensile testing. Specimen manufacture was also done in the same way.

B. Machine Description

Mechanical testing was performed on an Instron Tensile Testing Machine, Model TT-C. The cross-head was moved at a constant speed utilizing an amplidyne drive and selsyn control elements. A Leeds and Northrup chart recorder (1.5 seconds full scale response time) was driven by the output from the extensometer LVDT. Load was measured by an Instron Load Cell. The chart was operated at 100 lbs full scale to provide good sensitivity of the load-displacement curve. The load cell and the LVDT gain control were calibrated prior to each test. The load train and furnace assembly were essentially the same as shown in Figure 3 for the LCF testing.

C. Computation of Stress and Strain

Stress was simply computed by dividing the load by the cross-sectional area of the specimen. The strain was computed in an analogous manner to that for the LCF data. Thus, a relationship was required to convert displacement to strain. It is certainly true that

$$\epsilon_t = \epsilon_e + \epsilon_p \quad (6)$$

where ϵ_t is total strain, ϵ_e is elastic strain, and ϵ_p is plastic strain. But

$$\epsilon_e = \frac{\sigma}{E} = \frac{u_e}{L_{eff}^e} \quad (7a)$$

$$\text{and} \quad \epsilon_p = \frac{u_p}{L_{eff}^p} = \frac{u_t - u_e}{L_{eff}^p} \quad (7b)$$

where σ is the stress (in psi), E is Young's Modulus (in ksi), u_p is the plastic displacement of the gauge section (in inches), u_t is the total displacement of the gauge section (in inches), u_e is the elastic displacement of the gauge section (in inches), L_{eff}^e is the effective gauge length in the elastic regime (in inches), and L_{eff}^p is the effective gauge length in the plastic regime (in inches). Thus, it is apparent that:

$$\epsilon_t = \frac{\sigma}{E} + \frac{u_t - \frac{\sigma \cdot L_{eff}^e}{E}}{L_{eff}^p} \quad (8)$$

So, Equation 8 is the desired relationship.

V. REJUVENATION TREATMENTS

A. Thermal Treatments

The only thermal rejuvenation treatment which was investigated was STA 3A which is defined in Table 4. It was necessary to suspend the specimen vertically in the furnace in order to minimize creep effects which could warp the specimen. A heat treating fixture, shown in Figure 8(a) and Figure 8(b), was designed to support the specimens in the center of the furnace hot zone. This fixture minimized the

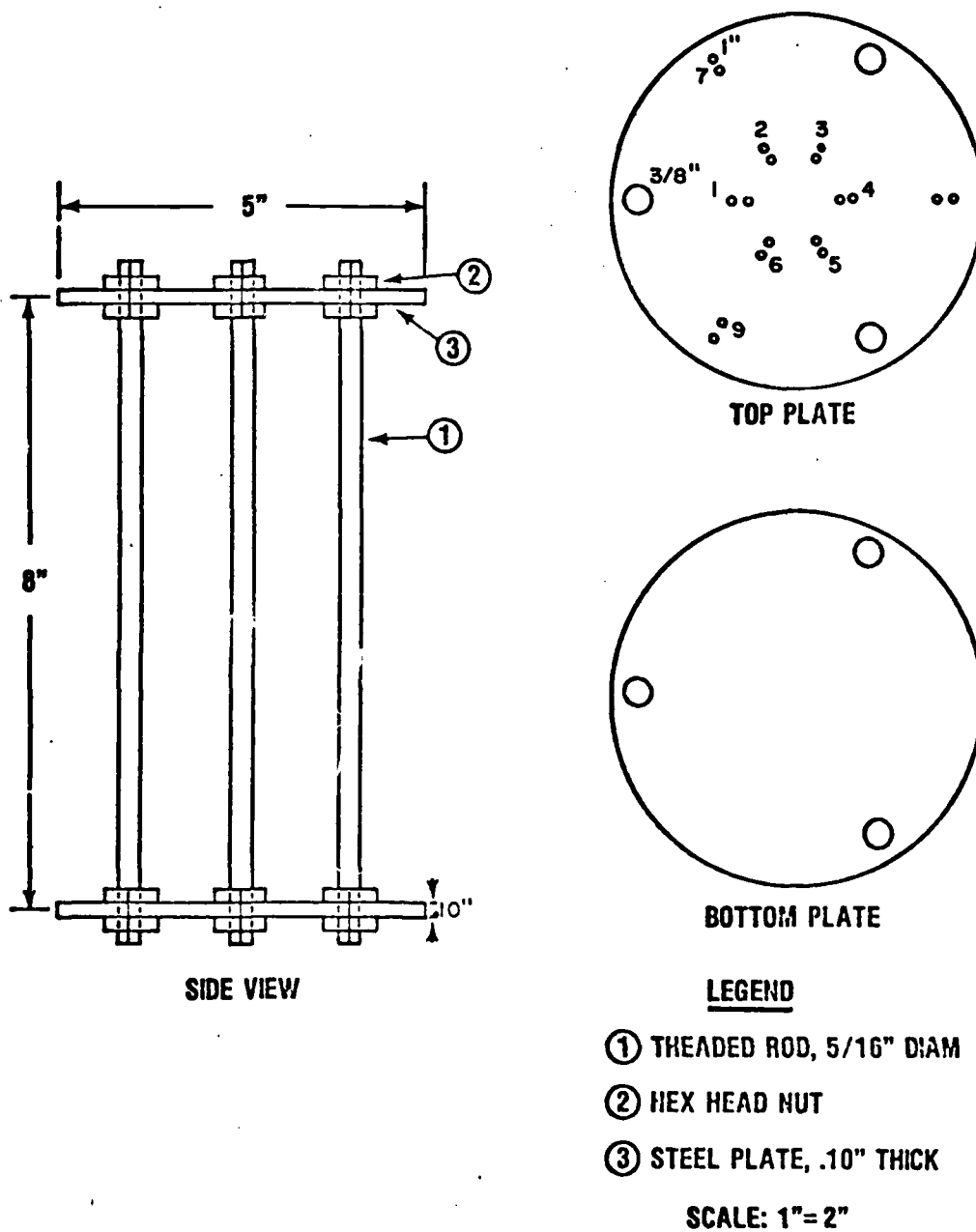
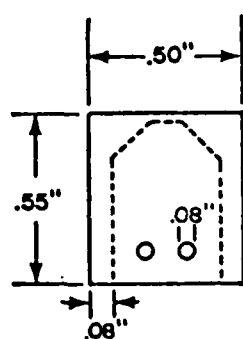
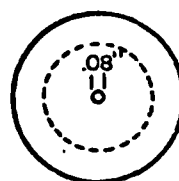


Figure 8a. Heat Treatment Fixture Design



SIDE VIEW



TOP VIEW

Figure 8b. Button Head Cap Design

possibility of specimen distortion, did not adversely affect critical machined surfaces, and was fairly simple to use. It held nine specimens. The cap, depicted in Figure 8(b), fit over the LCF specimen button head. Fine Nichrome wire was threaded into the two holes on each side of the cap, and thus the specimen was supported on the surface under the button head. Chromel wire, with a bead on one end, was threaded through the hole at the top of the cap. This wire was then pulled through a hole on the top plate of the fixture shown in Figure 8(a). The material used to manufacture the fixture and cap was AISI 1020 steel.

B. Hot Isostatic Pressing (HIP) Treatments

The HIP processing was conducted in a small, high-pressure, 7-in. i.d. × 14-in. long, HIP unit at Kelsey-Hayes, Detroit, Michigan. The chamber was designed by Autoclave Engineering, Erie, Pennsylvania. The heating elements were Kanthal wound, supplied by Conway Pressure Systems, Columbus, Ohio.

The fatigue specimens were vertically supported in a special fixture, shown in Figure 9. The same button head cap design, depicted in Figure 8(b) was used.

The temperature and pressure profiles for the HIP run are shown in Figures 10 and 11. The autoclave gas used was commercially pure argon.

A summary of the HIP run is as follows: The specimens mounted in the fixture were loaded into the HIP chamber. The system was flushed with argon gas until the atmosphere was primarily argon. The unit was slowly heated to 2050°F and the pressure was raised to 15 ksi. The 2050°F temperature was maintained for one hour, then the temperature

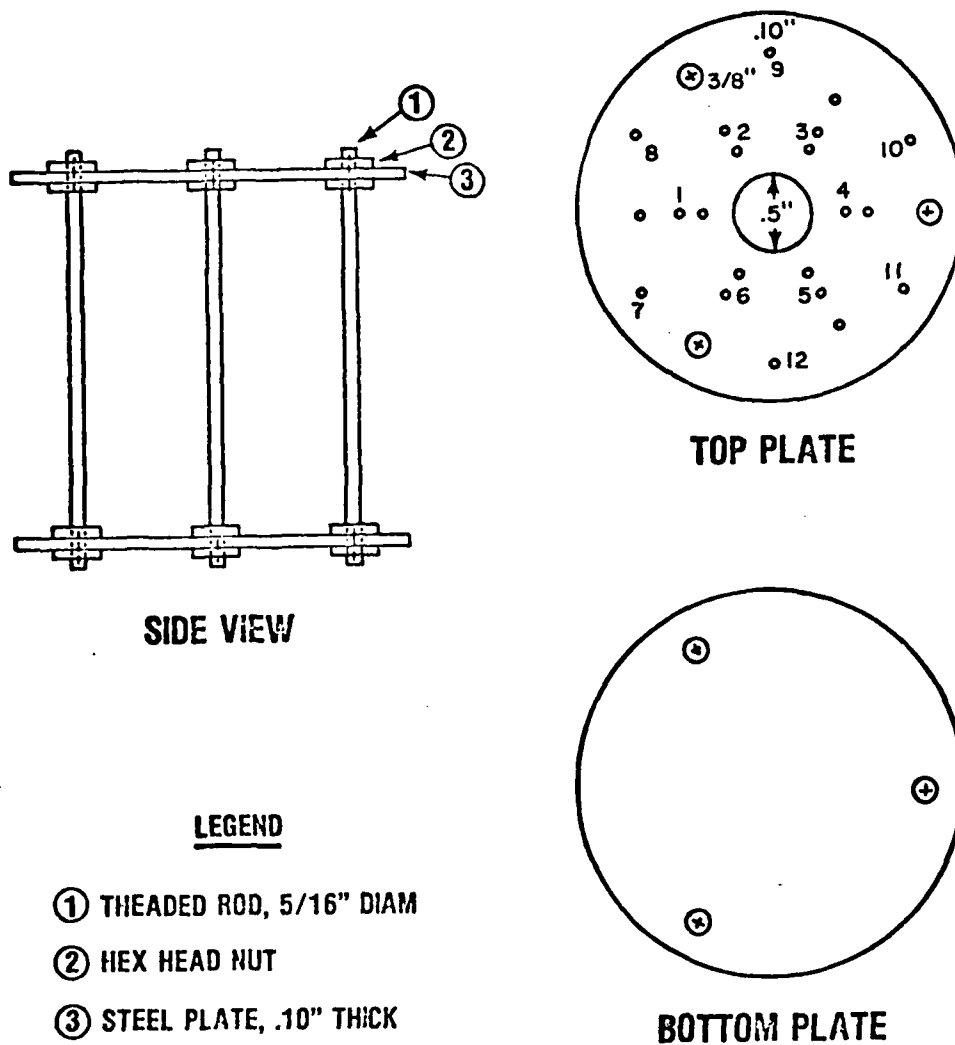


Figure 9. HIP Fixture Design

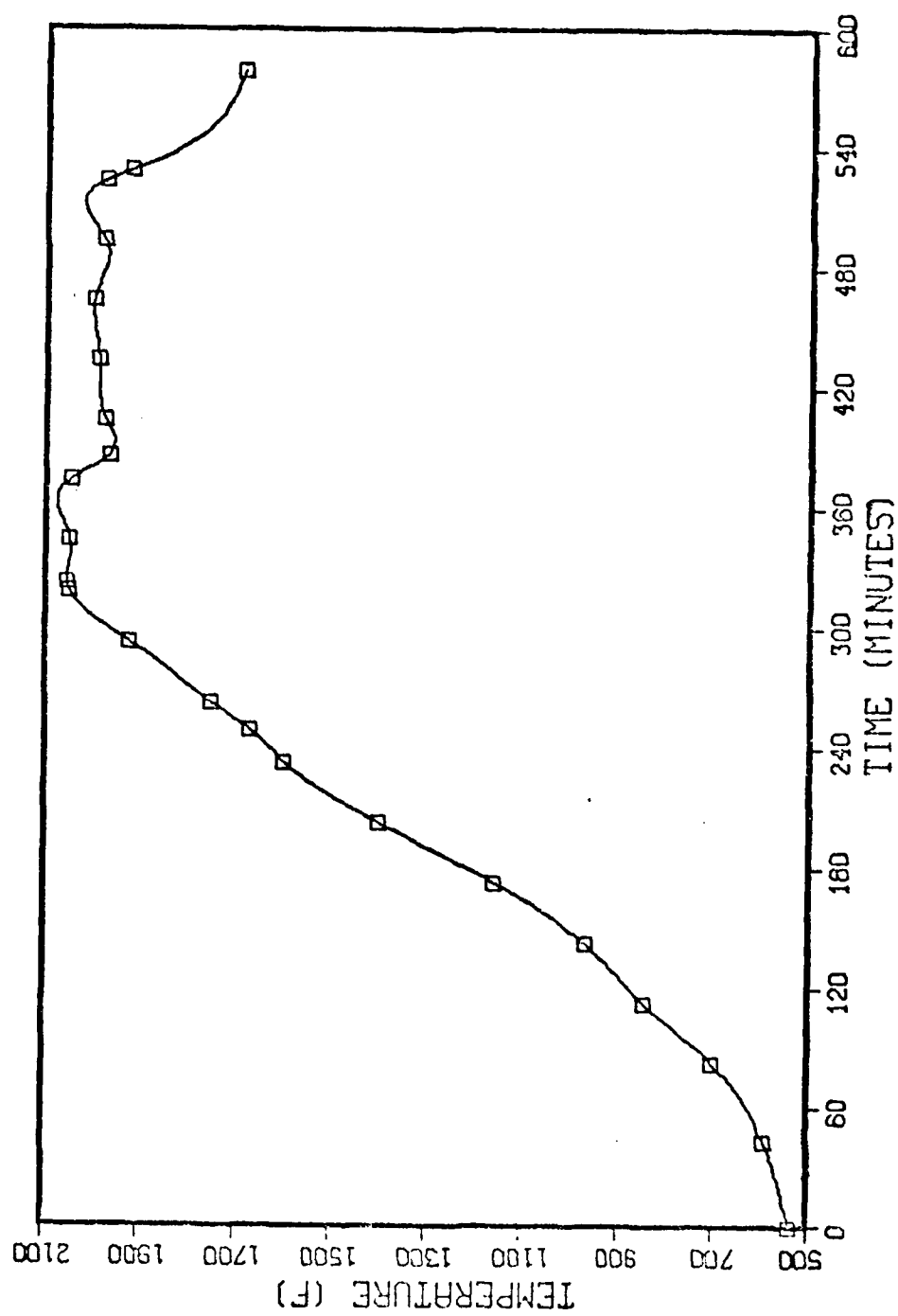


Figure 10. Plot of Temperature vs Time for HIP Run

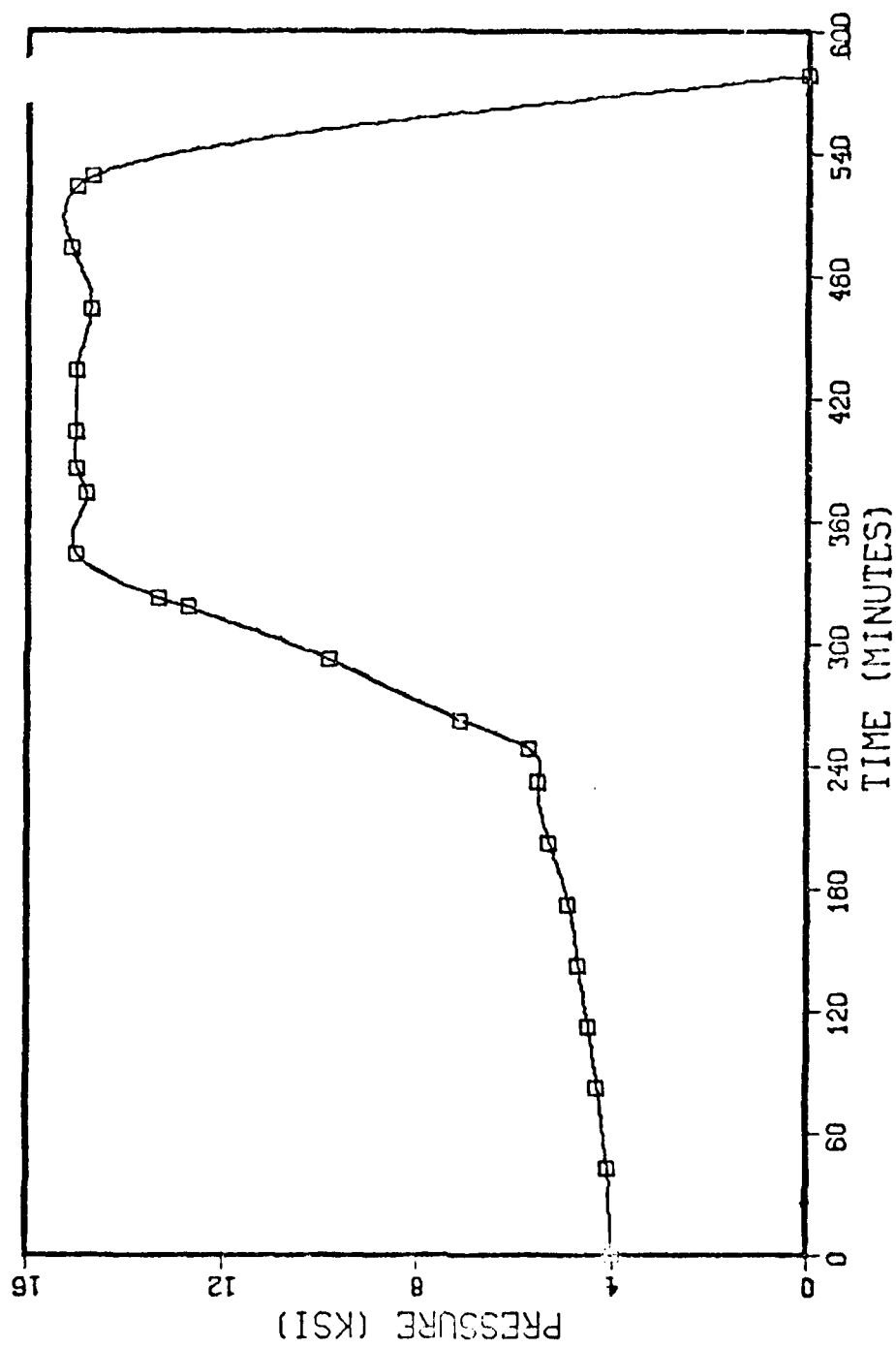


Figure 11. Plot of Pressure vs Time for HIP Run

was lowered to 1975°F while maintaining 15 ksi. After two hours at 1975°F, the pressure was released and the heating elements were turned off. When the chamber temperature reached 1700°F, the unit was opened, and the fixture removed. It was then placed in an argon gas stream until it reached ambient temperature.

VI. SONIC MODULUS TESTING

Moduli of elasticity were measured at room temperature using a Magnaflux FM-500 Elastomat. A right cylindrical rod was centerless ground to a uniform diameter of 0.4983 inches. The rod was 4.483 inches long and weighed 117.625 g.

The test rod was suspended at its nodal points by adjustable cross wires. Mechanical vibration was transmitted to the sample by a piezoelectric transducer by means of a 0.004-inch Nichrome wire spot welded to the rod about 0.010 inch from the circumference. Another transducer, similarly connected on the other side of the rod, received the mechanical vibration from the specimen. The rod was excited by means of a variable frequency oscillator which contained a digital counter. The resonant frequency was determined by the appearance of a circular Lissajou figure on an oscilloscope. The oscilloscope had the voltage output of one transducer connected to the x-axis and the voltage output of the other transducer connected to the y-axis. In such a manner, the resonant frequencies for the longitudinal (Young's) modulus, transverse modulus, and shear modulus were measured. The following equations were then used to compute the moduli:

Longitudinal (Young's) Modulus (39):

$$E = \frac{4.00 \times 10^{-4} \rho \ell^2 f_L^2}{6.895} \quad (9)$$

Shear Modulus (39):

$$G = \frac{4.00 \times 10^{-4} \rho \ell^2 f_G^2}{6.895} \quad (10)$$

Transverse Modulus (40):

$$E_T = \frac{1.261886 \times 10^{-4} \rho \ell^2 f_T^2 T_1}{6.895 d^2} \quad (11)$$

Shape Correction Factor, T_1 (41):

$$T_1 = 1 + 4.88669 \left[\frac{1 + 1.26225 v + 0.2098 v^2}{1 + v} \right] \left(\frac{d}{\ell} \right)^2 \quad (12)$$

where ρ is density (in g/cc); ℓ is length (in cm); d is diameter (in cm); f_L , f_G , and f_T are the resonant frequencies; E , G , and E_T are the elastic moduli (in psi); and v is Poisson's ratio.

Chapter 3

RESULTS AND DISCUSSION

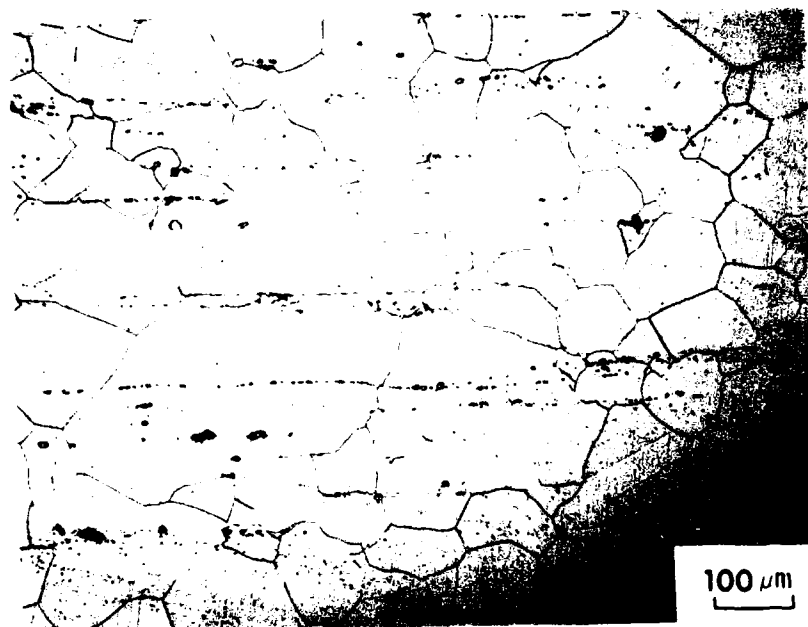
I. AGING RESPONSE OF INCOLOY 901

A. Characterization of As-Received Microstructure

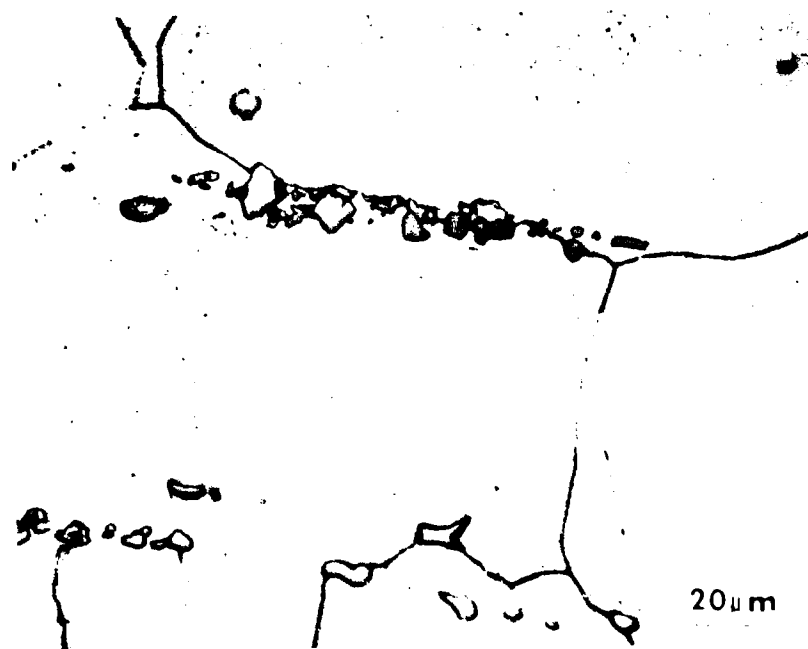
The microstructure of the Incoloy 901 forging was examined using a metallograph, a transmission electron microscope, and an electron microprobe.

Figure 12 shows a typical microstructure. Using the ASTM Linear Intercept Method to measure grain size (42), the grain size was determined to be 90 μm or ASTM Equivalent Grain Size 3.5. Particularly evident in Figure 12(a) are the inclusion stringers which parallel the forging direction. Figures 12(b) and 12(c) are higher magnification photographs of these inclusions. It is evident that these particles act as obstacles to grain boundary migration and thus assist in controlling the grain size during processing and thermal treatment. Figures 12(a) and 12(c) contain several annealing twins. These twins were commonly observed in the as-received material. Also evident in Figures 12(b) and 12(c) are much smaller particles.

Figure 13 is an electron image produced in a microprobe of a lightly etched sample. This clearly shows that there are two different particle morphologies.



a. General Microstructure



b. Inclusion Stringers

Figure 12. Micrograph of As-Received Material



c. Inclusion Stringers



Figure 13. Electron Micrograph of Inclusion

Qualitative electron probe analysis, shown in Figure 14, clearly identifies the large, blocky phase as a titanium/molybdenum carbide. Quantitative analysis indicates that these are MC-type carbides with slightly varying proportions of titanium and molybdenum. A typical carbide had the composition $Ti_{0.8}Mo_{0.2}C$. The sizes of these primary carbides typically ranged from 2-15 μm .

The small symmetrical particles in Figures 13 and 14 were approximately 1 μm in size and thus were difficult to quantitatively analyze. However, the results from an electron microprobe quantitative analysis indicated the following composition in weight percent: Ti-9.88, Co-13.52, Fe-8.55, Ni-3.42, Mo-52.23; difference from 100% is 12.40. Although boron could not be analyzed for in the microprobe, this analysis is consistent with the hypothesis that these particles are M_3B_2 borides. Furthermore, Beattie electrolytically extracted similar particles from Incoloy 901 and analyzed them chemically and by x-ray diffraction (69). His conclusion was that these particles were M_3B_2 borides.

Transmission electron microscopy was used to characterize the small γ' precipitates and the grain boundary precipitates. Figure 15 shows γ' in dark field. The particles have a spherical morphology and an average diameter of 300 \AA units. Figure 16 shows the grain boundary precipitates. These are MC carbides of the type (Ti,Mo)C rather than $M_{23}C_6$ carbides (70). It should be noted that some grain boundaries, as indicated in Figure 17, were relatively free of precipitates.

B. Development of Standard Solution and Double-Aged Treatment

Since the LCF test specimens were cut from different portions of a shaft forging, it was desired to subject them all to a standard,

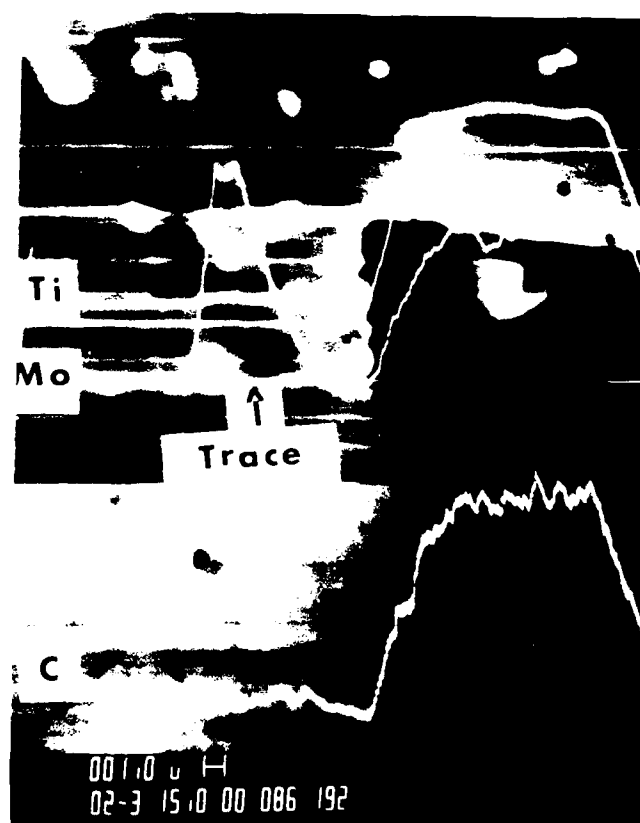


Figure 14. Electron Microprobe Trace of Carbide Inclusion

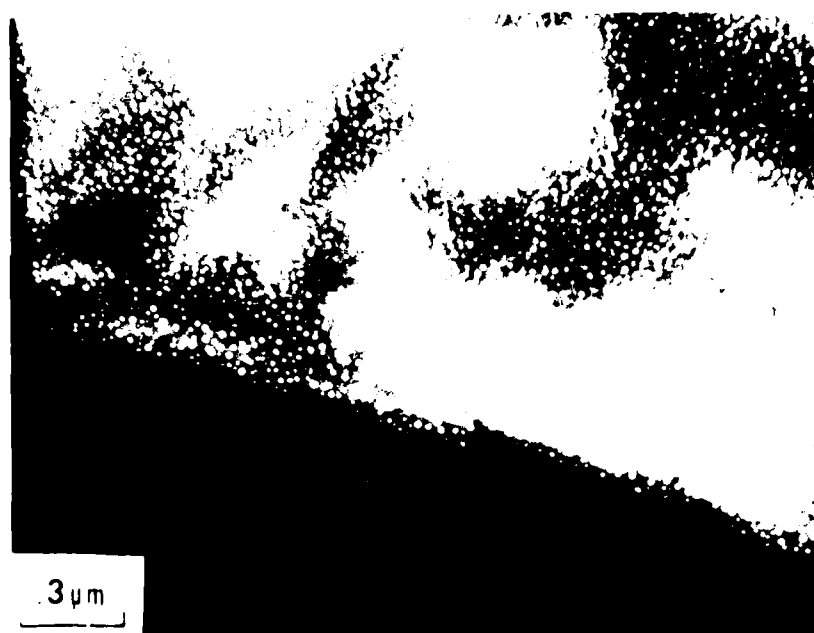


Figure 15. TEM Micrograph of γ'



a. Typical Grain Boundary MC Precipitates



b. Typical Grain Boundary MC Precipitates

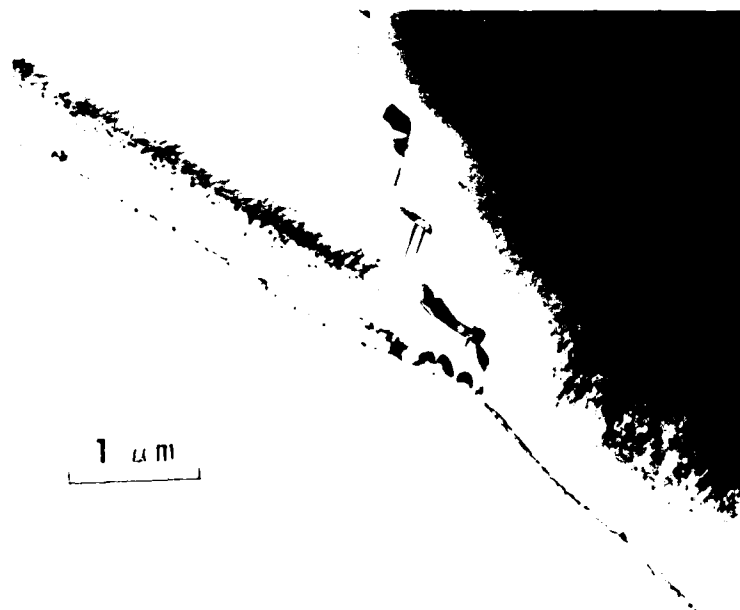
Figure 16. TEM Micrograph of Grain Boundary MC Carbides



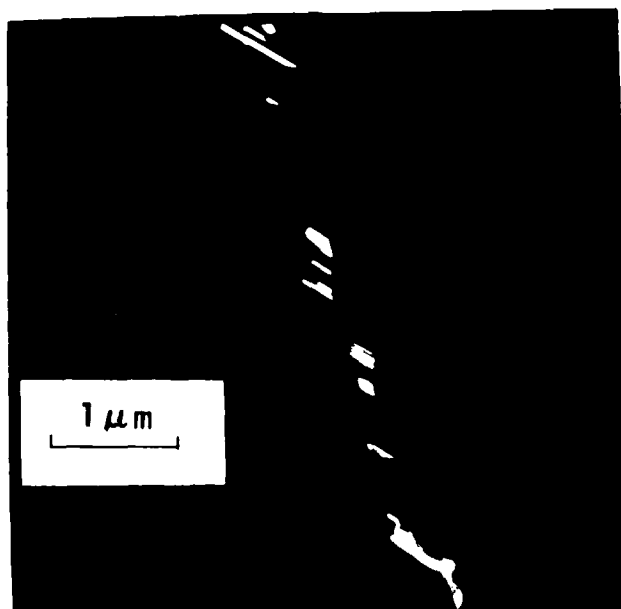
Figure 17. TEM Micrograph of Precipitate-Free Grain Boundary

known heat treatment prior to testing. Also, this standard heat treatment could be used for thermal rejuvenation and to restore the microstructure of hot isostatically pressed specimens. Table 2 contains the specification for the commercial heat treatment. Since the minimization of grain growth was an important consideration in developing the standard heat treatment, the lowest portion of the time and temperature ranges were selected for the solutioning treatment. The drop furnace was used to rapidly quench a piece of material which was subsequently examined by transmission electron microscopy. It was determined that 2 hours at 1975°F was sufficient to dissolve all phases except for the primary MC carbides.

All heat treatments were done in a vacuum furnace to minimize surface contamination. However, it was necessary to backfill the furnace with helium gas in order to obtain a high enough cooling rate to prevent the nucleation and growth of undesirable precipitates and precipitate morphologies. Such undesirable grain boundary morphologies are shown in Figure 18. Figure 18(a) shows needles of a η phase growing out from a grain boundary MC precipitate in a platelet morphology, and Figure 18(b) is a dark field view of the MC platelets growing out from a grain boundary. These precipitates were formed during vacuum cooling from the solutioning temperature because the cooling rate was too slow. It was found that backfilling the furnace to 640 torr of helium gas produced the proper grain boundary morphology. The standard heat treatment, designated as STA 3A, is presented in Table 4.



a. Needle-Shaped η Phase and MC Platelets



b. MC Platelets (Dark Field)

Figure 18. TEM Micrograph of Unidirectional Grain Boundary Precipitate Morphology

The effect of STA 3A on grain size was measured. The average grain size was increased to 120 μm (ASTM Equivalent Grain Size 3), but remained fairly stable at this size with subsequent heat treatments. The matrix was not dislocation-free, but the dislocations were randomly oriented.

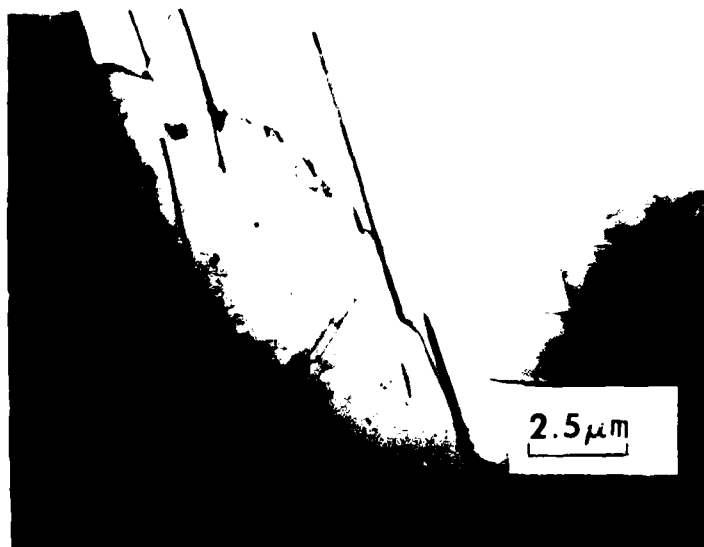
C. Microstructure Response at Elevated Temperatures

In order to better understand the physical metallurgy of Incoloy 901, the microstructure which developed at 1500°F and 1700°F was studied using a drop furnace. After 6 hours at 1500°F, no change in the grain size occurred. The fine γ' coarsened appreciably, approximately doubling in size to 600 \AA units. The grain boundary carbides developed a blocky morphology.

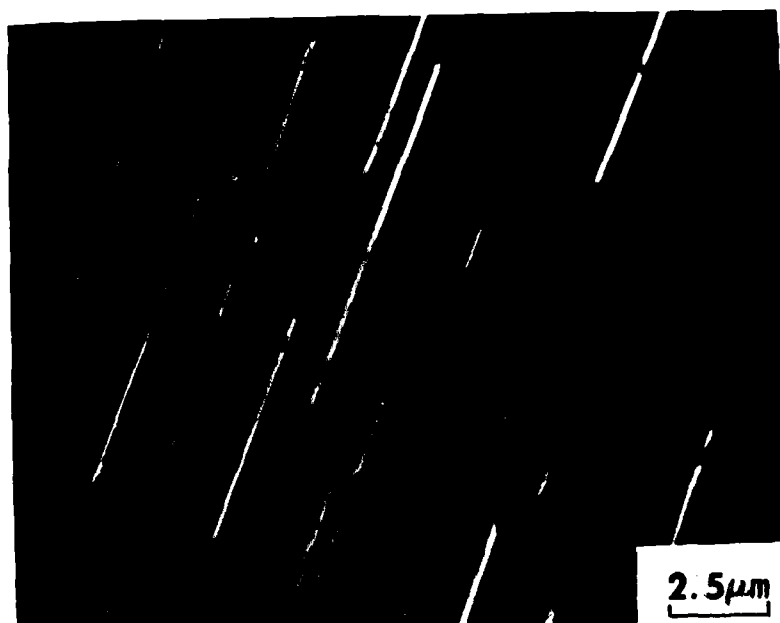
After 6 hours at 1700°F, no change in the grain size occurred. The change in precipitates was dramatic. No γ' was seen, although the solvus temperature is assumed to be 1725°F (17). The platelet morphology of the η phase is evident from the transmission electron micrographs in Figure 19. Figure 20 shows these η platelets at lower magnification as seen in a metallograph.

D. Microstructure Resulting from Hot Isostatic Pressing (HIP)

Hot isostatic pressing of superalloys is normally accomplished at very high temperatures; i.e., above the 1975°F solutioning temperature of Incoloy 901. In an attempt to measure the effect on grain growth of these high HIP temperatures, one piece of material was heated in a vacuum furnace to 2100°F for five hours and another piece was heated to 2050°F for three hours. The average grain size after the 2100°F

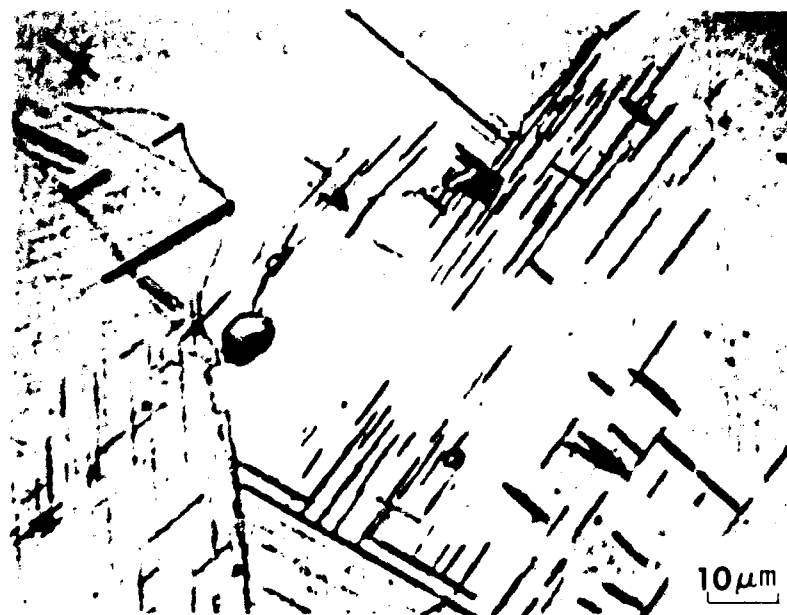


a. Nucleation of η at Grain Boundary

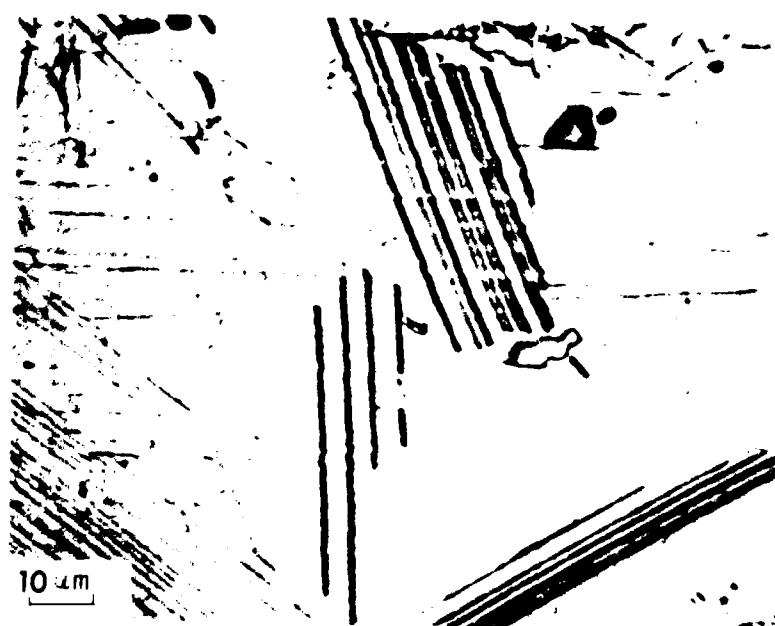


b. Matrix Nucleation of η

Figure 19. TEM Micrograph of η Platelets



a. Typical η Platelets



b. Typical η Platelets

Figure 20. Micrographs of η Platelets

heat treatment was 237 μm (ASTM Equivalent Grain Size 1). The average grain size which resulted from the 2050°F heat treatment was 181 μm (ASTM Equivalent Grain Size 1.5).

Figure 21 shows photomicrographs of as-HIPed material (15 ksi pressure, 1 hour at 2050°F, 2 hours at 1975°F). Note that the primary carbides helped to control grain growth. There also appears to be some η -phase precipitation which occurred during cooling. Except for the primary carbides and η platelets, transmission electron microscopy did not reveal any other precipitates. The grain size was about 150 μm , or ASTM Equivalent Grain Size 2.

When the as-HIPed material was given the standard STA 3A heat treatment, the desirable morphology and distribution of precipitates was restored.

II. MECHANICAL PROPERTIES

A. Tensile Properties

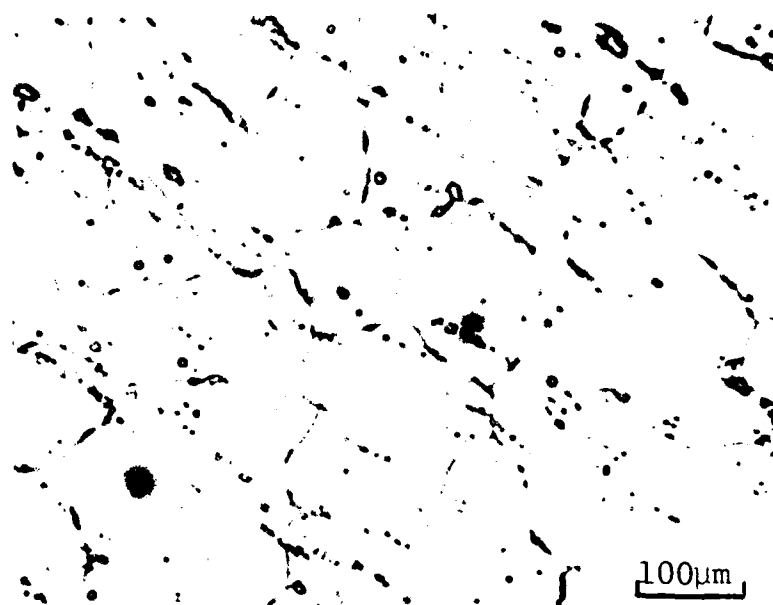
The measured tensile properties of the Incoloy 901 test specimens, after STA 3A, are summarized in Table 7. These properties (at room temperature) are well above the specified minimums of 100 ksi yield strength and 150 ksi ultimate tensile strength (43).

B. Elastic Constants

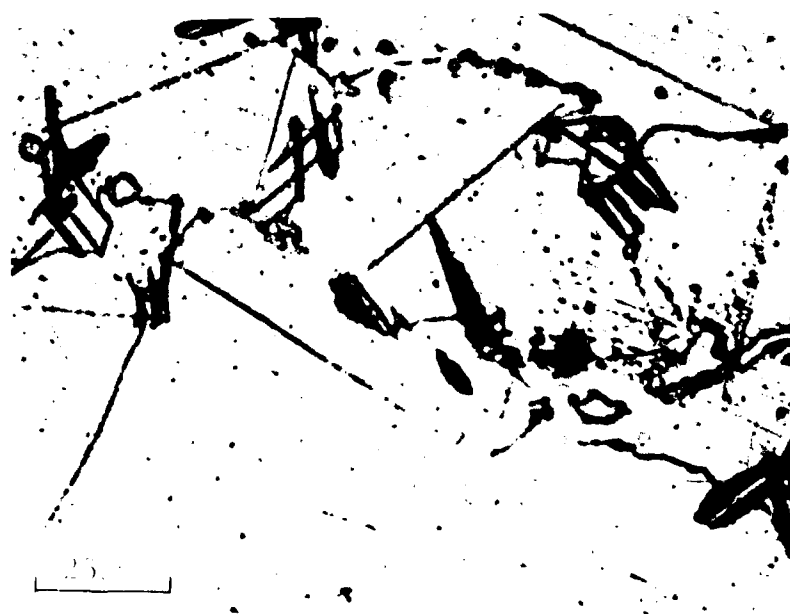
The elastic moduli were measured at room temperature using an Elastomat Sonic Modulus Tester. Young's Modulus was determined to be 30.2×10^6 psi; the corrected transverse modulus was 30.3×10^6 psi; the shear modulus was 11.2×10^6 psi; and Poisson's ratio was 0.35. Young's Modulus of 29.9×10^6 psi at room temperature and 27.51×10^6 psi at 500 °F have been reported from mechanical test data (44).

TABLE 7
INCOLOY 901 TENSILE DATA

Specimen	Test Temperature (°F)	Yield Stress (ksi)	Tensile Stress (ksi)	Fracture Stress (ksi)	Reduction in Area (%)	Strain Rate (in./in./min.)
B2	70	135.3	178.3	207.6	14.3	2×10^{-2}
B1	500	119.4	155.4	175.4	12.6	2×10^{-2}
B3	500	123.3	165.7	194.3	14.9	2×10^{-2}
B4	500	123.7	161.3	189.0	15.1	2×10^{-3}



a. Typical Microstructure



b. Grain Boundary Region

Figure 21. Micrographs of As-HIP'd Material

III. LOW-CYCLE FATIGUE BASELINE TESTING

A. Determination of Effective Gauge Length

The low-cycle fatigue specimen design (Figure 1) requires the use of an effective gauge length in order to compute a strain from the measured displacement between the flanges. A plot of Stress vs Displacement at room temperature is shown in Figure 22, and Figure 23 shows Stress vs Displacement at 500°F. The slope of the linear portions of these curves is an effective modulus, $\Delta\sigma/\Delta u$ (recall Equation 4). Thus, Equation 4 allows computation of the effective elastic gauge length, L_{eff}^e , once the effective modulus, $\Delta\sigma/\Delta u$, is known. Using a linear least square error curve fit to the linear portion of the data in Figures 22 and 23, the effective modulus at 70°F was found to be 58.76×10^6 psi/in. with a correlation coefficient of 0.9999. At 500°F, the effective modulus was found to be 54.89×10^6 psi/in. with a correlation coefficient of 0.999. The results are summarized in Table 8. Strain was then computed using Equations 2 and 8.

Table 8

EFFECTIVE ELASTIC GAUGE LENGTH

Temperature (°F)	Young's Modulus ($\times 10^{-6}$ psi)	Effective Modulus ($\times 10^{-6}$ psi/in.)	Effective Elastic Gauge Length (in.)
70	30.2	58.76	0.51
500	27.5	54.89	0.50

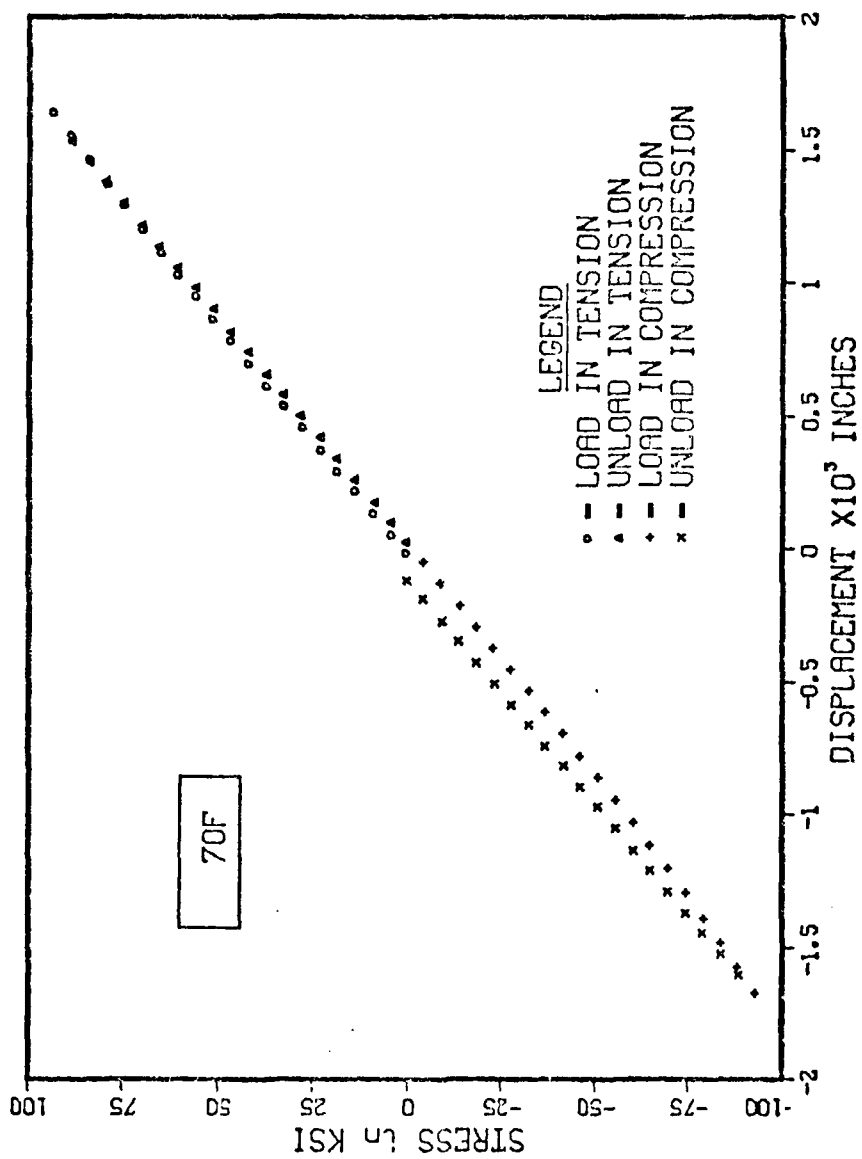


Figure 22. Plot of Stress vs Displacement at 70°F

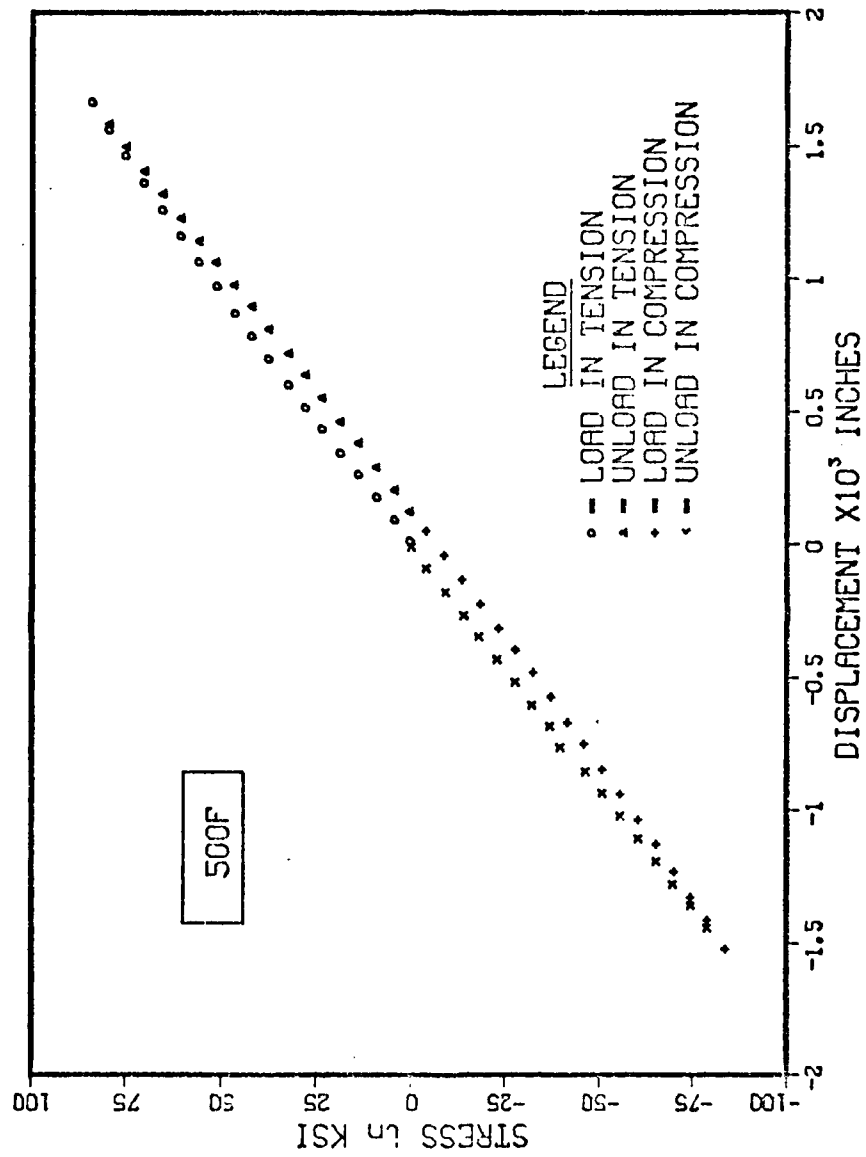


Figure 23. Plot of Stress vs Displacement at 500°F

B. Cyclic Stress-Strain Curve

Using the methodology described by Manson (3), a comparison of a 500°F static stress-strain curve with the 500°F cyclic stress-strain curve was made. For experimental ease, the tensile data used was measured at a strain rate of 2×10^{-2} in./in./min., while the cyclic data was obtained at a higher strain rate of 3.3×10^{-1} in./in./min. The tensile data presented in Table 7 shows that the mechanical properties of this alloy at 500°F are not very sensitive to strain rate within the range studied; thus, this comparison is not expected to be in significant error.

Figure 24 is the cyclic stress-strain curve compared to the static curve. At the lower strain ranges, the alloy cyclically softens; and, at the higher strain ranges, it cyclically hardens. For total strain ranges greater than 2.0%, Merrick observed rapid strain hardening of Incoloy 901 at room temperature and at 1000°F (16). The strain rate was not specified. Hardening peaked at about 10 cycles, then gradual softening occurred. Very rapid strain hardening was observed in this work also. The strain softening which occurred happened very gradually.

Cyclic strain hardening has been explained phenomenologically as being caused by dispersal of slip onto neighboring slip planes, and analogous to unidirectional hardening (4,66,67). The cyclic softening is due to the concentration of cyclic slip in the active slip bands (4,64,65,68). Thus, the shape of the cyclic stress-strain curve can be explained as follows: At the higher strain ranges, strain hardening has occurred but since the lifetimes at these high ranges is short, there was insufficient time for appreciable strain softening to

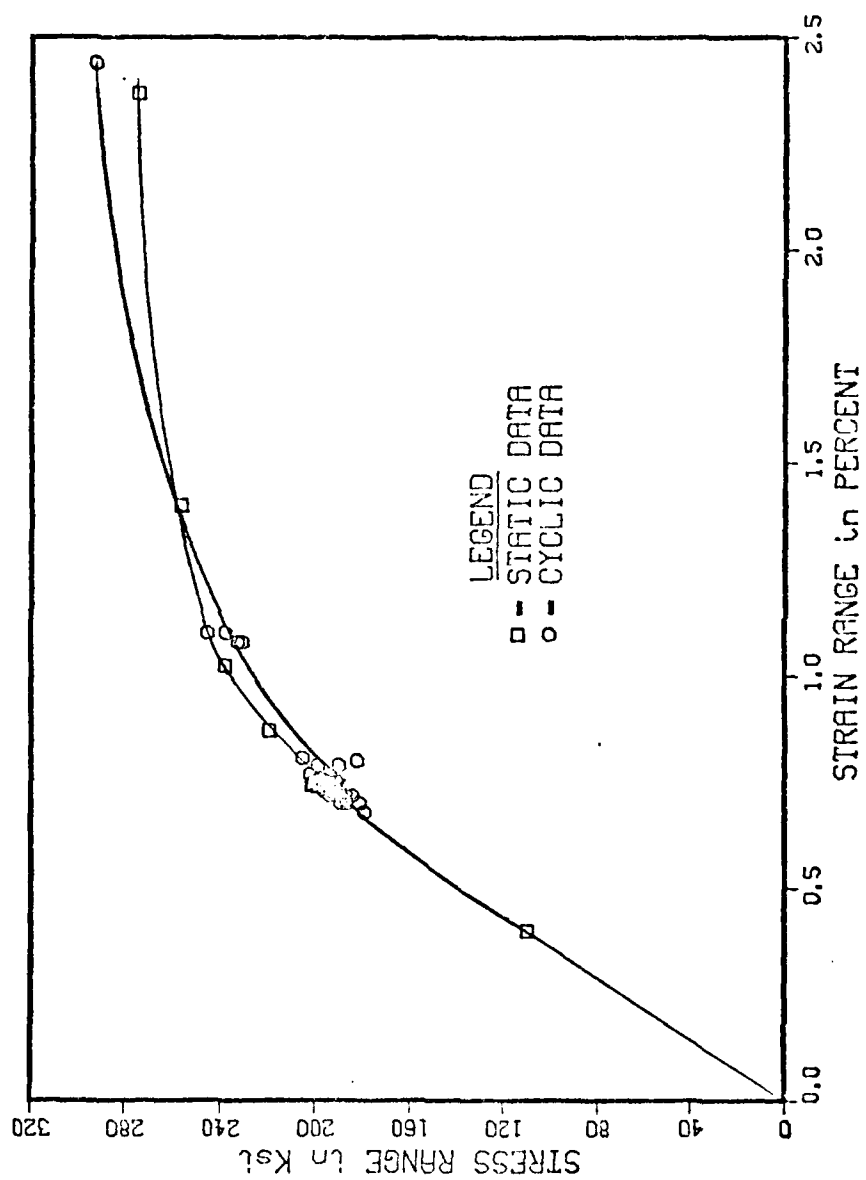


Figure 24. Plot of Cyclic Stress-Strain Curve

occur. At the lower strain ranges, the lifetimes are relatively long and hence there was time for softening to occur.

C. Characterization of Fatigue Damage

i. Baseline Data

A summary of the baseline data is presented in Table 9. The stress range reported is the stabilized range. The initiation cycle, N_i , was determined by extrapolating the asymmetric load drop back to the stable stress range on a plot of expanded Stress Range vs Cycles (2). A typical plot of this type is shown in Figure 25. The transition to the rapid load decrease, N_i' , was determined by the point at which the load drop-off was no longer linear. The cycles to failure, N_f , was determined when the maximum tensile stress was 20 ksi. Figure 26 is a log-log plot of Strain Range vs Cycles. Table 10 contains the constants for the linear least square fit lines of Figure 26. Using the data in Table 10, the following Coffin-Manson type equations can be derived:

$$\Delta \epsilon_t = 8.15 N^{-0.295} \quad (13a)$$

$$\Delta \epsilon_e = 1.75 N^{-0.114} \quad (13b)$$

$$\Delta \epsilon_p = 71.29 N^{-0.898} \quad (13c)$$

The data estimated from Merrick (16) was obtained by merely averaging his room temperature and 1000°F data. Figure 27 compares the trend line for Cycles to Initiation with Cycles to Failure.

Plots of Stress Range vs Cycles for the baseline specimens listed in Table 9 are contained in Figures 28-38, respectively. Note that these plots, in general, contain data obtained by measurement of hysteresis loops and by output from the Instron Minicomputer. The computer data

TABLE 9
SUMMARY OF BASELINE LCF PROPERTIES

Specimen	Strain Range (%)			Stress Range (ksi)	Cycles			
	$\Delta\epsilon_t$	$\Delta\epsilon_p$	$\Delta\epsilon_e$		N_i	N_i'	N_f	N_i'/N_f
2	1.08	0.25	0.83	232	780	-	1139	0.68
3	2.44	1.37	1.07	292	-	-	58	-
5	1.10	0.27	0.83	237	480	760	852	0.89
6	0.71	0.07	0.64	187	1400	2610	3263	0.43
7	0.72	0.05	0.67	191	1600	3200	3752	0.43
8	0.72	0.05	0.67	184	1200	3300	3820	0.31
11	0.70	0.05	0.65	181	2350	3800	4025	0.58
12	0.79	0.04	0.75	190	1300	2550	3398	0.38
32	0.70	0.04	0.66	189	1350	2900	4059	0.33
33	0.76	0.05	0.71	196	1000	2300	2965	0.34
53*	0.72	0.03	0.69	191	900	2600	3264	0.28

*Electropolished before test

TABLE 10
LINE CONSTANTS FOR $\log \Delta \epsilon$ vs $\log N$ CURVES

	<u>b*</u>	<u>m*</u>
$\Delta \epsilon_t$	0.911	-0.295
$\Delta \epsilon_p$	1.853	-0.898
$\Delta \epsilon_e$	0.242	-0.114

*Equation is of the form:

$$\log \Delta \epsilon = m \log N + b$$

where $\Delta \epsilon$ is strain range (%)

N is number of cycles

m is slope of the line

b is the y-intercept

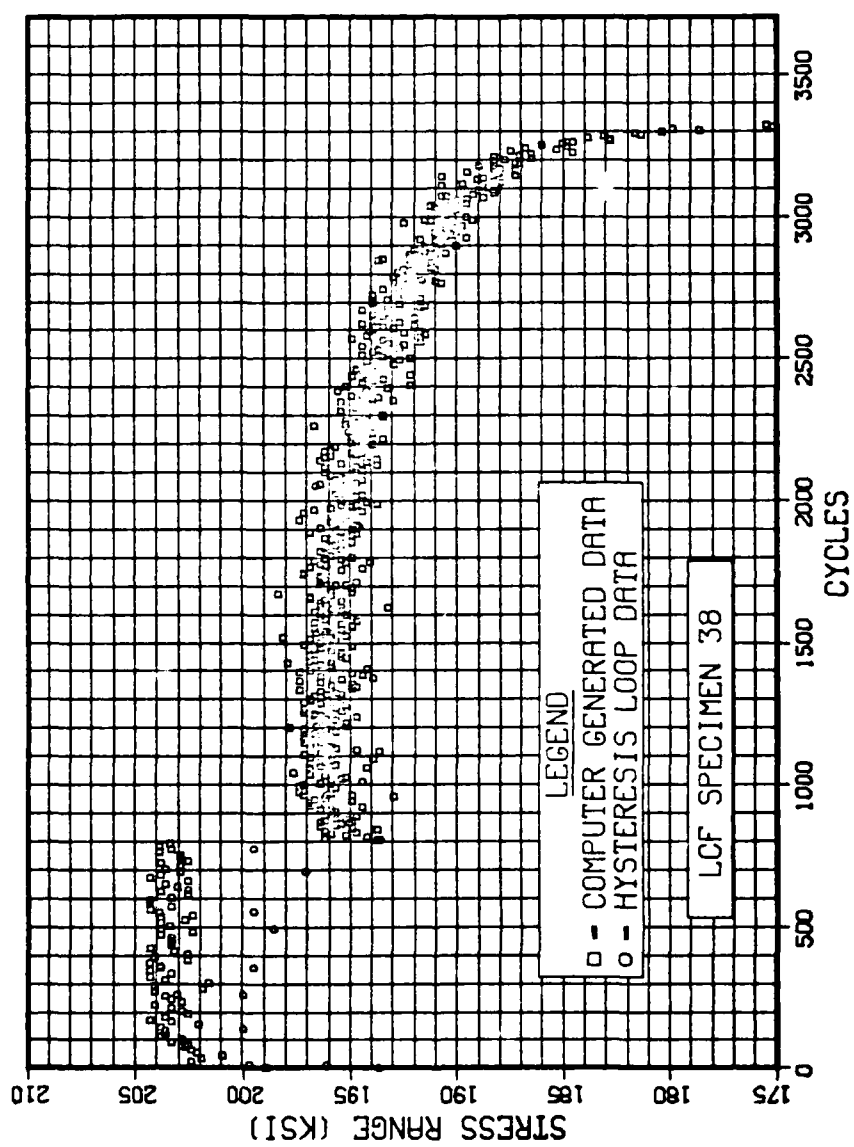


Figure 25. Plot of Stress Range vs Cycles - Expanded Scale

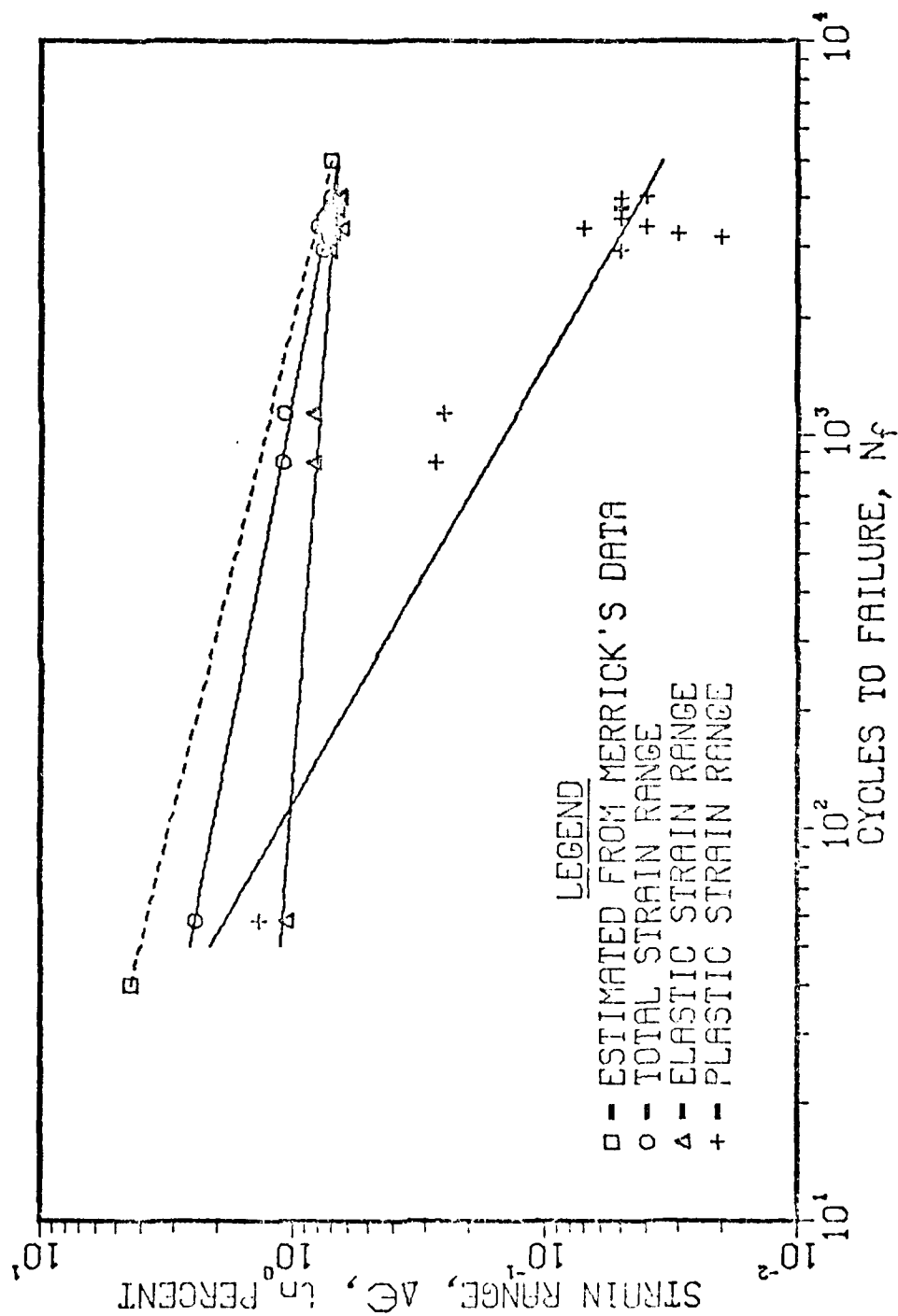


Figure 26. Plot of Baseline Strain Range vs Cycles to Failure

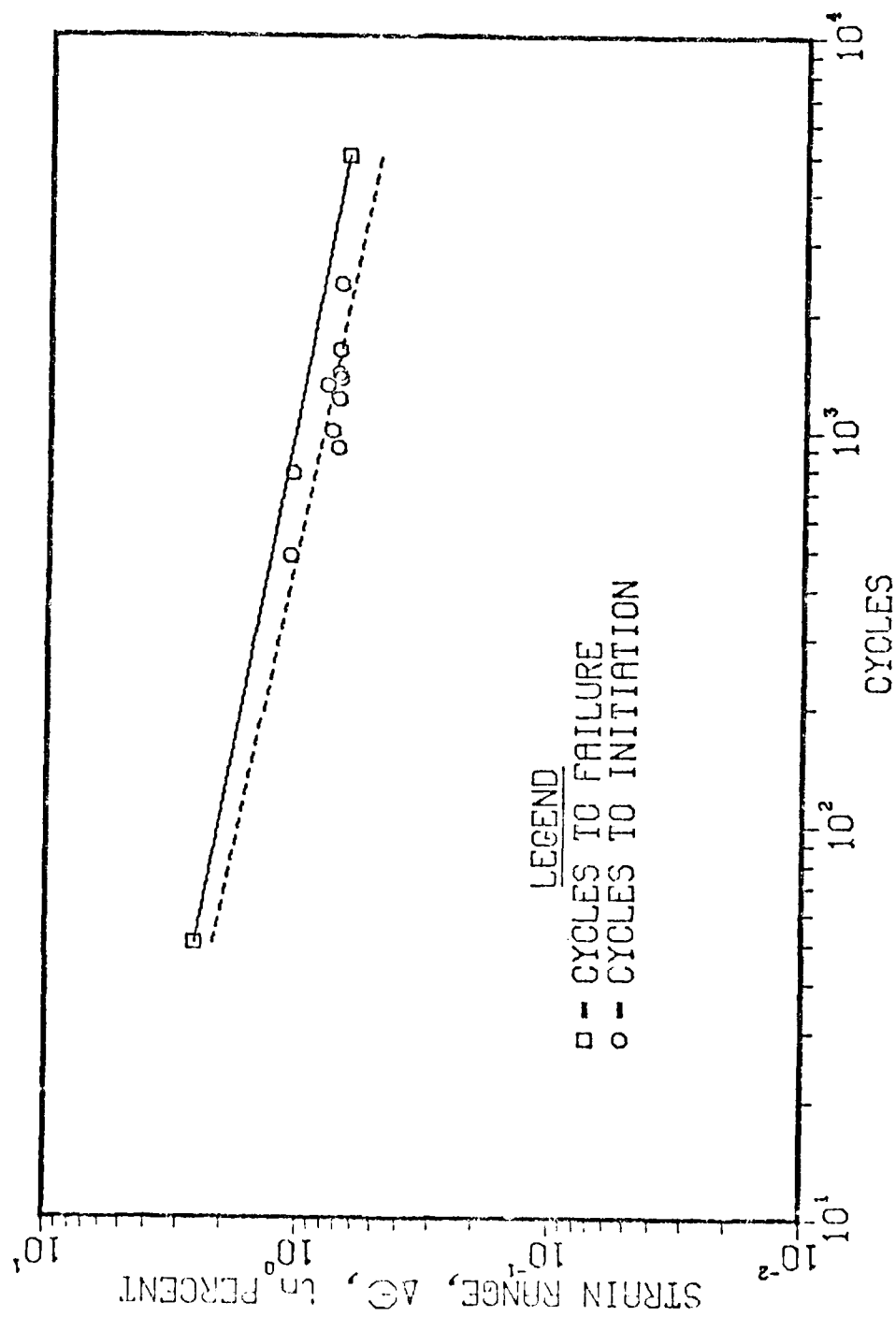


Figure 27. Plot of Baseline Strain Range vs Cycles to Initiation

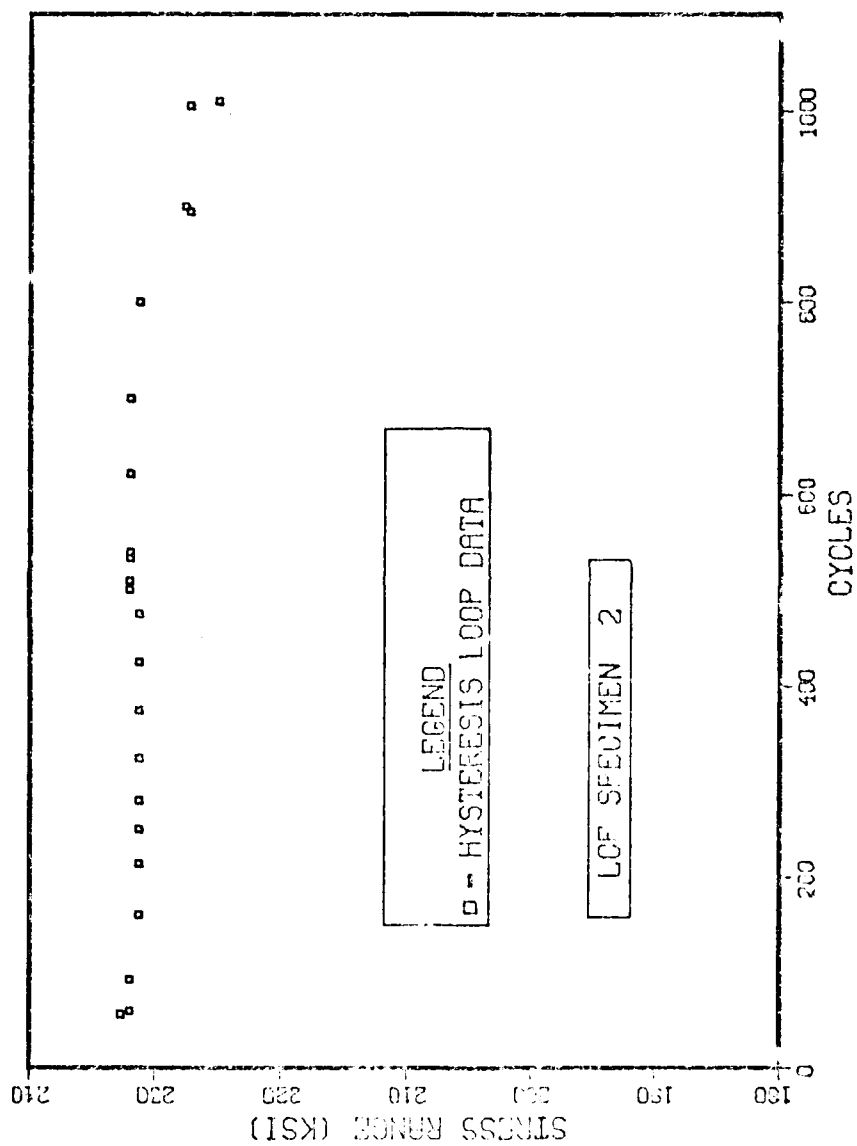


Figure 28. Plot of Stress Range vs Cycles - LCF Specimen 2

AD-A107 255

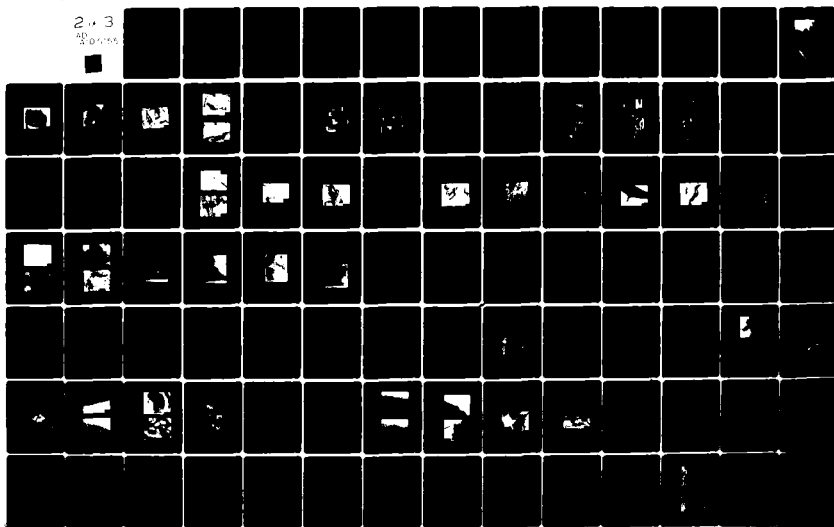
AIR FORCE INST OF TECH WRIGHT-PATTERSON AFB OH
MECHANISMS OF RECOVERING LOW CYCLE FATIGUE DAMAGE IN INCOLOY 90--ETC(U)
1979 R E SCHAFRIK
AFIT-C1-79-212D

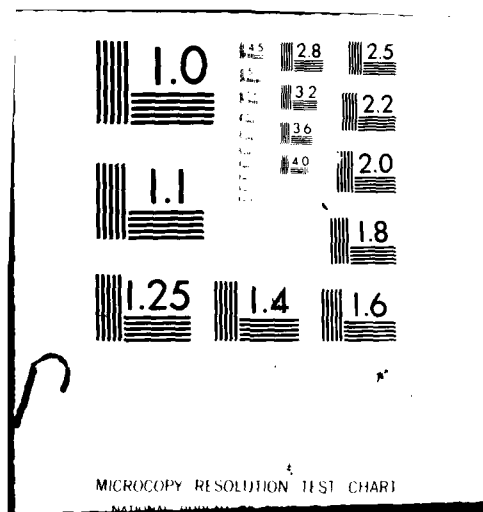
F/6 11/6

UNCLASSIFIED

NL

2.3
AD-A107 255





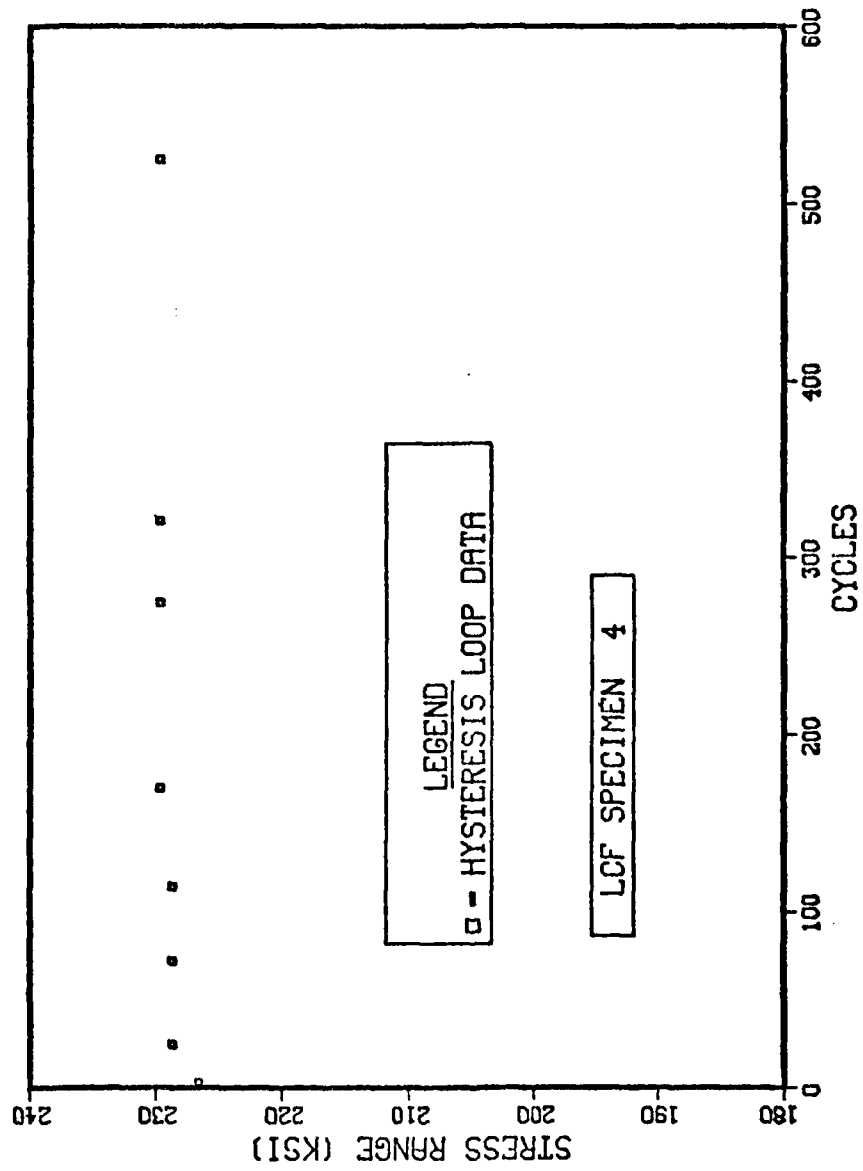


Figure 29. Plot of Stress Range vs Cycles - LCF Specimen 4

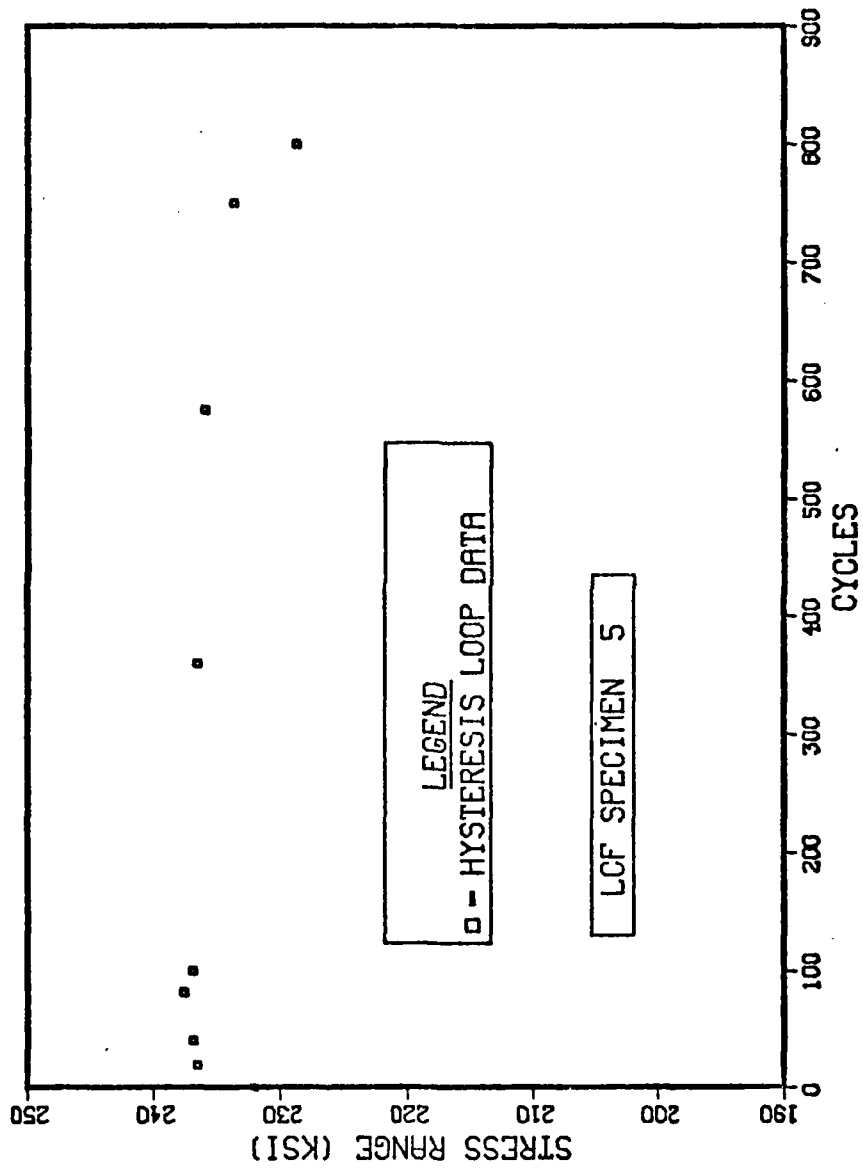


Figure 30. Plot of Stress Range vs Cycles - LCF Specimen 5

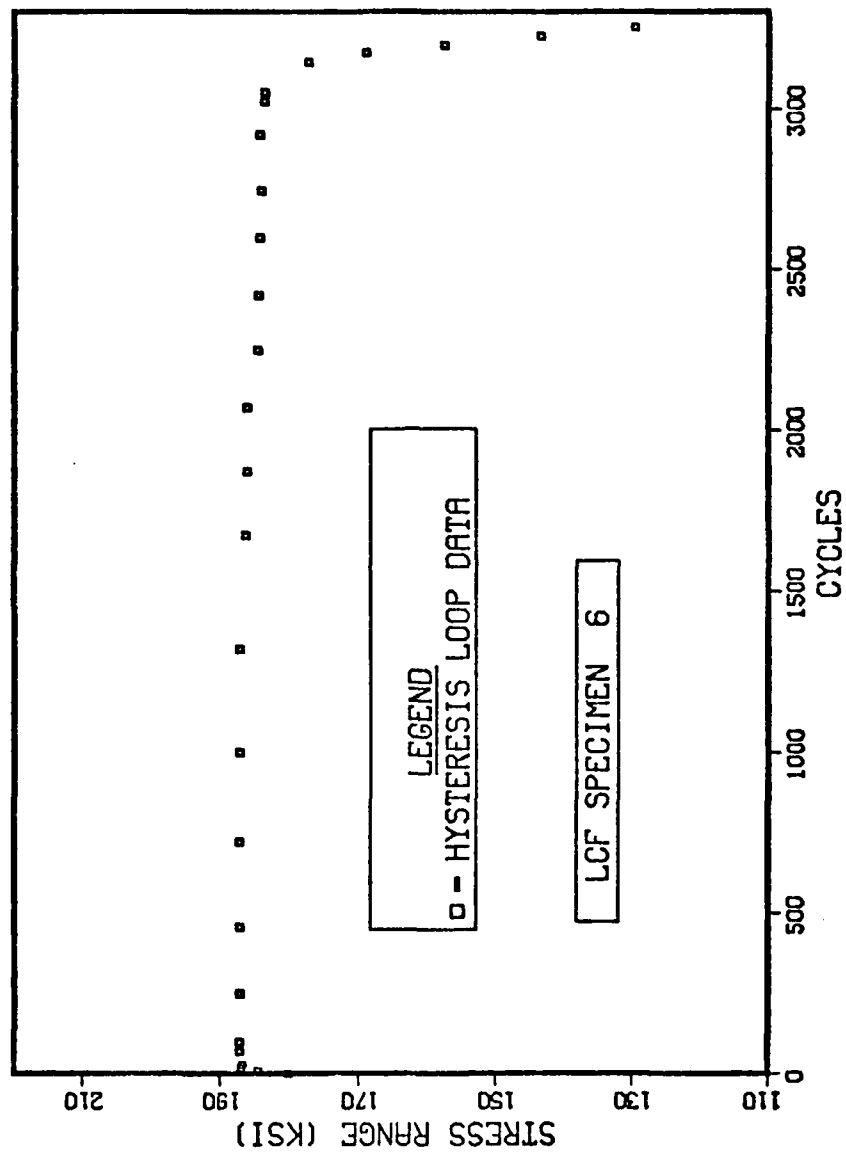


Figure 31. Plot of Stress Range vs Cycles - LCF Specimen 6

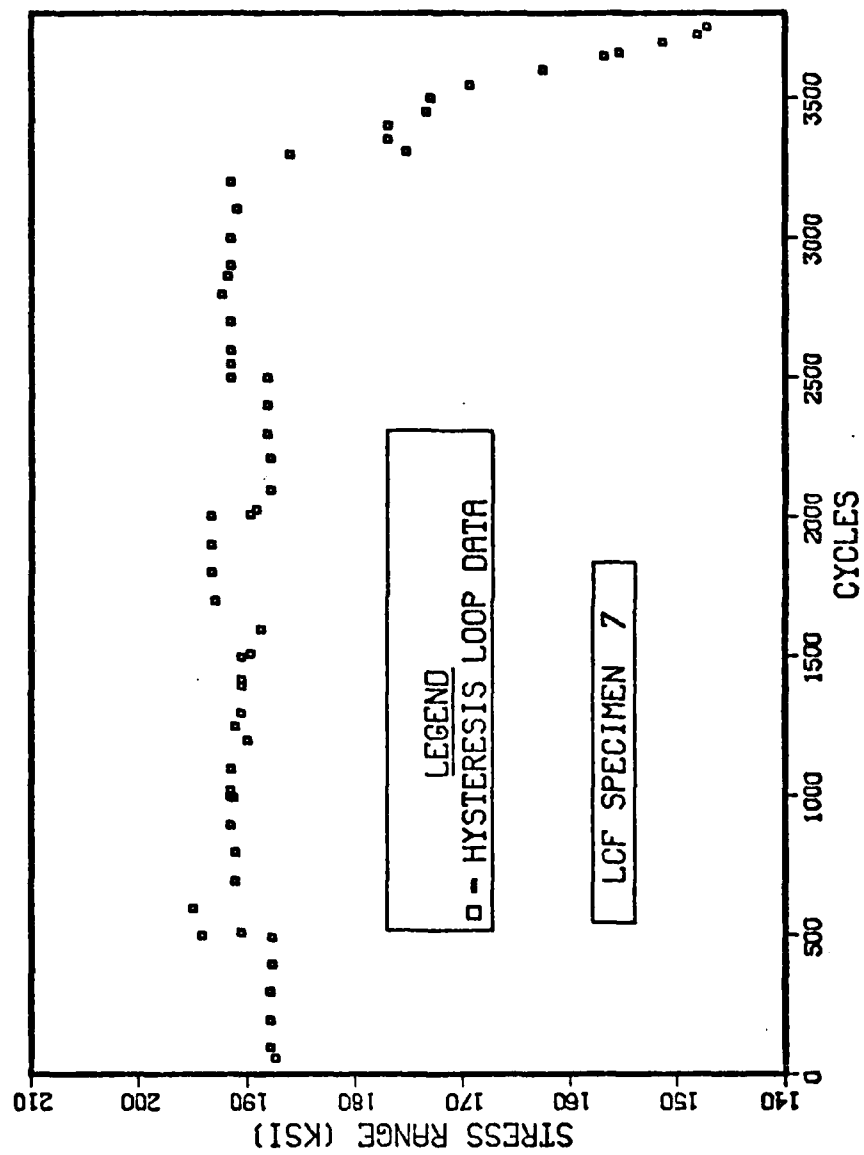


Figure 32. Plot of Stress Range vs Cycles - LCF Specimen 7

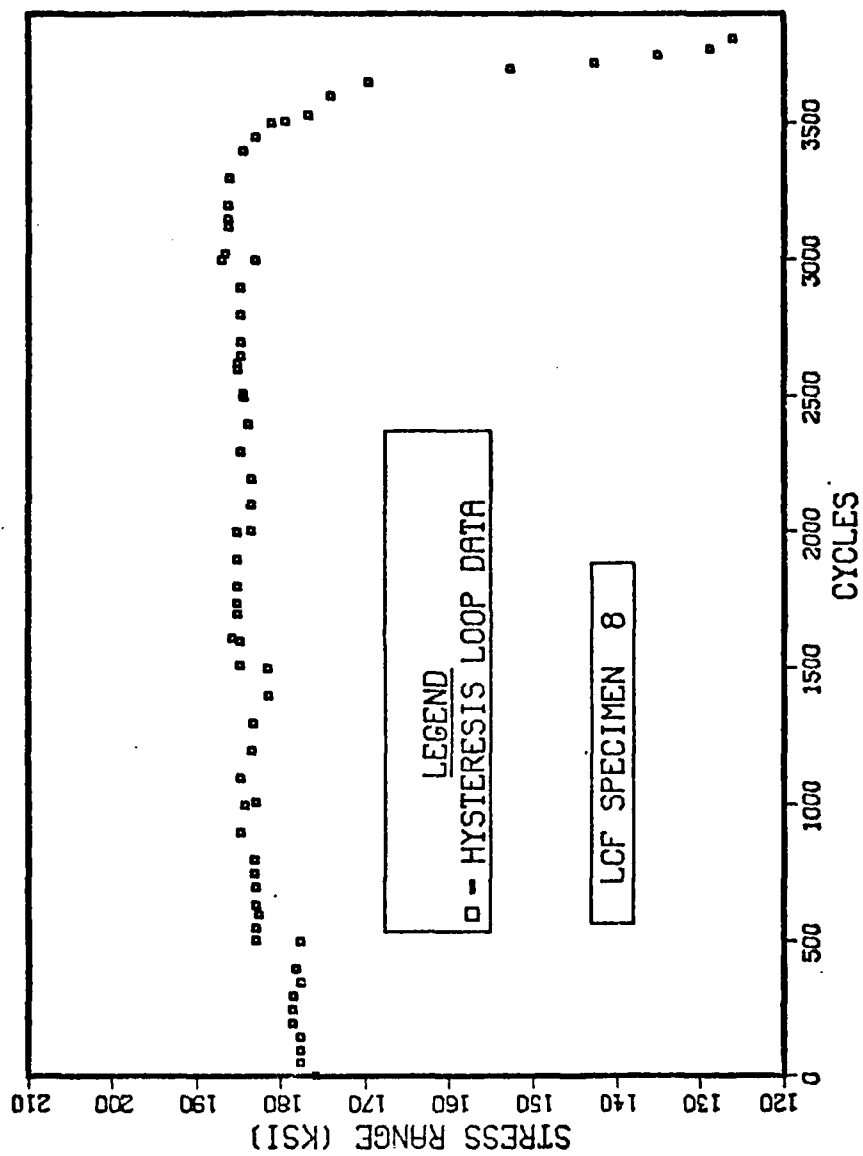


Figure 33. Plot of Stress Range vs Cycles - LCF Specimen 8

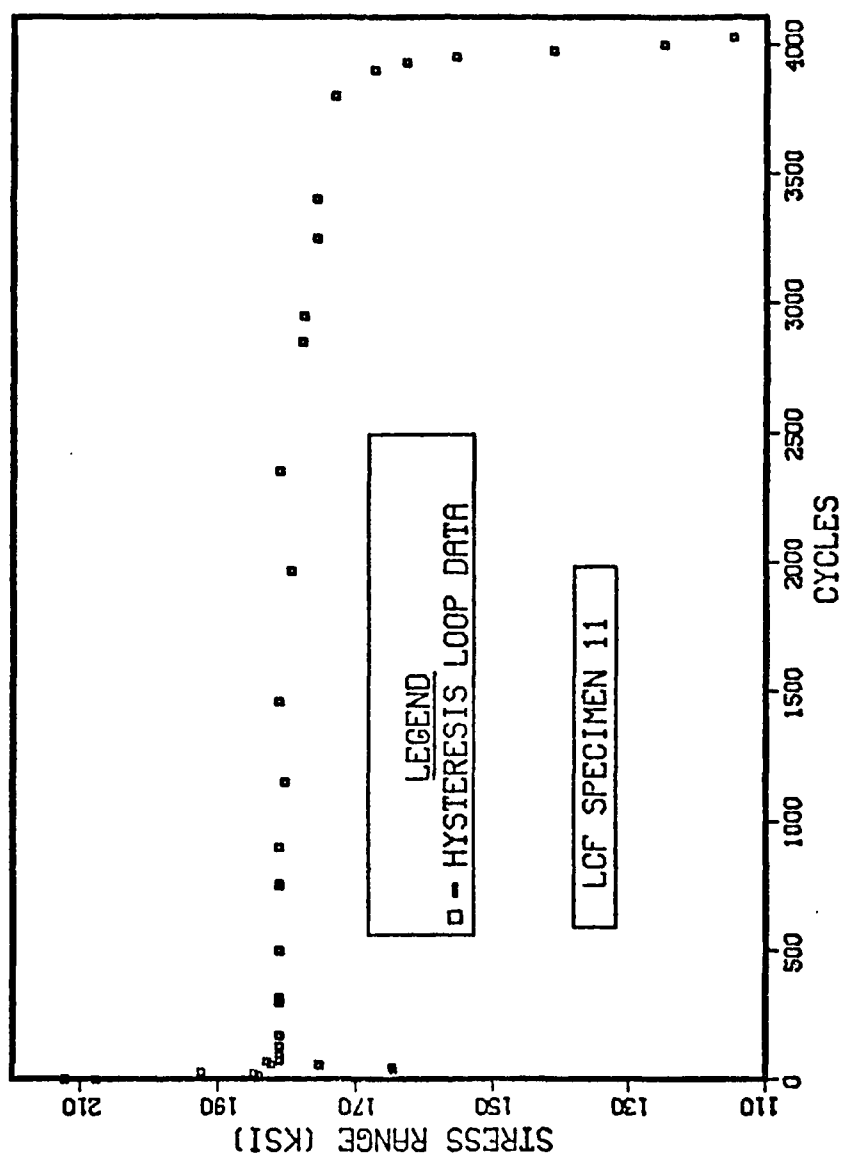


Figure 34. Plot of Stress Range vs Cycles - LCF Specimen 11

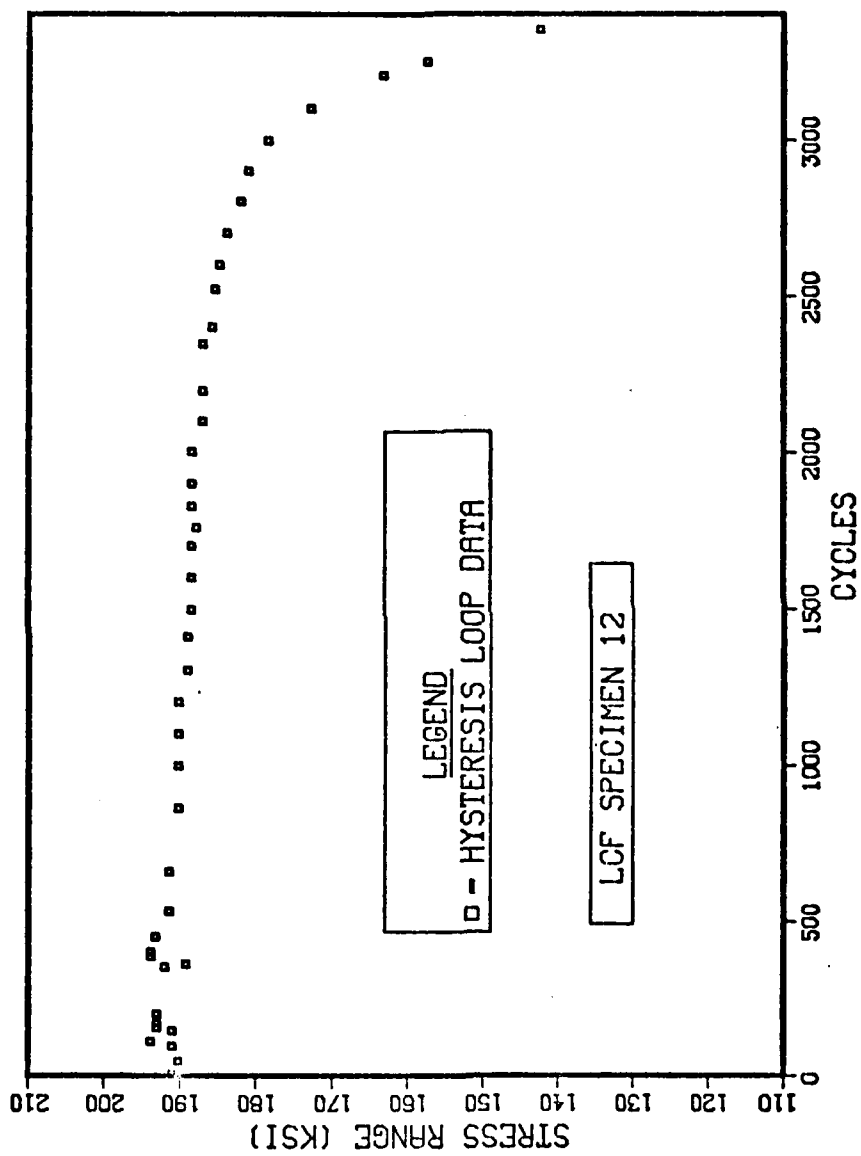


Figure 35. Plot of Stress Range vs Cycles - LCF Specimen 12

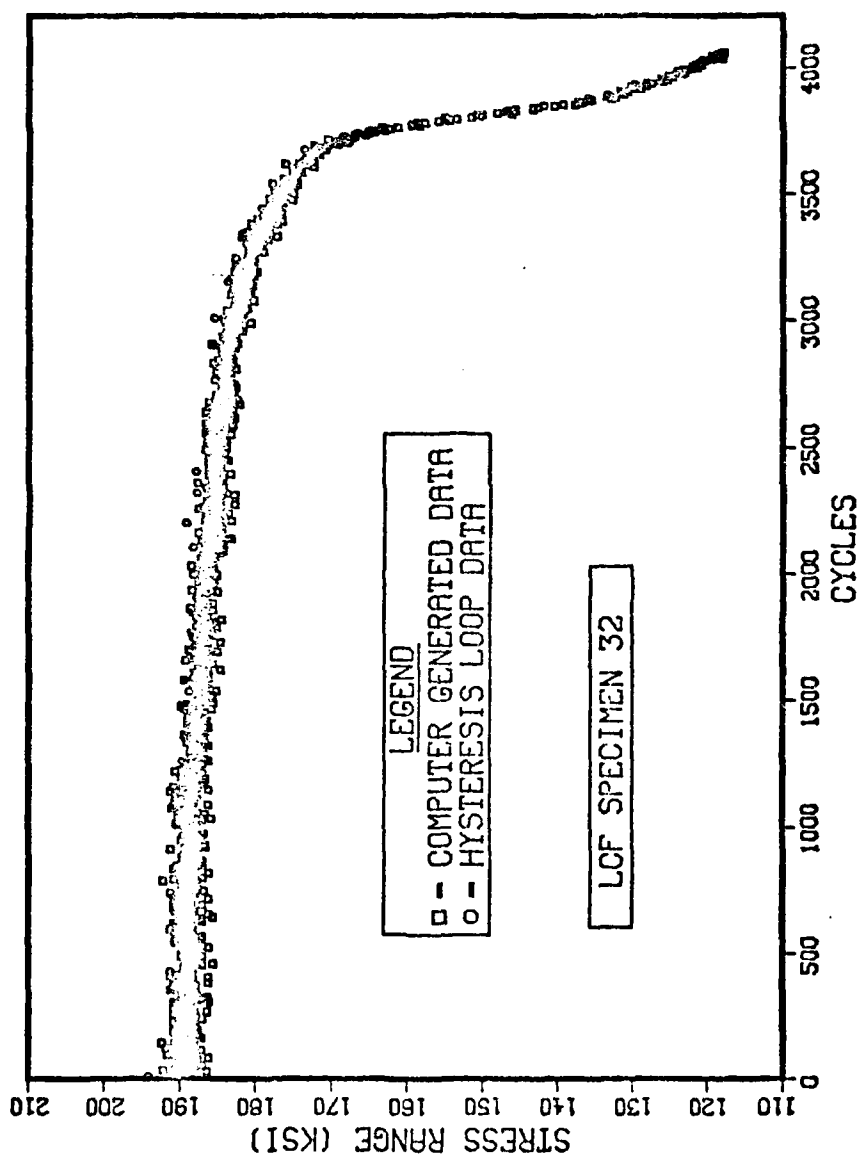


Figure 36. Plot of Stress Range vs Cycles - LCF Specimen 32

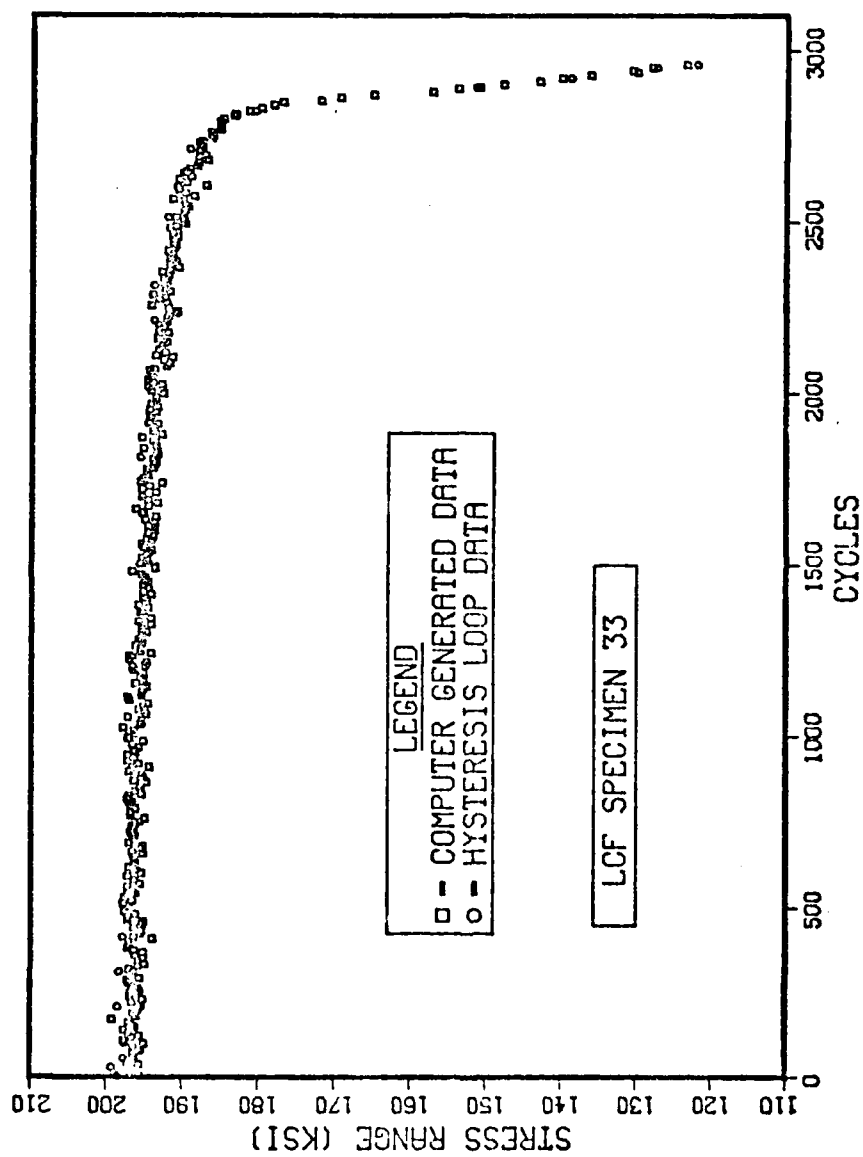


Figure 37. Plot of Stress Range vs Cycles - LCF Specimen 33

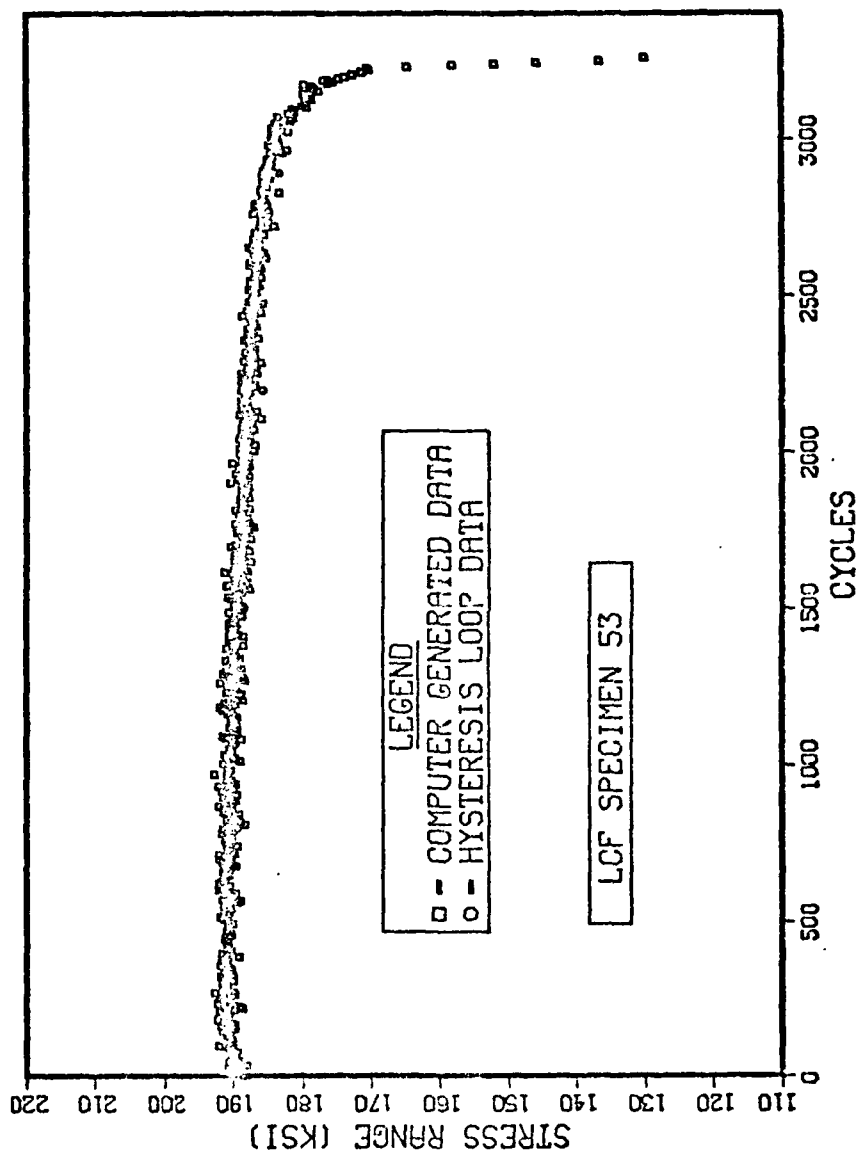


Figure 38. Plot of Stress Range vs Cycles - LCF Specimen 53

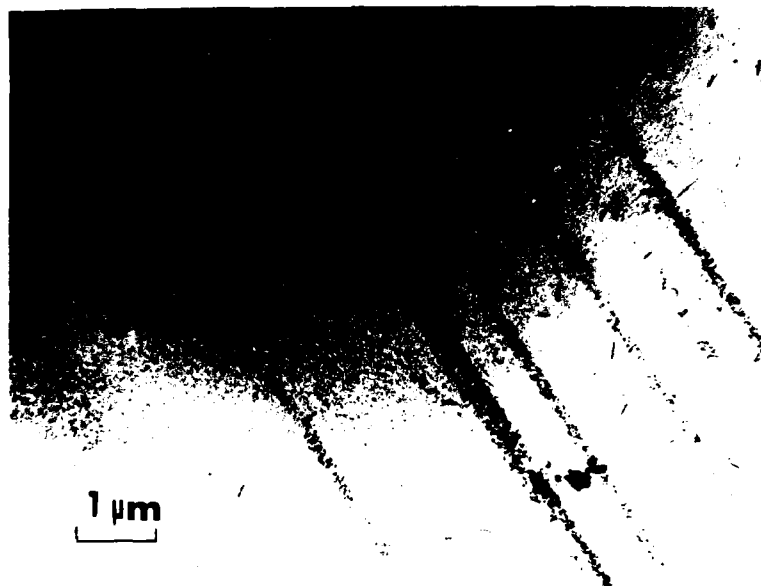
was obtained, in general, at every fifth cycle. The hysteresis loop data was usually obtained every 100 cycles. The effect of rejuvenation efforts will be discussed with respect to this baseline data.

ii. Dislocation Substructure

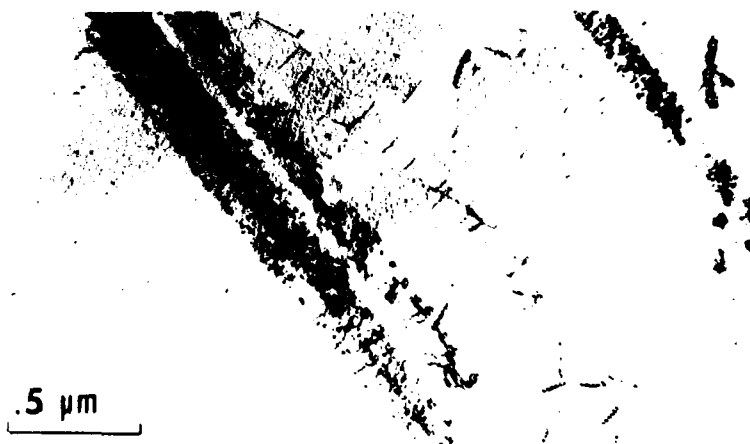
A typical dislocation substructure after a test is shown in Figure 39. The dislocations are aligned in bands, giving rise to the planar slip characteristics of this alloy. The dislocations are bowed around and looped around γ' precipitates, although cutting of the precipitates cannot be ruled out. Stacking fault contrast was observed in some precipitates, leading to the conclusion that they had been sheared. Using surface replication techniques, others have observed sheared γ' on the surface (16). Not every foil showed the concentration of slip bands depicted in Figure 39. Thus, deformation even at these higher strain ranges, is still somewhat localized.

iii. Fractography

Extensive fractography was carried out on samples which were removed unbroken from the fatigue machine and subsequently broken in tension. This procedure preserved the character of the fracture surface. The fractures were mixed mode, with both intergranular and transgranular regions. This behavior has been observed by others (16,45). A typical fractograph for LCF Specimen 33 is shown in Figure 40. Figure 41 is a higher magnification view of a likely crack initiation area. This was determined by following fatigue striations back to the edge. Typical fatigue striations are shown in Figure 42. Striations were seen close to the edge. Figures 43(a) and 43(b) demonstrate the cracking of carbides which lie on the fracture surface. The morphology of the



a. Planar Dislocations



b. Planar Dislocations

Figure 39. TEM Micrograph of Fatigued Specimens with Planar Dislocations

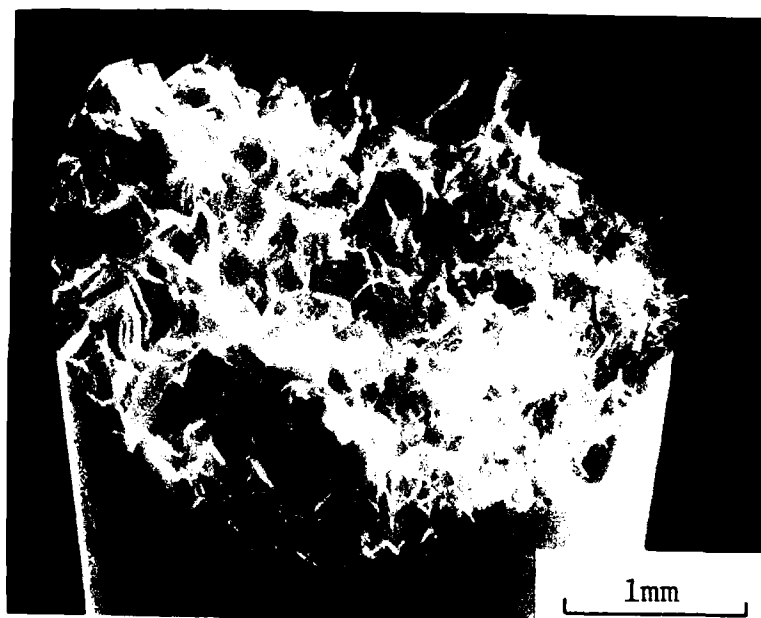


Figure 40. SEM Fractograph -- LCF Specimen 33

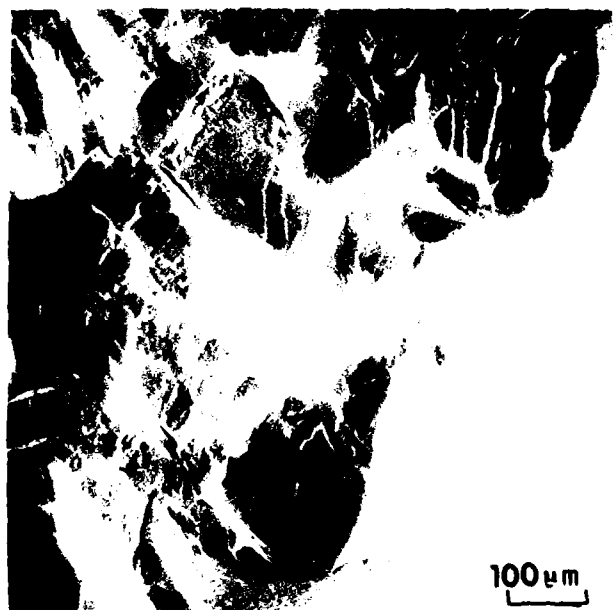
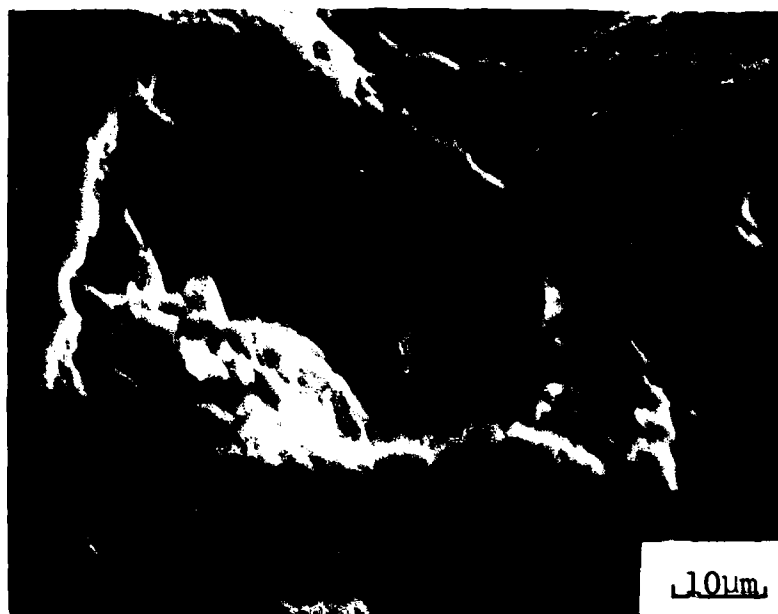


Figure 41. SEM Fractograph, Initiation Site - LCF Specimen 33



Figure 42. SEM Fractograph, Fatigue Striations - LCF Specimen 33



a. Cracked Titanium Carbide Particle



b. Cracked and Pull-Out Titanium Carbide Particles

Figure 43. SEM Fractograph, Cracked Carbides

carbide shown in Figure 43(a) suggests it may be a carbo-sulfide. The presence of these carbides may contribute to the large amount of longitudinal cracking which has been observed in this alloy (9).

D. Crack Initiation Mechanisms

i. Surface Replication

Surface replication during the course of fatigue testing was done in order to find the fraction of life at which crack initiation at 500°F occurred for total strain range of 0.75%. Two specimens, LCF Specimen 7 and LCF Specimen 8, were replicated at 500-cycle intervals. A composite of the replicas' photomicrographs are presented in Figures 44 and 46. Figure 44(a) shows the replication after 500 cycles of the area where the crack will initiate in LCF Specimen 7. At this magnification, there is no apparent crack, but persistent slip lines are evident. Figure 44(b), after 1000 cycles, still does not show a microcrack, but more intense deformation concentrated in the slip bands and grain boundaries is evident. Figure 44(c), after 1500 cycles, shows the first indication of microcracking. In Figure 44(d), after 2000 cycles, the cracking has extended into a persistent slip band. In Figure 44(e), after 2500 cycles, another microcrack becomes evident on the left-hand side. By Figure 44(f), after 3305 cycles, the two cracks have lined up and further extended. In the final series, Figure 44(g), after 3752 cycles (the last cycle), substantial crack propagation had occurred. A plot of Crack Length vs Cycles for LCF Specimen 7 is shown in Figure 45. When the crack length is extrapolated to zero length, the x-ordinate is intercepted at approximately 1500 cycles. The transition to rapid crack growth, N_1' , occurred at approximately 3400 cycles.



Figure 44. Micrographs of Replicas, Cracks - LCF Specimen 7



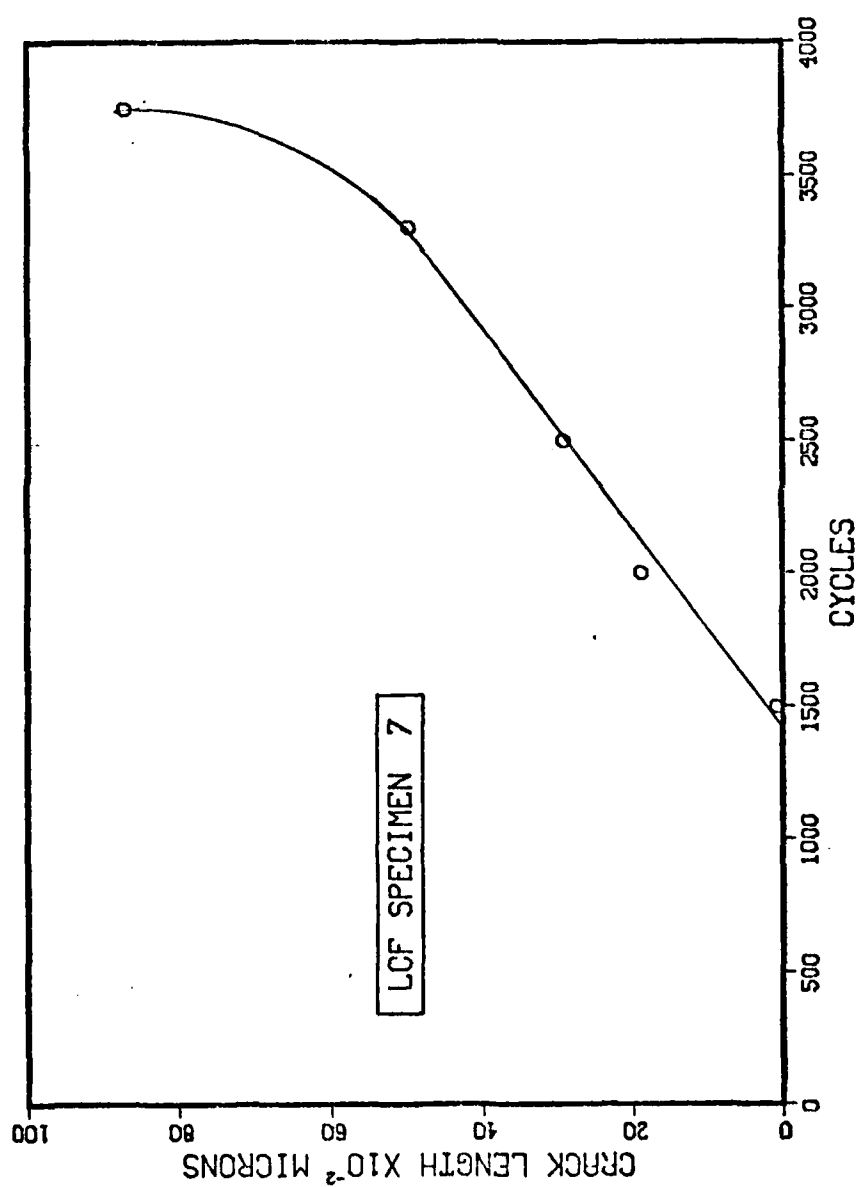


Figure 45. Plot of Crack Length vs Cycles - LCF Specimen 7

A composite of the photomicrographs of the surface replicas for LCF Specimen 8 is contained in Figure 46. In this specimen, three separate cracks form. Figure 46(a), taken after 500 cycles, shows the development of slip lines but no cracks are apparent. In Figure 46(b), after 1000 cycles, there is a persistent slip band evident in the upper right-hand portion of the collage which eventually becomes the upper crack. In Figure 46(c), after 1500 cycles, the V-shaped beginning of the middle crack is apparent. At 2000 cycles, Figure 46(d), the lower crack is evident as is a portion of the upper crack. Unfortunately, the middle crack is obscured by artifacts in the replica. In Figure 46(e), after 2500 cycles, all three cracks are clearly visible and several microcracks at either end of the middle crack are visible. By 3000 cycles, shown in Figure 46(f), the microcracks of the middle crack have linked up. Further crack extension by 3500 cycles, Figure 46(g), is readily apparent. A plot of Crack Lengths vs Cycles for LCF Specimen 8 is contained in Figure 47. The crack lengths plotted are the sum of the individual lengths. Since the measured crack lengths entailed some judgment, the scatter is not unreasonable. At the early cycles, it is especially difficult to ascertain if a crack exists and to measure its extent. Extrapolating the data back to zero crack length, it appears that crack initiation occurred at approximately 1300 cycles.

If the Stress Range vs Cycles plot for Specimens 7 and 8, contained in Figures 32 and 33, are closely examined, the asymmetric stress drop-off for LCF Specimen 7 occurs at about 1500 cycles and at about 1300 cycles for Specimen 8. These cycles correlate reasonably well with those determined from the crack length measurements. Therefore, the

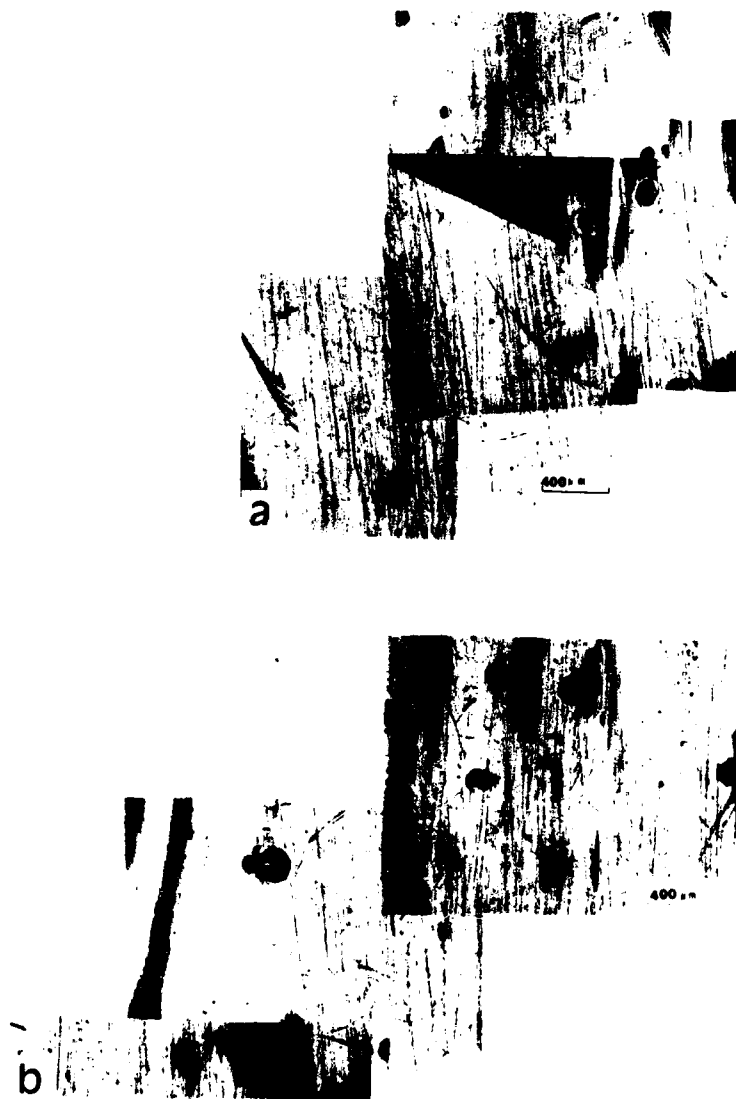
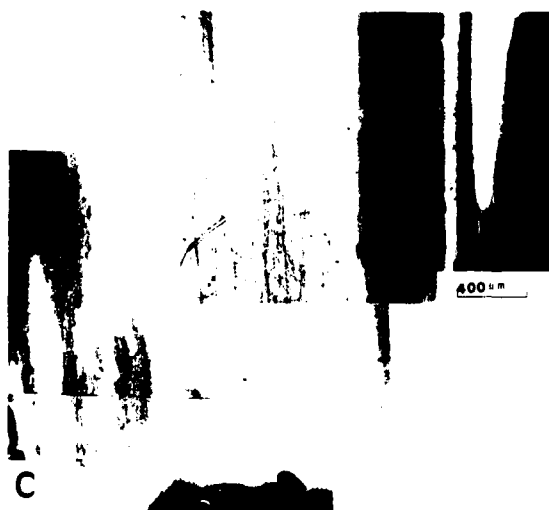


Figure 46. Micrographs of Replicas, Crack - LCF Specimen 8





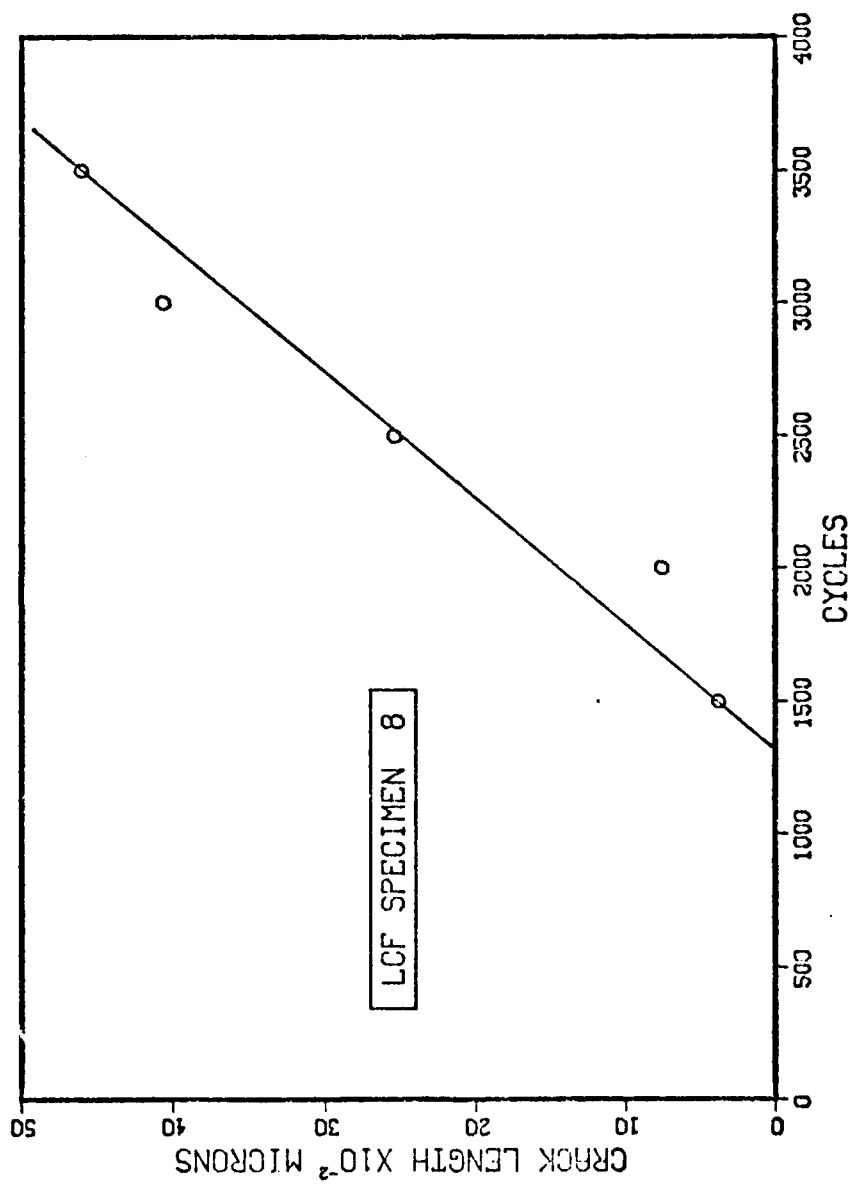


Figure 47. Plot of Crack Length vs Cycles - LCF Specimen 8

asymmetric load drop-off is used in the remainder of this dissertation as evidence that a definite crack exists. In Table 9, N_i is thus a measure of the crack initiation cycle. Furthermore, a damage level of 800 cycles was selected for rejuvenation efforts since it seemed well below the actual crack initiation point.

The slope of the lines in Figures 45 and 47 yields a crack growth rate, da/dN , of $0.27 \mu\text{m}/\text{cycle}$ or $1.07 \times 10^{-4} \text{ in.}/\text{cycle}$. Macha has determined crack growth rates as a function of ΔK at 400°F and 600°F (62). At 400°F he found that:

$$\frac{da}{dN} = 0.15 \times 10^{-9} (\Delta K)^{2.9} \quad (14)$$

where da/dN is crack growth rate in $\text{in.}/\text{cycle}$, and ΔK is stress intensity range in $\text{ksi} \sqrt{\text{in.}}$. At 600°F , he found:

$$\frac{da}{dN} = 0.10 \times 10^{-9} (\Delta K)^{3.2} \quad (15)$$

Since these expressions have the form:

$$\frac{da}{dN} = C (\Delta K)^m \quad (16)$$

C and m can be estimated to be 0.125 and 3.05, respectively, at 500°F , by simple averaging. Thus, at 500°F it is estimated that:

$$\frac{da}{dN} = 0.125 \times 10^{-9} (\Delta K)^{3.05} \quad (17)$$

By finding ΔK for a fatigue crack in the LCF test specimen, Equation 17 can be used to verify the replication-derived crack growth rate. Irwin's methodology for a semi-elliptical crack, correcting for the plane strain plastic zone in a finite body, was used (63). It is only an approximation for the geometry of the LCF specimen. The details of the calculation are presented in Table 11. The computed value of

TABLE 11
CALCULATION OF CRACK GROWTH RATE FROM FRACTURE MECHANICS

- Assumptions:
1. Initial flaw size, $2c$, of 0.118 in. (3000 μm)
 2. Crack aspect ratio, $a/2c$, of 0.30
 3. Stress range, $\Delta\sigma$, of 190 ksi
 4. Ratio $\sigma_{\text{max}}/\sigma_{\text{y.s.}}$ of 0.75
 5. $da/dN = 0.125 \times 10^{-9} (\Delta K)^{3.05}$

Calculation: Irwin's equation of interest is

$$K_I = \frac{1.1 \sigma \sqrt{\pi a}}{\sqrt{Q}}$$

$$\text{where } Q = \int_0^{\pi/2} \left[1 - \left(\frac{c^2 - a^2}{c^2} \right) \sin^2 \phi \right] d\phi = 1.12 \left[\frac{\sigma}{\sigma_{\text{y.s.}}} \right]^2$$

Using the above assumptions, $Q = 1.4$. Thus $\Delta K = 107.5 \text{ ksi } \sqrt{\text{in.}}$

From Assumption 5,

$$\frac{da}{dN} = 1.96 \times 10^{-4}$$

$da/dN = 1.96 \times 10^{-4}$ in./cycle agrees reasonably well with the measured value.

Higher magnification photographs of the replicas taken for Specimens 7 and 8 revealed evidence of a concentrated deformation zone along grain boundaries. But since these specimens were not lightly etched prior to testing, these observations were inconclusive.

ii. Surface Scanning Electron Microscopy

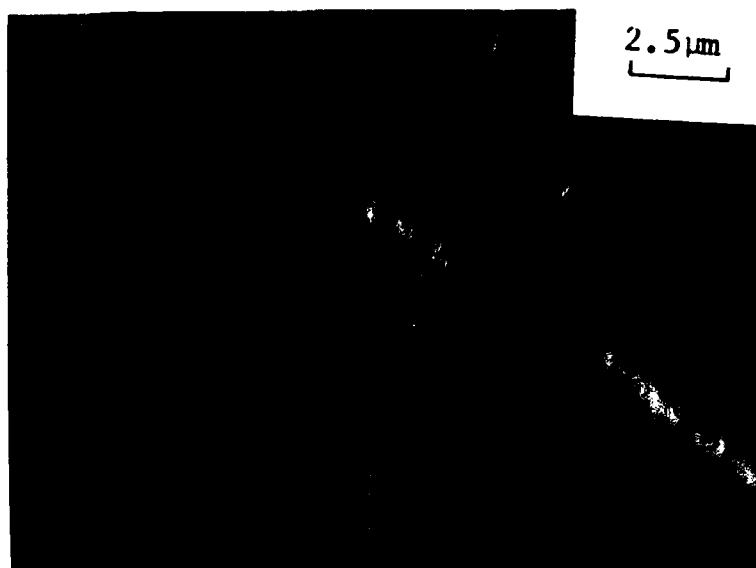
The above replication procedure was invaluable for finding cracks during a fatigue test, but it was not suitable for defining the crack initiation mechanisms for the following reasons: (1) The sharp radius of curvature of the LCF specimen made the replication process extremely difficult to accomplish without producing artifacts in the replica; and (2) A cycle of cooling the specimen, replicating it, and reheating the specimen for further testing took 3-4 hours with the consequence that a great deal of time was consumed in the testing.

With these difficulties in mind, several different approaches were taken to better determine the crack initiation mechanism: (1) A LCF specimen was lightly etched prior to testing and a search was made for offsets in the longitudinal polishing scratches at grain boundaries; (2) A LCF specimen had two parallel flats machined longitudinally and the specimen was electropolished (one flat was lightly etched), and after 1800 cycles of testing at 500°F at a strain range of 0.75%, the flats were examined in the SEM; (3) A specimen was tested at room temperature and replicated every 300 cycles until the asymmetric load drop-off occurred and a definite microcrack could be seen; (4) A specimen, after complete testing, was placed directly in the SEM for

surface observation; (5) The gauge section of a specimen was examined in the SEM after 800 cycles of testing; and (6) A longitudinal section of a gauge section was made of a specimen tested to 2103 cycles. The results of these metallographical investigations are detailed below, and a proposed mechanism for crack initiation at 500°F at $\Delta\epsilon_t = 0.75\%$ is presented.

LCF Specimen 42 was lightly etched after polishing through 4/0 emery paper. After testing was completed, the gauge section was placed in the SEM. Using the straight polishing scratches as fiduciary marks, offsets of them along grain boundaries were observed. Figure 48(a) and (b) show typical offsets at grain boundaries. There is an apparent curvature of the scratches in the vicinity of the grain boundary indicating the existence of a band of deformation along the boundary. Also, the offsets along a boundary are not uniform. The formation of grain boundary ledges was not readily apparent, but this experimental technique may not have been sensitive enough to detect them. Figure 48(c) shows offsets along a persistent slip band. Note that the polishing scratches which pass through a persistent slip band are relatively straight right up to the band, and that the offsets along the length of the band are reasonably uniform.

LCF Specimen F2 had two flats machined which were mechanically polished and then electropolished. One flat was lightly etched before testing. The stabilized stress range was 190.5 ksi, at total strain range of 0.75%. Crack initiation, as determined by the asymmetric load drop-off, occurred at 875 cycles. The fatigue test was halted at 1800 cycles and the flat surfaces examined in the SEM. Figure 49 shows

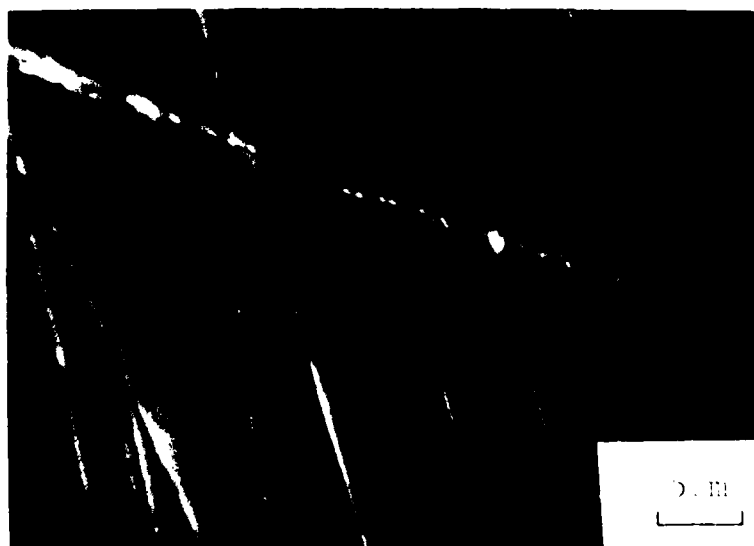


a. Offset of Polishing Scratch at a Grain Boundary



b. Offset of Polishing Scratches at a Grain Boundary

Figure 48. Electron Micrographs Depicting Grain Boundary Offsets



c. Offset of Polishing Scratches at a Persistent Slip Band



Figure 49. SEM Micrograph, Crack at Carbide - LCF Specimen F2

cracks leading away from a large carbide inclusion. Figure 50 graphically shows slip lines and cracks associated with two blocky carbides. The slip lines are at nearly a 45° angle with respect to the longitudinal stress axis.

LCF Specimen 36 was tested at room temperature after light etching. The stress range, after 500 cycles, constantly decreased at the rate of 3.2 psi/cycle. The stabilized stress range was 222 ksi at a total strain range of 0.73%. The test was stopped at 3900 cycles and the specimen broken in liquid nitrogen for fractographic examination. Figure 51 is a 100 \times view of a replica of a typical area after 3900 cycles. The slip lines within each grain are clearly evident. As the test progressed, there appeared to be a gradual thickening of the grain boundary regions. Using the longitudinal polishing scratches as fiduciary marks, higher magnification definitely revealed offsets along the grain boundaries. Figure 52 shows a typical crack which apparently initiated at a grain boundary carbide. On the fractograph, it was difficult to differentiate the fatigue initiated fracture from the tensile overload fracture.

LCF Specimen 53, which was electropolished before testing, was placed directly in the SEM after testing at 500 $^{\circ}$ F. Table 9 has a summary of its properties. Figure 53 shows a portion of the main crack. Note the grain which pulled out in the center of the photograph. This crack follows a combined transgranular and intergranular path on the surface. Figure 54 shows fatigue striations in an intergranular crack region which are obvious from looking in from the surface. Figure 55



Figure 50. SEM Micrograph, Crack at Carbide - LCF Specimen P2



Figure 51. Micrograph of Replica - LCF Specimen 36

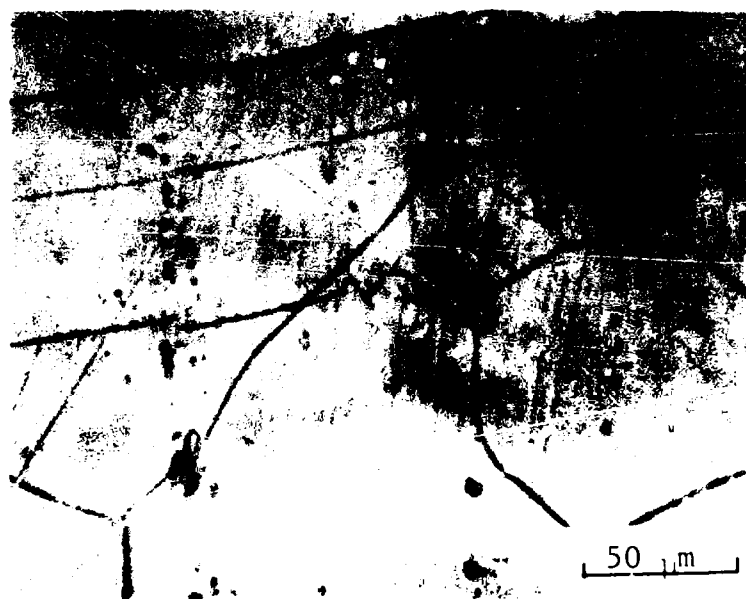


Figure 52. Micrograph of Euphlea, Crack at Carbide - LCI Specimen 26



Figure 53. SEM Micrograph, Main Crack - ICF Specimen 53



Figure 54. SEM Micrograph of bat fecal stratification + EPR Spectroscopy

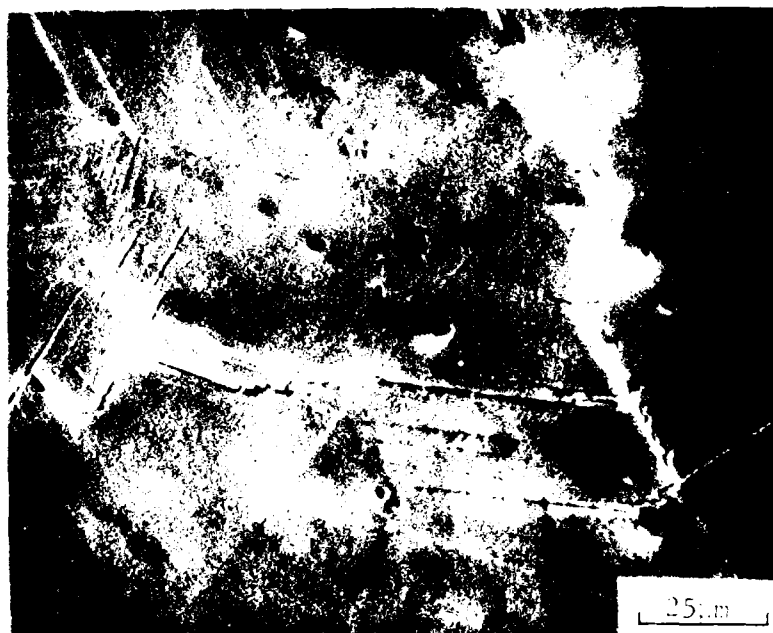
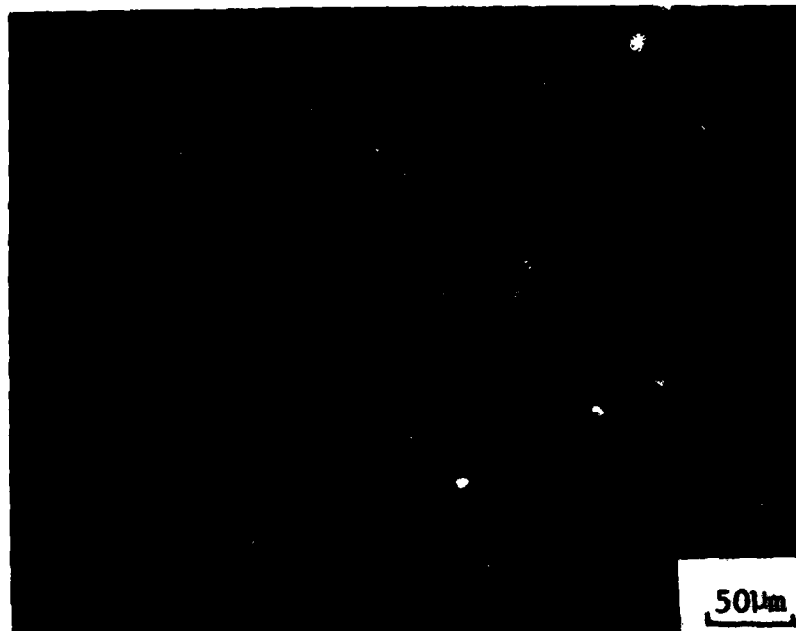


Figure 55. SEM Micrograph, Secondary Cracking - UGP Specimen 53

shows surface cracking which occurred at some distance from the main crack. The crack associated with the carbide is normal to the loading direction.

LCF Specimen 38 was removed from the Instron after 800 cycles at 500°F at a total strain range of 0.77%. It was lightly etched before testing. Figure 56(a) shows the general microstructure as viewed in the SEM. Figure 56(b) is a high magnification view of the slip line in the center of Figure 56(a). At this magnification, the slip line is seen to be an extrusion band. These extrusions were also commonly seen on other fatigue specimens examined in the SEM with greater than 800 cycles of damage. Figure 57(a) shows a blocky carbide in a grain boundary. Figure 57(b) shows that this carbide is beginning to de-cohere. The microstructural damage observed in this specimen at this stage of testing occurred well before the asymmetric load drop-off or the initiation of microcracking.

LCF Specimen 39 was tested at 500°F at a total strain range of 0.77%. The test was stopped after 2103 cycles. Crack initiation, determined by the asymmetric load drop method occurred at 1300 cycles. The specimen was sectioned longitudinally, lightly etched, gold plated, and examined in the SEM. Figure 58 shows the general microstructural appearance. The blocky carbide stringers and the grain boundary Laves phase are clearly evident, as are the small spherical precipitates. Figure 59(a) shows a crack along an apparent slip plane which is oriented 60° with respect to the applied load. Figure 59(b) is a magnified view of the edge of the crack. Figure 59(c) shows a crack running from the edge along a grain boundary oriented at 30° with respect to the applied



a. General Microstructure

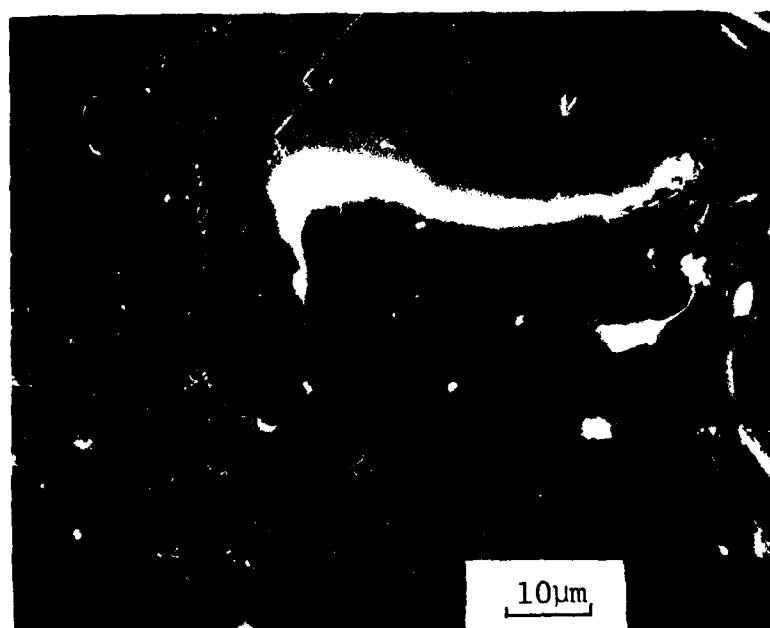


b. Extrusion

Figure 56. SEM Micrograph, Extrusion after 800 Cycles - ICF Specimen 38



a. Blocky Carbide

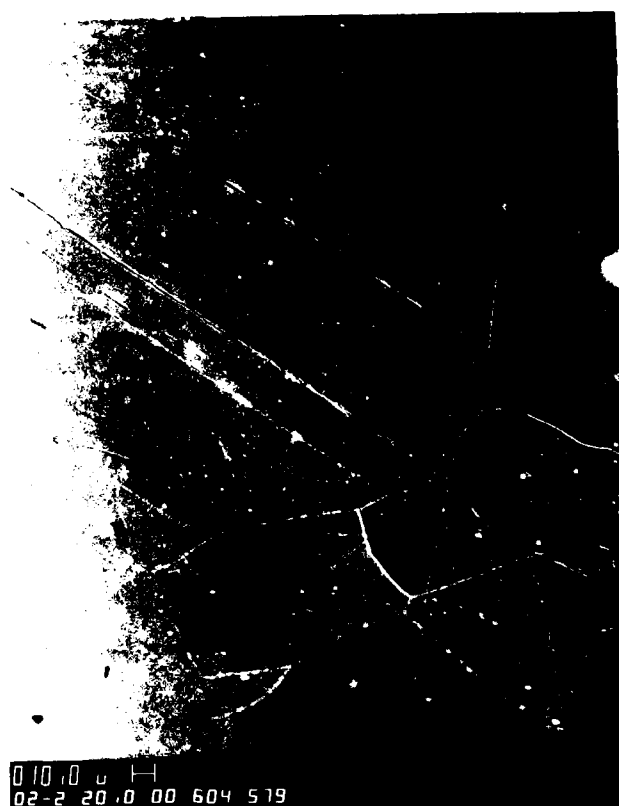


b. Magnified View of Carbide

Figure 57. SEM Micrograph, Decohering Carbide after 800 Cycles -
LCP Specimen 38



Figure 58. SEM Micrograph, Longitudinal Section after 2103 Cycles - LCF specimen 39



a. Crack 1

Figure 59. SEM Micrograph, Cracks in Longitudinal Section after 2103 Cycles - LCF Specimen 39



b. Higher Magnification View of Crack 1



c. Crack 2

stress. Note that as predicted by Kim and Laird, the crack is not symmetric with respect to the boundary, but propagates primarily in one grain (48). These cracks, as they progressed into the specimen, followed a path either along another slip plane in a grain or along a grain boundary, but not deviating by more than 15° from a 45° angle with respect to the applied stress. Blocky carbides did seem to be associated with crack propagation into the thickness.

iii. Proposed Mechanism

At 500°F and within the total strain range 0.7-0.8%, this material can initiate cracks at persistent slip bands or at grain boundaries, whichever is energetically favorable. Generally, cracks initiate at blocky carbide inclusions in those grain boundaries oriented between 30° and 60° with respect to the principle tensile direction. The combination of a deformation zone along a grain boundary, as evidenced by the offsets of polishing scratches across the boundaries, and the tendency to develop grain boundary steps, as developed by Kim and Laird (47,48), results in large compatibility strains between the carbide and the grains which are relieved by the decohering of the carbide. This marks the start of Stage I propagation and is noted by the start of the asymmetric load drop-off. Once the crack begins to propagate along a grain boundary away from the carbide, it either continues growing along the boundary both on the surface and into the material, or it turns and begins to propagate along a favorably oriented persistent slip band which had already formed a crack embryo in the form of intrusions/extrusions. Since the strain range is fairly high, these nucleation events occur at multiple locations. Once these cracks begin to link up, the crack

grows more rapidly, leading to a much larger decrease in stress drop-off per cycle. The point at which this happens corresponds to N_i' in Table 9.

Thus, the carbides play a key role in the crack initiation process, but are not as important during crack propagation. Stage I cracking generally ends when the crack reaches the end of a grain or a grain boundary triple point in terms of through the thickness of the crack dimension.

The material is ductile enough so that Stage II cracking leads to the formation of fatigue striations. It is not surprising that the fracture surface shows both intergranular and transgranular cracking.

It is clear that after 800 cycles, well before the start of Stage I crack growth, substantial microstructural damage in the form of partially de-cohered carbides and persistent slip bands already exists. This information is crucial in evaluating the effects of the rejuvenation treatments.

IV. REJUVENATION EFFECTS

A. Results of HIP Treatments

i. Presentation of Data

The results of the 11 specimens, pre-damaged in LCF to a given number of cycles, hot isostatically pressed and heat treated, and then retested to failure, are summarized in Table 12. The plots of stress range vs cycles are contained in Figures 60-70. Specimen 16 was mechanically polished and electro-polished three times before retesting.

It is apparent from this data, in comparison with the baseline data of Table 9, that no rejuvenation by HIP occurred. The ceramic

TABLE 12
SUMMARY OF HIP REJUVENATION ON LCF PROPERTIES

Specimen	Prior Damage Cycles	Strain Range (%)			Stress Range (ksi)	Cycles			N _f /N _f	N _f '/N _f	Remarks
		Δε _t	Δε _p	Δε _e		N _i	N _i '	N _f			
14	800	0.73	0.02	0.71	196.0	801	1750	2297	0.35	0.76	
16	800	0.73	0.03	0.70	193.0	1350	1800	2134	0.63	0.84	Electro-polished
18	800	0.72	0.03	0.69	189.0	1750	2250	2619	0.67	0.86	
19	800	0.76	0.05	0.71	195.5	1450	1650	1933	0.75	0.85	
20	800	0.73	0.02	0.71	194.8	1750	2350	3147	0.56	0.75	Coated
21	800	0.74	0.02	0.72	200.0	1150	1450	1797	0.64	0.81	Coated
22	800	0.76	0.05	0.71	197.0	1400	1700	2287	0.61	0.74	Coated
23	2100	0.76	0.05	0.71	195.0	2650	2950	3286	0.81	0.90	Coated
24	2100	0.70	0.04	0.66	186.5	801	2900	3862	0.21	0.75	
25	0	0.68	0.03	0.65	179.4	700	950	1573	0.45	0.60	Coated
29	0	0.77	0.04	0.73	202.0	900	1250	1660	0.54	0.75	

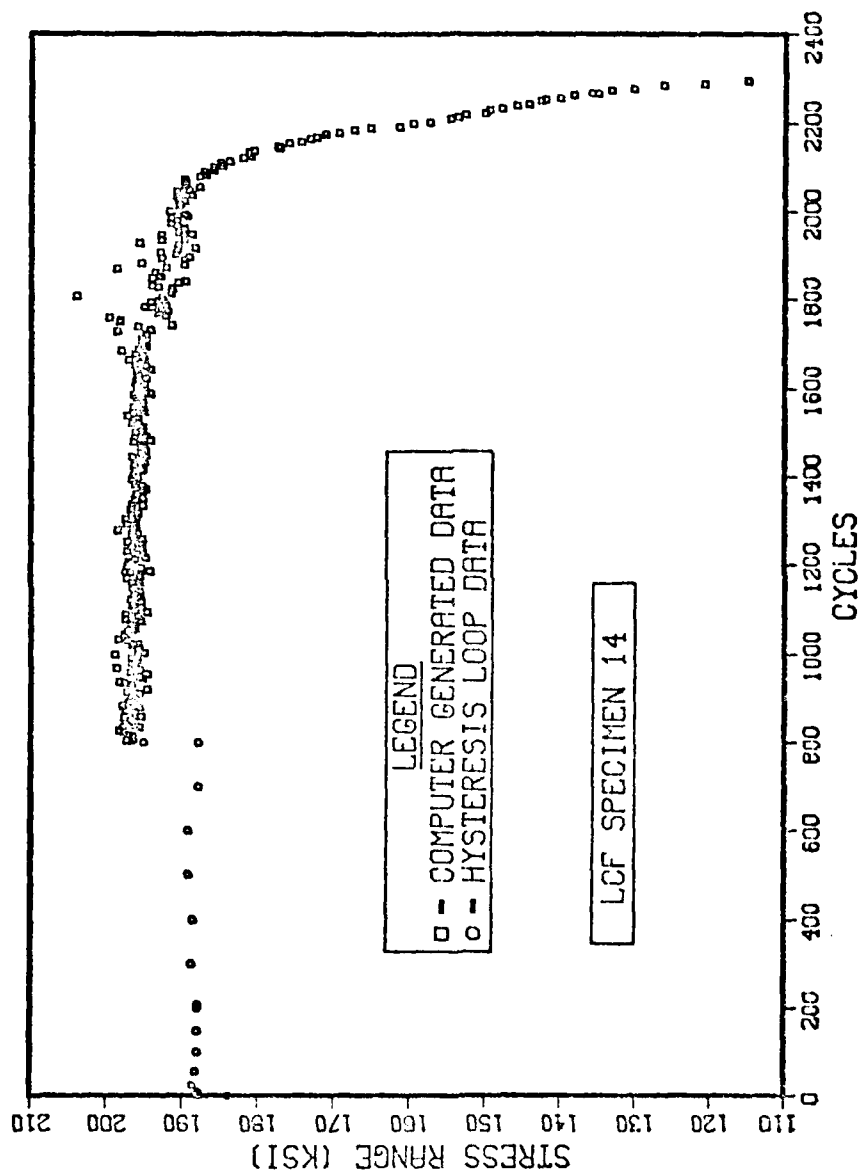


Figure 60. Plot of Stress Range vs Cycles - LCF Specimen 14

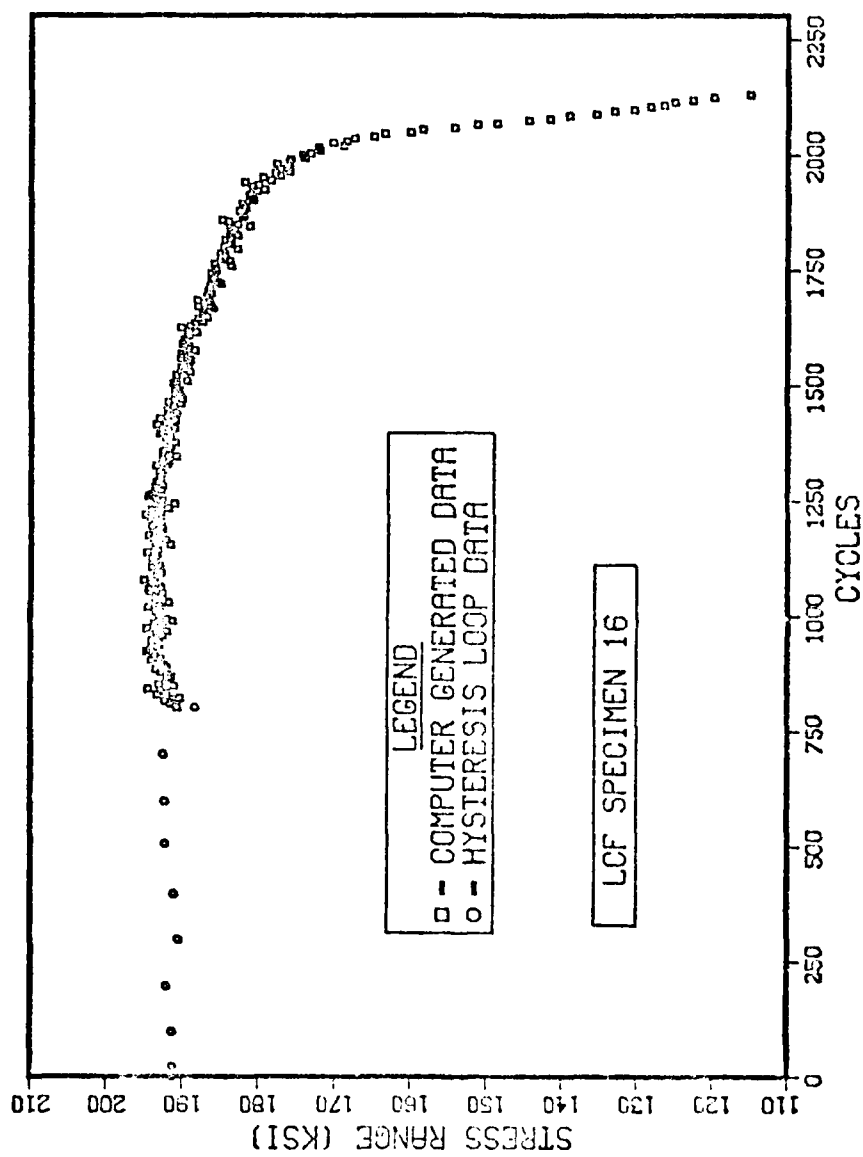


Figure 61. Plot of Stress Range vs Cycles - LCF Specimen 16

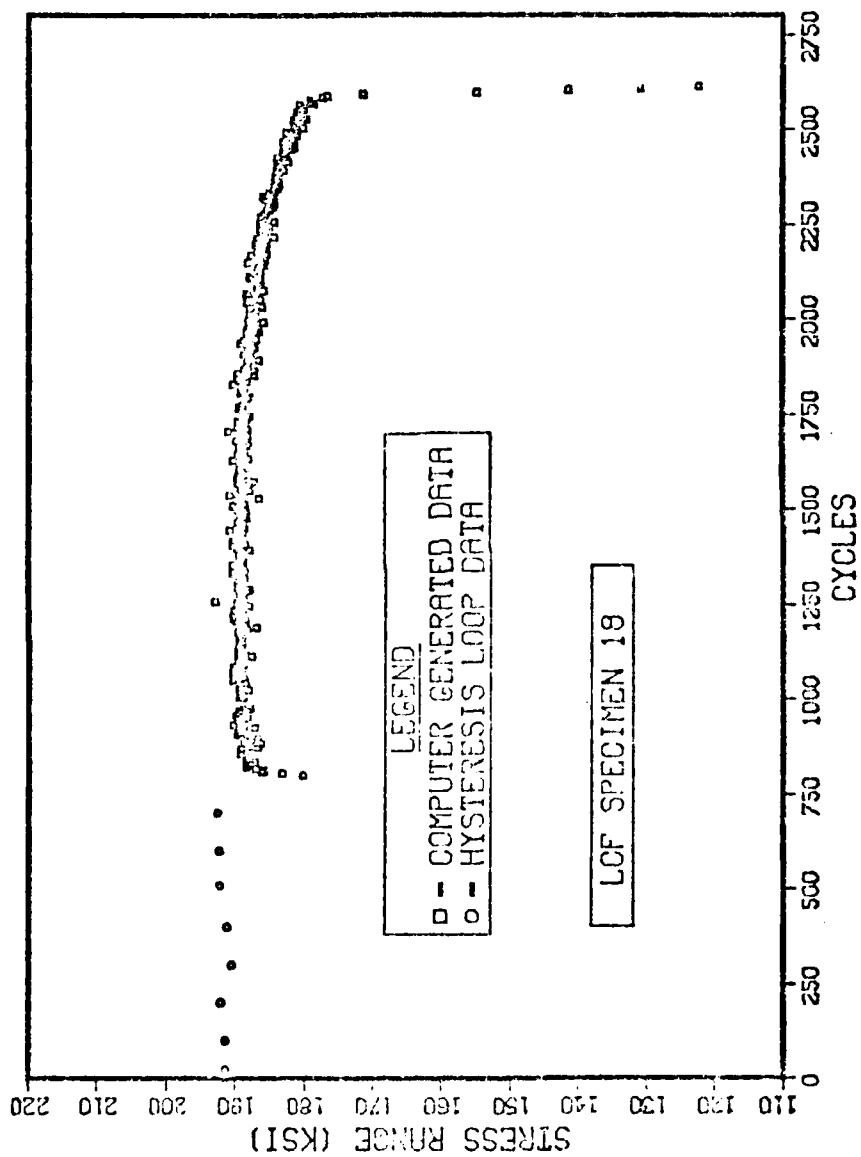


Figure 62. Plot of Stress Range vs Cycles - LCF Specimen 18

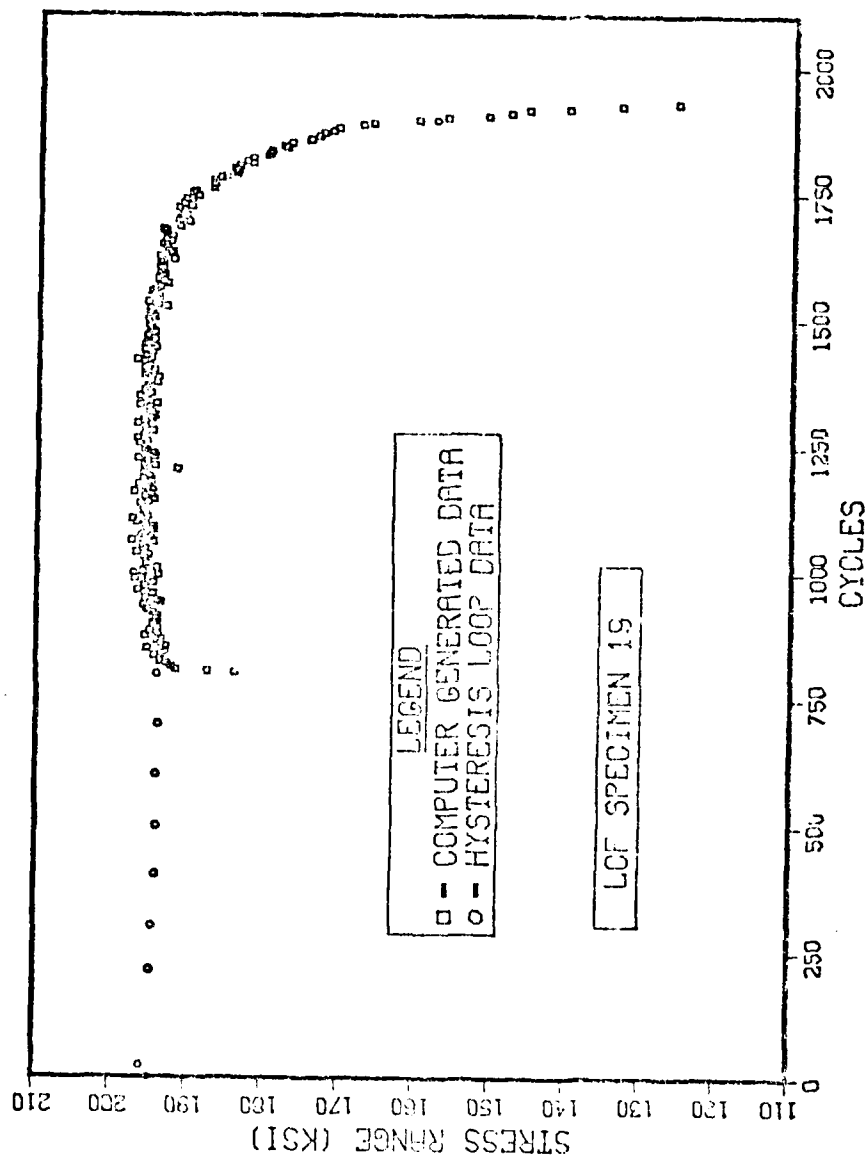


Figure 63. Plot of Stress Range vs Cycles - LCF Specimen 19

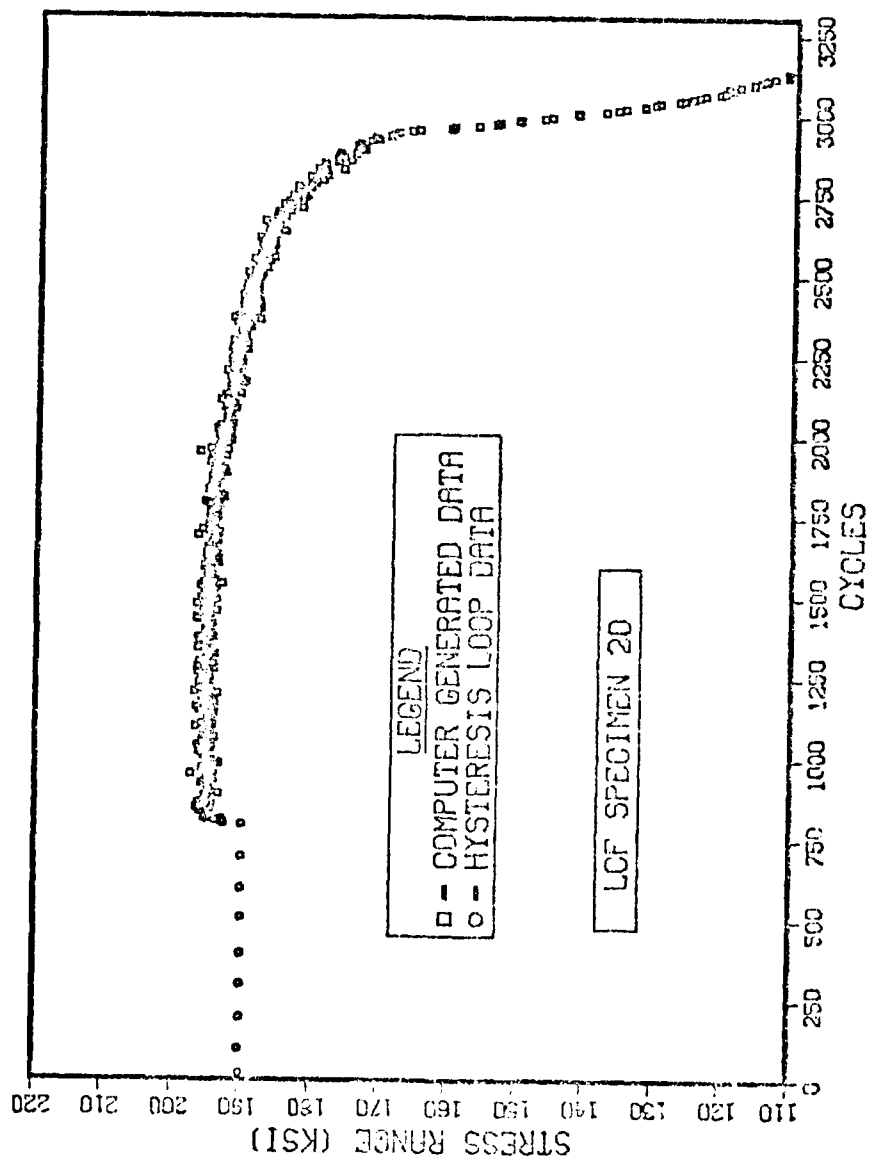


Figure 64. Plot of Stress Range vs Cycles - LCF Specimen 20

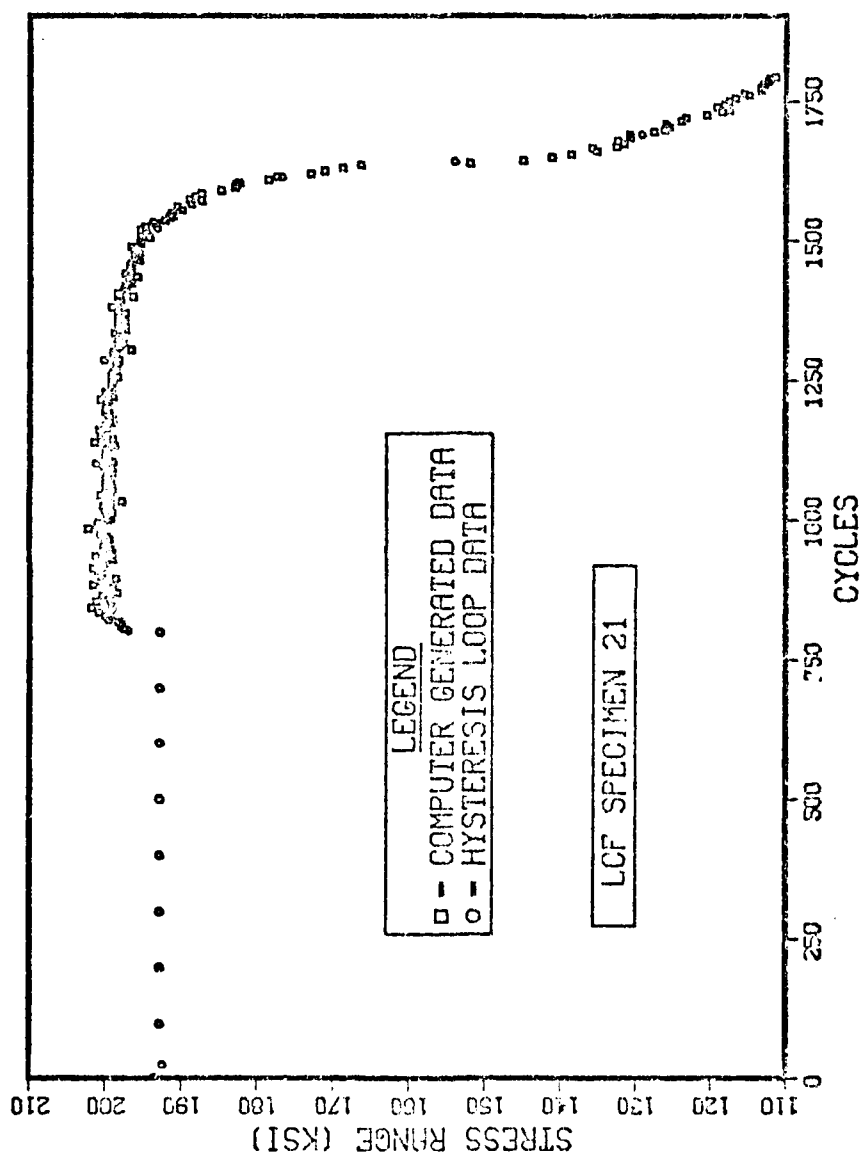


Figure 65. Plot of Stress Range vs Cycles - LCF Specimen 21

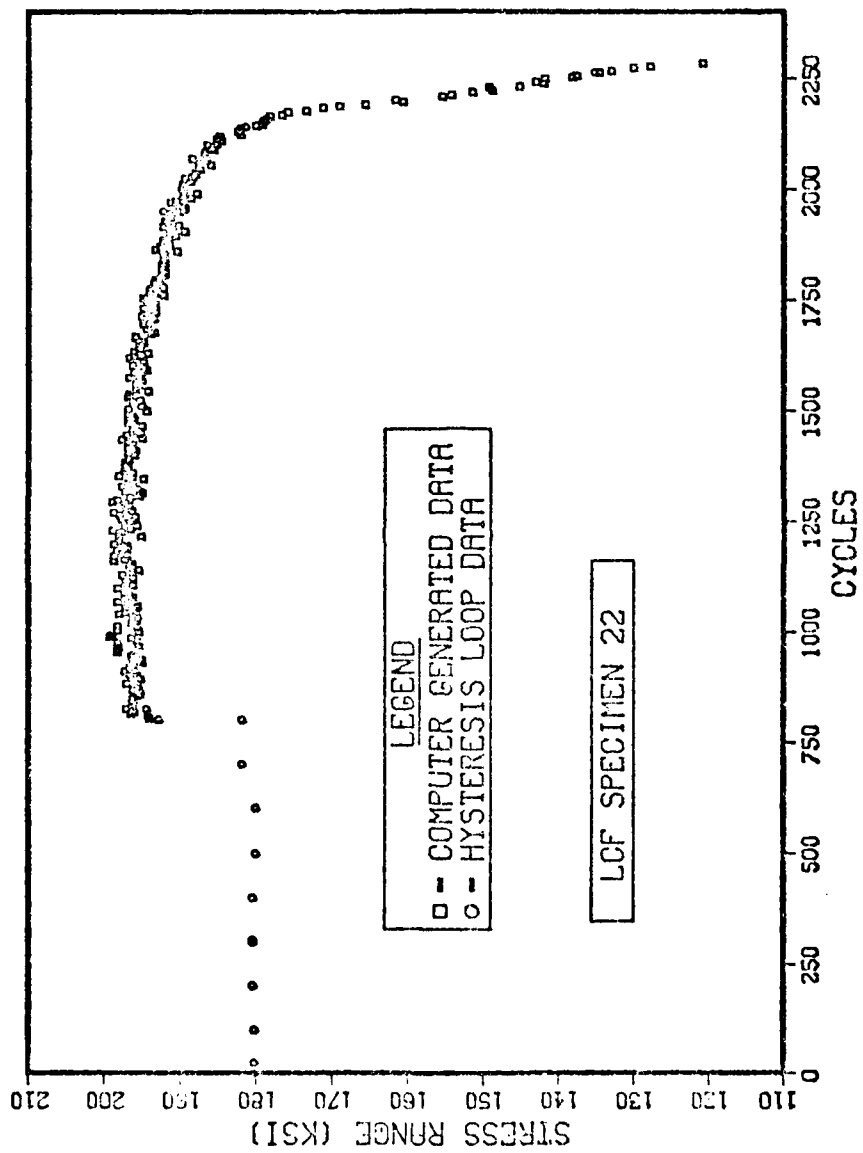


Figure 66. Plot of Stress Range vs Cycles - LCF Specimen 22

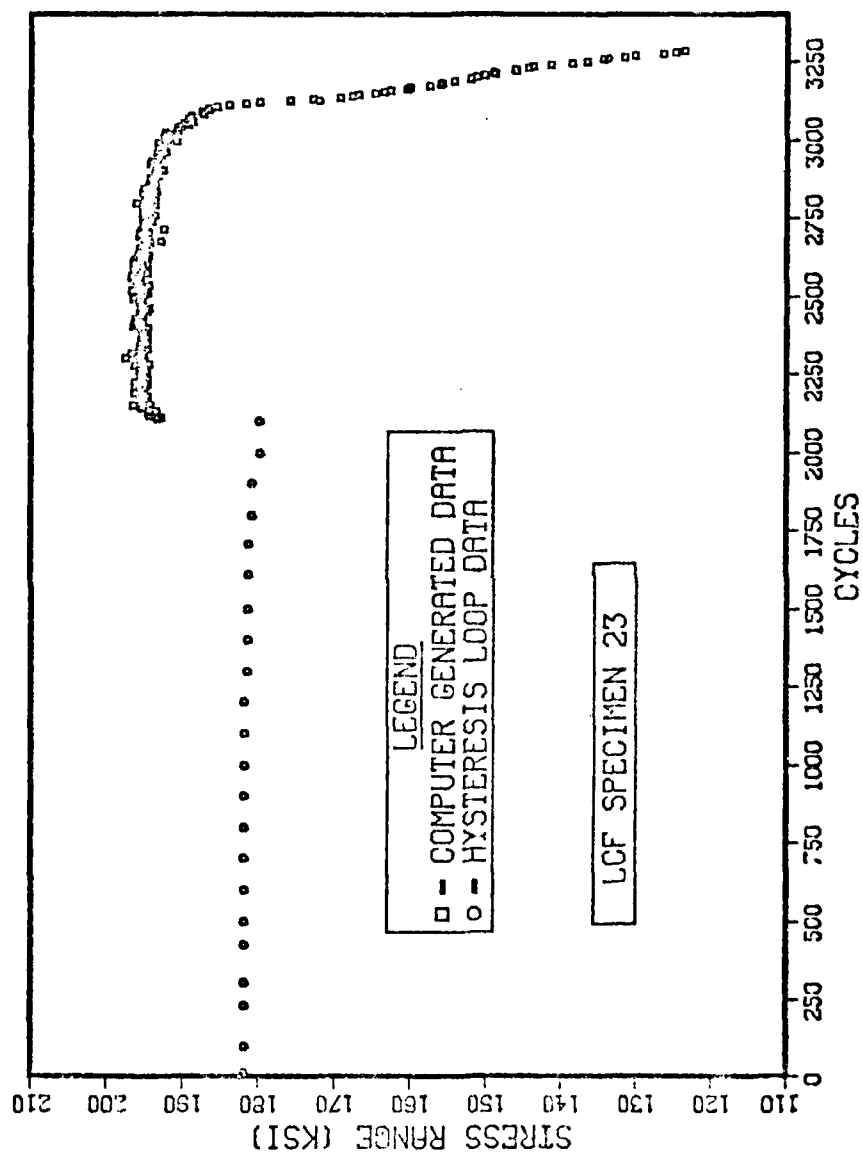


Figure 67. Plot of Stress Range vs Cycles - LCF Specimen 23

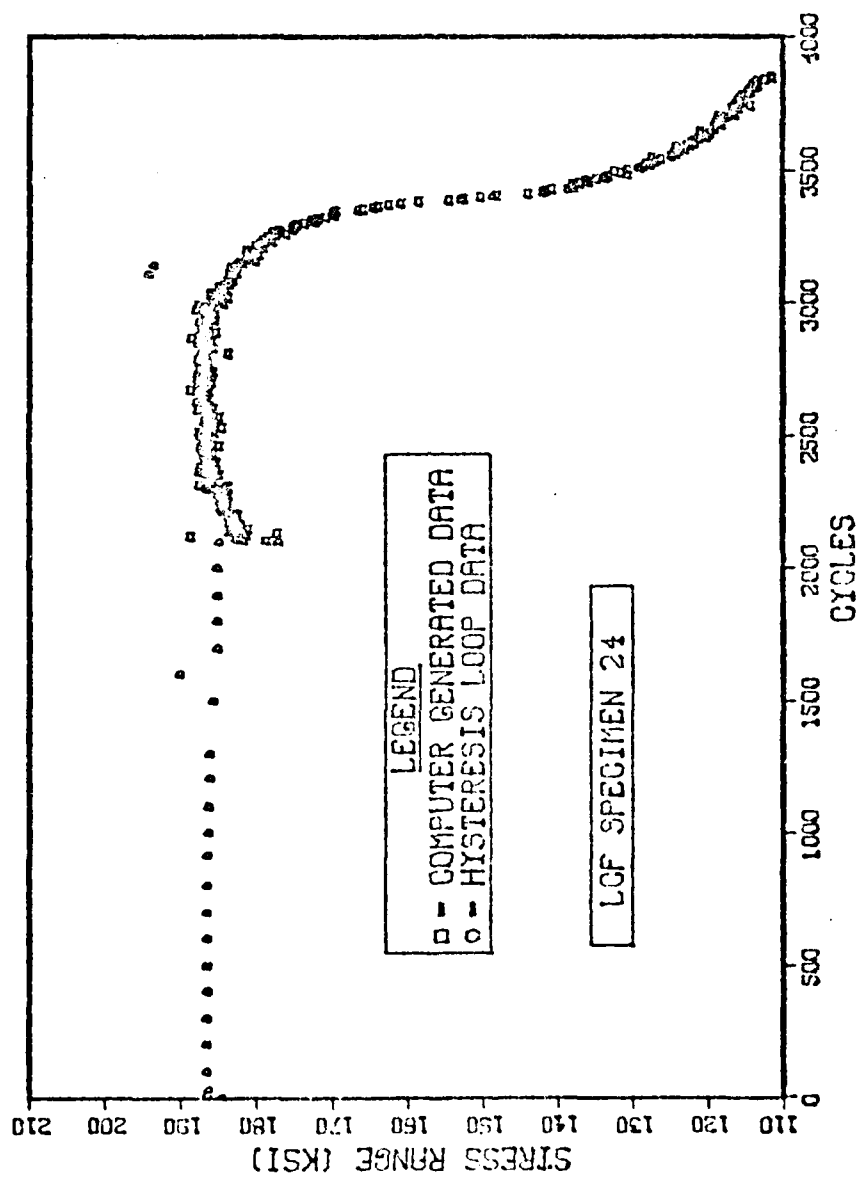


Figure 68. Plot of Stress Range vs Cycles - LCF Specimen 24

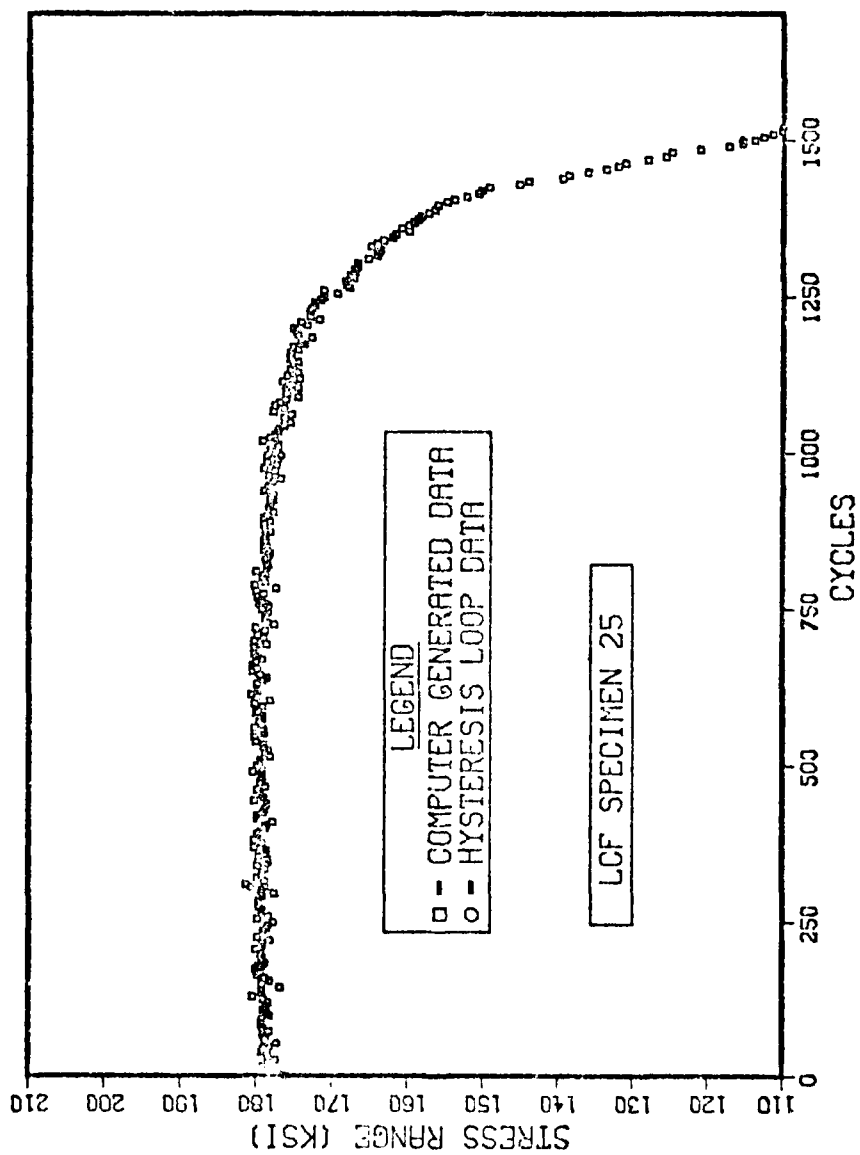


Figure 69. Plot of Stress Range vs Cycles - LCF Specimen 25

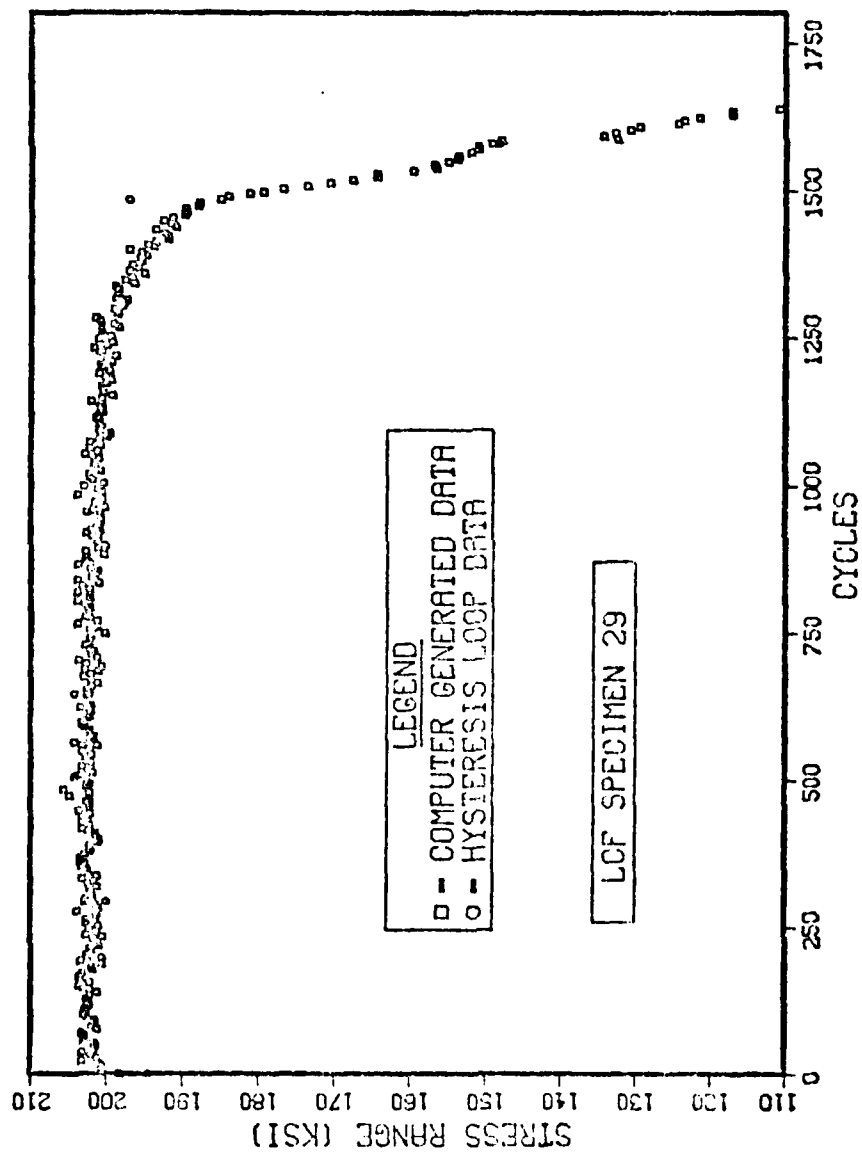


Figure 70. Plot of Stress Range vs Cycles - LCF Specimen 29

coated and the uncoated specimens performed about the same; although Specimen 20, which was coated, performed the best. On the basis of total life, these HIP specimens were clearly inferior to the baseline specimens. Specimens 25 and 29, which were HIP'd without prior damage, failed within the range of about 1600-1700 cycles. The remaining HIP'd specimens with different levels of pre-HIP damage also failed within this range of cycles after retesting commenced, regardless of the level of pre-HIP damage. This includes two specimens which were predamaged to 2100 cycles; crack initiation had already occurred in these specimens prior to the HIP treatment. This is strong evidence that the HIP processing itself adversely damaged the microstructure at the surface of the material.

Those specimens which were to be ceramic coated were first vapor honed to provide a suitable surface for the coating to adhere to. The effect of the vapor honed surface on the LCF properties was investigated. Figure 71 shows a SEM photomicrograph of the as-vapor-honed surface. The surface is fairly rumpled and some inclusions appear to have already decohered from the microstructure. The gauge section of two vapor-honed specimens was repolished and then tested at 500°F. The Stress Range vs Cycles for these specimens, Specimens 27 and 28, are shown in Figures 72 and 73. Table 13 is a summary of the LCF data. It is clear that vapor honing, even after repolishing, was deleterious to the fatigue life. During repolishing, the diameter was reduced from 0.118 in. to about 0.116 in., or by 25 μ (about one-fifth of a grain diameter) along the specimen radius. Specimen 28, after testing, was placed in the SEM. In addition to the main crack, extensive cracking along the gage

TABLE 13
EFFECT OF VAPOR HONING ON LCF PROPERTIES

Specimen	Strain Range (%)			Stress Range (ksi)	Cycles			
	$\Delta\epsilon_t$	$\Delta\epsilon_p$	$\Delta\epsilon_e$		N_i	N_i'	N_f	N_i'/N_f
27	0.81	0.06	0.75	205.0	900	1200	1505	0.80
28	0.76	0.04	0.72	198.0	1100	1850	1995	0.93



Figure 71. SEM Micrograph, As-Vapor-Honed Surface - LCF Specimen 55

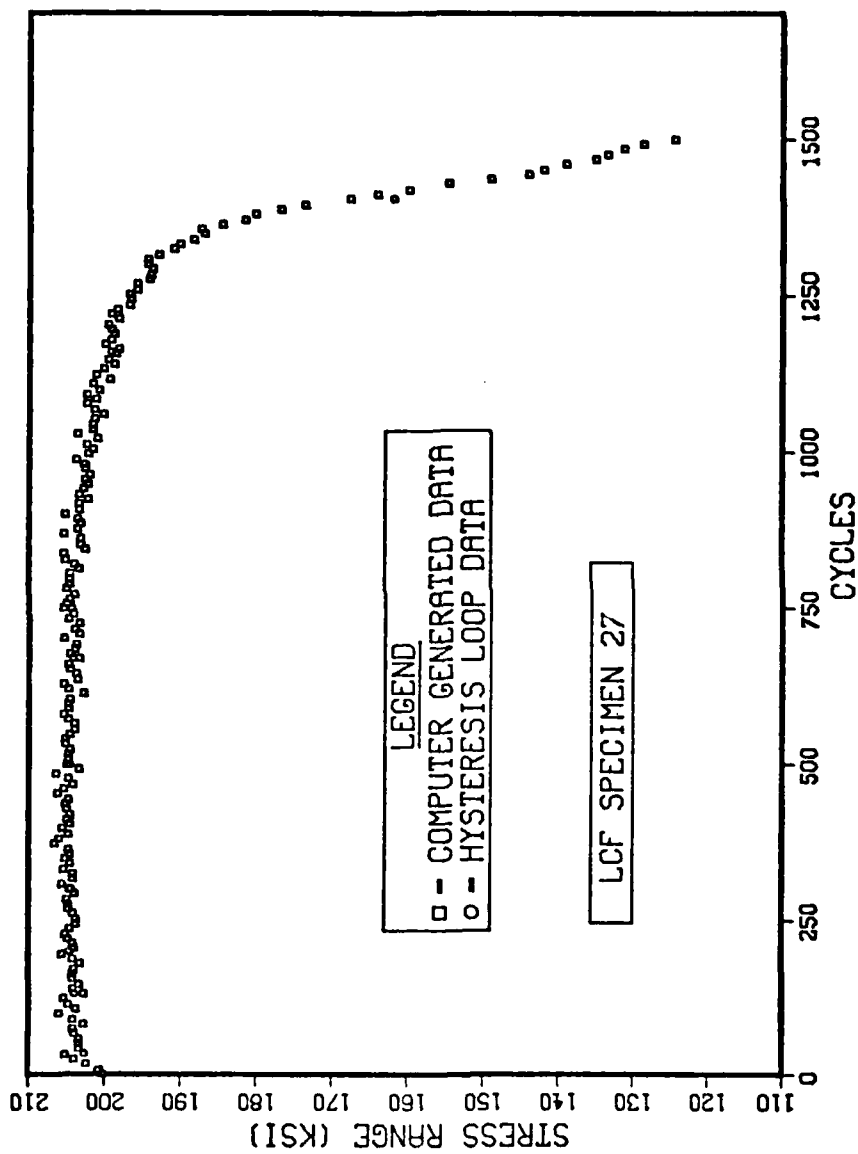


Figure 72. Plot of Stress Range vs Cycles - LCF Specimen 27

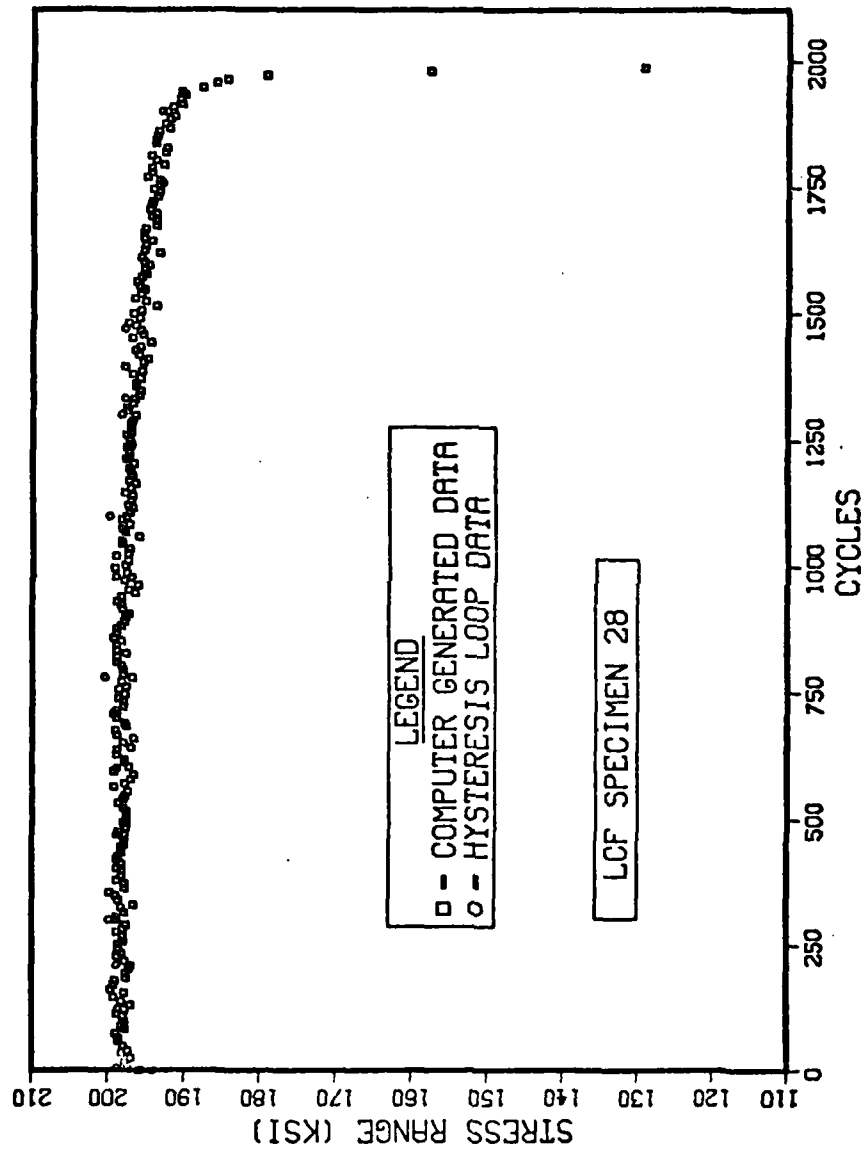


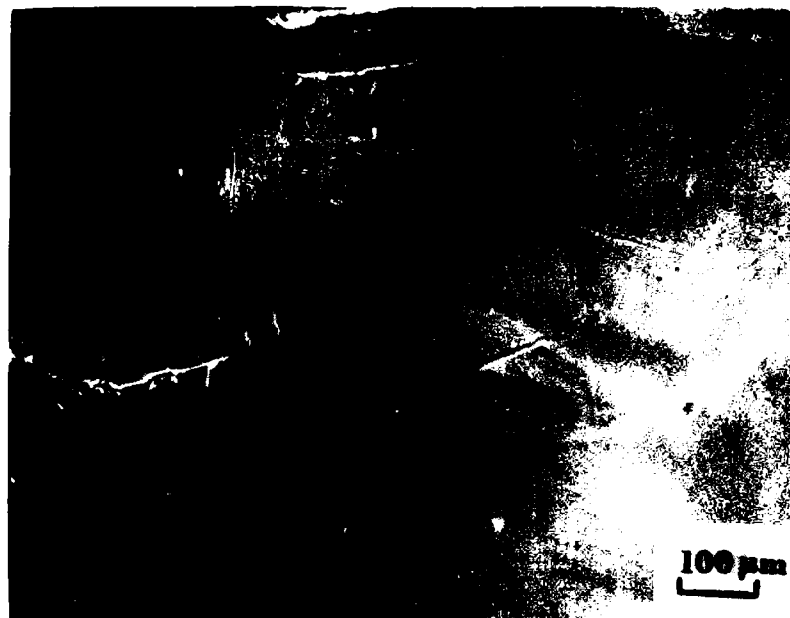
Figure 73. Plot of Stress Range vs Cycles - LCF Specimen 28

length was observed. Typical examples of secondary cracks are shown in Figures 74, 75, and 76. All three of these cracks seem to be associated with inclusions which have decohered, cracked, or fallen out.

There was a reaction between the ceramic coating and the base material during HIPing. Figure 77 shows a typical reaction zone from LCF Specimen 20. This reaction was observed in the shank region, above the extensometer flange. It is assumed a similar reaction occurred in the gauge section. The apparent penetration depth of the reaction zone was at least 5 μ . This zone should have been removed during the polishing operation prior to retesting. However, the grain boundaries may have been damaged to much greater penetration depths by alloy depletion. Greater material removal than that accomplished by repolishing was deemed unwise due to the already small specimen diameter.

Figure 78 shows some fractographs taken of ceramic-coated LCF Specimen 25. The fracture appears much more intergranular in nature than for the baseline specimens.

Crack growth rate in another ceramic-coated specimen, LCF Specimen 21, was also measured by the surface replication technique. Photomicrographs of the replicas are shown in Figure 79. The plot of Crack Length vs Cycles is contained in Figure 80. Extrapolation of the crack length to zero shows that initiation occurred between 1100 and 1200 cycles. This agrees with the asymmetric load drop-off point, N_1 , in Table 12 of 1150 cycles. Note that the slope of this curve is about 1.5 μ m/cycle. This is 5.5 times the slope of the two baseline specimens plotted in Figures 45 and 47. Thus, the crack growth rate was greatly accelerated in the HIP rejuvenated specimen.

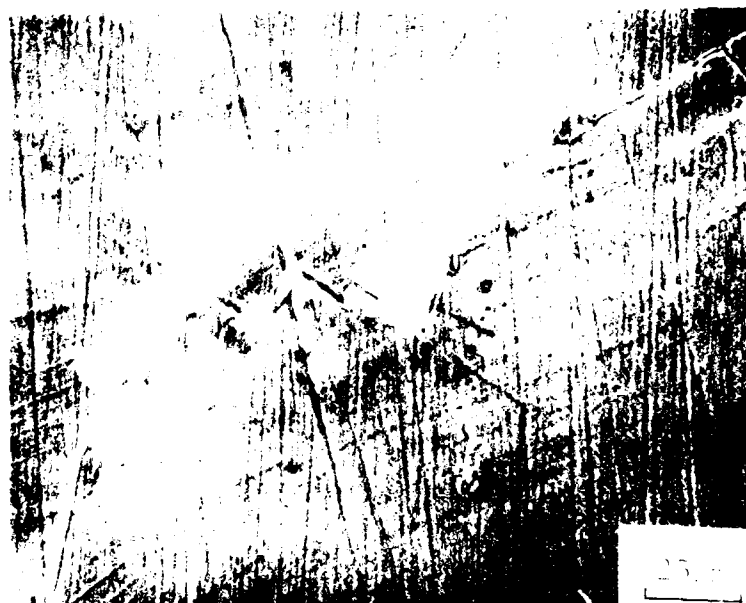


a. Low Magnification View of Crack



b. High Magnification View of Crack

Figure 74. SEM Micrograph, Secondary Cracking - LCF Specimen 28



a. General Crack



b. Higher Magnification View of Crack

Figure 75. SEM Micrograph, Secondary Cracking - LCF Specimen 28

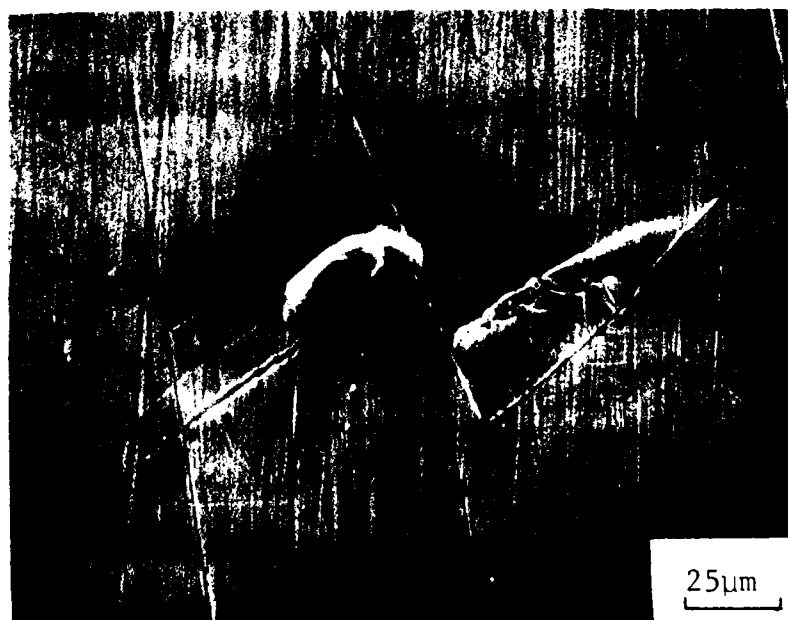
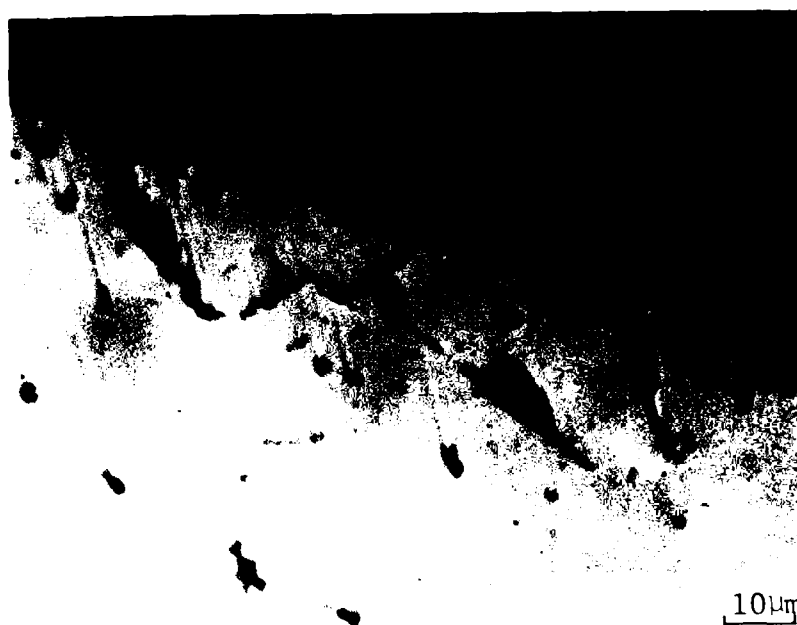


Figure 76. SEM Micrograph, Secondary Cracking - LCF Specimen 28



a. General Area

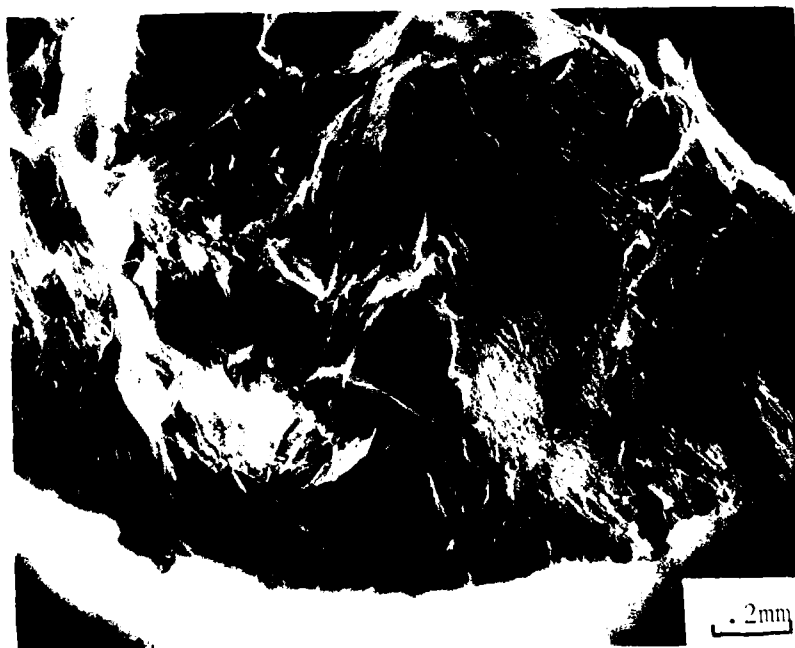


b. Higher Magnification of Reaction Zone

Figure 77. Micrograph, Coating Reaction



a. Fractograph



b. Possible Crack Initiation Area

Figure 78. SEM Fractography - LCF Specimen 25



Figure 79. Micrographs of Replicas, Cracks - LCF Specimen 21

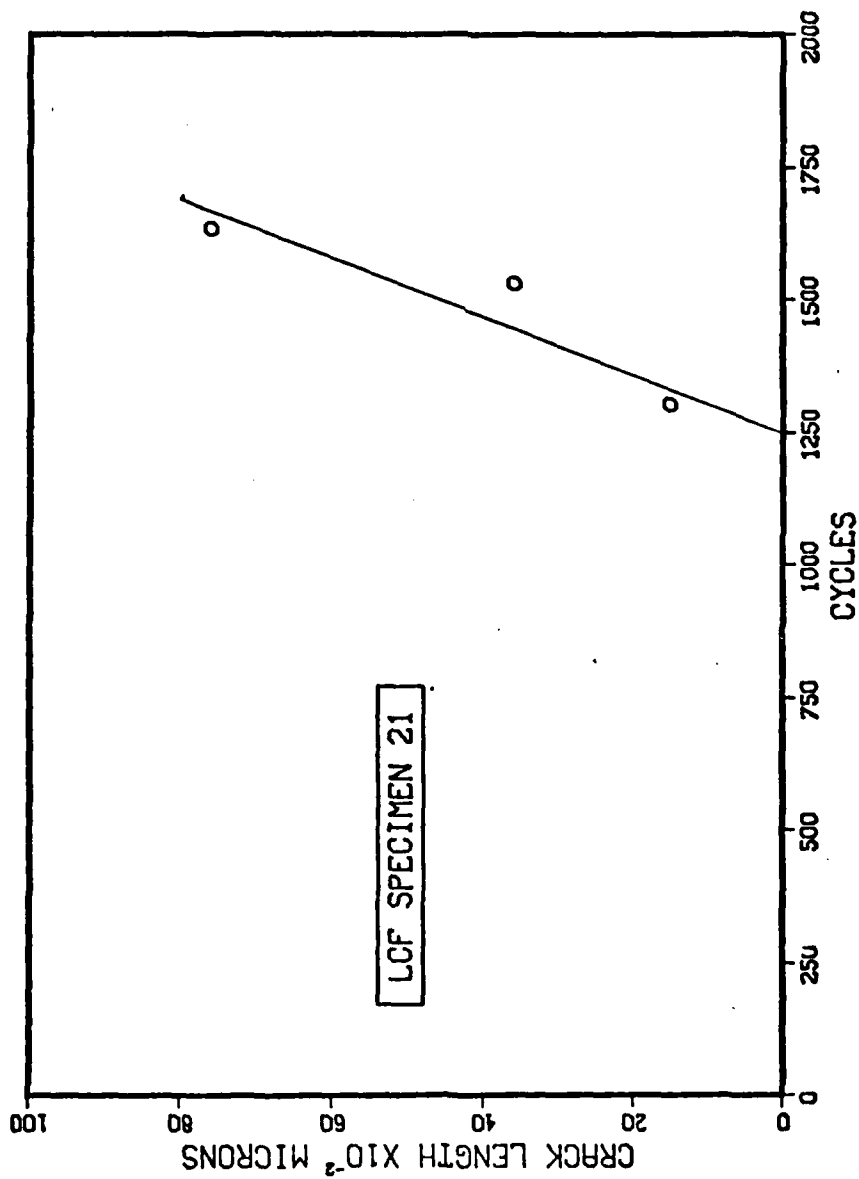


Figure 80. Plot of Crack Length vs Cycles - LCF Specimen 21

The uncoated specimens were badly contaminated after HIP processing. Figure 81 shows the reaction zone for LCF Specimen 26. The apparent reaction zone is 5-10 μ in depth. After HIP processing, alloy depletion along the grain boundaries to much greater depths has been observed in IN-713 (54). Thus, even after repolishing, the grain boundaries were still substantially weakened compared to the baseline. Figure 82 contains SEM photomicrographs of the primary crack in LCF Specimen 16. This crack had progressed completely around the circumference of the specimen. No baseline specimen had a complete circumferential crack, but it was not unusual for the HIP processed specimens (both coated and bare) to have one. Note that the crack in Figure 82(a) is both intergranular and transgranular. The role of a fractured blocky carbide in promoting cracking is graphically shown in Figures 82(b) and (c). Cracking throughout the gauge length was extensive. Figure 83 shows a typical intergranular crack located at some distance from the main crack. The fracture appearance for the uncoated specimens was very similar to that of the coated specimens.

HIP processing increased the material grain size from 120 μm to 150 μm . It is known that LCF life is usually sensitive to grain size. Merrick found an inverse relationship between grain size and fracture life for two different grain sizes at room temperature and at 1000 $^{\circ}\text{F}$ (16). Handbook data at room temperature for three grain sizes also shows an inverse relationship with fracture life for stress-controlled tests (43). When this data is plotted, it is apparent that the relationship follows a Hall-Petch dependency:

$$N_f \propto \frac{1}{\sqrt{\text{g.s.}}} \quad (18)$$



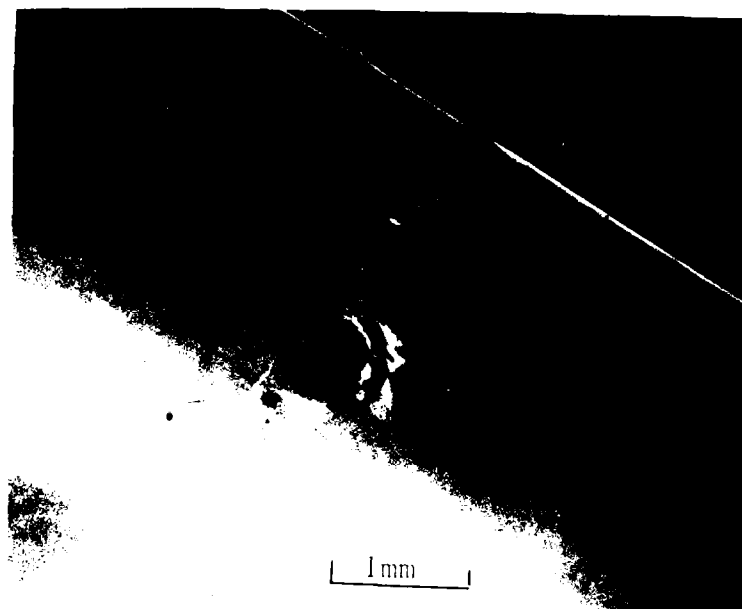
10 μ m

a. Surface Contamination, Area 1



b. Surface Contamination, Area 2

Figure 81. Micrograph, Surface Oxidation - LCF Specimen 26

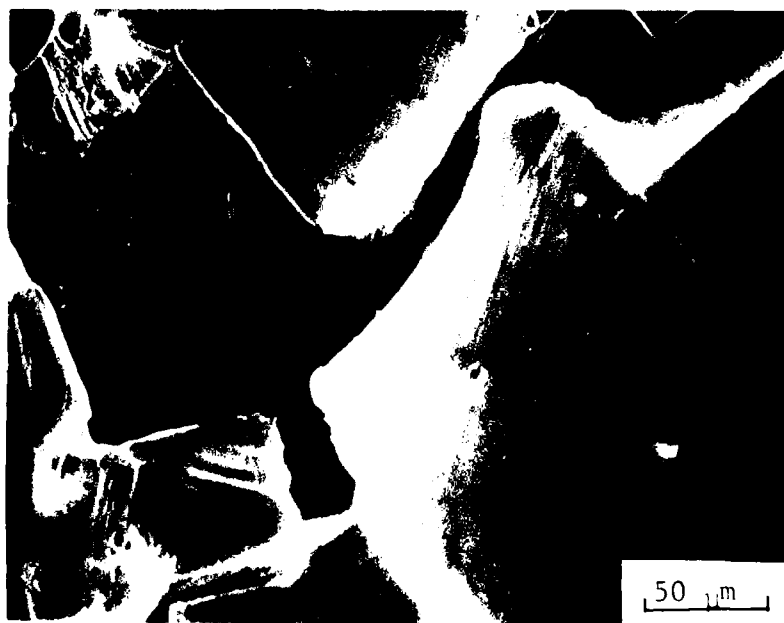


a. Main Crack



b. Magnification of Center Portion of Crack

Figure 82. SEM Micrographs, Main Crack - LCF Specimen 16



c. Possible Carbide Pullout



Figure 83. SEM Micrographs, Secondary Cracking - LCF Specimen 16

where N_f is the cycles to failure, and g.s. is the grain size. Thus, the effect of increased grain size from the rejuvenation processing on the cycles to failure can be estimated:

$$N_{f_2} = N_{f_1} \times \frac{g.s._1}{g.s._2} \quad (19)$$

Using Equation 18, a decrease in cycles to failure of 12% can be estimated to be due to the grain size changes alone.

iii. Mechanisms

Considering the data presented in Tables 12 and 13, the fatigue behavior for the HIP'd specimens (both coated and uncoated) and the vapor-honed specimens is similar. But the mechanisms of crack nucleation and growth are most likely not the same. Recall that the previous section demonstrated that the critical step for crack initiation in the baseline specimens was the decohering of a grain boundary carbide. Clearly, vapor honing, even with repolishing, can decohere or fracture carbides. This not only would greatly shorten the initiation time, but would provide many crack initiation sites. Thus, once crack growth began, it would progress very rapidly due to microcrack linkup. This is what was observed for the vapor-honed specimens.

The ceramic coating reacts with the matrix during HIP processing. Even though optical microscopy showed that the reaction depth was such that it should be removed by repolishing, localized contamination along the grain boundaries and existing persistent slip bands can be substantially greater. This would promote the early intergranular failure as was observed. This investigation is inconclusive, however,

in differentiating between the damage due to vapor honing and the damage due to contamination by the ceramic coating.

The uncoated specimens had contaminated grain boundaries which were relatively weak. Thus, the carbides readily decohered and crack propagation was fairly rapid.

B. Results of Thermal Treatments

1. Presentation of Data

The results of seven thermally rejuvenated specimens are contained in Table 14. A comparison of this data with the baseline data (Table 9) and the HIP rejuvenated data (Table 12) reveals that some rejuvenation definitely occurred as a result of the thermal treatment. The plots of Stress Range vs Cycles are contained in Figures 84-90. Note that LCF Specimen 13 was heat treated in a poor vacuum and, as a result, the surface was badly oxidized. It was tested without repolishing. The remaining specimens, except for LCF Specimen 54, were all repolished after thermal treatment.

An investigation was made to determine the effect of repolishing alone on enhancing the fatigue properties. A summary of the data is contained in Table 15. The plots of Stress Range vs Cycles are shown in Figures 91 and 92. These data are essentially no different than the baseline properties. Also, since LCF Specimen 54 was not repolished after the thermal treatment and yet was clearly rejuvenated, it can be concluded that repolishing alone does not recover LCF damage for the conditions studied in this investigation.

Table 14 indicates that complete recovery of LCF damage was not accomplished. But, it was previously shown that after 800 cycles,

Specimen	Total Process		Steady Range (3)				Cyclic			
	Cycles	ΔT	ΔT_p	ΔT_d	ΔT_d	(kat)	N_f	N_f'	N_f	N_f'/N_f
13*	800	0.79	0.07	0.72	0.72	198.0	1650	2100	2504	0.66
34	400	0.75	0.05	0.70	0.70	194.5	1800	2700	3333	0.54
35	800	0.74	0.03	0.71	0.71	194.0	1800	3900	5384	0.33
42	803	0.74	0.02	0.72	0.72	197.6	1800	3300	4134	0.44
43	803	0.75	0.02	0.73	0.73	200.5	2000	2650	2890	0.69
51	803	0.72	0.02	0.70	0.70	194.0	1700	3700	4475	0.38
54**	803	0.75	0.04	0.71	0.71	194.2	1900	3200	4106	0.46

*Heat treated in a poor vacuum

**Retested without repolishing

TABLE 15
SUMMARY OF REPOLISHING ON LCF PROPERTIES

Specimen	Prior Damage Cycles	Strain Range (%)			Stress Range (ksi)	Cycles			
		$\Delta\epsilon_t$	$\Delta\epsilon_p$	$\Delta\epsilon_e$		N_i	N_i'	N_f	N_i'/N_f
38	803	0.76	0.05	0.71	196.0	1575	2700	3562	0.76
40	803	0.73	0.02	0.71	194.5	1300	2800	3206	0.87

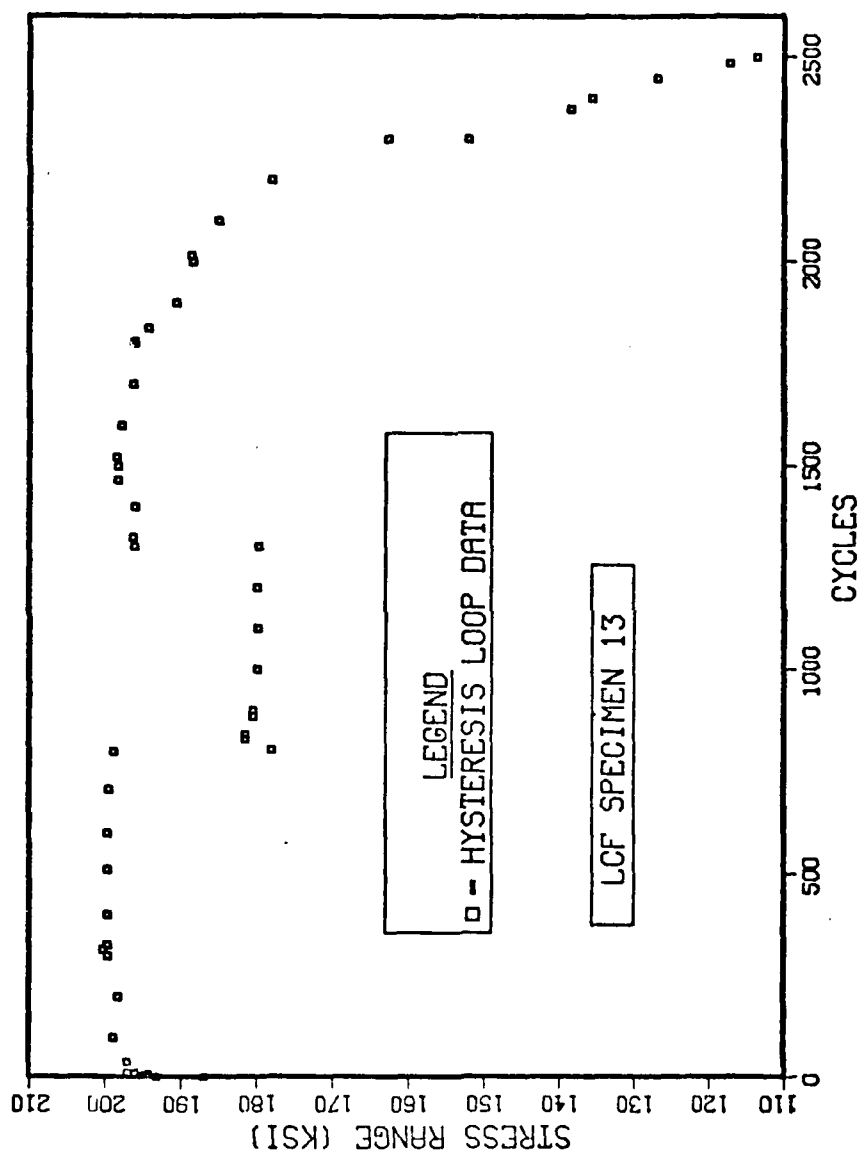


Figure 84. Plot of Stress Range vs Cycles - LCF Specimen 13

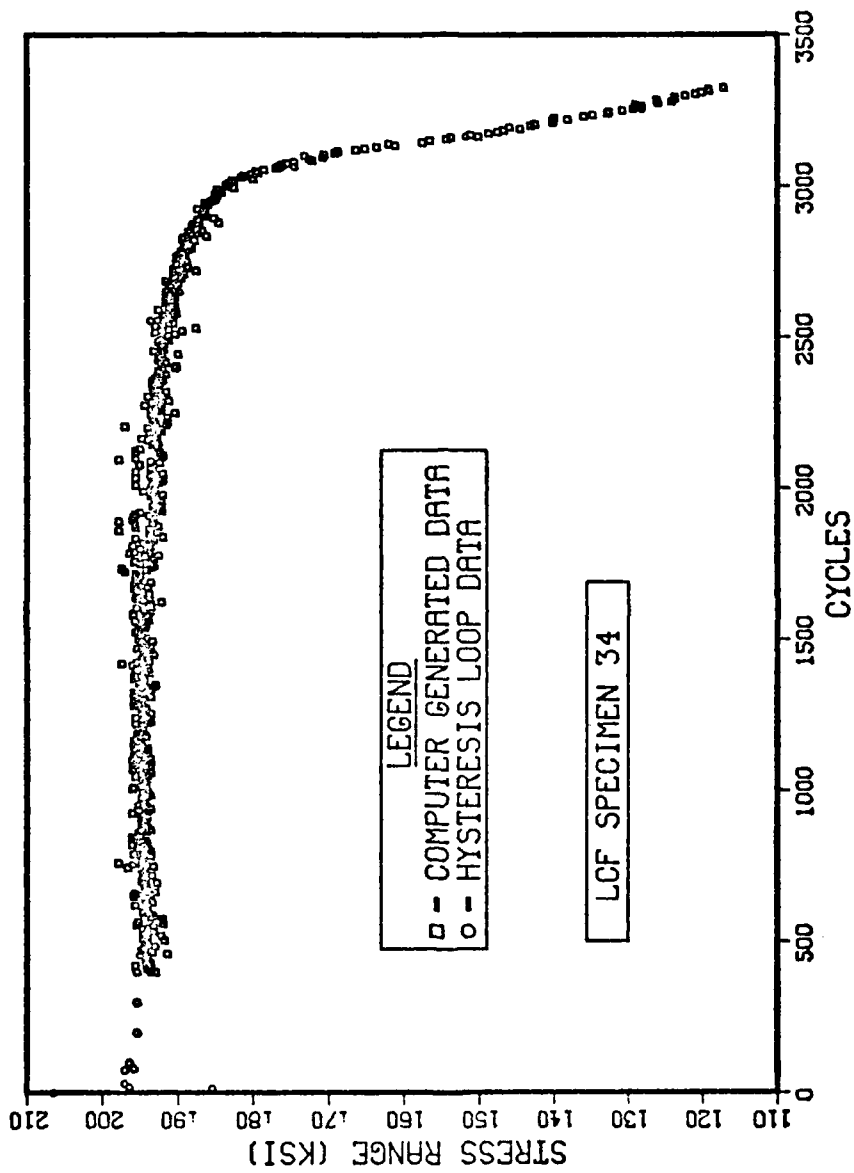


Figure 85. Plot of Stress Range vs Cycles - LCF Specimen 34

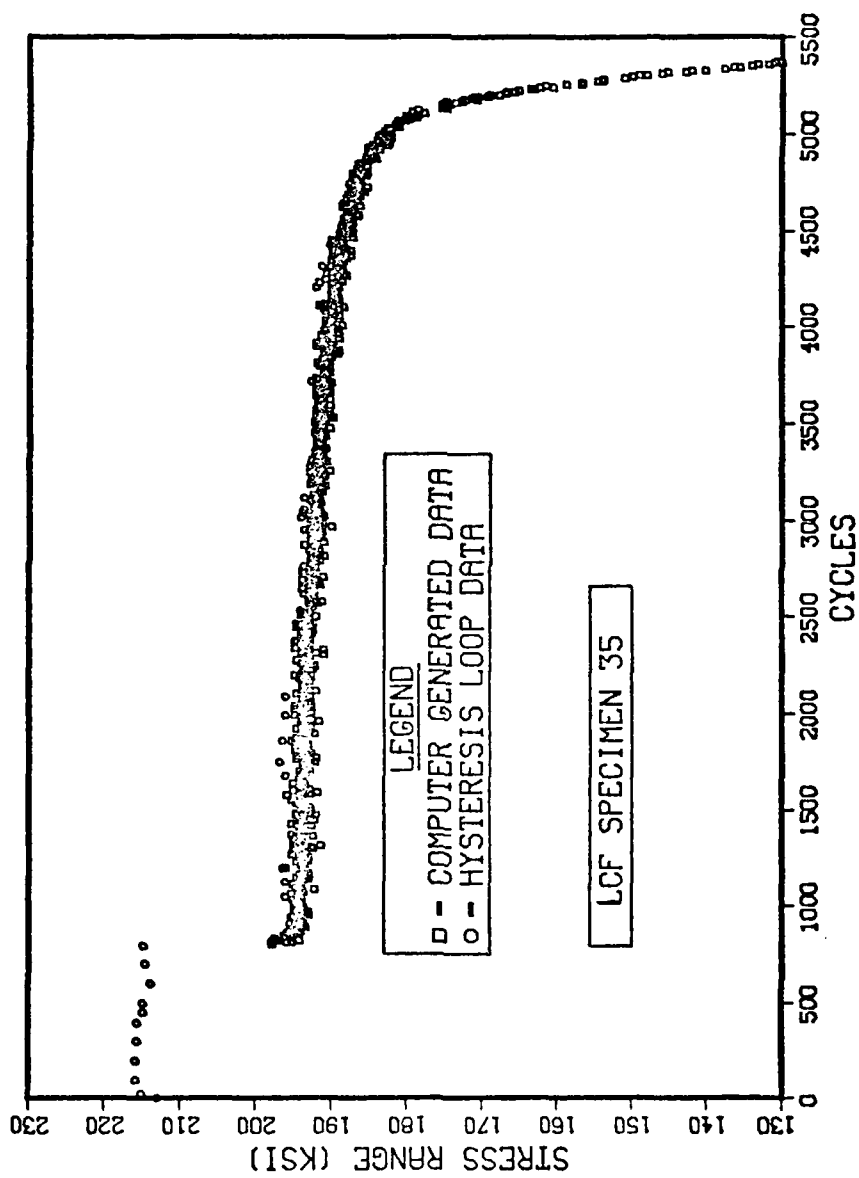


Figure 86. Plot of Stress Range vs Cycles - LCF Specimen 35

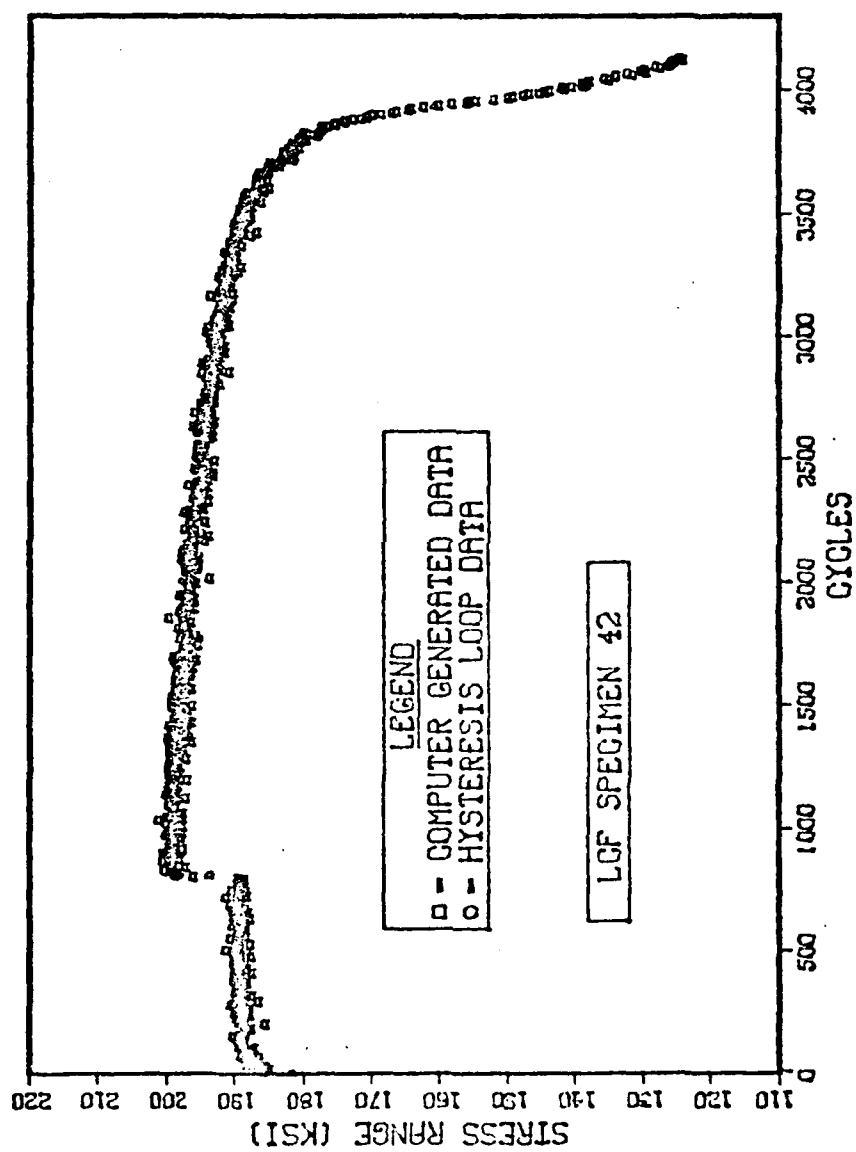


Figure 87. Plot of Stress Range vs Cycles - LCF Specimen 42

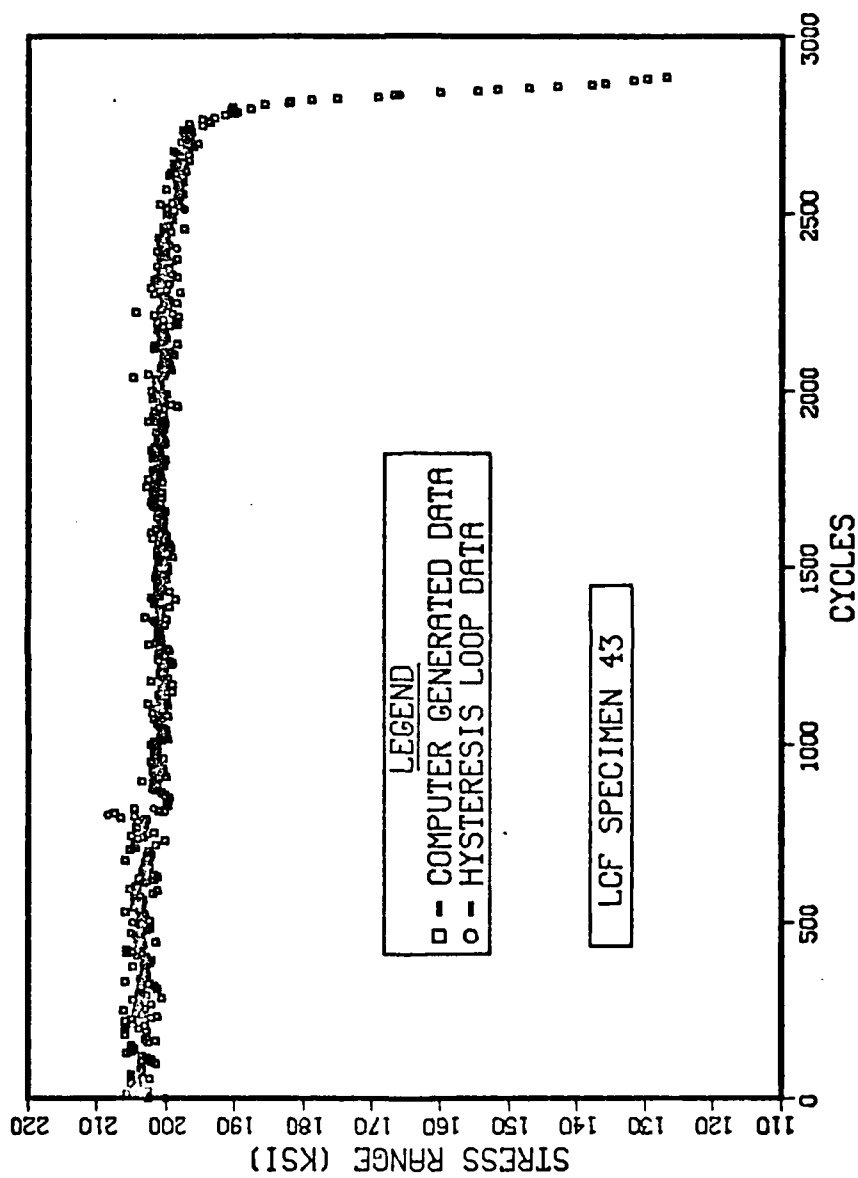


Figure 88. Plot of Stress Range vs Cycles - LCF Specimen 43

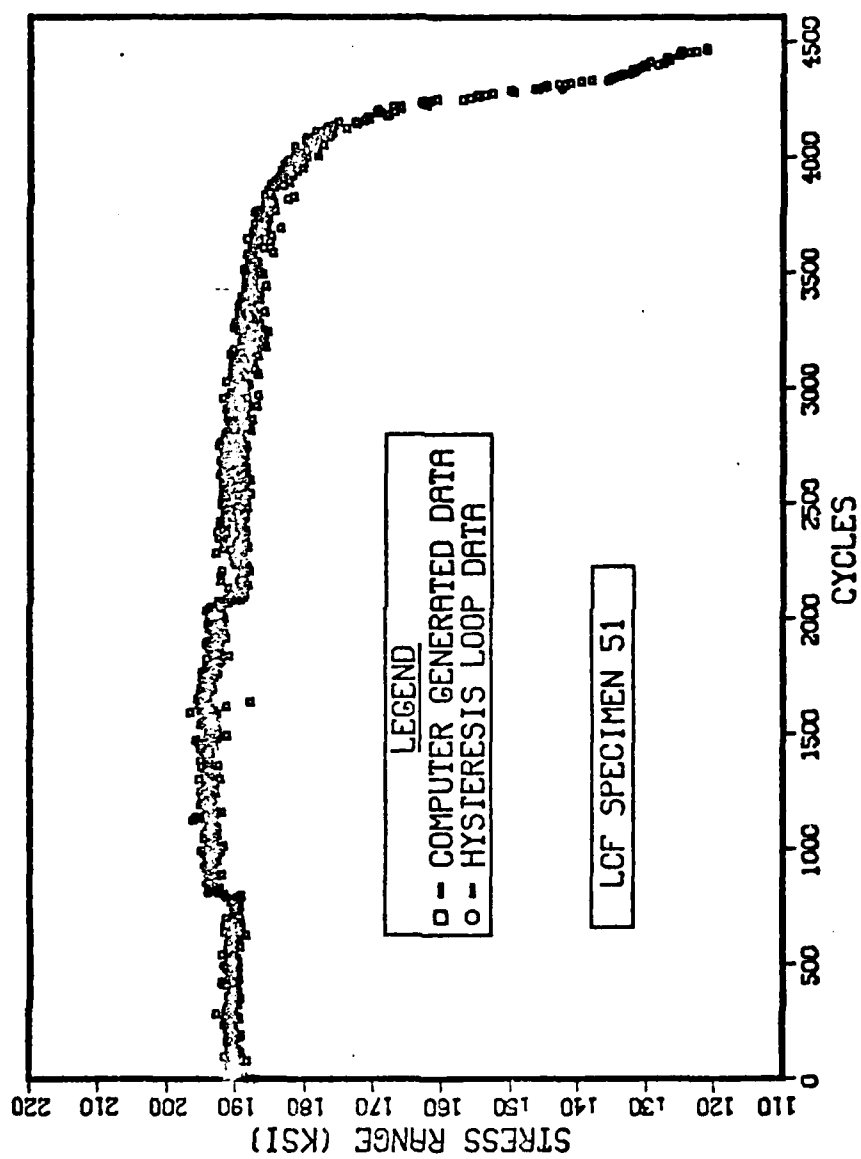


Figure 89. Plot of Stress Range vs Cycles - LCF Specimen 51

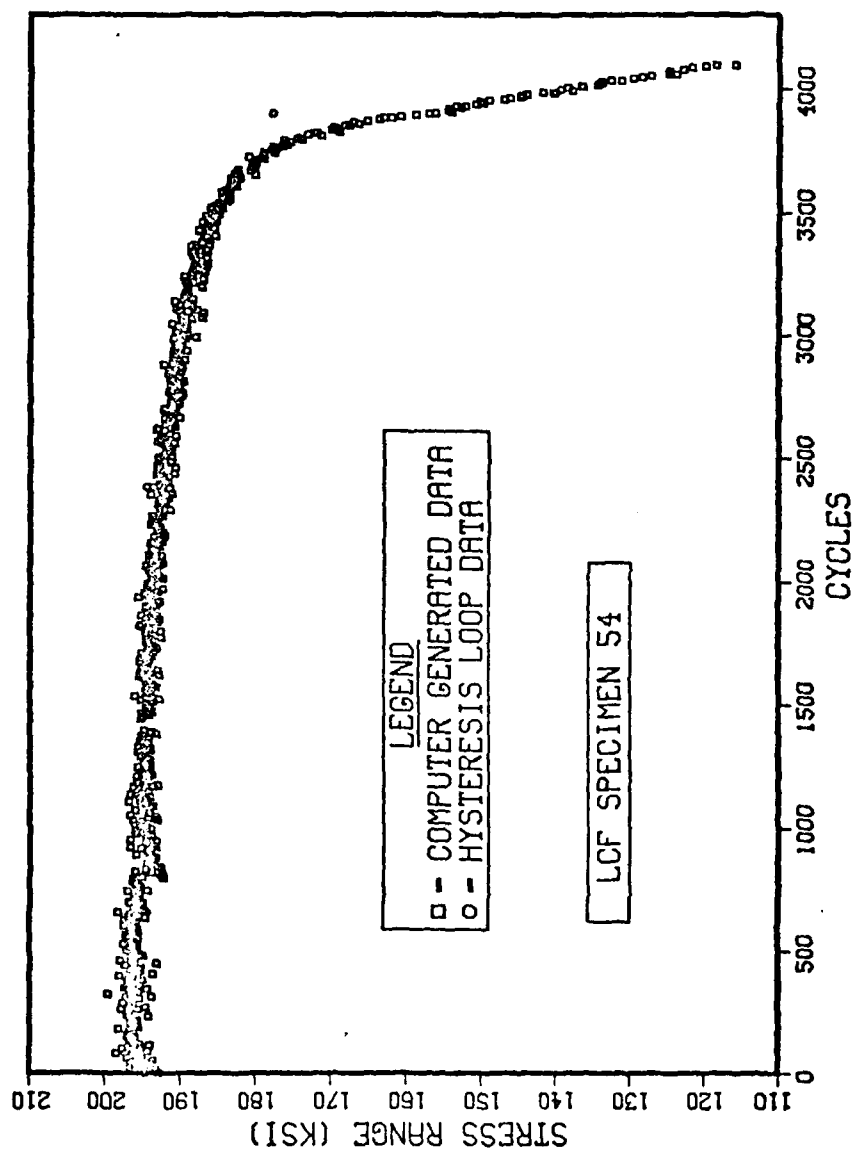


Figure 90. Plot of Stress Range vs Cycles - LCF Specimen 54

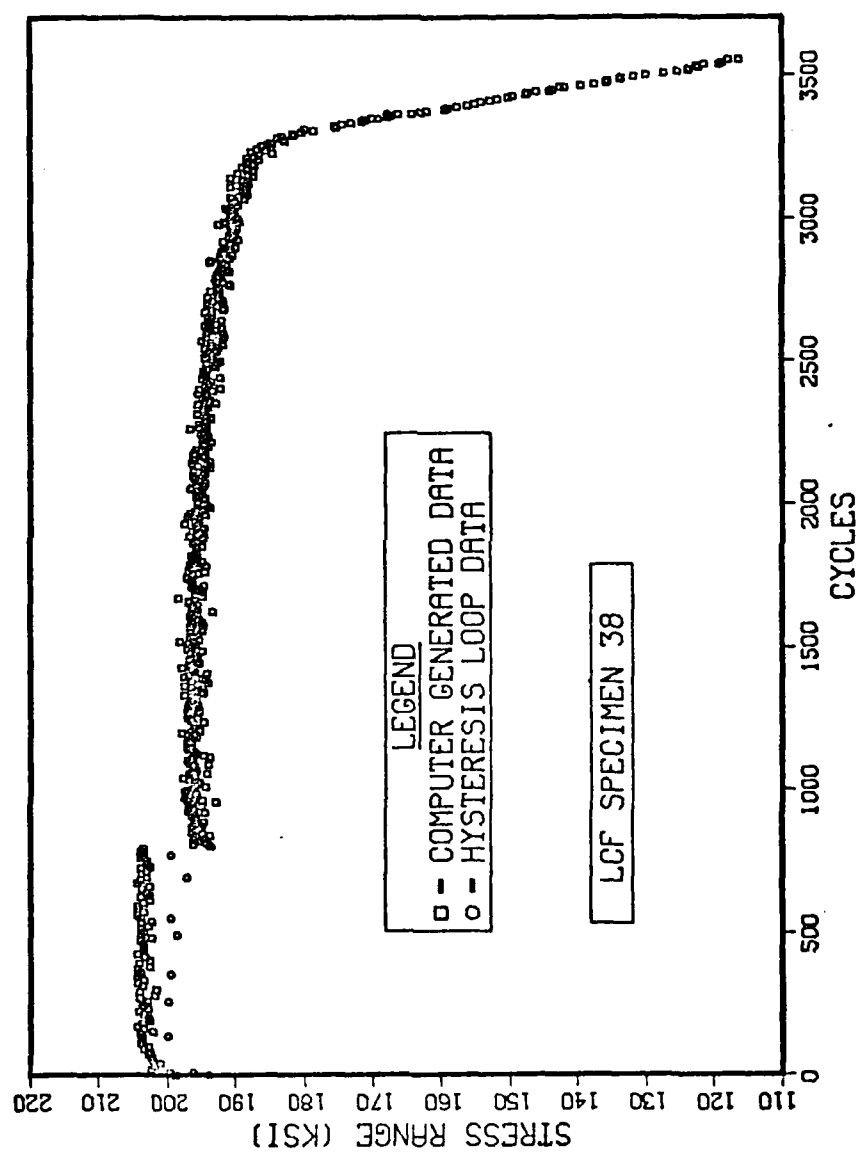


Figure 91. Plot of Stress Range vs Cycles - LCF Specimen 38

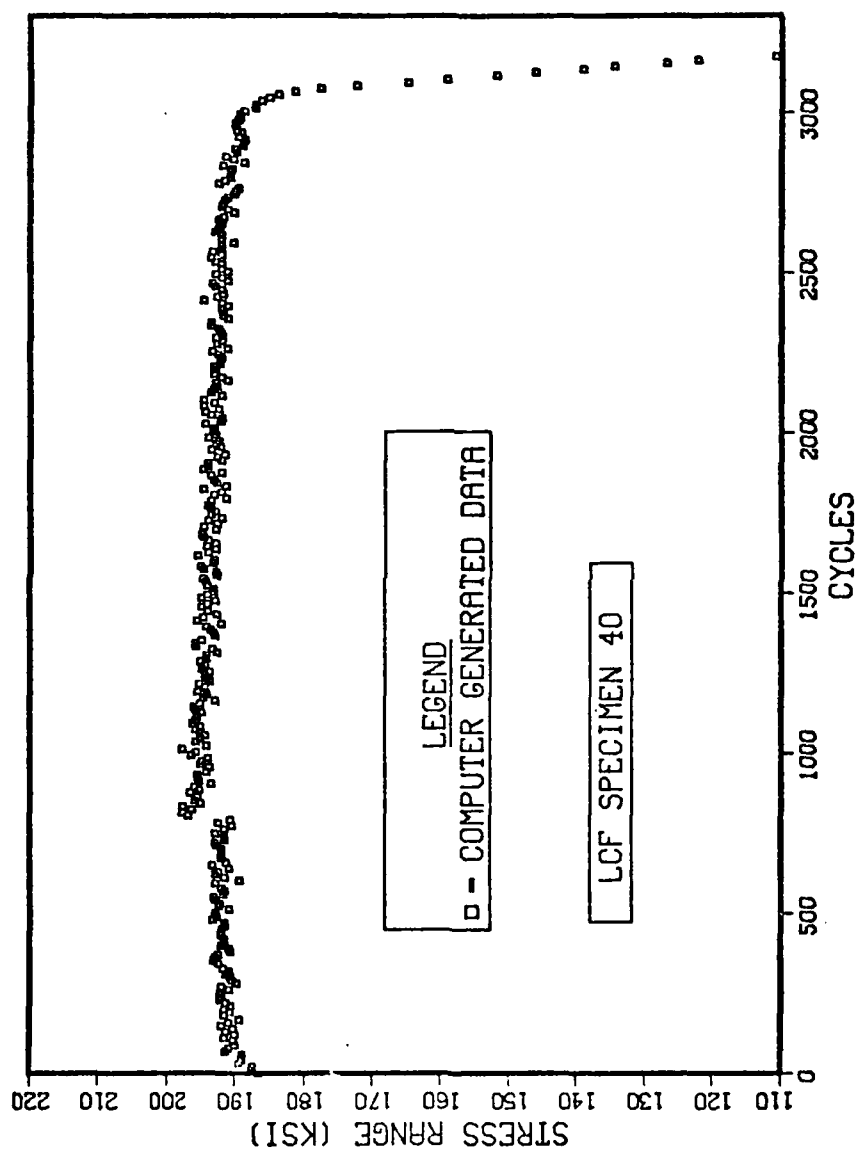


Figure 92. Plot of Stress Range vs Cycles - LCF Specimen 40

blocky carbides in the grain boundary began to decohere (Figure 51), and extrusions at persistent slip bands occurred (Figure 50). This is not the type of damage that thermal treatment can remove.

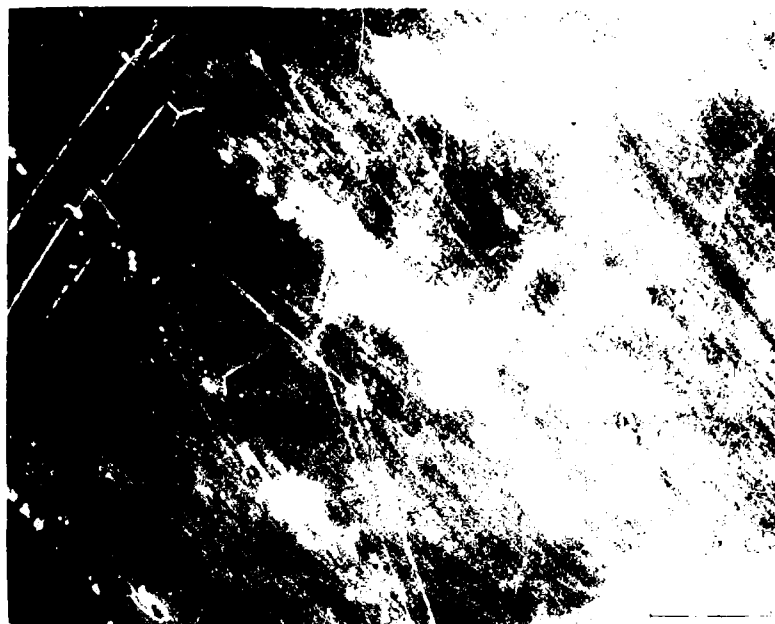
SEM photomicrographs of the gauge section of the thermally rejuvenated specimens after N_f revealed extensive cracking and decohering of inclusions. A typical example is shown in Fig. 93 from LCF Specimen 42.

LCF Specimen 31 was damaged in LCF at 500°F at a total strain range of 0.75% (stabilized stress range was 191 ksi). The gauge section was cut in two. Foils were made from one half for TEM investigation. The other half was given the thermal rejuvenation treatment, and the foils were prepared for TEM investigation. Figure 94 shows a network of dislocations beginning to form after 800 cycles. Figure 95, after the thermal treatment, shows that most of the dislocations have been annealed out.

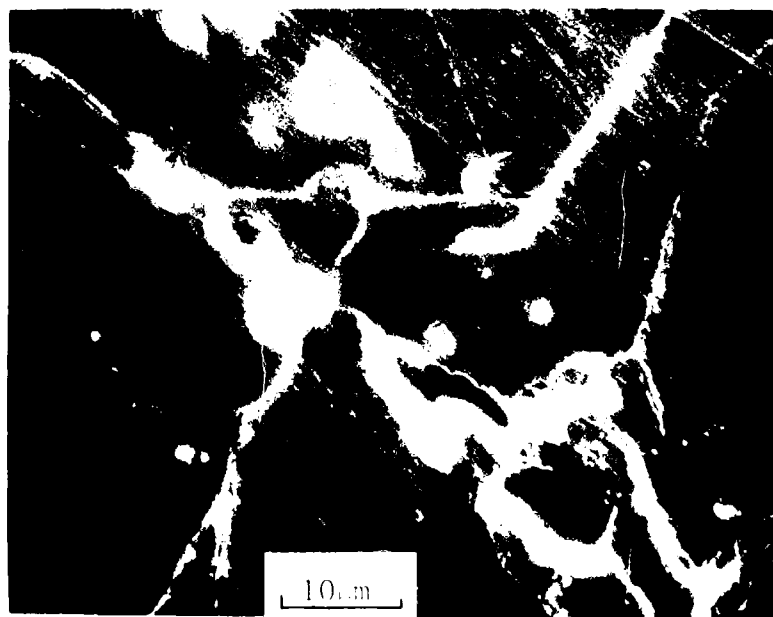
The previous results were for a single rejuvenation treatment. In an attempt to determine the effect of multiple rejuvenations, LCF Specimen 41 was subjected to multiple blocks of 803 cycles of LCF damage plus thermal rejuvenation. The plot of Stress Range vs Cycles is contained in Figure 96. Table 16 summarizes the LCF data. Note that the thermal rejuvenation treatments seemed to have forestalled the onset of crack initiation as determined by the asymmetric load dropoff, but once the dropoff occurred, the crack progressed very rapidly. The surface of this specimen was examined in the SEM after the second block of 803 cycles (i.e., after 1606 cycles) and after failure. Figure 97 shows photomicrographs taken after 1606 cycles. Figure 97(a) shows the development of persistent slip bands

TABLE 16

Prior Damage Cycles	Strain Range (%)			Stress Range (ksi)	Cycles			N_f'/N_f
	$\Delta\epsilon_t$	$\Delta\epsilon_p$	$\Delta\epsilon_e$		N_f	N_f'	N_f/N_f	
0	0.76	0.05	0.71	197.0	-	-	-	-
803	0.77	0.07	0.70	201.0	-	-	-	-
1606	0.77	0.06	0.71	193.0	-	-	-	-
2409	-	-	-	195.5	2500	2700	3134	0.86



a. General Appearance of Cracking



b. Decohered Inclusions and Cracking

Figure 93. SEM Micrograph, Cracking at Inclusions - LCF Specimen 42

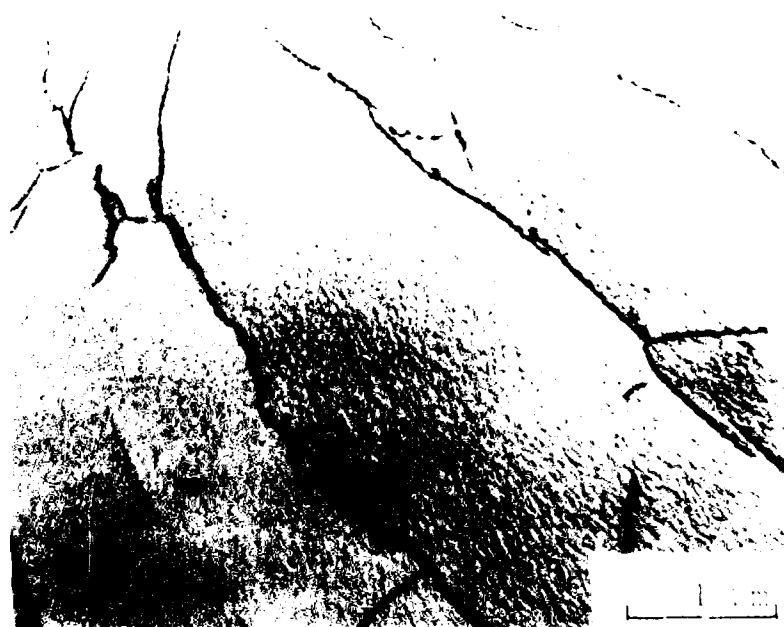


Figure 94. TEM Micrograph, Dislocation Network after 800 Cycles -
LCF Specimen 31



Figure 95. TEM Micrograph, Annealed Dislocation Network - 1CF Specimen

AD-A107 255

AIR FORCE INST OF TECH WRIGHT-PATTERSON AFB OH
MECHANISMS OF RECOVERING LOW CYCLE FATIGUE DAMAGE IN INCOLOY 90--ETC(U)
1979 R E SCHAFRIK
AFIT-CI-79-212D

F/G 11/6

NL

UNCLASSIFIED

3 x 3

AD-A107 255

■

END

DATE

FILED

12-81

DTIC

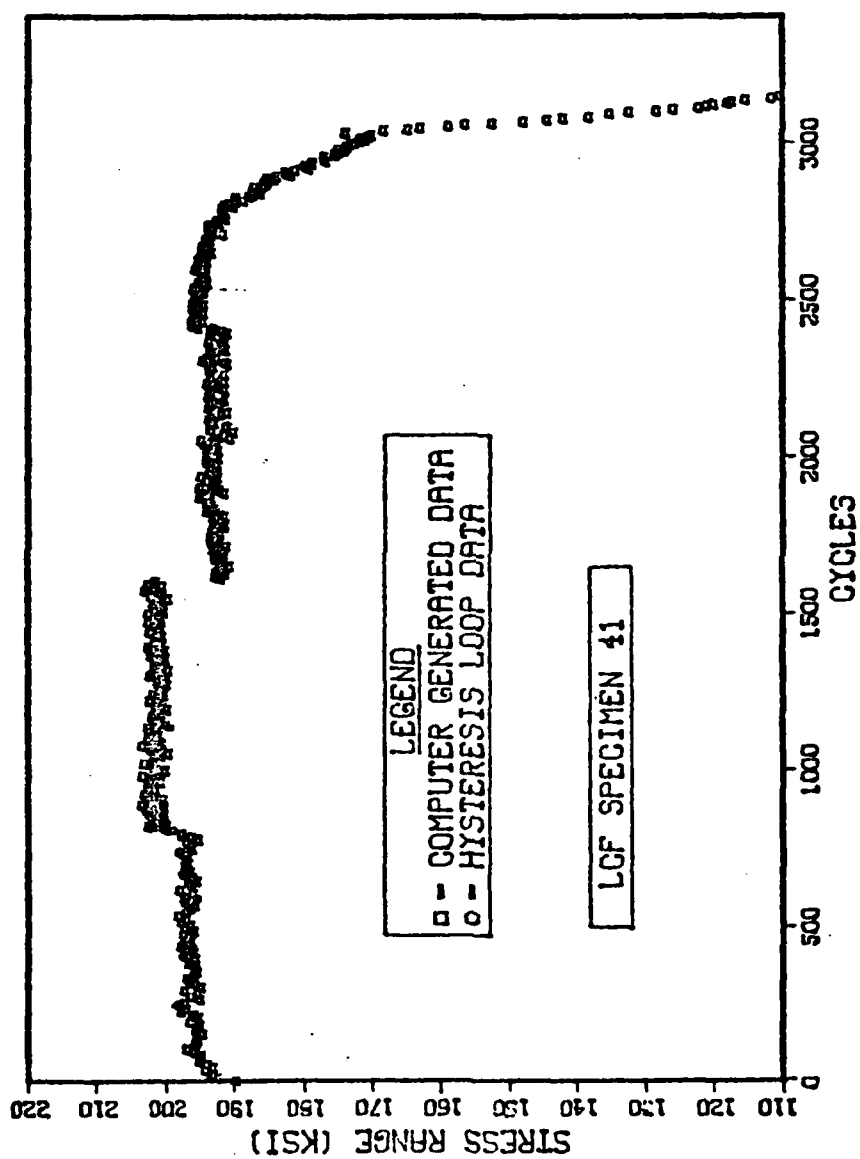
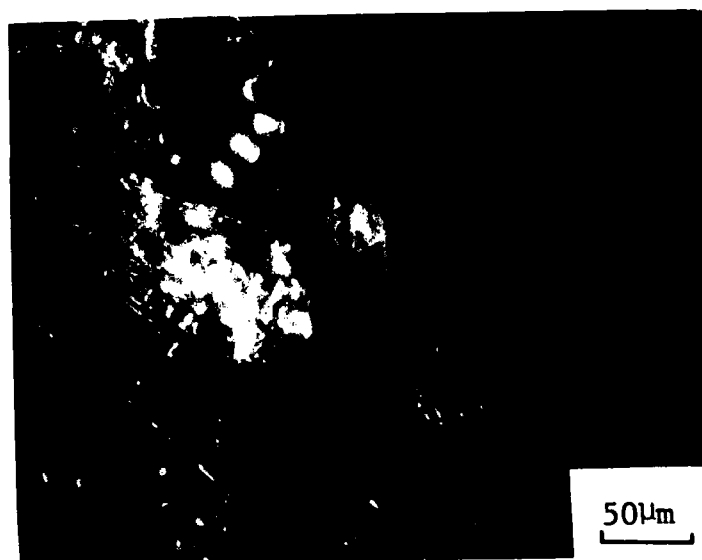


Figure 96. Plot of Stress Range vs Cycles - LCF Specimen 41

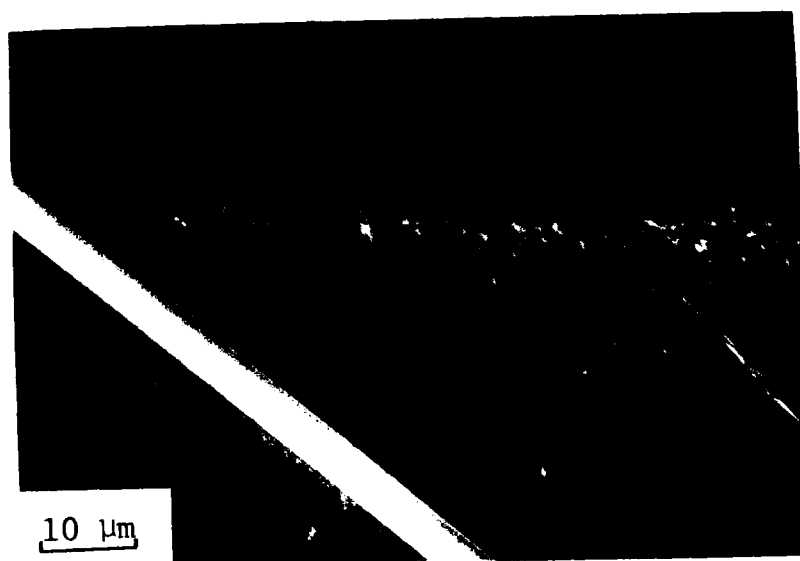


a. General Appearance of Cracking



b. Decohered Inclusion

Figure 97. SEM Micrograph, Surface Cracking after 1606 Cycles -
LCF Specimen 41

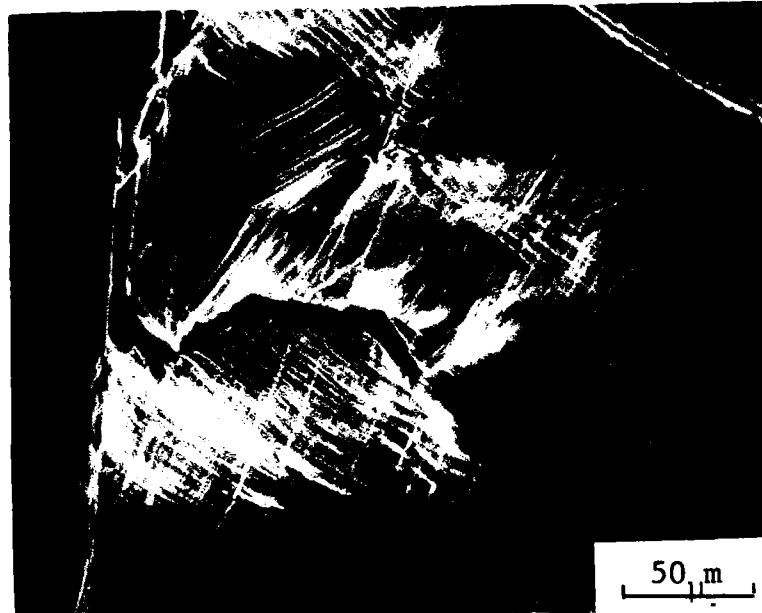


c. Possible Cracked Grain Boundary

and the effect of polishing a group of carbides. Figure 97(b) shows a blocky grain boundary carbide in the process of decohering. Figure 97(c) shows a grain boundary beginning to crack or form a ledge. Figure 98 are photomicrographs taken after failure. Figure 98(a) shows extensive deformation and cracking in a region near the principle crack. Figure 98(b) is a typical area located at some distance from the main crack. The grain boundary cracking and persistent slip bands are readily apparent. Note that the total life for LCF Specimen 41 was the same as could be expected for a baseline specimen. Thus, no overall rejuvenation was accomplished although the onset of gross microcracking may have been significantly retarded.

ii. Mechanisms

The rejuvenation effect of the thermal treatment was primarily due to the recovery of dislocations in the persistent slip bands and the deformation zone along the grain boundary. The fact that dislocation recovery can occur at elevated temperatures is well established, and several mechanisms have been postulated (55,56,57). Thus, after thermal rejuvenation and during subsequent testing, the planar dislocation arrays must re-form the persistent slip bands and the deformation zone along the grain boundary must be re-established. Also, the γ' precipitates which were sheared and possibly disordered are restored to their original distribution and morphology (65). The result is that the processes which lead to the decohering of the blocky grain boundary carbides are retarded. However, the decohering itself is not repaired by thermal treatment. Nor are the voids healed on the interior of a persistent slip band which developed intrusions and extrusions.



a. Surface Deformation Near Crack



b. General Cracking

Figure 98. SEM Micrograph, Cracking after Failure - LCF Specimen 41

Also, the rejuvenation process acts to disperse slip throughout the gauge section, leading to a greater number of decohering carbides. Thus, when microcracks begin to propagate, they readily link up, leading to an accelerated crack growth rate. If the grain boundaries are simultaneously weakened during the thermal rejuvenation processing, such as by contamination from a poor vacuum, crack growth is accelerated even more.

C. Conclusions

Table 17 summarizes the cycles to crack initiation as a function of the processing, and Table 18 similarly summarizes the cycles to failure. It is evident that the data for the repolishing treatment alone belongs to the same population as the baseline data. The vapor-honed plus repolished data indicates crack initiation at about 400 cycles earlier than the baseline data, and less than half the total lifetime to failure. The HIP samples did not show any rejuvenation of LCF properties. The uncoated HIP specimens performed slightly worse than the coated HIP specimens. Crack initiation for the HIP samples (with 800 cycles of pre-HIP damage) occurred at about the same point as for the baseline specimens. But failure occurred 1300-1500 cycles earlier than the baseline data. Also, the data indicates that failure occurred within about 1600 cycles after HIP processing regardless of the level of initial damage (Table 12). The conclusion is that vapor honing and HIP processing damaged the surface of the test specimens. Vapor honing caused fracturing and decohering of blocky grain boundary carbides. Ceramic-coated plus HIP specimens not only had the deleterious effects of the vapor-honing induced damage, but also contamination due to reaction

TABLE 17
SUMMARY OF CYCLES TO CRACK INITIATION
0.70-0.80 TOTAL STRAIN RANGE
500 F TEST TEMPERATURE

	Treatment					
	Baseline	Repolish	Vapor Honed	HIP-Bare	HIP-Coated	Thermal
Prior Damage (cycles)	0	803	0	800	800	800-803 400
No. of Data Points	8	2	2	4	3	5* 1
Mean	1388	1438	1000	1338	1433	1840 1800
Standard Deviation	448	194	141	396	301	114 -

*Excludes LCF Specimen 13

TABLE 18

SUMMARY OF CYCLES TO FAILURE

0.70-0.80 TOTAL STRAIN RANGE

500 F TEST TEMPERATURE

	Treatment				
	Baseline	Repolish	Vapor Honed	HIP-Bare	HIP-Coated Thermal
Prior Damage (cycles)	0	803	0	800	800-803 400
No. of Data Points	8	2	2	4	5* 1
Mean	3568	3384	1750	2246	2410 4198 3333
Standard Deviation	401	252	346	290	683 895 -

*Excludes LCF Specimen 13

between the ceramic coating and the superalloy. The uncoated HIP specimens were badly contaminated from impure argon in the HIP unit.

The thermally rejuvenated specimens definitely showed some rejuvenation. Those specimens damaged to 800 cycles before rejuvenation increased their initiation time by about 450 cycles and their total lifetime by about 630 cycles on the average (but note the high standard deviation in Table 18). The specimen predamaged 400 cycles before rejuvenation increased its initiation time by 400 cycles, but no increase in total lifetime was obtained. The experience with multiple rejuvenation (Table 16) indicates that damage accumulation in the form of decohering carbides, which are not affected by thermal treatments, leads to eventual very rapid crack extensions.

Chapter 4

SUMMARY

The mechanisms of crack initiation and growth in strain-controlled low cycle fatigue (LCF) damage were determined for the iron-nickel superalloy, Incoloy 901. Testing was done in air at a temperature of 500°F (260°C) and total strain range of 0.75%. The effect of hot isostatic pressing (HIP) and thermal treatment in reducing LCF damage was investigated.

The LCF specimens were manufactured using a low stress grinding method to maintain surface quality. Specimens were hand polished along the axial direction through 4/0 emery paper. Prior to testing, all specimens were given a standard solution treatment and double age, referred to as STA 3A (Table 4), to insure the uniform precipitate morphology and distribution from specimen to specimen. The as-received grain size was 90 μm . After STA 3A, the grain size was increased to 120 μm , but remained stable after subsequent heating to the solutioning temperature. The 0.2% offset yield stress at 500°F was 122 ksi.

Initial LCF testing was conducted over the total strain range of 0.70% to 2.44%. The Cyclic Stress-Strain Curve (Figure 24) exhibited cyclic hardening at the high strain ranges and cyclic softening at the lower ranges. A log-log plot of Total Strain Range vs Cycles (Figure 26) exhibits a linear curve with a negative slope.

Crack initiation in the baseline specimens was due to the decohering of blocky grain boundary carbides. Pre-crack initiation damage consisted of planar dislocation arrays forming persistent slip bands and an intense deformation region adjacent to favorably oriented grain boundaries. The persistent slip bands formed intrusions and extrusions at a total strain range of 0.75% by 800 cycles (about 60% of crack initiation time). Stage I crack propagation occurred along the grain boundary or along a favorably oriented persistent slip band. Substantial Stage II crack propagation occurred, as evidenced by the formation of fatigue striations. Fractography revealed a mixed fracture mode, consisting of both intergranular and transgranular fracture.

The HIP-processed specimens were subjected to a HIP cycle of 2025°F for one hour and 1975°F for two hours at 15 ksi of argon (Figures 10 and 11). Both uncoated and ceramic-coated specimens were HIP'd. Specimens had pre-HIP LCF damage of 0 cycles, 800 cycles, and 2100 cycles. The HIP processing increased the grain size by 25%. The specimens were subjected to STA 3A to restore the original morphology and distribution of the precipitates. No rejuvenation occurred. In fact, the fatigue properties were worse than the baseline properties by a substantial amount. Even correcting for the grain size change utilizing a Hall-Petch-type equation, it is clear that the HIP processing itself produced surface-related damage in the microstructure. In fact, the HIP processing caused more damage than the LCF pre-HIP damage levels.

In the case of the ceramic-coated specimens, damage resulted from at least two sources: (1) vapor honing the specimen surface to provide

a matte finish for the coating to adhere to, damaged the blocky carbides by decohering and cracking them; and (2) the ceramic coating reacted with the superalloy. As a consequence, intergranular cracking was promoted, and crack growth rates were greater than five times the rate in the baseline specimens.

The uncoated HIP specimens were damaged by contamination from the HIP atmosphere. Preferential formation of oxides and nitrides along the grain boundaries led to weakening of the boundaries. This promoted intergranular cracking, accelerated crack growth rates, and early failures. Overall, there was not much apparent difference between the behavior of the coated and uncoated specimens, although the coated ones were slightly superior.

Figure 99 plots the rejuvenation data and the trend line for the baseline data on a log-log plot of Total Strain Range vs Cycles to Failure.

The thermally rejuvenated specimens were given STA 3A after 800 cycles of damage. As long as the heat treating was done in a good vacuum so that surface contamination did not occur, partial rejuvenation was accomplished. Initiation life was increased by 400 cycles and the failure cycle was increased by 600 cycles. Complete rejuvenation was not attained because the grain boundary carbides had already begun to decohere after 800 cycles and persistent slip bands had formed intrusions and extrusions. When a specimen was rejuvenated three times after blocks of 803 cycles of damage, it failed catastrophically due to rapid crack extension. Thus, the unrecovered microstructural damage can adversely affect the fatigue life.

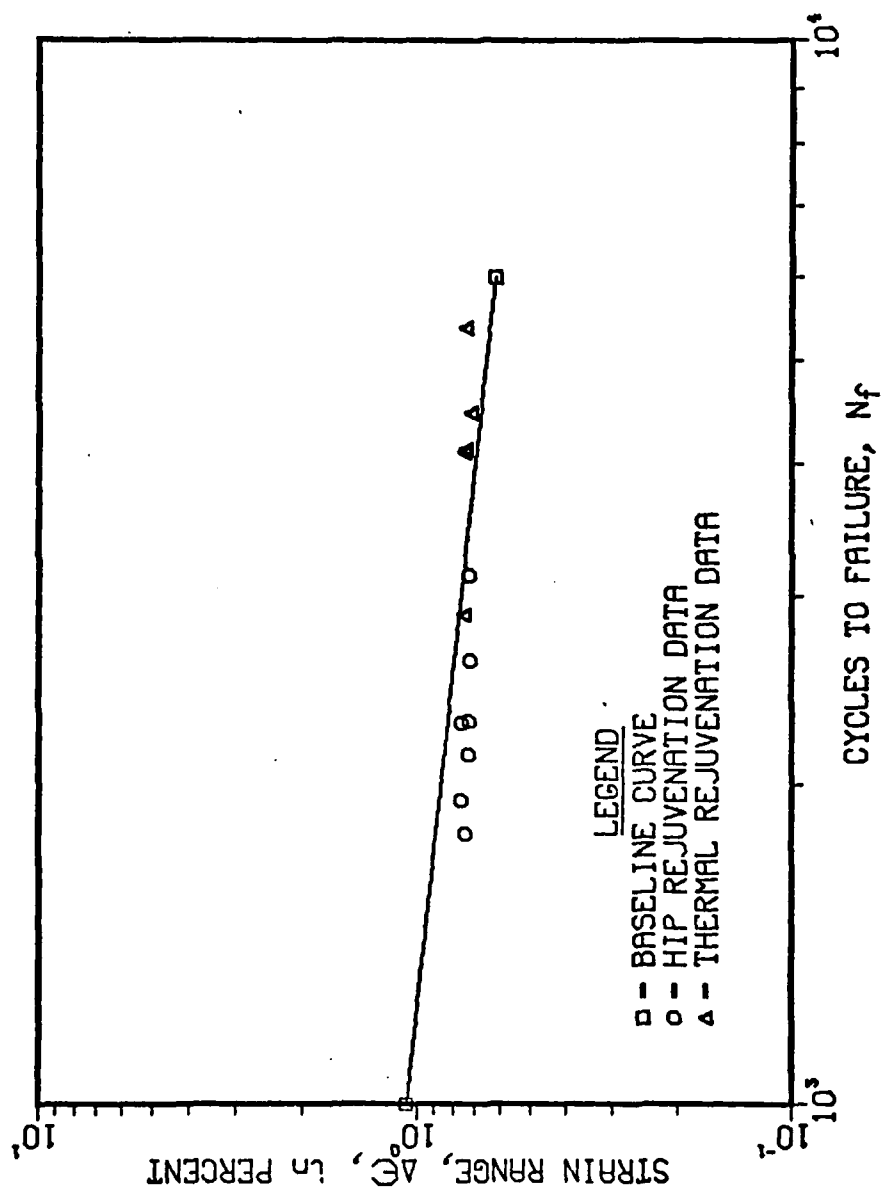


Figure 99. Plot of Strain Range vs Cycles to Failure with Baseline Trend Line and Rejuvenation Data

APPENDIX
LISTING OF COMPUTER PROGRAMS

APPENDIX I

SOURCE LISTING OF MODIFIED INSTRON LOW CYCLE FATIGUE
APPLICATION PROGRAM APP-900-A3A8

PAGE 0001

```
0001 *****
0002 *
0003 *
0004 *      LOW CYCLE FATIGUE
0005 *
0006 *      APP-900-A3A8+MOD2
0007 *
0008 *      04/04/75
0009 *
0010 *
0011 *****
0012 *
0013 *      COPYRIGHT INSTRON CORPORATION
0014 *      DECEMBER 1974
0015 *
0016 *      MODIFIED BY STEVE LEFFLER &
0017 *      BOB SCHAFRIK
0018 *
0019 *      4/13/79
0020 *
0021 *****
```

```

PAGE 0003                                LOW CYCLE FATIGUE

0039                                     *
0040      ***** BEGIN SECTION *****
0041                                     *
0042      001B F98E      BEGIN  ITBL TABLE1,33
           001C 0468
           001D 0021
0043      001E F98E      ITBL TABLE2,33
           001F 0489
           0020 0021
0044      0021 F98E      ITBL TABLE3,23
           0022 04AA
           0023 0017
0045      0024 F98E      ITBL TABLE4,33
           0025 04C1
           0026 0021
0046      0027 F95E      INID BUFFID
           0028 053E
0047      0029 F947      FMOV F0,AUGSTN
           002A 006E
           002B 0450
0048      002C F947      FMOV F0,DATPX AND DATPY
           002D 006E
           002E 0173
0049      002F F997      JST *GETSTA
0050      0030 EA3C      STX INDEX1
0051      0031 9900      STA INDEX      ALSO XB
           0172
0052      0032 C2B1      AXI '1'
0053      0033 0E00      SEM
0054      0034 EB3D      STXB *CURSTP
0055      0035 0F00      SWM
0056      0036 F947      FMOV F1,FCYCLE
           0037 045E
           0038 043A
0057      0039 FA71      JST INITCY
0058      003A F90F      CRLF
0059      003B F909      TYPE MAREA      ASK AREA DIMS.
           003C 04F7
0060      003D F93D      IFLT FTHICK      GET THICKNESS
           003E 043C
0061      003F F93D      IFLT FWIDTH      GET WIDTH
           0040 043E
0062      0041 F90F      CRLF
0063      0042 F948      FCMP FWIDTH,F0
           0043 043E
           0044 006E
0064      0045 2105      JAZ ROUND      ZERO = ROUND
0065      0046 F943      FMPL FTHICK,FWIDTH,FAREA
           0047 043C
           0048 043E
           0049 0442
0066      004A F20C      JMP CLEAR1
0067      004B F944      ROUND FDVD FTHICK,F2,FACT1

```

```

PAGE 0002                                LOW CYCLE FATIGUE

0023 0000                                REL 0
0024                                     *
0025                                     ***** SSP-LINKAGE *****
0026                                     *
0027 0007 0007 0007                      DATA NAME
0028 0001 0013 0013                      DATA BEGIN
0029 0002 00D6 00D6                      DATA RESTRT
0030 0003 0017A 0017A                    DATA UPDATE
0031 0004 0027A 0027A                    DATA FINAL
0032 0005 0066 0066                      DATA STAT: A
0033 0006 0069 0069                      DATA STAT: B
0034                                     *
0035 0007 CID0 NAME TEXT 'APP-900-A3'
0008 D0AD
0009 B9B0
000A BFAD
000B C1B3
0036 000C C1B8 TEXT 'A8+MOD2'
000D ABCD
000E CFC4
000F B2A0
0037 0010 A0A0 TEXT ' LOW CYCLE FATIGUE'
0011 APCC
0012 CFC7
0013 A0C3
0014 D0C3
0015 CCC5
0016 A0C6
0017 CID4
0018 C9C7
0019 D5C5
001A C0A0

```



```

PAGE 0004                                LOW CYCLE FATIGUE

      004C 043C
      004D 0070
      004E 0426
0068 004F F943      FMPL FAC:1,FAC:1,FAC:1
      0050 0426
      0051 0426
      0052 0426
0069 0053 F943      FMPL FAC:1,F:PI,FAREA
      0054 0426
      0055 007A
      0056 0442
0070 0057 F909      CLEAR1 TYPE MSTPLM      ASK STRAIN LIMITS
      0058 050D
0071 0059 F93D      IFLT MAXLIM      MAX. LIMIT
      005A 0446
0072 005B F93D      IFLT MINLIM      MIN. LIMIT
      005C 0448
0073 005D E100      LDX XABC
      0170
0074 005E F944      FDVD MAXLIM,*STVALP,HLIMIT
      005F 0446
      0060 80B4
      0061 00BE
0075 0062 F944      FDVD MINLIM,*STVALP,LLIMIT
      0063 0448
      0064 80B4
      0065 00C0

0076                                     ***
0077 0066 F90F      CRLF
0078 0067 F909      TYPE FNDMES      RANDOM LIMITS?
      0068 0518
0079 0069 F90B      IKB
0080 006A 00AC      CAI ', '      LEAVE AS IS?
0081 006B F20A      JMP CLEAR2      YES
0082 006C 00D9      CAI 'Y'
0083 006D F202      JMP FNDMLT
0084 006E 0110      ZAR      RQSTD/ASS'D NO
0085 006F F201      JMP S+2
0086 0070 0350      RNDMLT APP      SET RANDOM FLAG
0087 0071 9900      STA FNDFLG
      0175
0088 0072 F90B      WTCLP IKB      TERMINATION CHAR?
0089 0073 00AC      CAI ', '
0090 0074 F201      JMP CLEAR2
0091 0075 F603      JMP WTCLR      NO
0092                                     ***
0093 0076 B2FE      CLEAR2 LDA FNDFLG
0094 0077 3125      JAV CLR2
0095 0078 F90F      CPLF
0096 0079 F909      TYPE MISTRS      ASK MIN. STRESS
      007A 0503
0097 007B F93D      IFLT STRSLM      GET STRESS LIMIT
      007C 0444

```

PAGE	0005	LOW CYCLE FATIGUE	
0098	007D F944	CLR2	FDVD HLIMIT,F32767,HPNGE
	007E 00BE		
	007F 0074		
	0080 0452		
0099	0081 F944		FDVD LLIMIT,F32767,LPNGE
	0082 00C0		
	0083 0074		
	0084 0454		
0100	0085 F945	FIX	HLIMIT,HLIMIT
	0086 00BE		
	0087 00BE		
0101	0088 F945	FIX	LLIMIT,LLIMIT
	0089 00C0		
	008A 00C0		
0102	008B F947	FMOV	FI,NN
	008C 045E		
	008D 045B		
0103	008E F947	FMOV	F0,XX CALC. MD AFTER
	008F 006E		
	0090 045A		
0104		* GET CYCLE #'S & INCREMENTS	
0105	0091 F90F	CPLF	
0106	0092 F909	TYPE	NMMESS
	0093 00CC		
0107	0094 F93D	IFLT	FNMI
	0095 00C4		
0108	0096 F93D	IFLT	FNMI
	0097 00C6		
0109	0098 F93D	IFLT	FNMI
	0099 00C8		
0110	009A F90F	CPLF	
0111	009B 0010	ARM	1 PASS INITIALLY
0112	009C 9ADA	STA	CNT
0113	009D 9AD5	STA	XC NEEDED FOR FINAL
0114	009E C70A	LAM	10
0115	009F 9AC9	STA	CNTNI INITIALIZE
0116	00A0 B0CA	LDA	NUM1 SLOPE ROUTINE
0117	00A1 9ACA	STA	NUM
0118	00A2 9A95	STA	DLTLD
0119	00A3 8A97	ADD	1300
0120	00A4 9A97	STA	LOAD2
0121	00A5 0110	ZAR	
0122	00A6 9900	STA	BRANCH
	01C7		
0123	00A7 9AD0	STA	DATPX
0124	00A8 9AD0	STA	DATPY
0125	00A9 9AC3	STA	MDFLG
0126	00AA F22B	JMP	RESTR

```

PAGE 0006                                LOW CYCLE FATIGUE

0128 00AB 0000 INITCY ENT
0129 00AC 0350 APP
0130 00AD 9AC3 STA XBPT OR XA
0131 00AE F947 FMOV F1,CMPTEL
      00AF 045E
      00B0 058A
0132 00B1 F947 FMOV F2,CMPTEL+2
      00B2 0070
      00B3 058C
0133 00B4 F941 FADD F1,F2,F3
      00B5 045E
      00B6 0070
      00B7 00CA
0134 00B8 F947 FMOV F3,CMPTEL+4
      00B9 00CA
      00BA 058E
0135 00BB DABC IMS DATPX PRINT FIRST CYCLE
0136 00BC F711 RTN INITCY
0137 *
0138 *
0139 *
0140 00BD 0000 INDEX1 DATA 0
0141 00BE 0000 HLIMIT RES 2.0
0142 00C0 0000 LLIMIT RES 2.0
0143 00C2 0000 CURSTP BAC STAVUM+9
0144 00C3 00D9 FNDM DATA 'Y'
0145 00C4 0000 FNM1 RES 2.0 CUT-OFF CYCLE 1 INC
0146 00C6 0000 FNM2 RES 2.0 INCREMENT TWO
0147 00C8 0000 FNM3 RES 2.0 LAST CYCLE
0148 00CA 0000 F3 RES 2.0
0149 00CC C5CE NMMESS TEXT 'ENTER NM1,NM2,NM3:0'
      00CD D4C5
      00CE D2A0
      00CF CECD
      00D0 B1AC
      00D1 CECD
      00D2 B2AC
      00D3 CECD
      00D4 B3BA
      00D5 C0A0

```

PAGE 0007

LOW CYCLE FATIGUE

```

0151      *
0152      ***** RESTART SECTION *****
0153      *
0154      00D6 F93D RESTPT STOP
0155      00D7 B29D LDA FNDFLG RANDOM LIMITS
0156      00D8 2114 JAZ PSTEX NO
0157      00D9 F90F CRLF
0158      00DA F909 TYPE RESETM RESET RANDOM SEQUENCE
           00DB 0531
0159      00DC F90B IKB
0160      00DD 0C48 TAX
0161      00DE C0AC CAI ',' DO THE SAME AS LAST TIME?
0162      00DF F20B JMP SAME2 YES
0163      00E0 EE1D STX ENDM
0164      02E1 C0CE RESETI CAI 'N' RESET SEQUENCE?
0165      00E2 F202 JMP PSTRT0 NO
0166      02E3 C603 LAP 3 YES
0167      02E4 9B3F STA *ENIPTR
0168      00E5 C1AC RSTRTO CXI ',' SAME AS LAST TIME?
0169      00E6 F206 JMP RSTEX YES
0170      02E7 F92B IKB INPUT TERMINATION?
0171      00E8 C7AC CAI ','
0172      02E9 F203 JMP RSTEX
0173      00EA F625 JMP RSTRTO NO, KEEP WAITING
0174      00EB 9629 SAME2 LDA ENDM
0175      00EC F60B JMP RESETI
0176      *
0177      00ED F90F RSTEX CRLF
0178      00EE F909 TYPE MRATE
           00EF 0522
0179      00F0 F93D IFLT SRRATE
           00F1 044A
0180      00F2 F90F CRLF
0181      00F3 E27C LDX XABC
0182      00F4 F944 FDVD SPRATE,*STVALP,CLKRT
           00F5 044A
           00F6 80B4
           00F7 044C
0183      00F8 F90F CRLF
0184      00F9 F913 PATE CLKRT SET TIME VALUE
           00FA 044C
0185      00FB E274 LDX XABC FORCE INDEX IN XA
0186      00FC 0129 IXR
0187      00FD F944 FDVD *LDVALP,FAREA,STRESS
           00FE 80A7
           00FF 0442
           0100 044E
0188      0101 F944 FDVD STRSLM,STRESS,STRESS
           0102 0444
           0103 044E
           0104 0272
0189      0105 F945 FIX STRESS,STRESS
           0106 0272

```

PAGE	0008	LOW CYCLE FATIGUE	
	0107 0272		
0190	0108 F912	MODE STROKE	
	0109 0001		
0191	010A F90F	CPLF	
0192	010B F909	TYPE MEXEC	PRINT EXECUTE
	010C 052D		
0193	010D F90F	CPLF	
0194	010E F909	TYPE MHEAD	
	010F 0553		
0195	0110 F90F	CPLF	
0196	0111 F951	CLOS	
0197		*	
0198	0112 0800	SETTBL ENT	
0199	0113 DA64	IMS DATPX	PRINT ALL TRIGGER CYCLES
0200		* STORE CURRENT CYCLE - END OF TEST?	
0201	0114 F947	FMOV FTCYC, FTCYC	
	0115 043A		
	0116 013F		
0202	0117 F949	FCMP FNM3, F0	SEE IF DEFAULT
	0118 00C8		
	0119 006E		
0203	011A 2104	JAZ SETTBL	
0204	011B F948	FCMP FTCYC, FNM3 LAST CYCLE?	
	011C 013F		
	011D 00C8		
0205	011E 3095	JAP INCDNE	
0206	011F B251	SETTB2 LDA XBPT	
0207	0120 0150	IAR	
0208	0121 C004	CAI 4	
0209	0122 F202	JMP INCTBL	
0210	0123 9A4D	STA XBPT	
0211	0124 F712	RTN SETTBL	
0212	0125 0350	INCTEL ARP	
0213	0126 9A4A	STA XBPT	
0214	0127 FA19	INCTB2 JST CYADJ	
0215	0128 F947	FMOV FTCYC, CMPTBL	
	0129 013F		
	012A 058A		
0216	012B FA15	JST CYADJ	
0217	012C F947	FMOV FTCYC, CMPTBL+2	
	012D 013F		
	012E 058C		
0218	012F FA11	JST CYADJ	
0219	0130 F947	FMOV FTCYC, CMPTBL+4	
	0131 013F		
	0132 058E		
0220	0133 F721	RTN SETTBL	
0221	0134 0010	INCDNE ARM	
0222	0135 9A91	STA BRANCH	FINI
0223	0136 F956	EXIT	
0224		*	
0225	0137 0000	OLDLD DATA 0	
0226	0138 0000	DLTLD DATA 0	

```

PAGE 0009                                LOW CYCLE FATIGUE

0227 0139 0000 DLTSTN DATA 0,0
      013A 0000
0228 013B 012C 1300 DATA 300
0229 013C 0000 LOAD2 DATA 0
0230 013D 0000 CUPLD DATA 0
0231 013E 0020 CUPSTN DATA 0
0232 013F 0000 FTCYC RES 2,0      CYCLE VALUE
0233
0234 *
0235      * ADJUST CYCLE TRIGGER VALUE
0235 0141 0800 CYADJ ENT
0236 0142 F948      FCMP FTCYC,FNM1 SEE IF INC BY 1
      0143 013F
      0144 00C4
0237 0145 3085      JAP CYAD2      INC BY MORE
0238 0146 F941      FADD F1,FTCYC,FTCYC
      0147 045E
      0148 013F
      0149 013F
0239 014A F204      JMP CYAD3
0240 014B F941 CYAD2 FADD FNM2,FTCYC,FTCYC INC BY FNM2
      014C 00C6
      014D 013F
      014E 013F
0241 014F F70E CYAD3 RTN CYADJ
0242
0243

```

PAGE 0010

LOW CYCLE FATIGUE

```

0245
0246 0150 B218 *      LDA CNTN1
0247 0151 2103      JAZ NIX
0248 0152 B219      LDA NUM
0249 0153 9616      SUB CUPLD      SAVE POINTS
0250 0154 2031      JAM DATN1
0251 0155 F236      NIX      JMP NOT1
0252 0156 B214      DATN1     LDA NUM1      OF LOAD
0253 0157 8A14      ADD NUM1
0254 0158 9A13      STA NUM1      AND STRAIN
0255 0159 B61C      LDA CUPLD
0256 015A F991      GIVE TABLE3
015B 04AA
0257 015C F206      JMP FULLN1
0258 015D B61F      LDA CURSTM      IN 5%
0259 015E F991      GIVE TABLE3
015F 04AA
0260 0160 F202      JMP FULLN1
0261 0161 DA27      IMS CNTN1
0262 0162 F279      JMP NOT1
0263 0163 0110      FULLN1     ZAP
0264 0164 9A04      STA CNTN1      SLOPE
0265 0165 F957      CUE      SLOPE: 1000
0166 03B9
0167 03E3
0266 0168 F273      JMP NOT1
0267
0268 0169 0000      *      CNTN1     DATA 0      CALCULATION
0269 016A 0190      BREAK     DATA 400      20% FS
0270 016B 0004      NUM1      DATA 100
0271 016C 0000      NUM1      DATA 0
0272 016D 0000      MDPLG     DATA 0
0273 016E 0000      UTEMP1     DATA 0
0274 016F 0000      UTEMP2     DATA 0
0275 0170 0171      XABC       DATA 5+1
0276 0171 0000      XBPT       DATA 0      OR XA
0277 0172 0000      INDEX      DATA 0      OR XB
0278 0173 0000      XC         DATA 0
0279 0004      VALPTR     SCU 14
0280 0174 0395      ENIPTR     DATA ENI
0281 0175 0000      ENDPLG     DATA 0
0282 0176 0368      GETNUM1     DATA RANDOM
0283 0177 0000      CNT         DATA 0
0284 0178 0000      DATPX       DATA 0
0285 0179 0000      DATPY       DATA 0

```

PAGE 0011

LOW CYCLE FATIGUE

0287

*

PAUSE

0288

*

0289

***** UPDATE SECTION *****

0290

*

0291

017A F910

UPDATE READ LOAD, CUPLD

017B 0000

017C 013D

0292

017D F910

READ STROKE, CURSTN

017E 0001

017F 013E

0293

0180 B246

LDA BRANCH

0294

0181 3031

JAP S+2

IF < 0 THEN

0295

0182 F95F

DONE

REQUESTED DONE

0296

0183 3181

JAG S+2

0297

0184 F243

JMP UP:

0298

0185 E6C8

LDX INDEX1

0299

0186 E648

LDA CURSTN

0300

0187 9504

SUB @*VALPTR

0301

0188 D61E

CMS BREAK

0302

0189 F202

JMP S+3

0303

018A 0000

NOP

0304

018B F95F

DONE

0305

018C B64E

LDA CURSTN

0306

018D D6CD

CMS LLIMIT

0307

018E F2C6

JMP REVUP

0308

018F 0000

NOP

0309

0190 B653

LDA CUPLD

0310

0191 9E5A

STA OLDDLD

0311

0192 F911

RAMP DOWN

0312

0193 9000

0313

0194 F956

EXIT

0314

0195 B61C

* REVUP

LDA DATPY

0315

0196 210A

JAZ XX3

0316

0197 B659

LDA CURSTN

0317

0198 BE29

EMA UTEMP2

0318

0199 0048

TAX

0319

019A B65D

LDA CUPLD

0320

019B BE2D

EMA UTEMP1

0321

019C F957

CUE PRINT, 2900

019D 02F6

019E 0B54

0322

019F 0110

ZAR

0323

01A0 9E27

STA DATPY

0324

01A1 E631

XX3

LDY XABC

0325

01A2 F948

FCMP *C1PTL, FCYCLE

01A3 858A

01A4 043A

0326

01A5 3189

JAG DATAP1

FILL TABLE UNLESS CYCLE <

0327

01A6 B669

LDA CUPLD

VALUE SOUGHT

0328

01A7 0000

NOP

0329

01A8 0000

NOP

0330

01A9 0000

NOP

PAGE	0012		LOW CYCLE FATIGUE
0331	01AA	B66C	LDA CURSTN
0332	01AB	0000	NOP
0333	01AC	0000	NOP
0334	01AD	0000	NOP
0335	01AE	FE9C	JST SETTEL
0336	01AF	F941	DATA01 FADD F1,FCYCLE,FCYCLE
	01B0	045E	
	01B1	043A	
	01B2	043A	
0337	01B3	B67C	LDA OLDDLD
0338	01B4	8E49	ADD NUM1
0339	01B5	9E7D	STA DLTLD
0340	01B6	8E7B	ADD 1302
0341	01B7	9E7B	STA LOAD2
0342	01B8	F911	RAMP UP
	01B9	0000	
0343	01BA	E645	LDA MIDFLG
0344	01BB	2108	JAZ RMPUP
0345	01BC	FF46	JST *GETNUM
0346	01BD	F943	FMPL HFNGE,PNDTMP,HLIMIT
	01BE	0452	
	01BF	0456	
	01C0	00BE	
0347	01C1	F945	FIX HLIMIT,HLIMIT
	01C2	00BE	
	01C3	00BE	
0348	01C4	0110	RMPUP ZAR
0349	01C5	9A01	STA BRANCH
0350	01C6	F956	EXIT
0351			*
0352	01C7	0000	BRANCH DATA 0
0353			*
0354	01C8	E100	UP: LDX INDEX1
		00BD	
0355	01C9	B504	LDA @*VALPTR
0356	01CA	968C	SUB CURSTN
0357	01CB	D661	CMS BREAK
0358	01CC	F202	JMP S+3
0359	01CD	0000	NOP
0360	01CE	F95F	DONE
0361	01CF	B100	LDA HLIMIT
		00BE	
0362	01D0	D692	CMS CURSTN
0363	01D1	F24C	JMP REVDUN
0364	01D2	0000	NOP
0365	01D3	E696	LDA CUPLD
0366	01D4	9E9D	STA OLDDLD
0367	01D5	F911	RAMP UP
	01D6	0000	
0368	01D7	F948	FCMP FCYCLE,F1
	01D8	043A	
	01D9	045E	
0369	01DA	3101	JAN NOT1

PAGE 0013

LOW CYCLE FATIGUE

0370	01DB	F69B		JMP	NI	RETURNS TO NOT1
0371	01DC	B66F	NOT1	LDA	MDFLG	
0372	01DD	20DF		JAM	UPEXIT	
0373	01DE	3189		JAG	MD2ND	
0374	01DF	B6A2		LDA	CUPLD	AT 1ST SMPL PT?
0375	01E0	D6A8		CMS	DLTLD	
0376	01E1	F23B		JMP	UPEXIT	NO
0377	01E2	0000		NOP		
0378	01E3	9EAB		STA	DLTLD	YES, STORE DATA
0379	01E4	B6A6		LDA	CURSTN	
0380	01E5	9EAC		STA	DLTSTN	
0381	01E6	DE79		IMS	MDFLG	
0382	01E7	F235		JMP	UPEXIT	
0383	01E8	B6AE	MD2ND	LDA	CUPLD	AT 2ND SMPL PT?
0384	01E9	D6AD		CMS	LOAD2	
0385	01EA	F232		JMP	UPEXIT	
0386	01EB	0000		NOP		
0387	01EC	B6AF		LDA	CUPLD	YES, CALC. MD
0388	01ED	96B5		SUB	DLTLD	
0389	01EE	9E86		STA	DLTLD	
0390	01EF	B6E1		LDA	CURSTN	
0391	01F0	96B7		SUB	DLTSTN	
0392	01F1	9E83		STA	DLTSTN	
0393	01F2	F946		FLT	DLTLD,MOD	
	01F3	0138				
	01F4	045C				
0394	01F5	F943		FMPL	MOD,STRESV,MOD	
	01F6	045C				
	01F7	044E				
	01F8	045C				
0395	01F9	F946		FLT	DLTSTN,DLTSTN	
	01FA	0139				
	01FB	0139				
0396	01FC	E68C		LDX	XABC	XB=INDEX
0397	01FD	F943		FMPL	DLTSTN,*STVALP,DLTSTN	
	01FE	0139				
	01FF	80B4				
	0200	0139				
0398	0201	F944		FDVD	MOD,DLTSTN,MOD	
	0202	045C				
	0203	0139				
	0204	045C				
0399	0205	F943		FMPL	MOD,F1000,MOD	
	0206	045C				
	0207	0466				
	0208	045C				
0400	0209	F941		FADD	MOD,XX,XX	CALC. NEW
	020A	045C				
	020B	045A				
	020C	045A				
0401	020D	DE96		IMS	CNT	MODULUS
0402	020E	F2FC		JMP	XIT	EVERY 4TH
0403	020F	F944		FDVD	XX,NN,MD	CYCLE

PAGE 0014

LOW CYCLE FATIGUE

	0210	045A			
	0211	0458			
	0212	0274			
0404	0213	C704	LAM	4	AVERAGE OVER
0405	0214	9E9D	STA	CNT	4 CYCLES
0406	0215	F947	FMOV	F0,XX	
	0216	006E			
	0217	045A			
0407	0218	F947	FMOV	F4,NN	
	0219	0460			
	021A	0458			
0408	021B	0010	XIT	APM	RESET FLAG
0409	021C	9EAF	STA	MDFLG	
0410	021D	F956	UFEXIT	EXIT	
0411			*		
0412	021E	B6A9	REVDN	LDA	ENDFLG
0413	021F	3104	JAN	RVDN	NO STRESS TEST
0414	0220	B251	LDA	STRESS	WITH RANDOM OPTION
0415	0221	96E4	SUB	CURLD	
0416	0222	2031	JAM	S+2	
0417	0223	F95F	DONE		END OF TEST
0418	0224	B6AC	RVDN	LDA	DATPX
0419	0225	210D	JAZ	XX2	
0420	0226	B6E9	LDA	CURLD	
0421	0227	9EB9	STA	UTEMP1	
0422	0228	B6EA	LDA	CURSTN	
0423	0229	9E2A	STA	UTEMP2	
0424	022A	F947	FMOV	FCYCLE, FAC:3	
	022B	043A			
	022C	0278			
0425	022D	F947	FMOV	MD, FAC:4	
	022E	0274			
	022F	02F4			
0426	0230	0110	ZAP		
0427	0231	9EB9	STA	DATPX	
0428	0232	DEB9	IMS	DATPY	
0429	0233	F946	XX2	FLT	CURSTN, TEMPAV
	0234	013E			
	0235	0438			
0430	0236	F941	FADD	TEMPAV, AUGSTN, AUGSTN	
	0237	0438			
	0238	0450			
	0239	0450			
0431	023A	E6CA	LDX	XABC	
0432	023B	F948	FCMP	*CMPTEL, FCYCLE	
	023C	858A			
	023D	043A			
0433	023E	3190	JAG	DATA02	
0434	023F	B100	LDA	CURLD	
		013D			
0435	0240	0000	NOP		
0436	0241	0000	NOP		
0437	0242	0000	NOP		

PAGE 0015

LOW CYCLE FATIGUE

0438	0243	B100	LDA	CURSTN	
		013E			
0439	0244	0000	NOP		
0440	0245	0000	NOP		
0441	0246	0000	NOP		
0442	0247	B22C	LDA	MD	
0443	0248	0000	NOP		
0444	0249	0000	NOP		
0445	024A	0000	NOP		
0446	024B	B229	LDA	MD+1	
0447	024C	0000	NOP		
0448	024D	0000	NOP		
0449	024E	0000	NOP		
0450	024F	F911	DATA02	RAIP DOWN	
		0250			
0451	0251	0110	ZAR		
0452	0252	9EE5	STA	MDFLG	
0453	0253	B6DE	LDA	MDFLG	
0454	0254	2109	JAZ	RMPDN	
0455	0255	FFDF	JST	*GETNUM	
0456	0256	F943	FMPL	LENGL, PNDTMP, LLIMIT	
		0257			
		0258			
		0259			
0457	025A	F945	FIX	LLIMIT, LLIMIT	
		025B			
		025C			
0458	025D	0350	RMPDN	ARP	
0459	025E	9E97	STA	BRANCH	
0460	025F	F956	EXIT		
0461			*		
0462	0260	F957	FULL	CUE WINKER, 1005 FLASH STATUS 1	
		0261			
		0262			
0463	0263	0010	ARM		REQUEST A DONE
0464	0264	9E9D	STA	BRANCH	IN UPDATE
0465	0265	F956	EXIT		
0466			*		
0467	0266	0010	STAT:A	ARM	REQUEST A DONE
0468	0267	9EAC	STA	BRANCH	IN UPDATE
0469	0268	F951	CLOS		
0470			*		
0471	0269	DEF1	STAT:B	IMS DATPX	
0472	026A	F959		WINK 2	
		026B			
0473	026C	F951		CLOS	
0474			*		
0475	026D	F958		WINKER WINK 1	
		026E			
0476	026F	F951		CLOS	
0477			*		
0478	0270	00AB	INITCX	DATA INITCY	
0479	0271	0112	SETPTR	DATA SETTDL	

PAGE 0016

LOW CYCLE FATIGUE

```

0480 0272 0000 STPESS RES 2,0
0481 0274 0000 MD PES 2,0
0482 0276 0000 FAC:2 RES 2,0
0483 0278 0000 FAC:3 RES 2,0
0484 *

PAUSE
0485 ***** FINAL SECTION *****
0486 *
0487 027A 0110 FINAL ZAR
0488 027B 9EB4 STA BRANCH
0489 027C F90F CRLF
0490 027D F90F CRLF
0491 * TYPE TRAILER
0492 027E F909 TYPE NULL
0493 027F 04E2
0494 0280 F909 TYPE NULL
0495 0281 04E2
0496 0282 0000 NOP
0497 0283 F993 DATE
0498 0284 F90F CRLF
0499 0285 F909 TYPE BUFFID
0500 0286 053E
0501 0287 F90F CRLF
0502 0288 F90F CRLF
0503 0289 F900 JST SWAP SAVE CYCLE
0504 028A 0398
0505 028B B400 LDA 00 DATA IN CASE OF
0506 028C 3181 JAG LOOP3 START
0507 028D FF1C JST *INITCX
0508 028E E265 LOOP3 LDX XABCP
0509 028F F947 FMOV *CMPTBL,FAC:1
0510 0290 859A
0511 0291 0426
0512 0292 F992 GET TABLE1
0513 0293 0468
0514 0294 F242 JMP EMPTY
0515 0295 9E1C STA FAC:3
0516 0296 F992 GET TABLE4
0517 0297 04C1
0518 0298 F23E JMP EMPTY
0519 0299 9E22 STA FAC:2
0520 029A F992 GET TABLE4
0521 029B 04C1
0522 029C F23A JMP EMPTY
0523 029D 9E25 STA FAC:2+1
0524 * TAB 2
0525 * WDEC FAC:1,9,0 CYCLE #
0526 029E F94D WFLT FAC:1
0527 029F 0426
0528 * TAB 5
0529 * WDEC FAC:2,10,0 MODULUS
0530 029F F94D WFLT FAC:2
0531 02A0 0276
0532 * TAB 6

```

PAGE	0017	LOW CYCLE FATIGUE
0522	02A1 FA0C	JST PRINTV
0523	02A2 C6A0	LAP
0524		LXP 31
0525	02A3 C41C	LXP 28
0526	02A4 F92E	OTT
0527	02A5 00A9	DXR
0528	02A6 3342	JXN 5-2
0529	02A7 F992	GET TABLE1
	02A8 0469	
0530	02A9 F22C	JMP EMPTY
0531	02AA 9E32	STA FAC:3
0532	02AB FAC2	JST PRINTV
0533	02AC FF3B	JST *SETPTR
0534	02AD F620	JMP LOOP3
0535		
0536	02AE 0300	* PRINTV ENT
0537	02AF F946	FLT FAC:3, FAC:3
	02B0 0279	
	02B1 0278	
0538	02B2 F943	FMPL FAC:3, STRESS, FAC:3
	02B3 0278	
	02B4 044E	
	02B5 0278	
0539		* WDEC FAC:3, 8, 3 STRESS
0540	02B6 F94D	WFLT FAC:3
	02B7 0278	
0541		* TAB 6
0542	02B8 E23A	LDX XABCP
0543	02B9 F992	GET TABLE2
	02BA 0489	
0544	02BB F21A	JMP EMPTY
0545	02BC 9A37	STA FAC:4
0546	02BD F946	FLT FAC:4, FAC:4
	02BE 02F4	
	02BF 02F4	
0547	02C0 F943	FMPL FAC:4, *STVALP, FAC:4
	02C1 02F4	
	02C2 80B4	
	02C3 02F4	
0548		* WDEC FAC:4, 7, 4 STRAIN
0549	02C4 F94D	WFLT FAC:4
	02C5 02F4	
0550		* TAB 7
0551	02C6 F944	FDVD FAC:3, FAC:2, FAC:3
	02C7 0279	
	02C8 0276	
	02C9 0273	
0552	02CA F943	FMPL FAC:3, F1000, FAC:3
	02CB 0273	
	02CC 0466	
	02CD 0279	
0553	02CE F942	FSUB FAC:4, FAC:3, FAC:3
	02CF 02F4	

PAGE 0018

LOW CYCLE FATIGUE

	02D0	0278		
	02D1	0278		
0554			*	WDEC FAC:3,9,7 PLASTIC STPAIN
0555	02D2	F94D		WFLT FAC:3
	02D3	0278		
0556	02D4	F90F		CPLF
0557	02D5	F727		RTN PRINTV
0558			*	
0559	02D6	F90F	EMPTY	CPLF
0560	02D7	F90F		CPLF
0561	02D8	F909		TYPE MLAST
	02D9	0575		
0562			*	WDEC FCYCLE,9,0 FINAL CYCLE #
0563	02DA	F94D		WFLT FCYCLE
	02DB	043A		
0564	02DC	F90F		CPLF
0565	02DD	F909		TYPE MAVGS
	02DE	057A		
0566	02DF	F944		FDVD AUGSTN,FCYCLE,AUGSTN
	02E0	0450		
	02E1	043A		
	02E2	0450		
0567	02E3	E20F		LDX XABCP
0568	02E4	F943		FMPL AUGSTN,*STVALP,FAC:3
	02E5	0450		
	02E6	80E4		
	02E7	0278		
0569			*	WDEC FAC:3,7,4 PEAK STPAIN
0570	02E8	F94D		WFLT FAC:3
	02E9	0278		
0571	02EA	F90F		CPLF
0572	02EB	F909		TYPE MSLOPE
	02EC	0583		
0573			*	WDEC RESULT,10,0 SLOPE
0574	02ED	F94D		WFLT RESULT
	02EE	0436		
0575	02EF	FA08		JST SWAP
0576	02F0	F90F		CPLF
0577	02F1	F90F		CPLF
0578	02F2	F951		CLOS
0579			*	
0580	02F3	0171	XABCP	DATA XBPT
0581	02F4	0000	FAC:4	RES 2,0
0582			*	
0583	02F6	9900	PRINT	STA FAC:1
		0426		
0584	02F7	EE31		STX FAC:2
0585	02F8	F946		FLT FAC:1,FAC:1
	02F9	0426		
	02FA	0426		
0586	02FB	F946		FLT FAC:2,FAC:2
	02FC	0276		
	02FD	0276		

PAGE	0019	LOW CYCLE FATIGUE
0587	02FE F943	FMPL FAC:1, STRESV, FAC:1
	02FF 0426	
	0300 044E	
	0301 0426	
0588	0302 E60F	LDX XABCP
0589	0303 F943	FMPL FAC:2, *STVALP, FAC:2
	0304 0276	
	0305 80B4	
	0306 0276	
0590	0307 C606	LAP 6
0591	0308 9902	STA OUFLEN FIELD LENGTH = 6
	05EE	
0592	0309 FAA5	JST CPLF2
0593		TAB 2
0594		* WDEC FAC:3, 9.0 CYCLE #
0595		* OUTPUT CYCLE #
0596	030A F947	FMOV FI, OUF LZ / 1.
	030B 045E	
	030C 05F2	
0597	030D F947	FMOV FAC:3, OUF LX
	030E 0278	
	030F 05F0	
0598	0310 F941	FADD FIE14, OUF LX, OUF LX ELIM 13.99
	0311 05F8	
	0312 05F0	
	0313 05F0	
0599	0314 F900	JST OUF LFX
	0596	
0600	0315 FA95	JST SPACE
0601		* OUTPUT MODULUS
0602	0316 F947	FMOV FIE6, OUF LZ / 1.E6
	0317 05F4	
	0318 05F2	
0603	0319 F947	FMOV FAC:4, OUF LX
	031A 02F4	
	031B 05F0	
0604	031C F900	JST OUF LFX
	0596	
0605	031D FA9D	JST SPACE
0606		* OUTPUT MAX STRESS
0607	031E F947	FMOV FAC:1, OUF LX
	031F 0426	
	0320 05F0	
0608	0321 F947	FMOV FI, OUF LZ / 1.
	0322 045E	
	0323 05F2	
0609	0324 F900	JST OUF LFX PRINT NUM
	0596	
0610	0325 FA95	JST SPACE
0611		* STORE STRAIN
0612	0326 F947	FMOV FAC:2, OUTMPI
	0327 0276	
	0328 03B5	

PAGE	0020	LOW CYCLE FATIGUE
0613		* TAB 7
0614	0329 FASD	JST PRNTSB
0615	032A F946	FLT UTEMP1, FAC:1
	032B 016E	
	032C 0426	
0616	032D F946	FLT UTEMP2, FAC:2
	032E 016F	
	032F 0276	
0617	0330 F943	FMPL FAC:1, STRESV, FAC:1
	0331 0426	
	0332 044E	
	0333 0426	
0618	0334 E641	LDX XABCP
0619	0335 F943	FMPL FAC:2, *STVALP, FAC:2
	0336 0276	
	0337 80B4	
	0338 0276	
0620		* OUTPUT MIN STRESS
0621	0339 F947	FMOV FAC:1, OUFLX
	033A 0426	
	033B 05F0	
0622	033C F947	FMOV F1, OUFLZ / 1.0
	033D 045E	
	033E 05F2	
0623	033F F900	JST OUFLFX
	0596	
0624	0340 FA6A	JST SPACE
0625		* OUTPUT MAX STRAIN
0626	0341 F947	FMOV F1E13, OUFLZ / 1.E-3
	0342 05F6	
	0343 05F2	
0627	0344 F947	FMOV OUTMP1, OUFLX
	0345 03B5	
	0346 05F0	
0628	0347 F900	JST OUFLFX
	0596	
0629	0348 FA62	JST SPACE
0630		* OUTPUT MIN. STRAIN
0631	0349 F947	FMOV F1E13, OUFLZ / 1.E-3
	034A 05F6	
	034B 05F2	
0632	034C F947	FMOV FAC:2, OUFLX
	034D 0276	
	034E 05F0	
0633	034F F900	JST OUFLFX
	0596	
0634	0350 FA5A	JST SPACE
0635		* TAB 7
0636		* OUTPUT PLASTIC STRAIN MAX.
0637	0351 F947	FMOV F1E14, OUFLZ / 1.E-4
	0352 05F8	
	0353 05F2	
0638	0354 F947	FMOV OUTMP2, OUFLX

PAGE 0021

LOW CYCLE FATIGUE

```

0355 03B7
0356 05F0
0639 0357 F900      JST  OUFLEX
           0596
0640 0358 FA52      JST  SPACE
0641 0359 FA2D      JST  PR:TSB
0642          * OUTPUT MIN PSTRAIN
0643 035A F947      FMOV F1E14,OUFLZ / 1.E-4
           035B 05F8
           035C 05F2
0644 035D F947      FMOV OUTMP2,OUFLX
           035E 03D7
           035F 05F0
0645 0360 F900      JST  OUFLEX
           0596
0646 0361 FA49      JST  SPACE
0647 0362 FA4C      JST  CLF2
0648 0363 F95A      DIM  2
           0364 0002
0649 0365 F95A      DIM  1
           0366 0001
0650 0367 F951      CLOS
0651          *
0652          *
0653 0368 0800      RANDOM EIT
0654 0369 5804      DATA :5804      ICA, GET CONSOLE STATUS
0655 036A 9AEB      STA  PNDTMP      SAVE IT
0656 036B 06AA      LAP  :AA        IS THIS AN LSI OR ALPHA?
0657 036C 4404      DATA :4404      OCA
0658 036D 5804      DATA :5804      ICA
0659 036E 3107      JAY  LSI        IT'S AN LSI IF NON-ZERO RESPON
0660 036F E215      LDX  FN1        ELSE, IT'S AN ALPHA
0661 0370 11A9      RPX  1
0662 0371 6803      SIN  2
0663 0372 B213      LDA  RN2
0664 0373 0110      ZAP
0665 0374 19AE      DATA :19AE      MPS 15
0666 0375 F204      JMP  RNDFIN
0667 0376 0110      LSI  ZAP
0668 0377 E20E      LDX  RN2        ASSURE X-PEG POSITIVE FOR LSI
0669 0378 1960      DATA :1960,PN1 MPY FN1
           0379 0385
0670 037A B2DB      RNDFIN LDA  PNDTMP
0671 037B 4404      DATA :4404      OCA, RESTORE CONSOLE STATUS
0672 037C 13A3      LPX  1
0673 037D 3801      JXN  S+2
0674 037E C403      LXP  3
0675 037F EA05      STX  FN1
0676 0380 EAD5      STX  PNDTMP
0677 0381 F046      FLT  PNDTMP, PNDTMP
           0382 0456
           0383 0456
0678 0384 F71C      RTN  RANDOM

```

```

PAGE 0022                                LOW CYCLE FATIGUE

0679 0385 0003 FN1 DATA 3
0680 0386 00FD FN2 DATA 253
0681 *
0682 0387 0800 PRINTSB ENT
0683 0388 F944 FDVD FAC:1,FAC:4,FAC:1
      0389 0426
      038A 02F4
      038B 0426
0684 038C F943 FMPL FAC:1,F1000,FAC:1
      038D 0426
      038E 0466
      038F 0426
0685 0390 F942 FSUB FAC:2,FAC:1,FAC:1
      0391 0276
      0392 0426
      0393 0426

0686 * WDEC FAC:1,9.7 PLASTIC STRAIN
0687 * STORE MAX. PLASTIC STRAIN
0688      0394 F947 FMOV FAC:1,OUTMP2
      0395 0426
      0396 03B7

0689 0397 F710 RTN PRINTSB
0690 *
0691 0398 0800 SWAP ENT
0692 0399 E25B LDX ACMPTEB SWAP THE CONTENTS OF
0693 039A EA97 STX TEMPI CMPTBL & TMTPEL
0694 039B C206 AXI 6
0695 039C EA97 STX TEMP2
0696 039D C7C6 LAM 6
0697 039E 9AB7 STA RNDTMP
0698 039F E6AC LDX XABCP
0699 03A0 B472 LDA 02
0700 03A1 BC00 EIA 00
0701 03A2 9C02 STA 02
0702 03A3 B39E SWLOOP LDA *TEMP1
0703 03A4 B88F EIA *TEMP2
0704 03A5 9B8C STA *TEMP1
0705 03A6 DA3B IMS TEMP1
0706 03A7 DA3C IMS TEMP2
0707 03A8 DAAD IMS RNDTMP
0708 03A9 F6C6 JMP SWLOOP
0709 03AA F712 RTN SWAP
0710 * PRINT SPACE
0711 03AB 0800 SPACE ENT
0712 03AC C620 LAP 120
0713 03AD F9CE OTT
0714 03AE F703 RTN SPACE
0715 * DO CRLF - NO PARITY BIT
0716 03AF 0800 CRLF2 ENT
0717 03B0 C6FD LAP 100 CR
0718 03B1 F9CE OTT
0719 03B2 C60A LAP 10A LF
0720 03B3 F90E OTT

```

PAGE 0023

LOW CYCLE FATIGUE

0721	03B4	F725	RTN	CRLF2
0722	03B5	0000	OUTMP1	PES 2.0
0723	03B7	0000	OUTMP2	PES 2.0

PAGE 0024

LOW CYCLE FATIGUE

```

0725      *
0726      ***** CALCULATE SLOPE *****
0727      *
0728      03B9 F947      SLOPE: FMOV F0,NMBPTS
           03BA 006E
           03BB 0428
0729      03BC F947      FMOV F0,XSUM
           03BD 006E
           03BE 042A
0730      03BF F947      FMOV F0,YSUM
           03C0 006E
           03C1 042C
0731      03C2 F947      FMOV F0,XXSUM
           03C3 006E
           03C4 042E
0732      03C5 F947      FMOV F0,XYSUM
           03C6 006E
           03C7 0430
0733      03C8 F992      SLOPE1 GET TABLE3
           03C9 04AA
0734      03CA F228      JMP LAST
0735      03CB 0A66      STA TEMP1
0736      03CC F946      FLT TEMP1,TEMP2
           03CD 0432
           03CE 0434
0737      03CF F941      FADD TEMP2,YSUM,YSUM
           03D0 0434
           03D1 042C
           03D2 042C
0738      03D3 F992      GET TABLE3
           03D4 04AA
0739      03D5 F21D      JMP LAST
0740      03D6 0A5B      STA TEMP1
0741      03D7 F946      FLT TEMP1,TEMP1
           03D8 0432
           03D9 0432
0742      03DA F943      FMPL TEMP1,TEMP2,TEMP2
           03DB 0432
           03DC 0434
           03DD 0434
0743      03DE F941      FADD TEMP2,XYSUM,XYSUM
           03DF 0434
           03E0 0430
           03E1 0430
0744      03E2 F941      FADD TEMP1,XSUM,XSUM
           03E3 0432
           03E4 042A
           03E5 042A
0745      03E6 F943      FMPL TEMP1,TEMP1,TEMP1
           03E7 0432
           03E8 0432
           03E9 0432
0746      03EA F941      FADD TEMP1,XXSUM,XXSUM

```

PAGE	0025	LOW CYCLE FATIGUE
	03EB 0432	
	03EC 042E	
	03ED 042E	
0747	03EE F941	FADD FI,NMBPTS,NMBPTS
	03EF 045E	
	03F0 0428	
	03F1 0423	
0748	03F2 F62A	JMP SLOPE1
0749		*
0750	03F3 F943	LAST FMPL XSUM,YSUM,TEMP1
	03F4 042A	
	03F5 042C	
	03F6 0432	
0751	03F7 F943	FMPL NMBPTS,XYSUM,TEMP2
	03F8 0428	
	03F9 0430	
	03FA 0434	
0752	03FB F942	FSUB TEMP2,TEMP1,TEMP2
	03FC 0434	
	03FD 0432	
	03FE 0434	
0753	03FF F943	FMPL XSUM,XSUM,TEMP1
	0400 042A	
	0401 042A	
	0402 0432	
0754	0403 F943	FMPL NMBPTS,XXSUM,XXSUM
	0404 0428	
	0405 042E	
	0406 042E	
0755	0407 F942	FSUB XXSUM,TEMP1,TEMP1
	0408 042E	
	0409 0432	
	040A 0432	
0756	040B F944	FDVD TEMP1,TEMP2,RESULT
	040C 0432	
	040D 0434	
	040E 0436	
0757	040F E100	LDX XABCP
	02F3	
0758	0410 F944	FDVD FI,RESULT,RESULT
	0411 045E	
	0412 0436	
	0413 0436	
0759	0414 F943	FMPL RESULT,*LDVALP,RESULT
	0415 0436	
	0416 80A0	
	0417 0436	
0760	0418 F944	FDVD RESULT,*STVALP,RESULT
	0419 0436	
	041A 80D4	
	041B 0436	
0761	041C F944	FDVD RESULT,FAREA,RESULT
	041D 0436	

```

PAGE 0026                                LOW CYCLE FATIGUE

      041E 0442
      041F 0436
0762 0420 F943      FMPL RESULT, F1000, RESULT
      0421 0436
      0422 0466
      0423 0436
0763 0424 F951      CLOS
0764 *

PAUSE
0765 *
0766 *
0767 0425 058A ACMPTE DATA CMPTBL
0768 0426 0000 FAC:1 RES 2,0
0769 0428 0000 NMBPTS RES 2,0
0770 042A 0000 XSUM RES 2,0
0771 042C 0000 YSUM RES 2,0
0772 042E 0000 XYSUM RES 2,0
0773 0430 0000 XYSUM RES 2,0
0774 0432 0000 TEMP1 RES 2,0
0775 0434 0000 TEMP2 RES 2,0
0776 0436 0000 RESULT RES 2,0
0777 0438 0000 TEMPAV RES 2,0
0778 043A 0000 FCYCLE RES 2,0
0779 043C 0000 FTHICK RES 2,0
0780 043E 0000 FWIDTH RES 2,0
0781 0440 0000 WIDTH RES 2,0
0782 0442 0000 FAREA RES 2,0
0783 0444 0000 STRSLN RES 2,0
0784 0446 0000 MAXLIN RES 2,0
0785 0448 0000 MINLIN RES 2,0
0786 044A 0000 SPPATE RES 2,0
0787 044C 0000 CLMPT RES 2,0
0788 044E 0000 STPES" RES 2,0
0789 0450 0000 AUGSTN RES 2,0
0790 0452 0000 HENGES RES 2,0
0791 0454 0000 LENGES RES 2,0
0792 0456 0000 PNDTIP RES 2,0
0793 0458 0000 NN RES 2,0
0794 045A 0000 XX RES 2,0
0795 045C 0000 MOD RES 2,0
0796 045E 4090 F1 DATA :4080,0
      045F 0000
0797 0460 4180 F4 DATA :4180,0
      0461 0000
0798 0462 41A0 F5 DATA :41A0,0
      0463 0000
0799 0464 4220 F10 DATA :4220,0
      0465 0000
0800 0466 457A F1000 DATA :457A,0
      0467 0000

0801 *
0802 *
0803 *
0804 *

```

PAGE 0027

LOW CYCLE FATIGUE

```

0805      0000 LOAD EQU 0
0806      0001 STROKE EQU 1
0807      0002 STRAIN EQU 2
0808      *
0809      0000 UP EQU 0
0810      8000 DOWN EQU :8000
0811      *
0812      *
0813      0074 F32767 EQU :74
0814      007A F:PI EQU :7A
0815      006E F0 EQU :6E
0816      0070 F2 EQU :70
0817      0097 GETSTA EQU :97
0818      *
0819      *
0820      00A0 LDVALP EQU :A0
0821      00B4 STVALP EQU :B4
0822      *
0823      0469 0000 TABLE1 RES 33.0
0824      0439 0000 TABLE2 RES 33.7
0825      04AA 0000 TABLE3 RES 23.0
0826      04C1 0000 TABLE4 RES 33.0
0827      *
0828      04E2 0000 NULL RES 20.0
0829      04F6 0000 TEXT '00'
0830      *
0831      04F7 C4C9 MAREA TEXT 'DIMS. (THICK,WIDTH):: 0'
0832      04F8 CDD3
0832      04F9 AEA0
0832      04FA A3D4
0832      04FB C8C9
0832      04FC C3CB
0832      04FD ACD7
0832      04FE C9C4
0832      04FF D4C3
0832      0500 A9BA
0832      0501 EAA0
0832      0502 C0A0
0832      0503 CDC9 MMSTPS TEXT 'MIN. STRESS (KSI):: 0'
0832      0504 CEAE
0832      0505 A0D3
0832      0506 D4D2
0832      0507 C5D3
0832      0508 D3A0
0832      0509 A3CB
0832      050A D3C9
0832      050B A9BA
0832      050C A0C0
0833      050D D3D4 MSTPLM TEXT 'STRAIN LMTS (+,-):: 0'
0833      050E D2C1
0833      050F C9CE
0833      0510 A0CC
0833      0511 CDD4

```



```

PAGE 0028                                LOW CYCLE FATIGUE

0512 D3A0
0513 A8AB
0514 ACAD
0515 A9BA
0516 BAA0
0517 C0A0
0834 0518 D2C1  RMDES TEXT 'RANDOM LMTS (Y,N): 0'
0519 CEC4
051A CFCD
051B A0CC
051C CDD4
051D D3A0
051E A8D9
051F ACCE
0520 A9BA
0521 A0C0
0835 0522 D3D4  MPATE TEXT 'STRAIN RATE (1/SEC): 0'
0523 D2C1
0524 C9CE
0525 A0D2
0526 C1D4
0527 C5A0
0528 A8B1
0529 AFD3
052A C5C3
052B A9BA
052C A0C0
0836 052D C5D3  MEXEC TEXT 'EXECUTE0'
052E C5C3
052F D5D4
0530 C5C0
0837 0531 D2C5  PESETM TEXT 'RESET RANDOM NOS. (Y,N): 0'
0532 D3C5
0533 D4A0
0534 D2C1
0535 CEC4
0536 CFCD
0537 A0CE
0538 CFD3
0539 AEA0
053A A8D9
053B ACCE
053C A9BA
053D A0C0
0838
0839 053E C0C0  *
0840 *
0841 0558 C3D9  MHEAD TEXT 'CYCLES MODULUS (+)STRESS(-)'
0559 C3CC
055A C5D3
055B A0CD
055C CFC4
055D D5CC

```

```

PAGE 0029                                LOW CYCLE FATIGUE

055E D5D3
055F A0A3
0560 ABA9
0561 D3D4
0562 D2C5
0563 D3D3
0564 A3AD
0565 A9A0
0842 0566 A0A3      TEXT ' (+)T.DISPL.(-)'
0567 ABA9
0568 D4AE
0569 C4C9
056A D3D0
056B CCAE
056C A3AD
056D A9A2
0843 056E A3AB      TEXT '(+)PLASTIC(-)'
056F A9D0
0570 CCC1
0571 D3D4
0572 C9C3
0573 A3AD
0574 A9C0
0844 0575 C3D9      MLAST TEXT 'CYCLES= '
0576 C3CC
0577 C5D3
0578 BDA0
0579 C0A0
0845 057A C1D6      MAVGS TEXT 'AVG PEAK STRAIN= '
057B C7A0
057C D0C5
057D C1CB
057E ACD3
057F D4D2
0580 C1C9
0581 CEBD
0582 A7C0
0846 0583 D3CC      MSLOPE TEXT 'SLOPE(PSI)= '
0584 CFD0
0585 C5A3
0586 D0D3
0587 C9A9
0588 BDA0
0589 C0A0
0847 058A 0000      CMPTL RES 6.0
0848 0590 0000      TMPTL RES 6.0
0849 *
0850 *
0851 * SUBROUTINE TO CONVERT FLOAT TO FIX POINT.
0852 0596 0300      OUFLEX ENT
0853 *
0854 * OUTPUT FIX POINT NUMBERS
0855 * AT CALL: OUFLEN - CONTAINS (INT) FIELD LENGTH

```

PAGE 0030

LOW CYCLE FATIGUE

```

0856          *      OUFLEX - X (F.P.) # TO BE OUTPUT (LOST)
0857          *      OUFLEZ - Z (F.P.) NUM TO DIVIDE BY: Z=Z/10
0858          *
0859 0507 B256 LDA OUFLE1 SAVE LENGTH
0860 0508 9A56 STA OUFLE2
0861 0509 EA53 STX OUSAVX SAVE X-REG
0862 050A 0000 NOP
0863 050B 0000 NOP
0864 050C 0000 NOP
0865 050D 0000 NOP
0866 050E 0000 NOP
0867 050F 0000 NOP
0868 05A0 F944 FDVD OUFLEX,OUFLEZ,OUFLEZ Z=X/Z (RIGHT UNITS)
      05A1 05F0
      05A2 05F2
      05A3 05F2
0869 05A4 0110 ZAR
0870 05A5 9A46 STA OUPK K=0
0871 05A6 C701 LAM 1
0872 05A7 3A47 ADD OUFLE2 L=L-1
0873 05A8 2035 JAM A RETURN
0874 05A9 9A45 STA OUFLE2
0875          *
0876          * PRINT SIGN (+ OR -)
0877          *
0878 05AA F948 FCMF OUFLEZ,F0 SEE IF Z<0 OR >0, A=-1, OR +1
      05AB 05F2
      05AC 006E
0879 05AD 3096 JAP OU2 Z>0
0880 05AE 0043 TAX (SAVE A)
0881 05AF F942 FSUB F0,OUFLEZ,OUFLEZ Z=ABS(Z)
      05B0 006E
      05B1 05F2
      05B2 05F2
0882 05B3 0030 TXA (RESTORE A)
0883 05B4 3101 OU2 JAN S+2
0884 05B5 C601 LAP 1 A=1, IF Z=0
0885 05B6 0308 NAX X=-A
0886 05B7 C220 AXI :2C X=:2C -(A)
0887 05B8 0030 TXA A=X = "+" OR "-"
0888 05B9 F90E OTT PRINT "+" OR "-"
0889 05BA C601 LAP 1 A=1
0890 05BB 9A2F OU1 STA OUPJ J=1
0891 05BC C701 OLL00P LAM 1 A=-1
0892 05BD 9A31 ADD OUFLE2 L=L-1
0893 05BE 20AA JAM OUPET RETURN
0894 05BF 9A2F STA OUFLE2
0895 05C0 F948 OU3 FCMF OUFLEZ,F1
      05C1 05F2
      05C2 045E
0896 05C3 2089 JAM OU3B Z<1
0897 05C4 F944 FDVD OUFLEZ,F10,OUFLEZ Z=Z/10
      05C5 05F2

```

PAGE 0031

LOW CYCLE FATIGUE

```

05C6 0464
05C7 05F2
0898 05C8 C601      LAP 1
0899 05C9 9A21      ADD OUPJ      J=J+1
0900 05CA 9A20      STA OUPJ
0901 05CB F603      JMP O03
0902 05CC C601      OU3B LAP 1
0903 05CD 8A1E      ADD OUPK      K=K+1
0904 05CE 9A1D      STA OUPK      STORE K
0905 05CF 921B      SUB OUPJ      A=K-J
0906 05D0 3103      JAN O04
0907 * PRINT DECIMAL POINT
0908 05D1 C62E      LAP :2E
0909 05D2 F90E      OTT
0910 05D3 F617      JMP OUL00P
0911 05D4 F943      OU4 FMPL OUFLZ,F10,OUFLZ Z=Z*10
05D5 05F2
05D6 0464
05D7 05F2
0912 05D8 F945      FIX OUFLZ,OUFLX X=INT(Z)
05D9 05F2
05DA 05F0
0913 05DB F946      FLT OUFLX,OUFLX BACK TO F.P.
05DC 05F0
05DD 05F2
0914 05DE F942      FSUB OUFLZ,OUFLX,OUFLZ Z=10*Z-INT(10*Z)
05DF 05F2
05E0 05F0
05E1 05F2
0915 05E2 F945      FIX OUFLX,OUFLX BACK TO FIX
05E3 05F0
05E4 05F0
0916 * PRINT DIGIT
0917 05E5 C630      LAP :30
0918 05E6 9A09      ADD OUFLX
0919 05E7 F90E      OTT
0920 05E8 F62C      JMP OUL00P
0921 * RETURN
0922 05E9 E203      OUPET LDY OUSAVX      PESTORE X
0923 05EA F754      RTN OUFLX
0924 * DATA
0925 *
0926 05EB 0000      OUPJ DATA 0      DECIMAL POINT LOCATOR
0927 05EC 0000      OUPK DATA 0      CHARACTER POINTER
0928 05ED 0000      OUSAVX DATA 0      XREG
0929 05EE 0000      OUFLN1 DATA 0      FIELD LEN.
0930 05EF 0000      OUFLN2 DATA 0      TEMP
0931 05F0 0000      OUFLX RES 2,0      (F.P.) X
0932 05F2 0000      OUFLZ RES 2,0      (F.P.) Z
0933 05F4 4A74      F1E6 DATA :4A74,:2400 1.E6
05F5 2400
0934 05F6 3D83      F1E13 DATA :3B33,:126F 1.E-3
05F7 126F

```

PAGE 0032 LOW CYCLE FATIGUE
0935 05F8 39D1 FIEM4 DATA :39D1,:B717 1.E-4
05F9 B717
0936 *

END
0937

PAGE 0033

LOW CYCLE FATIGUE

AC1PTB	0425	AUGSTN	0450	A	05BE	BEGIN	001B
BRANCH	0107	SPEAK	016A	BUFFID	053E	CLEAR1	0057
CLEAR2	0076	CLKRT	044C	CLR2	007D	CMPTBL	058A
CNTN1	0169	CNT	0177	CPLF2	03AF	CUPLD	013D
CURSTN	013E	CURSTP	00C2	CYADJ	0141	CYAD2	014B
CYAD3	014F	DATA01	01AF	DATA02	024F	DATN1	0156
DATPX	0173	DATPY	0179	DLTLD	0139	DLTST1	0139
DOWN	0000	EMPTY	02D6	FAC:1	0426	FAC:2	0276
FAC:3	0273	FAC:4	02F4	FAREA	0442	FCYCLE	043A
FINAL	027A	FNM1	00C4	FNM2	00C6	FNM3	00C8
FTCYC	013F	FTHICK	043C	FULLN1	0163	FULL	0260
FWIDTH	043E	F0	006E	FIEM3	05F6	FIEM4	05F8
FIE6	05F4	F1	045E	F10	0464	F1000	0466
F2	0070	F3	00CA	F32767	0074	FA	0460
F5	0462	F:PI	007A	GETNUM	0176	GETSTA	0097
HLIMIT	00BE	HPNGE	0452	INCDEL	0134	INCTEL	0125
INCTB2	0127	INDEX	0172	INDEX1	00BD	INITCX	0270
INITCY	00A9	I300	0133	LAST	03F3	LDVALP	00A2
LLIMIT	00C0	LOAD	0000	LOAD2	013C	LOOP3	028D
LPNGE	0454	LSI	0376	MAPEA	04F7	MAVGS	057A
MAXLIM	0446	MDFLG	016D	MD	0274	MD2ND	01E3
MESEC	052D	MHEAD	0558	MINLIM	0448	MLAST	0575
MMSTPS	0503	MOD	045C	MPATE	0522	MSLOPE	0583
MSTPLM	050D	NAME	0007	NMBPTS	0428	NMMESS	0000
NN	0458	NOT1	01DC	NULL	04E2	NUM	0160
NUM1	016B	NIX	0155	N1	0150	OLDLD	0137
OUFLN	05EE	OUFLFX	0596	OUFLN2	05EF	OUFLX	05F0
OUFLZ	05F2	OULOPP	05EC	OUPI	05EB	OUPI	05EC
OURET	05E9	OUSAVX	05ED	OUTMPI	03B5	OUTMP2	03B7
OUI	05EB	OU2	05E4	OU3B	05CC	OU3	05CC
OUA	05D4	PRINTV	02AE	PRINT	02F6	PEVTSB	0387
RANDOM	0363	RESETM	0531	RESET1	00E1	RESTPT	00D6
RESULT	0436	REVDIN	021E	REVUP	0195	RMPDN	026D
RMPUP	0104	RNDFIN	037A	RNDFLG	0175	RNDMES	0518
RNDMLT	0070	RNDM	00C3	RNDTMP	0456	RN1PTR	0174
RNI	0385	RNI2	0386	ROUND	004B	RSTEX	00ED
RSTPT0	00E5	RVDN	0024	SAME2	00EB	SETPTR	0271
SETTEL	0112	SETTB2	011F	SLOPE1	03C8	SLOPE:	03B0
SPACE	03AB	SPRATE	044A	STAT:A	0266	STAT:B	0269
STRAIN	0002	STRESS	0272	STRESV	044E	STROKE	0201
STRSLM	0444	STVALP	00B4	SWAP	0399	SVLOOP	03A3
TABLE1	0469	TABLE2	0489	TABLE3	04AA	TABLE4	04C1
TEMPAV	0438	TEMP1	0432	TEMP2	0434	TEMPTEL	0590
UPDATE	017A	UPEXIT	021D	UP	0000	UP:	01C9
UTEMP1	016E	UTEMP2	016F	VALPTR	00C4	WIDTH	0440
WINKER	026D	WTCLR	0072	XABCP	02F3	XABC	0170
XBPT	0171	XC	0173	XIT	021B	XSUM	042A
XXSUM	042E	XX	045A	XY2	0233	XX3	01A1
XYSUM	0430	YSUM	042C				

APPENDIX II

SOURCE LISTING OF FORTRAN PROGRAM FOR STRESS
AND STRAIN COMPUTATIONS AND PLOTTING

```

PROGRAM DATA (OUTPUT,TAPE1,TAPE2,TAPE3,TAPE4,
1 TAPES,TAPE6,INPUT=7.)
C
C *****
C THIS PROGRAM DEVELOPED BY
C CAPT ROBERT SCHAFRIK
C MAY, 1979
C *****
C
COMMON /A/ N(1500),F(1500),SIGMA1(1500),SIGMA2(1500),ELONG1(1500),
AELONG2(1500),PLST1(1500),PLST2(1500),TITL(60),R1(1500),
BDELTER(1500)
REAL N
C
C IFLAG = YES FOR COMPUTER DATA
C IFLAG = NO FOR NO COMPUTER DATA
C IFLAG1 = YES FOR COMPUTER DATA PRINT-OUT (DATA ON P.F.)
C IUNIT IS THE TAPE NUMBER
C
READ 4,IFLAG,IUNIT,IFLAG1
4 FORMAT ( / A1,4X,I1,-X,A1)
C
IF (IUNIT.LE.3.OR.IUNIT.GT.6) IUNIT=1
PRINT 8,IFLAG,IUNIT,IFLAG1
8 FORMAT (1H1,I2,*FROM DATA : COMPUTER DATA = *,A1,
A/I2,*TAPE UNIT IS *,I1 /
BT4,*COMPUTER DATA FLAG IS *,A1//)
IF (IFLAG.NE.1HY) GO TO 50
C
READ (IUNIT,9) (TITL(JT),JT=1,60)
9 FORMAT(60A1)
C
IMAX=1500
I=0
1 CONTINUE
I=I+1
IF (I.GT.IMAX) GO TO 1000
C
READ (IUNIT,10) N(I),F(I),SIGMA1(I),SIGMA2(I),ELONG1(I),ELONG2(I),
1PLST1(I),PLST2(I)
10 FORMAT (9(F7.3,1X))
C
IF(N(I).LT.0.9) GO TO 3
IF (EOF(IUNIT))2,1
3 CONTINUE
PRINT 30
30 FORMAT (T2,*READ TERMINATED BY ZERO VALUE*)
I=I-1
GO TO 40
1000 CONTINUE
I=IMAX
PRINT 1001,I
1001 FORMAT(T2,*H**** ,2X,*IMAX = *,I5,2X,
1 *DATA PTS EXCEED ARRAY DIMENSIONS*,//)
GO TO 40
2 CONTINUE
PRINT 31
31 FORMAT (T2,*READ TERMINATED BY EOF*)
I=I-1
40 CONTINUE
PRINT 10,(TITL(JA),JA=1,60)
10 FORMAT (// T2,60A1, /T2,60(1H*))//
PRINT 11,I

```



```

11  FORMAT ( // T2,*NUMBER OF DATA PTS = *,I5
1, // )
IF (I.EQ.0) STOP
DO 20 J=1,I
IF (IFLAG1.NE.1HY) GO TO 45
PRINT 21, N(J),E(J),SIGMA1(J),SIGMA2(J),ELONG1(J),
1ELONG2(J),PLST1(J),PLST2(J)
21  FORMAT (T2,F7.0, 3(1X,F7.2), 4(1X,F7.3))
45  CONTINUE
E(J)=E(J)*1.E6
ELONG1(J)=ELONG1(J)*1.E-3
ELONG2(J)=ELONG2(J)*1.E-3
PLST1(J)=PLST1(J)*1.E-3
PLST2(J)=PLST2(J)*1.E-3
20  CONTINUE
CALL LCF(I)
GO TO 51
50  CONTINUE
I=0
PRINT 55
55  FORMAT (// T2,*NO COMPUTER DATA*, ///)
C
READ 9,TITL
C
PRINT 18, (TITL(JA),JA=1,50)
CALL LCF(I)
51  CONTINUE
CALL DATA1
CALL SUBPLOT(I)
STOP
END
C
C*****
C
SUBROUTINE LCF(I)
COMMON /A/ N(1500),E(1500),SIGMA1(1500),SIGMA2(1500),ELONG1(1500),
1ELONG2(1500),PLST1(1500),PLST2(1500),TITL(50),R1(1500),
1DELTEP(1500)
COMMON /D/ LPLST,LELST
REAL LPLST,LELST,N
DIMENSION MSIG(1500)
DIMENSION DELTSIG(1500),DELTEL(1500),DELTP(1500),DELTEE(1500),
1ADELTSTN(1500)
EQUIVALENCE (E(1),DELTSIG(1)), (ELONG1(1),DELTEL(1)),
1(ELONG2(1),DELTP(1)), (PLST1(1),DELTEE(1)),
1(PLST2(1),ADELTSTN(1))
C
DATA MSIG /1500*(1H )/
DATA IFLG /0/
C
C
READ *,EACT,LELST,LPLST,SFACTOR,DFACTOR,IFLG
C
EACT IS ACTUAL ELASTIC MODULUS IN EB PSI
LELST IS AN ASSUMED ELASTIC EFFECTIVE GAGE LENGTH
C
LPLST IS EFFECTIVE PLASTIC GAGE LENGTH
C
SFACTOR - COMPUTER STRESS CORRECTION FACTOR
C
DFACTOR - DISPL CORRECTION FACTOR, COMPUTER
C
IFLG IS USED TO SPECIFY DATA PRINT-OUT
C
FOR PRINT-OUT, USE 1
C
C
PRINT 23,EACT,LELST,LPLST,SFACTOR,DFACTOR,IFLG
23  FORMAT (T2,*FROM LCF* / T2,*EACT = *,E12.5,*, LELST = *, E12.5,
1* LPLST = *, E12.5 / T3,3H***,
1* SFACTOR = *, F12.5, *, DFACTOR = *, F12.5 /

```

```

C      AT3,*COMPUTER DATA PRINT-OUT FLAG IS = *,I1 //)      001400
C      IF (I.EQ.0) RETURN      001410
C      EACT=EACT*1.E+6      001420
C      DELTEET=0.0      001430
C      DO 9 J=1,I      001440
C      DELTEET=DELTEET+E(J)      001450
C      CONTINUE      001460
C      ASSUME MINI-COMPUTER INTERNAL ARITHMETIC IS OK      001470
C      DELTEET=DELTEET/I*(1.00/1.00)      001480
C      LELST=EACT/DELTEET      001490
C      DO 10 J=1,I      001500
C      SIGMA1(J)=SIGMA1(J)*SFACTOR      001510
C      SIGMA2(J)=SIGMA2(J)*SFACTOR      001520
C      ELONG1(J)=ELONG1(J)*DFACTOR      001530
C      ELONG2(J)=ELONG2(J)*DFACTOR      001540
C      DELTSIF=SIGMA1(J)-SIGMA2(J)      001550
C      DELTEK=ELONG1(J)-ELONG2(J)      001560
C      ELASTIC STRAIN = SIGMA/E = (UT-UP)/LELST      001570
C      PL1=PLST1(J)      001580
C      PLST1(J)=ELONG1(J)-(LELST*SIGMA1(J)*1.E+3/EACT)      001590
C      PL2=PLST2(J)      001600
C      PLST2(J)=ELONG2(J)-(LELST*SIGMA2(J)*1.E+3/EACT)      001610
C      DELTPK=PLST1(J)-PLST2(J)      001620
C      IF (DELTPK.LE.1.E-6) GO TO 11      001630
C      CONTINUE      001640
C      DELTED=(DELTEK-DELTPK)/LELST      001650
C      DELTEP(J)=(DELTPK/LELST)      001660
C      DELTSTM=DELTED+DELTEP(J)      001670
C      R1(J)=ABS(SIGMA1(J)/SIGMA2(J))      001680
C      GO TO 8      001690
C      CONTINUE      001700
C      PLST1(J)=PL1*LELST      001710
C      PLST2(J)=PL2*LELST      001720
C      MSIG(J)=1HX      001730
C      DELTPK=PLST1(J)-PLST2(J)      001740
C      RPL=DELTSIF/DELTEET      001750
C      DISPDIF=RPL/DELTEK      001760
C      DRATIO=DISPDIF*DFACTOR*1.E3      001770
C      PRINT 101, N(J),DRATIO      001780
C      101 FORMAT(T3,*CORRECTION FACTOR FOR DISPLACEMENTS: N = *,      001790
C      AF6.1,3X,*SUGGESTED DFACTOR = *,F6.4)      001800
C      IF (DELTPK.GT.1.E-6) GO TO 12      001810
C      MSIG(J)=1HX      001820
C      DELTPK=1.E-5      001830
C      GO TO 12      001840
C      CONTINUE      001850
C      E(J)=DELTSIF      001860
C      ELONG1(J)=DELTEK      001870
C      ELONG2(J)=DELTPK      001880
C      PLST1(J)=DELTED      001890
C      PLST2(J)=DELTSTM      001900
C      CONTINUE      001910
C      POINT 20,(TITL(JA),JA=1,31)      001920
C      20 FORMAT(1H1,T43,*INSTRON COMPUTER*/ T20,      001930
C      Z*DATA FOR *, 31A1 / T20,43(1H*), 3(/),      001940
C      XT59,*RATIO*, / T50,*MAX STRESS*,/      001950
C      1T11,*TOTAL*, T20,*PLASTIC*, T30 ,      001960
C      2*STRESS*, T40,*MAX*, T43,*MIN*,T60,*TO*, T68,*ELASTIC*,      001970
C      3T79,*PLASTIC*, T89,*STRAIN* /      001980
C      4 T2.*CYCLES*. T11.*ELONG*. T21.*ELONG*. T30. 001990

```

```

5      *RANGE*, T40,*STRESS*,
6      T48, *STRESS*, T56, *MIN STRESS*, T68, *STRAIN*,
7      T79, *STRAIN*, T89, *RANGE*/ ,
8      T10,*(INCHES)*, T20, *(INCHES)*, T30,
9      *(KSI)*, T4, *(KSI)*, T48,
A      *(KSI)*, T68, *(PCNT)*, T79, *(PCNT)*, T89, *(PCNT)* /)
C
DO 30 K=1,I
DELTEP(K)=DELTEP(K)*100.
DELTEE(K)=DELTEE(K)*100.
DELTSTN(K)=DELTSTN(K)*100.
NT=N(K)
C
C USE TO ELIMINATE PRINTING
C
IF (IFLG.NE.1) GO TO 99
C
PRINT 22,NT, DELTEL(K),DELTPL(K),
1DELTSIG(K),SIGMA1(K),SIGMA2(K),R1(K),DELTEE(K),
3DELTEP(K),DELTSTN(K),MSIG(K)
22  FORMAT (T2, I5, T11, F6.5, T21, F6.5, T30,
1 F7.2, T40, F5.1, T48, F6.1, T56, F7.3,
3 T58,F5.3,T79,F6.4, T89, F5.3,T120,A1)
C
99  CONTINUE
C
30  CONTINUE
PRINT 40
40  FORMAT(/// )
PRINT 31,DELTEET,LELST
31  FORMAT (1H1,
1 T, *THE AVERAGE MODULUS FOR THIS DATA WAS*,E12.5,* PSI*,
2 / T2,*EFFECTIVE ELASTIC GAGE LENGTH IS *,E12.5,* INCHES*/ )
RETURN
END
C
C*****
C
SUBROUTINE DATA1
COMMON /A/ BA(12000),TITL(60),BB(3000)
COMMON /C/ SIGC(70),STRT(70),STRP(70),STRNC(70),NC(70),KI,
ZDELTELC(70),DELTPLC(70)
INTEGER UNITS,DATASTS
REAL NC
C
READ 11,DATASTS
11  FORMAT(I1)
C
IF (DATASTS.LE.0) GO TO 50
C
KA=0
DO 15 M=1,DATASTS
C
FOR CHART DIMENS IN M4,USE M
C
FOR CHART DIMENSIONS IN INCHES, USE I
C
READ 2,UNITS,FCTR
2  FORMAT (A1,4X,F5.0)
C
PRINT 9,TITL
9  FORMAT(/ T2,BJ(145)/ T2,60A1)
PRINT 6,UNITS,FCTR
6  FORMAT (/T2,*FROM DATA1, UNITS = *,A1,/,
AT2,*ADD THESE NUMBER OF CYCLES TO DATA 1*,1X,F5.0/)
IF (UNITS.EQ.1HI.OR.UNITS.EQ.1HM) GO TO 51
GO TO 50

```

```

51  CONTINUE                                002720
C                                          002730
C  CALSIG IS CALIBRATION FACTOR FOR LOAD SCALE ON H-P CHART 002740
C  CALDIS1 IS EXTENSOMETER CALIB FACTOR 002750
C  CALDIS2 IS CALIBRATION FACTOR FOR H-P CHART 002760
C  SPECA IS SPECIMEN AREA 002770
C  READ *,CALSIG,CALDIS1,CALDIS2,SPECA 002780
C                                          002790
C  PRINT 10,CALSIG,CALDIS1,CALDIS2,SPECA 002800
10  FORMAT (// T2,*FROM DATA1*/ T2,*H-P CHART LOAD SCALE CALIBRATION 002810
1IS *, F7.5, 002820
2 / T2,*EXTENSOMETER CALIBRATION FACTOR IS *, F7.5, 002830
4 / T2,*H-P CHART DISPLACEMENT SCALE CALIBRATION IS *,F7.5, 002840
5 / T2,*SPECIMEN AREA = *,F7.5 /) 002850
C  PRINT 29,UNITS 002860
29  FORMAT (T2,* UNITS DESIG IS *, A2/) 002870
C  CALDIS=CALDIS1*CALDIS2 002880
C                                          002890
C  KT=KA 002900
100 CONTINUE 002910
C  KA=KA+1 002920
C  IF (KA.GT.70) GO TO 70 002930
C                                          002940
C  READ *,NC(KA),STRT(KA),STRP(KA),SIGC(KA) 002950
C  USE -1. TO TERMINATE READING DATA STRING 002960
C  PRINT *,NC(KA),STRT(KA),STRP(KA),SIGC(KA) 002970
C  IF(NC(KA).LT.0.3) GO TO 103 002980
C  NC(KA)=NC(KA)+FCTR 002990
C  GO TO 100 003000
70  CONTINUE 003010
C  PRINT 71 003020
71  FORMAT (4(/) T3,*EXCEEDED ARRAY DIMENSIONS IN DATA1*,3(/)) 003030
103 CONTINUE 003040
C  PRINT 4 003050
4  FORMAT(// T2,*CYCLES*, T10,*T.DISP*, T18,*PL.DISP*,T28, 003060
1*STRESS*/) 003070
C  KA=KA-1 003080
C  KI=KA 003090
C  KS=KT+1 003100
C                                          003110
C  DO 1 J=KS,KI 003120
C  PRINT 5,NC(J),STRT(J),STRP(J),SIGC(J) 003130
5  FORMAT (T2,F5.0,T10,F5.2,T18,F5.2,T29,F5.2) 003140
1  CONTINUE 003150
C  CALL DATA2 (CALSIG,CALDIS,SPECA,UNITS,KS) 003160
15 CONTINUE 003170
C                                          003180
C  PRINT 9 003190
C  PRINT 21,(TITL(JA),JA=1,31) 003200
21  FORMAT (1H1,T28,*HYSTERESIS LOOP*,/ 003210
AT16,*DATA FOR *, 31A1/ 003220
BT16,40(1+*), 3(/) 003230
CT10,*TOTAL*, T20,*PLASTIC*,T31, 003240
D*STRESS*, T42,*ELASTIC*, T53, 003250
E*PLASTIC*, T65,*STRAIN* / T2 003260
F,*CYCLES*, T11,*ELONG*, T21,*ELONG*, 003270
GT31,*RANGE*, T42,*STRAIN*, T53, 003280
H*STRAIN*, T65,*RANGE* , / T10, 003290
I*(INCHES)*, T20, *(INCHES)*, T31, 003300
J*(KSI)*, T42, *(PCNT)*, T53,*(PCNT)*, 003310
KT65, *(PCNT)* /) 003320
C                                          003330
C  DO 20 MC=1,KI 003340
C  NT=NC(MC) 003350
C  PRINT 22,NT,DELTELC(MC),DELTPLC(MC),SIGC(MC), 003360
ASTRT(MC),STRP(MC),STRNC(MC) 003370

```

```

22  FORMAT(T2,I5,T11,F6.5,T21,F6.5,T30,F7.2,T42,F5.3
    AT53,F6.4,T65,F5.3)
26  CONTINUE
    PRINT 27
27  FORMAT (1H1)
C
    RETURN
50  CONTINUE
    PRINT 7
7    FORMAT (/ T2,*NO HYSTERESIS LOOP DATA* ,/)
    KI=0
    RETURN
    END
C
C*****
C
    SUBROUTINE DATA2(CALSIG,CALDIS,SPECA,UNITS,KI)
    COMMON /C/ SIGC(70) ,STRT(70) ,STRP(70) ,STRNC(70) ,NC(70) ,KI
    A,DELTELC(70),DELTPLC(70)
    COMMON /D/ LP,LE
    INTEGER UNITS
    REAL NC
C LE IS EFF-ELAST GAGE LGTH,LP IS PL EFF GAGE LENGTH,
    REAL LE,LP
C
    SIG(C,CAL,A,F)=C/F*CAL*500./A
    E(C,CAL,F)=C/F*CAL
    STNE(UTOT,UPL,EE)=(UTOT-UPL)/EE
    STNP(UPL,EP)=UPL/EP
C
    PRINT 8,LE,LP,CALSIG,CALDIS
8    FORMAT (T2,* LE,LP,CALSIG,CALDIS ARE = *, 4F9.5, //)
    PRINT 6
6    FORMAT (3(/), T2,*CYCLES*, T9,*ELAST STN*, T22, *PL STRN*,
1 T35, *TOT STRN*,T48,*STRESS*,T57,*TOT DISPL* ,T70,*PL DISPL* //)
    IF (UNITS.EQ.1H) FACTOR=1.00
    IF (UNITS.EQ.1HM) FACTOR=2.54
C
    DO 5 K=KS,KI
    SIGC(K)=SIG(SIGC(K),CALSIG,SPECA,FACTOR)*1.E-3
    UT=E(STRT(K),CALDIS,FACTOR)
    UP=E(STRP(K),CALDIS,FACTOR)
    STNEL=STNE(UT,UP,LE)*1.E2
    STNPL=STNP(UP,LP)*1.E2
    STRNC(K)=STNEL+STNPL
C
    STORE ELAS & PLAST STRAIN
    STRT(K)=STNEL
    STRP(K)=STNPL
    DELTELC(K)=UT
    DELTPLC(K)=UP
    UT=UT*1.E3
    UP=UP*1.E3
    PRINT 7,NC(K),STRT(K),STRP(K),STRNC(K),SIGC(K),UT,UP
7    FORMAT (T2,F5.3,T9,F4.3,T22,F4.3 ,T35,F5.3, T48,F5.1,T57,
1 F4.2,T70,F4.3)
5    CONTINUE
    RETURN
    END
C
C*****
C
    SUBROUTINE SUBPLOT(I)
    COMMON /A/ N(1500),DELTSIG(1500),X(1500),Y(1500),DELTEL(1500),
    ADLTPL(1500),DELTEE(1500),DELTSTN(1500),TITL(60),
    DR1(1500),DELTEP(1500)
    COMMON /C/ SIGC(70),STRT(70),STRP(70),STRNC(70),NC(70),KI

```

```

A,DELTELC(70),DELTPLC(70)                                004040
REAL N,U(50),NC                                           004050
REAL XA(70),YA(70)                                         004060
DIMENSION IPAK(50),MPLOT(10)                               004070
LOGICAL HYPLOT,COMPLLOT,DUALPT                             004080
C                                                           004090
PRINT 10,I,KI                                              004100
10  FORMAT (1H1//T2,*FROM SUBPLOT : NO. OF COMPUTER DATA PTS IS = *, 004110
      A15 / T17,*NO. OF HYSTERESIS LOOP DATA PTS IS = *, I5/) 004120
      CALL COMPRS                                           004130
C                                                           004140
COMPLLOT=.T.                                               004150
HYPLOT=.T.                                                 004160
DUALPT=.F.                                                 004170
IF (I.LE.0) COMPLLOT=.F.                                   004180
IF (KI.LE.0) HYPLOT=.F.                                    004190
IF (HYPLOT.AND.COMPLLOT) DUALPT=.T.                       004200
C                                                           004210
PRINT 6, COMPLLOT,HYPLOT,DUALPT                           004220
6   FORMAT ( / * COMPLLOT = *, L3, 5X, *,HYPLOT = *, L3/, 004230
      AT3,*DUALPT = *,L3 /)                                004240
C                                                           004250
IF (.NOT.COMPLLOT.AND..NOT.HYPLOT) RETURN                 004260
C                                                           004270
LN2=1                                                       004280
IF (DUALPT) LN2=2                                           004290
C                                                           004300
C   DEFINE MESSAG LTR HEIGHT & BLNK1 SIZE                 004310
      HT=0.14                                               004320
C   ASSUMES 15 PLOTTED CHARACTERS                         004330
C                                                           004340
      XLNGTH=15.*HT+2.*HT                                  004350
      YLNGTH=2.*HT                                          004360
      XORGIN=1.0                                            004370
      YORGIN=1.0                                            004380
C   ESTABLISH LENGTHS FOR BLANKING                         004390
      XF=XORGIN+XLNGTH                                     004400
      YF=YORGIN+YLNGTH                                     004410
C   ESTABLISH MESSAG PRINT POSITIONS                      004420
      XO=XORGIN+HT*2.                                       004430
      YO=YORGIN+HT/2.                                       004440
C                                                           004450
C                                                           004460
C   FOR PLOTS 1-10   USE Y                                004470
C                                                           004480
      READ 1, (MPLOT(L),L=1,10)                             004490
1   FORMAT(10A1)                                           004500
C                                                           004510
      PRINT 9, (MPLOT(L),L=1,10)                             004520
9   FORMAT (T2, *MPLOT IS : *, 10(A1,1X) /)               004530
C                                                           004540
C   ASSUMES 15 CHARACTERS + $                             004550
      ENCODE (15,20,U) (TITL(KL),KL=1,15)                 004560
20  FORMAT (15A1, "$")                                       004570
C                                                           004580
C   YMIN2,YMAX2 - STRESS RANGE FOR PLOT 2                 004590
C   YMIN3,YMAX3 - STRAIN RANGE FOR PLOT 3                 004600
C   YMIN4,YMAX4 - STRESS RANGE FOR PLOT 4                 004610
C   YMIN5,YMAX5 - STRESS RANGE FOR PLOT 5                 004620
C   XMAX1 - DEFINED MAX NUMBER OF CYCLES FOR 2ND PLOT GROUP 004630
C                                                           004640
      READ *,YMIN2,YINC2,YMAX2                               004650
      READ *,YMIN3,YINC3,YMAX3                               004660
      READ *,YMIN4,YINC4,YMAX4                               004670
      READ *,YMIN5,YINC5,YMAX5                               004680
      READ *,X50RGN,XCYCL                                     004690

```

	READ *,XINC1,XMAX2	004700
C		004710
	PRINT 8,YMIN2,YINC2,YMAX2,YMIN3,YINC3,YMAX3,YMIN4,YINC4,YMAX4,	004720
	AYMIN5,YINC5,YMAX5,X5ORGN,XCYCLE,XINC1,XMAX2	004730
8	FORMAT (/T3,*YMIN2,YINC2,YMAX2 = *,3F10.2/	004740
	AT3,*YMIN3,YINC3,YMAX3 = *,3F10.2/	004750
	BT3,*YMIN4,YINC4,YMAX4 = *,3F10.2 /	004760
	CT3,*YMIN5,YINC5,YMAX5 = *,3F10.2/	004770
	ET3,*X5ORGN,XCYCLE = *,2F10.2/	004780
	DT3,*XINC1,XMAX2 = *,2F10.2/)	004790
C		004800
	JTEST=0	004810
	DO 507 JRS=1,10	004820
	IF (MPL0T(JRS).EQ.1HY) JTST=1	004830
	JTEST=JTEST+JTST	004840
607	CONTINUE	004850
	IF (JTEST.EQ.0) GO TO 1001	004860
	CALL 9GNPL(-1)	004870
	DO 1000 MINDEX=1,2	004880
	IF (MINDEX.EQ.1.AND.COMPLOT) GO TO 400	004890
	IF (MINDEX.EQ.1.AND..NOT.COMPLOT) GO TO 410	004900
	IF (MINDEX.EQ.2.AND.COMPLOT) GO TO 405	004910
	IF (MINDEX.EQ.2.AND..NOT.COMPLOT) GO TO 405	004920
400	CONTINUE	004930
C	FIND XMAX	004940
	XMAX=N(1)	004950
	DO 30 M=2,I	004960
	IF (N(M).GT.XMAX) XMAX=N(M)	004970
30	CONTINUE	004980
	XMAX=XMAX/100.	004990
	IXMAX=XMAX	005000
	XMAX=(IXMAX+1)*100.	005010
	IF (DUALPT) GO TO 402	005020
	GO TO 401	005030
402	CONTINUE	005040
	DO 32 M=1,KI	005050
	IF (NC(M).GT. XMAX) XMAX=NC(M)	005060
32	CONTINUE	005070
	XMAX=XMAX/100.	005080
	IXMAX=XMAX	005090
	XMAX=(IXMAX+1)*100.	005100
	GO TO 401	005110
C		005120
410	CONTINUE	005130
C	FIND NC=MAX	005140
	XMAX=NC(1)	005150
	DO 31 M=2,KI	005160
	IF (NC(M).GT.XMAX) XMAX=NC(M)	005170
31	CONTINUE	005180
	XMAX=XMAX/100.	005190
	IXMAX=XMAX	005200
	XMAX=(IXMAX+1)*100.	005210
	GO TO 401	005220
C		005230
405	CONTINUE	005240
415	CONTINUE	005250
	XMAX=XMAX2	005260
	GO TO 401	005270
C		005280
401	CONTINUE	005290
	PRINT 3, MINDEX,XMAX	005300
3	FORMAT (T2,*MINDEX= *, I3, 4X,*XMAX = *,F7.1 /)	005310
C		005320
	IF (MPL0T(MINDEX*5-4).NE.1HY) GO TO 502	005330
501	CONTINUE	005340
		005350

C	PLOT S-MAX/S-MIN VS CYCLES	PLOT #1	005360
C	*****		005370
C			005380
	IF (.NOT.COMPLOT) GO TO 120		005390
	PRINT 7,I		005400
7	FORMAT(///,* SUBPLOT *//,T2,* I= *,I5//)		005410
C	DO 10 J=1,I		005420
C	PRINT 1,J, N(J), R1(J)		005430
C1	FORMAT (T2, *J= *,I5,3X,* N= *,F7.1,3X,* R1= *,F5.3)		005440
C10	CONTINUE		005450
C			005460
	XLTH=7.0		005470
	YLTH=5.0		005480
	XMIN=0.0		005490
	XINC=500.		005500
	YINC=.1		005510
	YMIN=.4		005520
	YMAX=1.3		005530
C	ELIM OUT OF RANGE PTS		005540
	IT=C		005550
	DO 210 IJ=1,I		005560
	IF (R1(IJ).LT.YMIN.OR.R1(IJ).GT.YMAX) GO TO 211		005570
	IF (N(IJ).LT.XMIN.OR.N(IJ).GT.XMAX) GO TO 211		005580
	IT=IT+1		005590
	X(IT)=N(IJ)		005600
	Y(IT)=R1(IJ)		005610
	GO TO 210		005620
211	CONTINUE		005630
210	CONTINUE		005640
C			005650
	CALL BASALF("STANDARD")		005660
	CALL MIXALF ("INSTRUCTION")		005670
	CALL MX3ALF ("L/CGREEK" ,1H*)		005680
	CALL TITLE(1H,-1,"CYCLES",100,"RATIO (H2.)*S (LH.5) MAX (LXHX) TO		005690
	1 (H2.)*S (LH.5) MIN (LXHX)", 100, XLTH ,YLTH)		005700
	CALL HEADIN ("RATIO OF (H2.)*S (LH.5) MAX (LXHX) TO (H2.)*S (LH.5) MIN		005710
	1 (LXHX)", 100,3,2)		005720
	CALL HEADIN ("VERSUS CYCLES", +100, 3,2)		005730
	CALL BLNK1(XORGIN,XF,YORGIN,YF,+1)		005740
	CALL INTAXS		005750
	CALL FRAME		005760
	CALL GRAF(XMIN,XINC,XMAX,YMIN,YINC,YMAX)		005770
	CALL SCLPIC(0.5)		005780
	CALL CURVE (X,Y,IT,-1)		005790
	CALL RESET("BLNK1")		005800
	CALL HEIGHT (HT)		005810
	CALL MESSAG(U,100,XO,YO)		005820
	CALL ENOPL(MINDEX*5-4)		005830
	CALL RESET ("HEIGHT")		005840
C			005850
C			005860
502	CONTINUE		005870
	IF (MPLT(MINDEX*5-3).NE.1HY) GO TO 503		005880
C			005890
C			005900
C	PLOT STRESS RANGE VS CYCLES	PLOT #2	005910
C	*****		005920
C			005930
C	DO 11 J=1,I		005940
C	PRINT 2, J, N(J),DELTSIG(J)		005950
C2	FORMAT(T2,*J= *,I5,3X,*N= *,F7.1,3X,*DELTSIG= *, F6.1)		005960
C11	CONTINUE		005970
C			005980
	XLTH=7.0		005990
	YLTH=5.0		006000
	XMIN=XMIN		006010


```

      YINC=YINC2
      YMAX=YMAX2
      XMIN=0.0
      XINC=500.
      IF (MINDEX.EQ.1) XINC=XINC1
C
      IF (.NOT.COMPLOT) GO TO 120
      IT=0
      DO 220 IJ=1,I
      IF (DELSIG(IJ).LT.YMIN.OR.DELTSIG(IJ).GT.YMAX) GO TO 221
      IF (N(IJ).LT.XMIN.OR.N(IJ).GT.XMAX) GO TO 221
      IT=IT+1
      X(IT)=N(IJ)
      Y(IT)=DELSIG(IJ)
      GO TO 220
221 CONTINUE
220 CONTINUE
C
120 CONTINUE
      IF (.NOT.HYPLLOT) GO TO 227
      JT=0
      DO 225 IJ=1,KI
      IF (SIGC(IJ).LT.YMIN.OR.SIGC(IJ).GT.YMAX) GO TO 226
      IF (NC(IJ).LT.XMIN.OR.NC(IJ).GT.XMAX) GO TO 226
      JT=JT+1
      XA(JT)=NC(IJ)
      YA(JT)=SIGC(IJ)
      GO TO 225
226 CONTINUE
225 CONTINUE
227 CONTINUE
C
      CALL SCLPIC(1.0)
      CALL RESET ("XALFS")
      CALL BASALF("STANDARD")
      CALL TITLE(1H,-1, "CYCLESS", 100, "STRESS RANGE (KSI)",
1 100,XLTH, YLTH)
      CALL HEADIN ("STRESS RANGE VS CYCLESS", -100,3,1)
      CALL BLNK1(XORGIN,XF,YORGIN,YF,+1)
      CALL BLNK2(0.35,4.25,1.95,2.65,+1)
      CALL INTAXS
      CALL FRAME
      CALL GRAF (XMIN,XINC,XMAX,YMIN,YINC,YMAX)
      CALL SCLPIC(0.5)
      IF (COMPLOT) CALL CURVE (X,Y,IT,-1)
      IF (HYPLLOT) CALL CURVE(XA,YA,JT,-1)
      CALL RESET("BLNK1")
      CALL RESET("BLNK2")
      CALL HEIGHT (HT)
      CALL MESSAG(U,100,XO,YO)
      CALL SCLPIC(1.00)
      IF (COMPLOT) CALL LINES("COMPUTER GENERATED DATAS",IPAK,1)
      IF (HYPLLOT) CALL LINES ("HYSTERESIS LOOP DATAS",IPAK,LN2)
      CALL LEGEND(IPAK,LN2,1.0,2.0)
      CALL ENDFL(MINDEX*5-3)
      CALL RESET ("HEIGHT")
C
503 CONTINUE
      IF (HPLOT(MINDEX*5-2).NE.1HY) GO TO 504
C
C
C      PLOT STRAIN RANGE VS CYCLES      PLOT #3
C#####
C
C      DO 12 J=1,I

```

```

006020
006030
006040
006050
006060
006070
006080
006090
006100
006110
006120
006130
006140
006150
006160
006170
006180
006190
006200
006210
006220
006230
006240
006250
006260
006270
006280
006290
006300
006310
006320
006330
006340
006350
006360
006370
006380
006390
006400
006410
006420
006430
006440
006450
006460
006470
006480
006490
006500
006510
006520
006530
006540
006550
006560
006570
006580
006590
006600
006610
006620
006630
006640
006650
006660
006670

```

```

C      PRINT 3, J, N(IJ), DELTSTN(IJ)                                006680
C3     FORMAT(T2, *J= *, I5, 3X, *N= *, F7.1, 3X, *DELTSTN= *, F6.4) 006690
C12    CONTINUE                                                       006700
C                                           006710
C                                           006720
C      XLTH=7.0                                                         006730
C      YLTH=5.0                                                         006740
C      YMIN=YMIN3                                                       006750
C      YINC=YINC3                                                       006760
C      YMAX=YMAX3                                                       006770
C      XMIN=0.0                                                         006780
C      XINC=500.                                                       006790
C      IF (MINDEX.EQ.1) XINC=XINC1                                     006800
C                                           006810
C      IF (.NOT.COMPLOT) GO TO 130                                       006820
C      IT=0                                                             006830
C      DO 230 IJ=1, I                                                    006840
C      IF (DELTSTN(IJ).LT.YMIN.OR.DELTSTN(IJ).GT.YMAX) GO TO 231      006850
C      IF (N(IJ).LT.XMIN.OR.N(IJ).GT.XMAX) GO TO 231                  006860
C      IT=IT+1                                                           006870
C      X(IT)=N(IJ)                                                       006880
C      Y(IT)=DELTSTN(IJ)                                                 006890
C      GO TO 230                                                         006900
231    CONTINUE                                                         006910
236    CONTINUE                                                         006920
130    CONTINUE                                                         006930
C                                           006940
C      IF (.NOT.HYPLOT) GO TO 237                                       006950
C      JT=0                                                             006960
C      DO 235 IJ=1, KI                                                  006970
C      IF (STRNC(IJ).LT.YMIN.OR.STRNC(IJ).GT.YMAX) GO TO 236          006980
C      IF (NC(IJ).LT.XMIN.OR.NC(IJ).GT.XMAX) GO TO 236                006990
C      JT=JT+1                                                           007000
C      XA(JT)=NC(IJ)                                                     007010
C      YA(JT)=STRNC(IJ)                                                  007020
C      GO TO 235                                                         007030
236    CONTINUE                                                         007040
235    CONTINUE                                                         007050
237    CONTINUE                                                         007060
C                                           007070
C      CALL SCLPIC(1.0)                                                  007080
C      CALL TITLE (1H, -1, "CYCLES", 100, "STRAIN RANGE (PERCENT)S", 007090
C      1 100, XLTH, YLTH)                                               007100
C      CALL HEADIN ("STRAIN RANGE VS CYCLES", -100, 3, 1)             007110
C      CALL FRAME                                                         007120
C      CALL BLNK1 (XORIGIN, XF, YORIGIN, YF, +1)                      007130
C      CALL BLNK1 (0.95, 4.25, 1.95, 2.55, +1)                       007140
C      CALL XINTAX                                                         007150
C      CALL GRAF (XMIN, XINC, XMAX, YMIN, YINC, YMAX)                  007160
C      CALL SCLPIC(0.5)                                                  007170
C      IF (COMPLOT) CALL CURVE (X, Y, IT, -1)                          007180
C      IF (HYPLOT) CALL CURVE (XA, YA, JT, -1)                         007190
C      CALL RESET ("BLNK1")                                              007200
C      CALL RESET ("BLNK2")                                              007210
C      CALL HEIGHT (HT)                                                  007220
C      CALL MESSAG (U, 100, XO, YO)                                     007230
C      CALL SCLPIC(1.0)                                                  007240
C      IF (COMPLOT) CALL LINES ("COMPUTER GENERATED DATA", IPAK, 1) 007250
C      IF (HYPLOT) CALL LINES ("HYSTERESIS LOOP DATA", IPAK, LN2)    007260
C      CALL LEGEND (IPAK, LN2, 1.0, 2.0)                               007270
C      CALL ENOPL (MINDEX*5-2)                                           007280
C      CALL RESET ("HEIGHT")                                             007290
C                                           007300
C      504 CONTINUE                                                       007310
C      IF (HYPLOT (MINDEX*5-1).NE.1HY) GO TO 505                      007320
C                                           007330
C      PLOT EXPLODED STRESS RANGE VS CYCLES PLOT 04

```

CC

```

C
  XLTH=7.0
  YLTH=5.0
  YMIN=YMIN4
  YINC=YINC4
  YMAX=YMAX4
  XMIN=0.0
  XINC=500.
  IF (MINDEX.EQ.1) XINC=XINC1
C
  IF (.NOT.COMPLOT) GO TO 140
  IT=0
  DO 240 IJ=1,I
  IF (DELSIG(IJ).LT.YMIN.OR.DELTSIG(IJ).GT.YMAX ) GO TO 241
  IF (N(IJ).LT.XMIN.OR.N(IJ).GT.XMAX) GO TO 241
  IT=IT+1
  X(IT)=N(IJ)
  Y(IT)=DELSIG(IJ)
  GO TO 240
241 CONTINUE
240 CONTINUE
140 CONTINUE
C
  IF (.NOT.HYPLOT) GO TO 247
  JT=0
  DO 245 IJ=1,KI
  IF (SIGC(IJ).LT.YMIN.OR.SIGC(IJ).GT.YMAX) GO TO 246
  IF (NC(IJ).LT.XMIN.OR.NC(IJ).GT.XMAX) GO TO 246
  JT=JT+1
  XA(JT)=NC(IJ)
  YA(JT)=SIGC(IJ)
  GO TO 245
246 CONTINUE
245 CONTINUE
247 CONTINUE
C
  CALL SCLPIC(1.0)
  CALL TITLE(1H , -1, "CYCLESS", 100, "STRESS RANGE (KSI)",
1 100,XLTH, YLTH)
  CALL HEADIN ("STRESS RANGE VS CYCLES", -100,3,1)
  CALL FRAME
  CALL BLNK1(XORGIN,XF,.30,.60,+1)
  CALL BLNK2(0.60,3.90,3.90,1.6,+1)
  CALL INTAXS
  CALL GRAF (XMIN,XINC,XMAX,YMIN,YINC,YMAX)
  CALL GRID (5,5)
  CALL SCLPIC(0.5)
  IF (COMPLOT) CALL CURVE (X,Y,IT,-1)
  IF (HYPLOT) CALL CURVE(XA,YA,JT,-1)
  CALL RESET("BLNK1")
  CALL RESET("BLNK2")
  CALL HEIGHT (HT)
  CALL MESSAG(U,100,X0,.38)
  CALL SCLPIC(1.0)
  IF (COMPLOT) CALL LINES("COMPUTER GENERATED DATA",IPAK,1)
  IF (HYPLOT) CALL LINES ("HYSTERESIS LOOP DATA",IPAK,LN2)
  CALL LEGEND (IPAK,LN2,.05,.95)
  CALL ENDPL (MINDEX*5-1)
  CALL RESET ("HEIGHT")
C
C
505 CONTINUE
  IF (HYPLOT(MINDEX*5).NE.1HY) GO TO 99
C
C
  PIOT STRESS RANGE VS LOG CYCLES PLOT #5

```

007340
 007350
 007360
 007370
 007380
 007390
 007400
 007410
 007420
 007430
 007440
 007450
 007460
 007470
 007480
 007490
 007500
 007510
 007520
 007530
 007540
 007550
 007560
 007570
 007580
 007590
 007600
 007610
 007620
 007630
 007640
 007650
 007660
 007670
 007680
 007690
 007700
 007710
 007720
 007730
 007740
 007750
 007760
 007770
 007780
 007790
 007800
 007810
 007820
 007830
 007840
 007850
 007860
 007870
 007880
 007890
 007900
 007910
 007920
 007930
 007940
 007950
 007960
 007970
 007980
 007990

260	CONTINUE	008660
	PRINT 264,IT,JT	008670
264	FORMAT (T3, 34** , *NO DATA PTS WITH RANGE OF PLOT 5*/	008680
	AT*,*IT = *, I5, 3X, *,JT = *, I5/)	008690
C		008700
99	CONTINUE	008710
C		008720
C	CC	008730
1000	CONTINUE	008740
	CALL DONEPL	008750
1001	CONTINUE	008760
	RETURN	008770
	END	008780

BIBLIOGRAPHY

1. M. N. Menon and W. H. Reimann, "Low Cycle Fatigue Crack Initiation Study in René 95," J. Mater. Sci. 10, 1571-1581 (1975).
2. B. Leis and A. Clauer, Investigation of Rejuvenation of Fatigue Damage in IN-718, Air Force Materials Laboratory Technical Report, AFML-TR-78-90, AF Contract F33615-76-C-5100 (Air Force Materials Laboratory, Wright-Patterson Air Force Base, Ohio, 1978).
3. S. S. Manson, Thermal Stress and Low Cycle Fatigue, McGraw-Hill (1966).
4. M. Gill, G. R. Leverant, and C. H. Wells, "The Fatigue Strength of Nickel-Base Superalloys," Achievement of High Fatigue Resistance in Superalloys, ASTM STP 467, American Society of Testing and Materials, 53-76 (1970).
5. C. H. Wells and C. P. Sullivan, "Low Cycle Fatigue of Udimet 700 at 1700 F," Trans. ASM 61, 149-155 (1968).
6. C. H. Wells and C. P. Sullivan, "The Effect of Temperature on the Low Cycle Fatigue Behavior of Udimet 700," Trans. ASM 60, 217-222 (1967).
7. C. H. Wells and C. P. Sullivan, "The Low Cycle Fatigue Characteristics of a Nickel-Base Superalloy at Room Temperature," Trans. ASM 57, 841-855 (1964).
8. M. Gell and G. R. Leverant, "The Fatigue of the Nickel-Base Superalloy MAR-M-200 in Single Crystal and Columnar Grain Forms at Room Temperature," Trans. AIME 242, 1869-1879 (1968).
9. P. Gauthier, H. DeRandy, and J. Auvinet, "Secondary Cracking Process During Fatigue Crack Propagation," Eng. Fract. Mech. 5, 977-981 (1973).
10. W. H. Vaughan, R. J. Sanford, J. M. Krofft, W. H. Cullen, and J. W. Dolly, Failure Studies of a Third Stage Fan Disk from a TF-30 Turbine Engine, NRL Memorandum Report 3874, Naval Research Laboratories (1978).
11. A. H. Cottrell, "Fracture," Proc. Roy. Soc. London A 276, 1-18 (1963).

12. A. W. Funkenbusch and L. F. Coffin, "Low Cycle Fatigue Crack Nucleation and Early Growth in Ti-17," Met. Trans. 9A, 1159-1167 (1978).
13. J. C. Grosskreutz, Phys. Stat. Solidi (B) 47, 359-396 (1971).
14. G. E. Dieter, Mechanical Metallurgy, McGraw-Hill, 403-450 (1976).
15. C. H. Wells and C. P. Sullivan, "The Low Cycle Fatigue Characteristics of a Nickel-Base Superalloy at Room Temperature," Trans. ASM 57, 841-847 (1964).
16. H. F. Merrick, "The Low Cycle Fatigue of Three Wrought Nickel-Base Alloys," Met. Trans. 5, 891-897 (1974).
17. D. R. Muzyka, "The Metallurgy of Iron Nickel Alloys," The Superalloys (C. T. Sims and W. C. Hagel, eds.), John Wiley and Sons, New York (1972).
18. R. F. Decker and S. Floreen, "Precipitation from Substitutional Iron-Base Austenitic and Martensitic Solid Solutions," Precipitation from Iron Base Alloys (G. R. Speich and J. B. Clark, eds.), Gordon and Breach Scientific Publishers, New York (1965).
19. E. F. Bradley and M. J. Donachie, "Forgings for Jet Engines: More Quality at Less Cost," Metals Prog. 106/2, 80-82 (July 1974).
20. D. Raynor and J. M. Silcock, "Strengthening Mechanisms in Gamma-Prime Precipitating Alloys," Metal Sci. J. 4, 121-130 (1970).
21. D. R. Muzyka, "Controlling Microstructure and Properties of Superalloys Via Use of Precipitated Phases," Metals Eng. Qtrly 11/4, 12-20 (1971).
22. G. R. Speich, "Cellular Precipitation in an Austenitic Fe-30Ni-6Ti Alloy," Trans. AIME 227, 754-762 (1963).
23. C. C. Clark and J. S. Iwanski, "Phase Changes in Precipitation Hardening Nickel-Chromium-Iron Alloys during Prolonged Heating," Trans. AIME 215, 648-651 (1959).
24. H. J. Beattie and W. C. Hagel, "Intragranular Precipitation of Intermetallic Compounds in Complex Austenitic Alloys," Trans. AIME 221, 28-35 (1961).
25. E. E. Brown, R. C. Boettner, and D. L. Ruckle, Minigrain Processing of Nickel-Base Alloys, presented at the Metallurgical Society of AIME Fall Meeting, Cleveland, 1970.

26. R. F. Decker and C. T. Sims, "The Metallurgy of Nickel-Based Superalloys," The Superalloys (C. T. Sims and W. C. Hagel, eds.) John Wiley and Sons, New York (1972).
27. C. T. Sims, "The Occurrence of Topologically Close-Packed Phases," The Superalloys (C. T. Sims and W. C. Hagel, eds.), John Wiley and Sons, New York (1972).
28. J. P. Dennison and B. Wilshire, "Mechanisms of Improving Creep Rupture Lives by Re-Heat Treatments," Fracture 2, 635-639 (1977).
29. J. P. Dennison, P. D. Holmes, and B. Wilshire, "The Creep and Fracture Behavior of the Cast Nickel-Based Superalloy IN-100," Mater. Sci. & Eng. 33, 35-47 (1978).
30. K. C. Anthony and J. F. Rodavitch, The Effects of HIP Rejuvenation of Turbine Blades, presented at the AIME Annual Meeting, Atlanta, Georgia.
31. Summary Report on the Powder Metallurgy Seminar, Air Force Materials Laboratory Technical Report AFML-TM-LT-74-4 (Air Force Materials Laboratory, Wright-Patterson Air Force Base, Ohio, 1974).
32. ASTM Standard E407-70, "Standard Methods for Microetching Metals and Alloys," Annual Book of ASTM Standards, American Society of Testing and Materials, Philadelphia (1974).
33. M. F. Henry, A Technique for Monitoring Time Dependent Surface Damage, General Electric Report No. 71-C-338, Schenectady, New York (1971).
34. Pratt and Whitney Aircraft Specification 1003H, East Hartford, Conn. (November 1973).
35. W. P. Koster and J. B. Kohls, Relationship of Surface Integrity to Cost and Reliability of Structural Components, SME Technical Paper IQ72-207 (1972).
36. R. L. Ketter and S. P. Prawel, Modern Methods of Engineering Computation, McGraw-Hill (1969).
37. L. G. Heroux and C. P. Sullivan, "Metallographic Replication of Curved Surfaces," Trans. ASM 56, 861-863 (1963).
38. L. K. Singhal and M. L. Vaidya, "Precipitation of Sigma Phase in a Duplex Fe-Cr-Ni-Ti Alloy," Trans. ASM Qtrly 62, 879-885 (1969).
39. W. H. Hill, K. D. Shimmin, and B. A. Wilcox, "Elevated Temperature Dynamic Moduli of Metallic Materials," ASTM Proc. 61, 890-906 (1961).

40. S. Spinner and W. E. Tefft, "A Method for Determining Mechanical Resonance Frequencies and for Calculating Elastic Moduli from These Frequencies," ASTM Proc. 61, 1221-1238 (1961).
41. W. E. Tefft, "Numerical Solution of the Frequency Equations for the Flexural Vibration of Cylindrical Rods," J. Research NBS 64B, 237-242 (1960).
42. ASTM Standard E112-61, "Standard Methods for Estimating the Average Grain Size of Metals," Annual Book of ASTM Standards, American Society of Testing and Materials, Philadelphia (1974).
43. Aerospace Structural Metals Handbook, Code 4107, Mechanical Properties Data Center, Traverse City, Michigan (December 1973).
44. A. Green, H. Sieber, D. Wells, and T. Wolfe, Research Investigation to Determine Mechanical Properties of Nickel and Cobalt-Base Alloys for Inclusion in Military Handbook 5, Air Force Materials Laboratory Technical Report ML-TDR-64-116, DDC AD-608813, V1, 500-508 (1964).
45. SEM/TEM Fractography Handbook, MCIC-HB-06, compiled by McDonnell Douglas Astronautics Co., published by Metals and Ceramics Information Center, Battelle-Columbus Laboratories, Columbus, Ohio (1975).
46. C. Laird, Mechanisms and Theories of Fatigue, presented at the Materials Science Seminar, American Society for Metals, St. Louis, Missouri (1978).
47. W. H. Kim and C. Laird, "Crack Nucleation and Stage I Propagation in High Strain Fatigue - I. Microscopic and Interferometric Observations," Acta Met. 26, 777-787 (1978).
48. W. H. Kim and C. Laird, "Crack Nucleation and Stage I Propagation in High Strain Fatigue - II. Mechanism," Acta Met. 26, 789-799 (1978).
49. D. Kuhlmann-Wilsdorf and C. Laird, "Dislocation Behavior in Fatigue," Mater. Sci. and Eng. 31, 137-156 (1977).
50. W. A. Wood, Fatigue in Aircraft Structures, Academic Press, New York (1956).
51. C. Laird, Fatigue Crack Propagation, ASTM 415, American Society for Testing and Materials, Philadelphia (1967).
52. A. S. Tetelman and A. J. McEvily, Fracture of Structural Materials, 347-400 (1967).

53. American Society for Metals, Failure Analysis and Prevention, vol. 10, Metals Handbook (8th ed.), Metals Park, Ohio (1975).
54. F. Petit, Personal Communication, Materials Research Laboratory, Pratt and Whitney Aircraft, Commercial Products Division, East Hartford, Conn. (June 1979).
55. R. Sandström, "Subgrain Growth Occurring by Boundary Migration," Acta Met. 25, 905-911 (1977).
56. R. Sandström, "On Recovery of Dislocations in Subgrains and Subgrain Coalescence," Acta Met. 25, 897-904 (1977).
57. J. P. Hirth and J. Lothe, Theory of Dislocations, McGraw-Hill, New York (1968).
58. M. R. James and A. W. Sleeswyk, "Influence of Intrinsic Stacking Fault Energy on Cyclic Hardening," Acta Met. 26, 1721-1726 (1978).
59. R. W. Landgraf, "The Resistance of Metals to Cyclic Deformation," Achievement of High Fatigue Resistance in Metals and Alloys, ASTM STP 467, American Society of Testing and Materials, 3-36 (1970).
60. R. W. Smith, M. H. Hirschberg, and S. S. Manson, Fatigue Behavior of Materials under Strain Cycling in Low and Intermediate Life Range, NASA Technical Note D-1574, Lewis Research Center, Cleveland, Ohio (1963).
61. T. J. Dolan, "Designing Structures to Resist Low-Cycle Fatigue," Metals Eng. Qtrly 10, 18-25 (November 1970).
62. D. Macha, Unpublished Research, Air Force Materials Laboratory, Metals Behavior Branch (AFML/LLN), Wright-Patterson Air Force Base, Ohio 45433 (1977).
63. G. R. Irwin, Plastic Zone Near a Crack and Fracture Toughness, Seventh Sagamore Ordinance Materials Research Conference (August 1960).
64. C. Calabrese and C. Laird, "High Strain Fatigue Fracture Mechanics in Two Phase Alloys," Met. Trans. 5, 1785-1793 (1974).
65. C. Calabrese and C. Laird, "Cyclic Stress-Strain Response of Two-Phase Alloys; Part I. Microstructures Containing Particles Penetrable by Dislocations," Mater. Sci. and Eng. 13, 141-157 (1974).
66. C. Calabrese and C. Laird, "Cyclic Stress-Strain Response of Two-Phase Alloys; Part II. Particles Not Penetrated by Dislocations," Mater. Sci. and Eng. 13, 159-174 (1974).

67. W. H. Kim and C. Laird, "The Role of Cyclic Hardening in Crack Nucleation at High Strain Amplitude," Mater. Sci. and Eng. 33, 225-231 (1978).
68. C. Laird, V. J. Langelo, M. Hallrah, N. C. Yang, and R. DeLaVeaux, "The Cyclic Stress-Strain Response of Precipitation Hardened Al-15 wt% Ag Alloy," Mater. Sci. and Eng. 32, 137-160 (1978).
69. H. J. Beattie, Jr., "The Crystal Structure of a M_3B_2 -Type Double Boride," Acta Cryst. 11, 607-609 (1958).
70. M. J. Fleetwood and C. A. P. Horton, "The Use of the Microprobe Analyzer and the Electron Microscope for the Identification of Precipitate Particles in a Nickel-Chromium-Iron Alloy," J. Roy. Microsc. Soc. 83, 245-250 (1964).

**DA
FILM**